Ollscoil Chathair
Bhaile Átha Cliath
Dublin City University

REMOTE SENSING OF SURFACE WATER TEMPERATURE IN SOUTH AMERICAN LAKES

by

Dieu Anh Dinh

Research supervised by:

Dr. R Iestyn Woolway[1]

Prof. Eleanor Jennings[2]

Dr. Valerie McCarthy[3]

Dr. Siobhán Jordan[2]

[1]School of Ocean Sciences, Bangor University, Menai Bridge, Anglesey, UK

[2]Centre for Freshwater and Environmental Studies, Dundalk Institute of Technology, Dundalk, Ireland

[3]Dublin City University, Dublin, Ireland

A dissertation submitted in fulfilment of the requirements for the degree of Doctor of Philosophy registered at the Centre for Freshwater and Environmental Studies, Dundalk Institute of Technology, Dundalk, Ireland

July 2025

Student Declaration

I hereby certify that this material, which I now submit for assessment on the programme of study leading to the award of Doctor of Philosophy is entirely my own work, and that I have exercised reasonable care to ensure that the work is original and have conformed to the regulations on the use of and declaration of Generative AI, and does not to the best of my knowledge breach any law of copyright, and has not been taken from the work of others save and to the extent that such work has been cited and acknowledged within the text of my work.

Signed: Dieu Anh Dinh ID No.: D00253021 Date: 09/09/2026

Funding

Dieu Anh Dinh was co-funded by the Ireland's Higher Education Authority and Dundalk Institute of Technology through the Landscape and Technology University Transformation Fund (TUTF) programmes.

Acknowledgements

This dissertation would not have been possible without the guidance, support and encouragement of many individuals. I am truly thankful to everyone who provided valuable assistance from the beginning to the end of this incredible journey.

First of all, I would like to express my sincere gratitude to my PhD supervisors, Dr. R Iestyn Woolway, Prof. Eleanor Jennings, Dr. Valerie McCarthy, and Dr. Siobhán Jordan for their excellent guidance, advice and support. It is a great honour to learn from your expertise. Thank you for always making time for progress meetings and sharing your invaluable guidance through every stage of this research.

A big thank you to my family, my mother- mẹ Hương, my father- bố Tuyên, my sister- chị Thu, my brother-in-law- anh Hưng, my nephew-Bi and my niece-Táo Đỏ for always by my side with great support and encouragement. A heartfelt thanks to my husband- Stefan for his unconditional love, support, endless patience and a source of strength through every up-and-down moment. I also dedicate this work to my dear grandmother, Bà Ngoại, who passed away this year. Her belief in the importance of learning- "Knowledge is power"- has always motivated me and will keep inspiring me.

A great thanks to my colleagues and friends from the Centre for Freshwater and Environmental Studies (CFES), DkIT, especially Samuel, Trisha, Remember, Jimena, Ryan and Ricardo. Thank you all for your help, support and the wonderful memories we created together from our never-ending chats, lunchbreaks, dinners, seminars and road trips.

My special thanks to Pogonian friends- Pedro, Adreeja, Anto, Andrea, Sharloth, Jeffrey, Hadeer, and Akoko for their infinite support, for the laughs and conversations we shared and for keeping our birthday calls going strong. I also like to thank Eva and Baerbel from the Alfred Wegener Institute (AWI), Helgoland for their wonderful support during the time I was there and throughout my PhD journey.

I would like to thank the lecturers and technicians from CFES, DkIT staff from the RDC and IT staff for their assistance and help along the way.

Lastly, I thank the Irish Higher Education Authority and the DkIT Research Office for funding this PhD research and giving me the opportunities to attend international conferences,

workshops and summer school, which helped me enhance knowledge, improve professional development and build academic networks.

Abstract

Water temperature is an essential component that drives the physical and biogeochemical processes in lakes and also serves as an indicator of climate change impacts on lake ecosystems. Therefore, understanding lake surface water temperature (LSWT) variability is vital to assess the response of lakes to the effects of climate change. This study investigates LSWT and lake heatwave variability using satellite Earth Observation (EO) and model-derived data during historical period (1981-2020) and under various future scenarios (2021-2099). This dissertation focuses on a local case study of Lake Titicaca (Peru-Bolivia) and expands to a regional scale of South American lakes.

Firstly, the comparison of gap-filling methods for satellite EO data was assessed using Lake Titicaca because of its ecological and economic importance in the region. Several gap-filling methods, including machine learning algorithms, were evaluated to determine the most accurate reconstruction method. Data Interpolating Convolutional Auto-Encoder (DINCAE) was identified as the most accurate and suitable gap-filling method. DINCAE was then used to assess LSWT variability at different timescales during the period of 2000-2020.

Secondly, the result derived from the DINCAE algorithm was validated against a daily Global LAke Surface water Temperature (GLAST) dataset. The historical and future variability of Lake Titicaca's LSWT and lake heatwave using the GLAST dataset were analysed. Additionally, the meteorological drivers of LSWT changes, including surface air temperature, longwave downward radiation, shortwave downward radiation, specific humidity and wind speed, were assessed for their influence on LSWT changes. The results showed that there has been a warming trend over the past 40 years in Lake Titicaca, driven mainly by solar radiation and surface air temperature. LSWT and lake heatwave are projected to increase by 2100.

Thirdly, the study was upscaled to 2,046 lakes in South America, where limited in situ measurements have constrained LSWT research. The interannual and diurnal LSWT trends and heatwave variability in South America over the past 40 years and by the end of the 21st century were investigated. Most South American lakes experienced warming trends in daily and diurnal LSWT during the historical period (1981-2020). The main factors that influenced LSWT and diurnal LSWT variability were air temperature and solar radiation, respectively. LSWT and lake heatwave intensity and frequency are forecasted to increase in the future. Furthermore, a

typology of lake thermal responses based on diurnal and seasonal temperature range classification was developed.

In conclusion, this research highlights the rapid warming of LSWT and the increasing frequency and intensity of lake heatwaves across South American lakes. These findings suggest the need to enhance the lake monitoring systems and increase regional collaboration, as well as immediate action to mitigate the effects of climate change and to protect lake ecosystems in South America.

Table of Contents

Student Declaration....ii
Funding iii
Acknowledgements....iv
Abstract....vi
List of Figures....xii
List of Tables xvi
Acronyms and Abbreviations xvii
I. Introduction 1
1.1. Lakes as sentinels of climate change....1
1.2. Essential Climate Variables (ECVs) 2
1.3. Research aims and objectives....3
1.4. Thesis structure 5
II. Literature review 6
2.1. Climate change impacts on global lakes 6
2.1.1. Climate change impacts on lake physics 6
2.1.1.1. Lake surface water temperature 6
2.1.1.2. Lake ice cover 8
2.1.1.3. Stratification and mixing regimes 9
2.1.1.4. Lake water level and lake water volume....11
2.1.2. Climate change impacts on lake chemistry 14
2.1.3. Climate change impacts on biological communities 15
2.2. South American lakes....16
2.2.1. Climate change impacts in South America....19
2.2.1.1. Air temperature 19
2.2.1.2. Solar radiation....20
2.2.1.3. Humidity 21
2.2.1.4. Wind speed....22
2.2.2. Climate change and anthropogenic impacts on South American lakes....23
2.2.2.1. Lake surface water temperature 24
2.2.2.2. Lake water level/volume....25
2.2.2.3. Lake ice cover....25

2.2.2.4. Lake mixing regimes....26
2.2.2.5. Lake chemistry....27
2.2.2.6. Lake biology....28
2.2.3. Extreme events impact on South American climate and lakes....29
2.3. Lake Titicaca....33
2.3.1. Climate change and impacts on Lake Titicaca region....36
2.3.1.1. Air temperature....36
2.3.1.2. Other meteorological variables....37
2.3.1.3. Extreme events....38
2.3.2. Climate change and anthropogenic impacts on Lake Titicaca....39
2.3.2.1. Lake surface water temperature....39
2.3.2.2. Stratification and mixing regimes....40
2.3.2.3. Hydrology....41
2.3.2.4. Lake chemistry and biology....43
2.3.2.5. Extreme events....45
2.3.2.6. Socio-economy impacts....46
2.4. Application of Satellite Earth Observations for LSWT Dynamics Analysis....47
III. Evaluating gap-filling techniques for satellite-derived surface water temperature: A case study of Lake Titicaca....49
3.1. Introduction....49
3.2. Materials and Methods....52
3.2.1. Study site....52
3.2.2. Materials....52
3.2.3. Methods....53
3.2.3.1. Data Interpolating Empirical Orthogonal Functions (DINEOF)....54
3.2.3.2. Multi-model gap-filling approach....55
3.2.3.3. Data Interpolating Convolutional Auto-Encoder (DINCAE)....57
3.2.3.4. Validation and analysis....60
3.3. Results....61
3.3.1. Satellite-derived observations of LSWT and Chl-*a*....61
3.3.2. Comparison of gap-filling methods....64
3.3.3. Spatial and temporal variations in LSWT....66
3.4. Discussion....68
3.5. Conclusions....73

IV. The current and future warming of Lake Titicaca 74
4.1. Introduction 74
4.2. Study Area 76
4.3. Data and Methods 76
4.3.1. Data 76
4.3.1.1. GLAST Dataset 76
4.3.1.2. Satellite-derived lake surface water temperature 77
4.3.2. Methods 78
4.3.2.1. Bias correction for future projections of GLAST 78
4.3.2.2. Attribution analysis 80
4.3.2.3. Lake heatwaves 80
4.3.2.4. Statistical analysis 81
4.4. Results 81
4.4.1. Historical to contemporary temperature changes in Lake Titicaca 81
4.4.2. Contributions of meteorological drivers to LSWT trends 82
4.4.3. Future warming of Lake Titicaca 84
4.4.4. Persistence of extreme temperatures this century 86
4.5. Discussion 88
4.6. Conclusions 91
V. Emerging changes in lake temperature extremes and variability in South America 92
5.1. Introduction 92
5.2. Study area 94
5.3. Data and Methods 94
5.3.1. GLAST dataset 94
5.3.2. Lake Heatwaves 95
5.3.3. Lake classification 95
5.3.4. Diurnal to seasonal lake temperature typology 96
5.3.5. Data analysis 97
5.4. Results 97
5.4.1. Historic patterns of change in LSWT, lake heatwaves and diurnal-seasonal variability 97
5.4.2. Future changes during the 21st century 107
5.5. Discussion 110
5.6. Conclusions 113

VI. Conclusion and Future Perspectives 114
6.1. Summary of findings 114
6.2. Synthesis of contributions 116
6.3. Limitations and uncertainties 117
6.4. Implications for water management 119
6.5. Future research 121
6.6. Final remarks 122
References 123
Appendices 155
Appendix A 155
Appendix B 164
Appendix C 177
Appendix D. List of Publications, Conference Oral/Poster presentations and Trainings 183

List of Figures

Figure 2.1. The importance of LSWT in lake ecosystems.....7
Figure 2.2. South American Map (Source: Rivas Martínez et al. 2011).....17
Figure 2.3. The location of the study site, Lake Titicaca (Peru-Bolivia).....34
Figure 2.4. Lake Titicaca bathymetry map (Source: Duquesne et al. 2021).....36
Figure 3.1. Total number of annual (a) LSWT and (b) Chl-*a* observations, both temporally and spatially in Lake Titicaca during the study period (2000-2020). The percentage was calculated based on the ratio of observed or available pixels to the total potentially available pixels over 365 days in percentage.....62
Figure 3.2. Monthly observations, per 4 km^2 pixel, of LSWT from 2000 to 2020 in Lake Titicaca. Observation counts ranged between 0 and 400 per cell monthly. 63
Figure 3.3. Examples of a) Original, b) Added clouds, as well as the reconstructed images (c-f).....64
Figure 3.4. Comparison of the tested gap-filling algorithms in reconstructing LSWT in Lake Titicaca, shown in scatter plots of observed and predicted LSWTs. The red lines denoted the 1:1 line. 65
Figure 3.5. Annual, seasonal, and monthly gap-filled LSWTs in Lake Titicaca (2000 to 2020). Shown are the average (a) annual and (b, c) wet/dry season LSWTs throughout the study period, (d) monthly LSWT variations (error bars represent the standard deviation), and (e) the interannual variability in LSWT. Also shown are the LSWT trends, calculated (f) annually and (g, h) during the wet/dry season. The asterisk (*) shows statistically significant trends with $p < 0.05$. The LSWT data used in this analysis are those reconstructed using the DINCAE multivariate algorithm.....67
Figure 4.1. Annual temperature (black), wet season temperature (dashed dark grey), dry season temperature (dotted grey) derived from GLAST data from 1981 to 2020, with the trends respectively on the top right.....82
Figure 4.2. Contributions of meteorological variables (SAT- Surface Air Temperature, LWdown- Longwave Downward Radiation, SH- Specific Humidity, SWdown- Shortwave Downward Radiation, WindSpeed- Wind Speed) in driving lake surface water temperature changes in a) Annual; b) Dry Season and c) Wet Season.....83
Figure 4.3. Historical and future projections of temperature anomalies under different RCPs in a) Annual, b) Wet season, c) Dry season. The thick lines represent mean temperature anomalies and the shaded areas show the standard deviation across the multi-model ensemble. The historical temperature anomalies (black) from 1981 to 2020, the projections under RCP 2.6 (blue), RCP 6.0 (orange), RCP 8.5 (red) scenarios from 2021 to 2099. The three bars represent the mean temperature (central lines) from 2080-2099 and its standard deviation. ..85
Figure 4.4. Historical and future projections of extreme temperatures driven under different RCPs of a) Total days; b) Average duration; c) Average intensity; and d) Average Cumulative Intensity. The thick lines represent mean values, and the shaded areas show the standard deviation. The historical temperature anomalies (black) from 1981 to 2020, the projections under RCP 2.6 (blue), RCP 6.0 (orange), and RCP 8.5 (red) scenarios from 2021 to 2099. ..87

Figure 4.5. Boxplots represent the mean temperature (central lines) from 2080-2099 and its standard deviation of a) Total days; b) Average duration; c) Average intensity and d) Average Cumulative Intensity; Barplot of d) Total permanent heatwaves from 2080-2099. 88
Figure 5.1. Temporal and spatial pattern of LSWTs during the historical period (1981-2020). (a) Maps of thermal regions in South America (NH- Northern Hot, SH- Southern Hot, ST- Southern Temperate, SW- Southern Warm, TH- Tropical Hot); (b) Average LSWT of each lake map; (c) Total number of lakes per thermal region; (d) Average LSWT per thermal region; (e) Annual LSWT anomaly per thermal region; (f) LSWT Trends per thermal region; (g) LSWT trend per lake; (h) Contribution of meteorological variables to LSWT trend map (SAT- Surface Air Temperature, SH- Specific Humidity, WindSpeed- Wind Speed, LWdown- Longwave downward radiation, SWdown- Shortwave downward radiation).....98
Figure 5.2. Mean daily meteorological variables from 1981 to 2020- (b) air temperature, (c) longwave downward radiation, (d) shortwave downward radiation, (e) specific humidity, (f) wind speed. 100
Figure 5.3. Trends in daily meteorological variables from 1981 to 2020- (a) Maps of thermal regions in South America (NH- Northern Hot, SH- Southern Hot, ST- Southern Temperate, SW- Southern Warm, TH- Tropical Hot); (b) air temperature, (c) longwave downward radiation, (d) shortwave downward radiation, (e) specific humidity, (f)-wind speed. 101
Figure 5.4. Temporal and spatial pattern of diurnal LSWTs during the historical period (1981-2020). (a) Average diurnal LSWT of each lake map; (b) Annual diurnal LSWT anomaly per thermal region; (c) Average diurnal LSWT per thermal region; (d) Diurnal LSWT Trends per thermal region; (e) Diurnal LSWT Trends map; (f) Contribution of meteorological variables to diurnal LSWT trend map. 102
Figure 5. 5. Mean diurnal meteorological variables from 1981 to 2020- (b) air temperature, (c) longwave downward radiation, (d) shortwave downward radiation, (e) specific humidity, (f)-wind speed. 103
Figure 5.6. Trends in diurnal meteorological variables from 1981 to 2020- (b) surface air temperature, (c) longwave downward radiation, (d) shortwave downward radiation, (e) specific humidity, (f)-wind speed.....104
Figure 5.7. Historical mean heatwave (HW) and trend maps (1981-2020); (a) Mean HW duration, (b) Mean HW Intensity, (c) Mean HW Cumulative Intensity, (d) HW Duration Trend, (e) HW Intensity Trend and (f) HW Cumulative Intensity Trend. 105
Figure 5.8. Diurnal-seasonal variability during the historical period (1981-2020): (a) Historical DTR/STR ratio; (b) DTR/STR trend per decade, and (c) Thermal response type (grey circle defined as "Others" type).....106
Figure 5.9. Historical and future projections of lake heatwave anomalies in the studied lakes under different RCPs, including (a) Total heatwave days, (b) Heatwave duration, (c) Heatwave intensity, and (d) Heatwave cumulative intensity. The black points represent anomaly values during the historical period from 1981 to 2020. The thick lines represent heatwave anomalies and the shaded areas show the standard deviation across the multi-model ensemble. The projections under RCP 2.6 (blue), RCP 6.0 (orange), and RCP 8.5 (red) scenarios from 2021 to 2099. 107

Figure 5.10. Historical and future projections of LSWT anomalies under different RCPs per thermal region: (a) NH, (b) SH, (c) ST, (d) SW and (e) TH. The thick lines represent mean temperature anomalies and the shaded areas show the standard deviation across the multi-model ensemble. The historical temperature anomalies (black) from 1981 to 2020, the projections under RCP 2.6 (blue), RCP 6.0 (orange), RCP 8.5 (red) scenarios from 2021 to 2099. (f) Average LSWT during the period of 2080-2099 per thermal region. (g-i) LSWT anomalies from 2080 to 2099 under RCP 2.6, RCP 6.0 and RCP 8.5, respectively.....108
Figure 5.11. Future projections of lake heatwave anomalies (from left to right: total heatwave days, heatwave duration, heatwave intensity and cumulative intensity) of each studied lake under (a-d) RCP 2.6; (e-h) RCP 6.0; (i-l) RCP 8.5 scenarios between 2080 and 2099.....110
Figure A.1. Total observations of LSWT data (a), monthly (b) and yearly (c) time series of LSWT observations from 1995-1999 155
Figure A.2. Monthly/Annual Total Observations of LSWT and Chl-*a* from 2000 to 2020. 156
Figure A.3. Mean Chl-*a* Uncertainty (%) from 2002-2020 after removing outliers and uncertainty > 60%.....157
Figure A.4. Workflow.....158
Figure A.5. Monthly observations per cell of Chl-*a* from 2000 to 2020. Observation count ranged between 0 and 400 per cell monthly. 159
Figure A.6. Seasonal observations per cell of LSWT and Chl-*a* from 2000 to 2020. Seasonal observation count ranged between 0 and 3000 per cell seasonally. 160
Figure A.7. Total observations of only Chl-*a* from 2000 to 2020. 161
Figure A.8. Monthly observations per cell of only Chl-*a* from 2000 to 2020. Observation count ranged between 0 and 200 per cell monthly. 161
Figure A.9. Seasonal observations per cell of only Chl-*a* from 2000 to 2020. Seasonal observation count ranged between 0 and 1200 per cell seasonally. 162
Figure A.10. Annual coefficient of determination between LSWT and Chl-*a*, the asterisk (*) shows statistically significant with $p < 0.05$. 162
Figure A.11. Monthly coefficient of determination between LSWT and Chl-*a*, the asterisk (*) shows statistically significant with $p < 0.05$. 163
Figure A.12. Trend *p*-values of annual and seasonal LSWT, the asterisk (*) shows statistically significant with $p < 0.05$. 163
Figure B.1. Temperature anomalies derived from GLAST data (1981-2020) in black and satellite data (2000-2020) in grey; shown in a) Annual, b) Wet season, c) Dry season. 170
Figure B.2. Monthly temperature anomalies derived from GLAST data (1981-2020) in black and satellite data (2000-2020) in grey. 171
Figure B.3. Seasonal temperature anomalies derived from GLAST data (1981-2020) in black and satellite data (2000-2020) in grey. 172
Figure B.4. Annual anomaly of LSWT and meteorological variables (1981-2020).....172
Figure B.5. Annual range during the historical and future periods driven under different RCPs. 173
Figure B.6. Monthly historical and future projections of temperature anomalies driven under different RCPs. The thick lines represent mean temperature anomalies and the shaded areas

show the standard deviation. The historical temperature anomalies (black) from 1981 to 2020, the projections under RCP 2.6 (blue), RCP 6.0 (orange), RCP 8.5 (red) scenarios from 2021 to 2099.....174
Figure B.7. Seasonal historical and future projections of temperature anomalies driven under different RCPs.....175
Figure B.8. Seasonal (3-month) sea surface temperature anomalies from 1980 to 2020. Warming phases show in red color while cooling phases show in blue color (Source: NOAA; https://www.cpc.ncep.noaa.gov/data/indices/oni.ascii.txt).....176
Figure C.1. Trend and relative contribution of daily LSWT (SAT- Surface Air Temperature, LWdown- Longwave Downward Radiation, SH- Specific Humidity, SWdown- Shortwave Downward Radiation, WindSpeed- Wind Speed) per thermal regions (NH- Northern Hot, SH- Southern Hot, ST- Southern Temperate, SW- Southern Warm, TH- Tropical Hot). 177
Figure C.2. Trend and relative contribution of diurnal LSWT per thermal regions (SAT- Surface Air Temperature, LWdown- Longwave Downward Radiation, SH- Specific Humidity, SWdown- Shortwave Downward Radiation, WindSpeed- Wind Speed).....178
Figure C.3. Total heatwave day anomalies per thermal regions (a) Northern Hot, (b) Southern Hot, (c) Southern Temperate, (d) Southern Warm, and (e) Tropical Hot. The thick lines represent total heatwave day anomalies and the shaded areas show the standard deviation across the multi-model ensemble. The historical temperature anomalies (black) from 1981 to 2020, the projections under RCP 2.6 (blue), RCP 6.0 (orange), RCP 8.5 (red) scenarios from 2021 to 2099.....179
Figure C.4. Heatwave duration anomalies per thermal regions (a) Northern Hot, (b) Southern Hot, (c) Southern Temperate, (d) Southern Warm, and (e) Tropical Hot. The thick lines represent average anomalies and the shaded areas show the standard deviation across the multi-model ensemble. The historical temperature anomalies (black) from 1981 to 2020, the projections under RCP 2.6 (blue), RCP 6.0 (orange), RCP 8.5 (red) scenarios from 2021 to 2099.....180
Figure C.5. Heatwave intensity anomalies per thermal regions (a) Northern Hot, (b) Southern Hot, (c) Southern Temperate, (d) Southern Warm, and (e) Tropical Hot. The thick lines represent average anomalies and the shaded areas show the standard deviation across the multi-model ensemble. The historical temperature anomalies (black) from 1981 to 2020, the projections under RCP 2.6 (blue), RCP 6.0 (orange), RCP 8.5 (red) scenarios from 2021 to 2099.....181
Figure C.6. Heatwave cumulative intensity anomalies per thermal regions (a) Northern Hot, (b) Southern Hot, (c) Southern Temperate, (d) Southern Warm, and (e) Tropical Hot. The thick lines represent average anomalies and the shaded areas show the standard deviation across the multi-model ensemble. The historical temperature anomalies (black) from 1981 to 2020, the projections under RCP 2.6 (blue), RCP 6.0 (orange), RCP 8.5 (red) scenarios from 2021 to 2099.....182

List of Tables

Table 3.1. List of input variables for DINCAE and DINCAE multivariate.....58

Table B.1. Bias correction results for 4 GCMs and 3 RCPs using 5 bias corrected methods (Linear Scaling- LS, Quantile Mapping- QM, Quantile Delta Mapping- QDM, Inter-Sectoral Impact Model Intercomparison Project- ISIMIP and Scale Distribution Mapping- SDM)...167

Table B.2. Simulations for relative contribution of meteorological variables using FLake model.....169

Acronyms and Abbreviations

BRT	Boosted Regression Tree
CDF	Cumulative Distribution Function
CH_4	Methane
Chl-a	Chlorophyll-a
CPU	Central Processing Unit
DINCAE	Data Interpolating Convolutional Auto-Encoder
DINEOF	Data Interpolating Empirical Orthogonal Functions
DO	Dissolved Oxygen
DOC	Dissolved Organic Carbon
DTR	Diurnal Temperature Range
ECMWF	European Centre for Medium-Range Weather Forecast
ECVs	Essential Climate Variables
ENSO	El Niño-Southern Oscillation
EO	Earth Observation
ESA CCI	European Space Agency Climate Change Initiative
GAM	Generalized Additive Model
GCMs	Global Climate Models
GCOS	Global Climate Observing System
GHG	Greenhouse Gas
GLAST	Global LAke Surface water Temperature
GPU	Graphics Processing Unit
HW	Heatwave
IOD	Indian Ocean Dipole
IPCC	Intergovernmental Panel on Climate Change
IQR	Interquartile Range
ISIMIP	Inter-Sectoral Impact Model Intercomparison Project
LIC	Lake Ice Cover
LIT	Lake Ice Thickness
LM	Linear Regression Model
LS	Linear Scaling
LSWT	Lake Surface Water Temperature
LWdown	Longwave Downward Radiation
LWE	Lake Water Extent
LWL	Lake Water Level
LWLR	Lake Water Leaving Reflectance
MAE	Mean Absolute Error
NAO	North Atlantic Oscillation
NH	Northern Hot
PBIAS	Percentage Bias
PDO	Pacific Decadal Oscillation
QDM	Quantile Delta Mapping
QM	Quantile Mapping
RCPs	Representative Concentration Pathways

RH	Relative Humidity
RMSE	Root Mean Square Error
SAT	Surface Air Temperature
SDM	Scale Distribution Mapping
SH	Specific Humidity
SH	Southern Hot
ST	Southern Temperate
STR	Seasonal Temperature Range
SW	Southern Warm
SWdown	Shortwave Downward Radiation
TDPS	Lake Titicaca, Desaguadero River, and Lake Poopó basins
TH	Tropical Hot
UNFCCC	United Nations Framework Convention on Climate Change
WHO	World Health Organization

I. Introduction

1.1. Lakes as sentinels of climate change

Lakes are frequently defined as sentinels of climate change because they are sensitive to climate-related changes, making them effective indicators of climatic forcing (Adrian et al. 2009). Several studies have found that lakes can give early warning signs of climate change by altering the lake environment and nearby catchment regions (Castendyk et al. 2016; Vinnå et al. 2021; Zhang and Duan 2021). These changes can include changes in Lake Surface Water Temperature (LSWT), Lake Water Level (LWL), Lake Ice Cover (LIC), and nutrient concentration in lakes and lake biota.

The rise in LSWT, which is highly correlated with air temperature, has a significant impact on lake ecosystems, affecting mixing and stratification patterns, and ice cover duration (O'Reilly et al. 2015; Piccolroaz et al. 2020). Lake mixing regimes are projected to change due to global warming, e.g., polymictic lakes (frequently mixing)/dimictic lakes (mixing twice per year) turn to monomictic lakes (mixing once per year) or oligomictic (rarely mixing) regimes (Shatwell et al. 2019; Woolway and Merchant 2019). Such changes can have a major impact on dissolved oxygen (DO) concentrations in the lake and aquatic life, such as levels of primary production and extent of fish habitats as they require DO to survive and reproduce (Ficker et al. 2017; Anushka and Mishra 2022).

Climate-driven water level fluctuations (Kraemer et al. 2020) and changes in ice formation and thawing regime, which regulate lake phenology (seasonal timing of lake processes) and morphology (Sharma et al. 2021), can disrupt ecosystem functions (fishing, transportation, regulation and recreation, etc) and structure (Sharma et al. 2021). Water level is a useful indicator of climate change as it represents the relationship between water input (precipitation, runoff) and water output (evaporation) (An et al. 2022) and the timing of the ice-free season (Adrian et al. 2009). The decrease in lake water level can cause an increase in salinity, and affect the community composition, biomass and aquatic diversity (Woolway et al. 2022c). In glacier lakes, increases in lake water level will be a particular issue owing to as glacier melts in Arctic areas (Woolway et al. 2022c).

Lake ice phenology is another important climate indicator (Imrit and Sharma 2021). Ice phenology includes ice-off (the date at the end of the season when ice is no longer visible/thawed), ice-on timing (the date at the beginning of the season when ice is first

observed) and ice duration (days between ice-on and ice-off dates) (Brown and Duguay 2022). Lake ice phenology is driven mainly by air temperature (Imrit and Sharma 2021; Sharma et al. 2021). Due to recent warming, several deep arctic lakes, which previously had a summer ice cover, have become ice-free during the summertime, resulting in a variety of physical, chemical, and biological effects (Woolway et al. 2022c).

Changes in the export of terrestrial nutrients and organic matter due to climate impacts or changes in terrestrial primary production can modify nutrient concentrations and ratios in lakes (Tong et al. 2022). Excessive inputs of nitrogen and/or phosphorus to aquatic systems can alter primary production, leading to eutrophication (excessive nutrients), increases in harmful algal blooms or changes in food web structure (Rathore et al. 2016; Tong et al. 2022). Decreasing trends in nutrient concentrations (dissolved inorganic nitrogen and total phosphorus), along with the increasing dissolved organic carbon (DOC) trend, influence phytoplankton quantity and quality (Bergström et al. 2020). These parameters are also sensitive to climate change induced change (altering primary production, causing toxic algal blooms or changes in food web structure).

The interactions between lake biota and climate change are complex (Armstrong et al. 2021; Kraemer et al. 2021). Because of their quick response to temperature changes, planktonic organisms can be particularly sensitive to climate change impacting primary production, zooplankton size and bacterial cell density (Adrian et al. 2009). Climate change effects can also be reflected in plankton phenology changes, growth rates, abundance, and species composition (Yang et al. 2020; Hebért et al. 2021; Moe et al. 2021).

Lakes can also be considered excellent sentinels of climate change as they are generally well-defined ecosystems which can integrate climate change impacts within the catchment and over time, and owing to their global distribution, lakes cover a wide range of geographic and climatic regions (Adrian et al. 2016).

1.2. Essential Climate Variables (ECVs)

LSWT, LWL, LIC, Lake Water Extent (LWE), Lake Ice Thickness (LIT) and Lake Water-Leaving Reflectance (LWLR) are all defined as Lake Essential Climate Variables (ECVs) by the Global Climate Observing System (GCOS) (GCOS 2022). These ECVs are important to understand and forecast the impacts of climate change on lakes. These variables are also a vital

component of the United Nations Framework Convention on Climate Change (UNFCCC) and the Intergovernmental Panel on Climate Change (IPCC) (Woolway et al. 2020b).

Lake ECVs have been shown to have changed significantly in recent decades as a result of climate change, for example, an increase in LSWT (O'Reilly et al. 2015), a decrease in LIC (Imrit and Sharma 2021; Sharma et al. 2021), changes in LWL and LWE (Busker et al. 2019; Kraemer et al. 2020), and in Chlorophyll-a (Chl-a) variability (which can be extracted from LWLR) (Kraemer et al. 2022). These variables differ substantially based on the lake types and climatic zones. They also interact with each other, which occasionally leads to a more robust response to climate change. Water temperature increases, for example, have been shown to lead to LIC decline (Sharma et al. 2021) and LWL and LWE decrease due to water loss through enhanced evaporation (Coppens et al. 2020).

Both in situ and satellite observation have been used over the past decades to quantify lake variability (Carrea et al. 2023). A limitation of in situ data, however, is that they might not give details of lake responses because they typically use single-point measures (Carrea et al. 2023). In addition, different instruments are used at different sites to collect in situ measurements and such data are only occasionally delivered with uncertainty estimations (Carrea et al. 2023). Nevertheless, in situ data are essential to validate satellite Earth Observation (EO) (Carrea et al. 2023). Satellite measurements, however, have the advantage that they can provide globally consistent observations for long-term monitoring even for lakes in remote and inaccessible areas that do not have in situ data (Carrea et al. 2023). Recently, the European Space Agency Climate Change Initiative (ESA CCI) has been developing multi-decadal EO products for Lake ECVs at a global scale called the Lakes CCI project. This dataset provides a consistent illustration of lakes around the world and allows their responses to climate change to be examined.

1.3. Research aims and objectives

Lakes are important water resources. There are around 117 million lakes in the world (Verpoorter et al. 2014), which contain 87% of the Earth's surface liquid fresh water (Woolway et al. 2020b). Lakes are considered as key indicators of water changes as they are useful to observe Earth's responses to climate change (Woolway et al. 2020b). Recently, there has been growing interest in how lake variables change globally, including changes in LSWT (Schmid

et al. 2014; O'Reilly et al. 2015; Desgué-itier et al. 2022; Woolway et al. 2022c), lake ice cover (Sharma et al. 2019; Sharma et al. 2021), lake water level and volume (Busker et al. 2019; Kraemer et al. 2020) in response to climate change. However, most studies often have a specific focus on the Northern Hemisphere, with little attention given to lake variability in the Southern Hemisphere (Aranda et al. 2021). Previous studies are also often limited to local, individual lakes, particularly glacial lakes (Quade and Kaplan 2017; Wilson et al. 2018; Mergili et al. 2020; Hata et al. 2022), rather than assessing a comprehensive analysis of lakes across the entire continent. Additionally, these studies often analysed only one lake variable, such as lake ice cover or lake water level (Zolá and Bengtsson 2006; Pasquini et al. 2008; Carabajal and Boy 2021). To date, few studies have been carried out on changes in LSWT in South American lakes due to a lack of in situ measurements. South America has a population of over 217 million inhabitants (Nuñez-Hidalgo et al. 2023). Freshwater resources, including lakes, are vital for economic and domestic activities in South America, such as agriculture, mining, hydropower, etc, and supplying from megacities to remote indigenous communities. However, climate change is projected to cause changes in water temperature and increased water scarcity, which will exacerbate social conflicts and negatively affect the livelihoods of vulnerable populations, particularly those in rural and indigenous areas (IPCC 2022). Therefore, this study evaluates the effectiveness of satellite EO and model-derived data in assessing the changes in LSWT in the South American continent and develops a better understanding of historical and future LSWT and lake heatwave trends under climate change. The specific objectives of this research are:

1. To evaluate the most suitable gap-filling methods for satellite EO data for lakes with a case study of Lake Titicaca (Peru-Bolivia) and to use the gap-filled data for analysing the spatial-temporal LSWT of Lake Titicaca;

2. To investigate the past, current and future climate change impacts on LSWT and lake heatwaves in Lake Titicaca on various timescales. To evaluate the performance of different bias correction methods for future projection data;

3. To analyse LSWT variability and lake heatwaves in response to climate warming across South America during both historical and future periods. To examine the diurnal and seasonal variability for classifying lake thermal response using the ratio of Diurnal Temperature Range (DTR) to Seasonal Temperature Range (STR).

1.4. Thesis structure

This dissertation includes seven chapters. The first chapter is the introduction to this study. Chapter 2 presents the literature review, focusing on climate change impacts on global lakes, South American lakes and particularly Lake Titicaca and a description of the study areas. Chapters 3 to 5 consist of the main results of this dissertation and provide a comprehensive understanding of LSWT extremes and variability in Lake Titicaca and South America. These chapters follow a scientific paper format, which contains Abstract, Introduction, Materials and Methods, Results, Discussion and Conclusion sections. Chapter 3 presents a submitted article titled "Evaluating gap-filling techniques for satellite-derived surface water temperature: A case study of Lake Titicaca", which analyses the most suitable gap-filling methods for satellite EO data for lakes with a case study in Lake Titicaca. Following by chapter 4- a published article titled "The current and future warming of Lake Titicaca", reports the variability of LSWT and lake heatwaves and the influence of meteorological variables during the historical and future periods. Chapter 5 is a published article titled "Emerging changes in lake temperature extremes and variability in South America", which expands the research from Chapter 4 to lakes in South America and reports novel findings of lake thermal response using the DTR/STR ratio. Finally, chapter 6 concludes the dissertation by summarising the key results, and contributions and proposing future research directions.

II. Literature review

This chapter presents an overall literature review on lake surface water temperature research. The physico-chemical and biological impacts of climate change on global lakes are discussed in the first section. The next section reviews South American regions and lakes under the changing climate. A review of climate change impacts on a specific lake- Lake Titicaca, is provided in the last section.

2.1. Climate change impacts on global lakes

2.1.1. Climate change impacts on lake physics

2.1.1.1. Lake surface water temperature

LSWT is critically important for lake ecosystems. It can influence physical (lake stratification length and period), chemical (solubility of gases and minerals, chemical reaction rate) and biological (changes in phytoplankton biomass and primary production) processes in lakes, which impacts lake ecological conditions (Adrian et al. 2009; Dokulil 2014; Jeppesen et al. 2014) (Fig. 2.1). LSWT is also considered as indicator of climate change (Adrian et al. 2009) as it responds directly to the changes in climate forcings such as air temperature, solar radiation, evaporation, etc (Rose et al. 2023). Additionally, LSWT effects stratification, seasonal deep convective mixing, ice cover (Schmid et al. 2014), light availability and DO concentrations (Kraemer et al. 2021). LSWT can also affect aquatic organisms (Desgué-itier et al. 2022) by causing ecological and physiological changes such as shifts in seasonality (Kraemer et al. 2021).

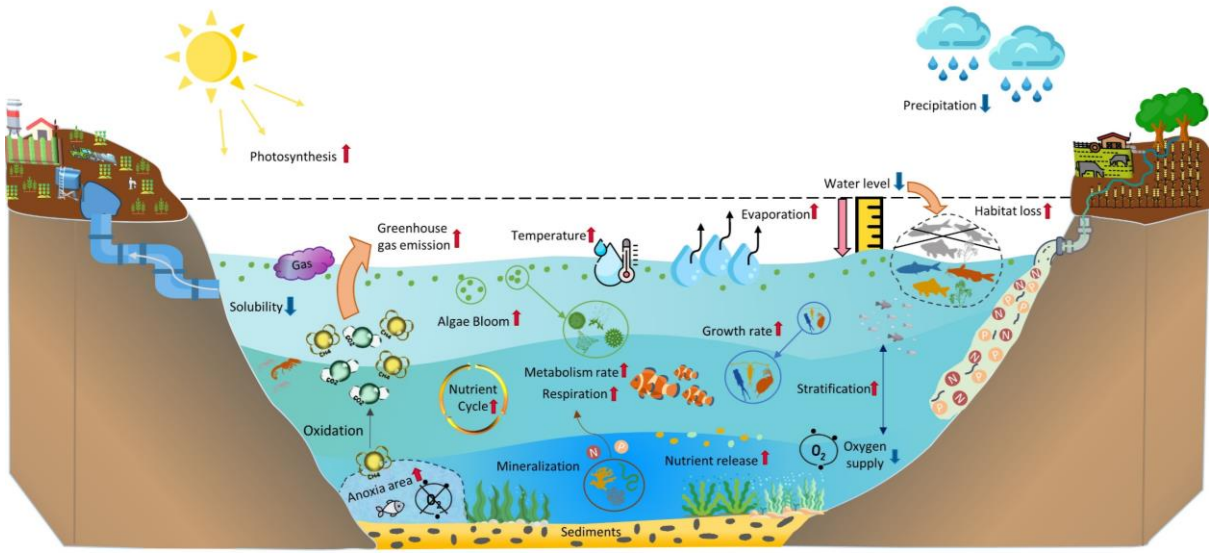


Figure 2.1. The importance of LSWT in lake ecosystems

LSWT has increased significantly in recent decades (Schmid et al. 2014; O'Reilly et al. 2015; Kraemer et al. 2021; Desgué-itier et al. 2022; Tong et al. 2023). According to O'Reilly et al. (2015), global LSWT had an increasing trend of 0.34°C decade^{-1} during the period 1985-2009, which was compatible with the surface air temperature trend (0.25°C decade^{-1}) and higher than the sea surface temperature trend (0.12°C decade^{-1}). Recent research of Tong et al. (2023) showed that LSWT of 92,245 lakes globally increased at a rate of 0.24°C decade^{-1} between 1981 and 2020. Additionally, daytime and nighttime LSWT trends range from -0.2 to 0.8°C decade^{-1} in the same period (Tong et al. 2023). Schneider and Hook (2010) analysed lakes globally from 1985 to 2009 and discovered that mean nighttime warming rate of LSWT was 0.45 ± 0.11°C decade^{-1} (Schneider and Hook 2010).

Recently, there has been growing attention to the diurnal temperature range (DTR), which represents temperature variations within a 24-hour period. DTR variability plays a crucial role in biogeochemical processes in lakes (Woolway et al. 2015; Woolway et al. 2016; Choiński and Strzelczak 2018) and is essential for the interpretation and analysis of LSWT trends (Woolway et al. 2016). LSWT is mainly influenced by air temperature (Schmid et al. 2014), resulting shifts in DTR and thermal regimes. LSWT has been forecast to increase by 70-85% of the increase in air temperature (Schmid et al. 2014). Thus, as local air temperature increases within a warming world, LSWT changes accordingly. However, some lakes have been shown to be warming at faster rates than air temperature. For example, lakes in northern Europe or the Great Lakes area in North America have experienced LSWTs increasing at a

more rapid rate than air temperature (Sharma et al. 2015). Other climate forcings that influence LSWT variation are solar radiation (Wetzel 2001), wind speed (Wüest and Lorke 2003), precipitation (Rooney et al. 2018), and lake properties such as lake area, depth, and volume (Schindler et al. 1990; Kraemer et al. 2015; Sharma et al. 2015). Overall, LSWT in shallow lakes can warm faster compared to deep lakes due to heat storage capacity (Kraemer et al. 2015; Sharma et al. 2015).

LSWT is projected to rise globally by +1-4^{o}C by the end of the century (Grant et al. 2021). The LSWT increase varies between regions, for example, lakes may warm more in southern temperate latitudes in North America and Eurasia (+4-5°C by 2077-2099 relative to 1971-2000) (Grant et al. 2021). The IPCC has introduced the Representative Concentration Pathways (RCPs) of greenhouse gas (GHG) emission scenarios for use in climate modelling and research. Four RCPs, including RCP 2.6 (low GHG), RCP 4.5 and RCP 6.0 (intermediate GHG), and RCP 8.5 (high GHG) (IPCC 2022) are considered. The GHG levels for the RCP 2.6 scenario reflect a world that aims to keep the temperature under 2°C by 2100, while those for RCP 4.5 and RCP 6.0 keep the temperature increase to 2-3°C and 3-4°C correspondingly (IPCC 2022). In the RCP 8.5 scenario, the temperature continues to warm during the 21st century (IPCC 2022). Lake bottom water temperatures are forecasted to also increase by 0.9 ± 0.3°C, 1.6 ± 0.4°C, and 2.6 ± 0.7°C under RCP 2.6, 6.0, and 8.5 respectively by 2099 relative to 1970-1999 (Jansen et al. 2022).

2.1.1.2. Lake ice cover

Ice plays an important role in ecosystem services for more than half of the world's lakes and influences hydrological cycle regulation, human transportation, fishing and cultural activities (Sharma et al. 2021). LIC affects other processes in lake, including lake physics, chemistry and biology (Sharma et al. 2019). Sharma et al. (2019) used LIC observations from 513 lakes in the Northern Hemisphere to predict winter ice cover loss. According to their results, 14,800 lakes currently have discontinuous winter ice cover, with the number increasing to 35,300 lakes (2.8%) and 230,400 lakes (18.4%) at increases in air temperature at +2^{o}C (from the Paris Agreement under the United Nations Framework Convention on Climate Change) and +8^{o}C (no climate change mitigation), respectively (Sharma et al. 2019). Under the RCP 6.0 scenario, 41,000-90,000 lakes are predicted to have intermittent winter ice cover by 2080, while under

the RCP 2.6 scenario, 27,000-48,000 lakes will lose ice cover in early 2080 (Sharma et al. 2019). This phenomenon could potentially impact 656 million people in 50 countries (Sharma et al. 2019).

Ice phenology refers to the study of the period of ice freezing and break up (Walsh et al. 1998). Phenology change in ice is affected by water temperature increase, ice cover decrease and longer thermal stratification (Jensen et al. 2007; Brown and Duguay 2010; Nõges and Nõges 2014). Ice break-up timing is affected by air temperature (Magnuson et al. 2000). In the Northern Hemisphere, ice freeze timing was found to be 11 days later since 2004 for 31 lakes, whereas ice break up timing was 6.8 days earlier for 58 lakes, with the ice duration reduced to 17 days per century for 30 lakes (Sharma et al. 2021). According to Wang et al. 2022, mean ice duration globally is projected to decrease to 49.9 days by 2099 compared with that recorded during the baseline period of 2001-2020 under RCP 8.5. Ice duration is forecasted to decline by > 45 days relative to the 1971-2000 baseline period, which is projected to be highest in coastal areas and in Scandinavia by the end of the century, under the RCP 8.5 (Grant et al. 2021). In the Northern Hemisphere, the availability of safe ice for recreation (ice thicker than 10 cm) has been projected to reduce to 13, 17, and 24 days under global warming of 1.5^{o}C (2024-2038), 2^{o}C (2037-2051) and 3^{o}C (2061-2075) (relative to 1900-1929) (Woolway et al. 2022b). Based on measured data, ice freeze timing and duration were found to be six times faster in the last 25 years (1992-2016) compared to the past quarter century (Sharma et al. 2021). Ice freeze timing is occurring later in winter and breaking up earlier in spring in recent decades and ice duration is decreasing by more than 2 weeks/year, leading to a loss in ice cover, intermittent ice cover or disappearance of ice (Parmesan et al. 2022).

2.1.1.3. Stratification and mixing regimes

Thermal stratification is a phenomenon due to temperature changes where the water column in lake divides into distinct layers, influencing lake vertical fluxes of dissolved and particulate material (Boehrer and Schultze 2008). Stratification occurs because of the thermal expansion characteristics of water, which creates a steady vertical density gradient (Boehrer and Schultze 2008). Generally, stratified lakes show three identifiable layers: epilimnion, metalimnion and hypolimnion. The epilimnion layer is the upper layer, directly below the water surface and interacts with atmospheric forcings such as wind and sunlight. Thus, it is the warmest layer and

is typically well mixed. The thermocline which occurs within the metalimnion, is the point of maximum temperature change and separates epilimnion and hypolimnion layers. The hypolimnion is the bottom layer, which is the densest and coldest layer (Woolway et al. 2017b). The duration of stratification can last from hours to months or even be permanent in certain lakes. However, some shallow lakes do not stratify in the summer or only for a short period of time. These lakes are called polymictic (mixing several times per year) and they can be divided into continuous (daily) and discontinuous polymictic (not occurring every day). Dimictic lakes are those that have two mixing periods per year while monomictic lakes are stratified once per year. Less common are lakes that circulate incompletely, causing stagnant conditions in the bottom layer. These partially mixing lakes are called meromictic (Woolway and Merchant 2019).

Many crucial lake processes such as nutrients and oxygen cycles, plankton composition, primary production and habitat availability are affected by thermal stratification patterns (Labaj et al. 2018). Exacerbated thermal stratification of lakes can increase lake anoxia, stimulate the growth of planktonic, bloom-forming cyanobacteria, and alter internal nutrient loading, all of which have an impact on lake productivity (Kraemer et al. 2015). Increases in air temperature affect stratification duration and intensity (Desgué-itier et al. 2022) and mixing regime (Vincent 2009). Depending on the changes in climatic factors such as air temperature, solar radiation, cloud cover, wind speed and humidity, which can affect the lake heat budget, the mixing regime will change (Woolway and Merchant 2019). Vertical mixing intensity, frequency and duration have been decreasing in deep temperate lakes, and hence vertical temperature gradient of the surface and deep layers rise (Desgué-itier et al. 2022).

Changes in lake mixing classification or mixing regime shifts as a consequence of climate change have been reported (Shatwell et al. 2019). Polymictic lakes have been identified as being particularly vulnerable to mixing regime shifts (Woolway et al. 2017b). In monomictic lakes, winter mixing can be inadequate and irregular, whilst polymictic or dimictic lakes can turn into monomictic lakes due to climate warming (Shatwell et al. 2019). Some deep lakes which are monomictic will encounter persistent stratification throughout the year, decreasing mixing intensity and inhibiting deep-water regeneration (Adrian et al. 2016). Therefore, monomictic lakes will have a tendency to become oligomictic, which are not fully mixed every year (Adrian et al. 2016). During winter, if the ice cover decreases, shallow polymictic lakes will experience permanent mixing throughout the year (Adrian et al. 2016). Woolway et al.

(2019) used numerical modelling to investigate global climate change impacts on mixing regimes in 635 lakes. Their results showed that some monomictic lakes will become meromictic (permanently stratified), while some dimictic lakes will become monomictic (Woolway and Merchant 2019). Due to climate change impacts, mixing frequency in lakes is projected to continue to reduce in the future (Woolway and Merchant 2019). Nevertheless, projecting mixing behaviour under climate change remains a challenge (Parmesan et al. 2022). Inverse thermal stratification is likely to stop due to rising LSWT and loss of ice cover during winter in the north temperate lakes (Parmesan et al. 2022). Under the high GHG emission scenario RCP 8.5, lake stratification in the Northern Hemisphere is projected to begin 22.0 ± 7.0 days earlier and finish 11.3 ± 4.7 days later than is experienced now by the end of the century (Woolway et al. 2021a).

2.1.1.4. Lake water level and lake water volume

The variability of precipitation and evaporation ratio affects water budget, lake retention time, lake depth and lake water extent (Vincent 2009). Lake levels and surface water extent are affected by ice cover, water temperature, and evaporation rate changes (Woolway et al. 2020b). Additionally, precipitation and land surface runoff impact lake level and water extent (Woolway et al. 2020b).

Vincent et al (2009) stated that large and shallow lakes have fluctuated and some have had reductions in their water budget due to climate warming. Lake water quantity can decrease rapidly as a consequence of higher evaporation rates during periods of increased temperature and sunlight or with a reduction in precipitation (Woolway et al. 2022c). Lake water level decreased intensely in some areas, for example, the water level and extent of Lake Chad in Africa dropped greatly due to the decline in precipitation and catchment discharge along with the rise in evaporation. Over the last few decades, Lake Chad's water level has decreased to less than 7 m deep because of climate change (Vincent 2009). The lake area decreased from 25,000 km^2 in the early 1960s to 1350 km^2 in the 1990s due to the reduction in precipitation (Vincent 2009). Both climate change impacts and water demand increases accounted for this decline in lake areas (Vincent 2009). Similarly, declining water levels have been recorded in Lake Poopó in Bolivia as a consequence of low discharge from the Desaguadero River. In 2015 and 2016, this lake recorded its lowest level in history (Woolway et al. 2022c).

Evaporation can cause a greater reduction in lake water from unfrozen and warmer lakes than other lakes (Wang et al. 2018b). Lake evaporation is projected to rise and will vary regionally due to global warming and dry areas such as tropical America, the Mediterranean and Southeast China will be particularly vulnerable, whereas lake evaporation will likely reduce in wet areas (for instance, high latitudes areas and the Tibetan Plateau) (Zhou et al. 2021). Lake evaporation change depends on regional hydro climate change (Zhou et al. 2021). According to La Fuente et al. (2024), global annual lake evaporation rates are likely to increase by 27% by the end of the 21st century, relative to the 1970-1999 base period under the RCP 8.5 (Fuente et al. 2024), which is higher than the 16% projected by earlier studies (Wang et al. 2018b; Woolway et al. 2020b).

Climate extremes such as storms or increased precipitation events can lead to an increase in flooding in some regions (Vincent 2009). Extreme precipitation affects lake ecosystems and their services such as drinking water provision, biodiversity or fish production and escalates the risk of disruption to these services (Eyto et al. 2016). Lake responses vary based on precipitation magnitude and timing (Jennings et al. 2012), however, extreme precipitation can disturb the water column's physical structure, nutrient cycle and lake biology (Eyto et al. 2016). Extreme precipitation leads to flood pulses, resulting in a rise in dissolved and suspended substances imported into the lake (Eyto et al. 2016). However, in certain areas such as the Mediterranean, precipitation is forecasted to decline (~25-30% runoff decrease by 2040-2061), which may cause a reduction in nutrient input to lakes (Jeppesen et al. 2014).

Other extreme events, such as El Niño and La Niña, also affect the lake's water level and volume. El Niño is a climate pattern characterized by unusually warm surface waters in the eastern tropical Pacific Ocean (Trenberth 1997). El Niño is the warm phase, while La Niña is the cold phase of the El Niño-Southern Oscillation phenomenon (ENSO) (Trenberth 1997). The ocean component of ENSO is represented by El Niño and La Niña, while the atmospheric component is represented by the Southern Oscillation (Trenberth 1997). El Niño events occur every one to five years in recent decades and are generally followed by La Niña events (Bergmann et al. 2021). ENSO causes weather pattern variability, leading to disasters such as drought, flood and storm events (Yang et al. 2018). As a result, these changes impact humans (e.g., diseases such as cholera, dengue and malaria), ecosystems (e.g., fish die or migrate) and the economy (e.g., food production and irrigation) (Yang et al. 2018). The Pacific Decadal Oscillation (PDO) is a long-term ocean fluctuation of the Pacific Ocean, over the period of 20

to 30 years (Mantua et al. 1997). PDO influences ENSO variability (Lima-quispe et al. 2021) and impacts the hurricane's intensity in the Atlantic and Pacific, drought and flood frequency in the Pacific basin, marine ecosystem productivity and global temperature trends (Mantua et al. 1997). The North Atlantic Oscillation (NAO) is the difference in surface sea-level pressure between the Subtropical (Azores) High and the Subpolar Low (Liu et al. 2023). NAO causes changes in temperature and precipitation trends from eastern North America to western and central Europe (Liu et al. 2023). The difference in sea surface temperature between two regions (or poles, thus a dipole) - a western pole in the Arabian Sea (western Indian Ocean) and an eastern pole in the eastern Indian Ocean south of Indonesia - is called the Indian Ocean Dipole (IOD) (Pillai et al. 2023). Both phases of IOD affect temperature, precipitation variability and wind anomalies (Pillai et al. 2023). Variation in lake water level is related to the oscillating dynamics in hydroclimate ENSO, PDO, NAO, and IOD (Kraemer et al. 2020). Because of the positive phase of NAO, the water level in some lakes in Poland might rise by 20 cm (Kraemer et al. 2020). During the late 1990s, water levels increased by 1 m in eight East African Great lakes in < 1 year because of the ENSO and IOD effects (Kraemer et al. 2020). However, the lake water storage forecast is limited due to the lack of reliable, long-term, homogenous and spatially hydrological observations (Parmesan et al. 2022).

Lake water volume is defined as the volume of the lake basin or the amount of water below the surface water level, and it is also called “lake storage mass” or “lake storage capacity” (An et al. 2022). The difference between the lake’s inflow and outflow is used to compute the change in lake water volume. Precipitation, runoff, and groundwater are often included in the inflow while evapotranspiration and surface runoff outflow are included in the outflow (An et al. 2022). Several studies, using various methods such as remote sensing, and modelling reveal that lake water volume has been decreasing in many lakes (Cretaux et al. 2013; Gronewold and Stow 2014; Wurtsbaugh et al. 2017; Wang et al. 2018a). A recent study from Yao et al. (2023) showed that 53% of the 1,972 studied lakes experienced water losses between 1992 and 2020 (Yao et al. 2023). It has been estimated that lake volume reduces globally at a rate of -26.38 ± 1.59 Gt year^{-1}, attributed to human activities, temperature changes and evapotranspiration (Yao et al. 2023). Lake water volume declines in certain lakes are due to temperature increases and precipitation decreases. For instance, Toshka lake (-0.13 ± 0.10 Gt year^{-1}) in Egypt, Lake Khyargas (-0.35 ± 0.03 Gt year^{-1}) in Mongolia, and Lake Good-e-Zareh (-0.48 ± 0.17 Gt year^{-1}) in Afghanistan have experienced water losses (Yao et al. 2023).

Conversely, the water volumes of other lakes have reduced because of changes in runoff and precipitation, for example, Lake Titicaca (-0.12 ± 0.08 Gt $year^{-1}$), the Caspian Sea (-18.80 ± 0.93 Gt $year^{-1}$), and the Great Salt Lake (-0.29 ± 0.08 Gt $year^{-1}$) in the United States (Yao et al. 2023). Changes in lake water volume can impact activities including water supply (irrigation, industrial), recreation and tourism (fishing and boating) (Busker et al. 2019; Feng et al. 2022).

2.1.2. Climate change impacts on lake chemistry

Changes in LSWT can influence the water's saturation capacity (Wilcock et al. 1998). Specifically, an increase in LSWT can result in a decrease in saturation capacity, consequently reducing dissolved oxygen concentrations (Wilcock et al. 1998). Thus, this decrease in DO level can lead to oxygen depletion in the lake (Jeppesen et al. 2009). Jane et al. (2021) also suggest that water temperature rise and a decrease in water column mixing may lead to a depletion of hypolimnetic DO concentrations (Jane et al. 2021). Their research also suggested that DO in surface and deep waters in 400 lakes from 1980 to 2017 decreased by 4.1 and 16.8% respectively. Oxygen-deficient conditions are projected to rise in the deepest water layers by more than 25% (Schwefel et al. 2016). Due to heatwaves, water temperature increases and mixing decreases, resulting in a decline in oxygen and deep-water oxygen replenishment (Parmesan et al. 2022).

Changes in weather patterns (temperature rise and precipitation, extreme events frequency and intensity) affect the composition and concentration of runoff (Dokulil 2014). Evapotranspiration is projected to increase which impacts the hydrological cycle, indirectly affecting other water resources and ecosystem services (Dokulil 2014). Other factors such as pH, ionic strength and composition, and conductivity are sensitive and used as indices for weather changes and water balance (Adrian et al. 2009).

Nutrient dynamics in lakes are projected to change as a consequence of climate change. Research has shown evidence that increases in lake water temperature by 2°C can lead to a rise in methane (CH_4) emissions by 101-183% and 47-56% in highly eutrophic lakes and oligotrophic lakes, respectively (Sepulveda-Jauregui et al. 2018). Total phosphorous concentration in lakes is affected by external loading variations and is lower during winter (Jeppesen et al. 2009). Phosphorous release from sediments may be associated with the increase in temperature in shallow, non-stratified lakes (Jeppesen et al. 2009). In many European

regions, the nitrate concentration in water has been rising, causing several issues such as acidification and phytoplankton composition changes (George et al. 2010). The ratio between nitrogen and phosphorous has been increasing due to imbalanced anthropogenic inputs, which impacts ecosystem function (e.g., food resource quality for secondary consumers) and ecosystem productivity in some regions (Wu et al. 2022). As the climate warms, nutrient-limited lakes are expected to be less productive, whereas nutrient-rich lakes will possibly become more productive (Adrian et al. 2016; Kraemer et al. 2017b). In two high Arctic lakes, major ion concentrations such as sulphate (SO_4^{2-}) have risen quickly up to 500% from 2006 to 2016 and 340% from 2008 to 2018 (Caretta et al. 2022).

2.1.3. Climate change impacts on biological communities

Due to warming trends, species' relative abundance, species composition and biodiversity are forecasted to change in lakes globally. Nevertheless, to date, the understanding of current and future climate change-driven changes in the global food web is limited (Parmesan et al. 2022). Physical and chemical changes in lakes affect aquatic organisms' physiology, distribution, composition and development (Adrian et al. 2009; Parmesan et al. 2022). Lake temperature rise can lead to a decrease in oxygen concentrations and affect the biological community structure (Caretta et al. 2022).

Climate change affects fish species' distributions, abundance and community structure (Adrian et al. 2009). Due to the increase in LSWT, cold-stenothermal abundance (*Arctic charr*) is decreasing while eurythermal fish abundance is increasing in northern temperate lakes (Jeppesen et al. 2012; Jeppesen et al. 2014). These changes will lead to an increase in phytoplankton biomass because predation pressure on zooplankton will escalate and grazing pressure on phytoplankton will decrease (Jeppesen et al. 2014; Adrian et al. 2016). Decreases in lake mixing may result in the reduction of nutrient concentrations and an increase in silicon to phosphorous ratios, which can affect diatom growth and primary productivity (Parmesan et al. 2022). For example, lake mixing declined because of warming in Lake Tanganyika, Zambia, causing a reduction in algal production, oxygenated benthic habitat (~38%), and fish and mollusc yield (Caretta et al. 2022). Fish and invertebrates are vulnerable to temperature and oxygen stress (Pauly and Dimarchopoulou 2022; Bonacina et al. 2023). Extreme heatwaves cause local fish mortality in lakes as the temperature rises and oxygen concentration exceeds

critical levels (Till et al. 2019). According to Till et al. (2019), from 2004 to 2014, 502 large fish died in Wisconsin lakes due to extreme heat in the summer (Till et al. 2019). When compared to historical levels, such events are expected to double by 2041-2059 and quadruple by 2081-2099 (Till et al. 2019). On the contrary, extreme cold temperatures with continuous ice cover led to fish kills in Scandinavia and North America (Abrahams et al. 2013).

Increased strength of vertical thermal stratification in lakes due to climate change can result in changes in phytoplankton species composition, particularly among taxonomic groups such as diatoms, flagellates or cyanobacteria (Adrian et al. 2009). Due to water temperature, atmospheric CO_2 and precipitation increases, freshwater macrophyte growth is expected to escalate (Hossain et al. 2017; Reitsema et al. 2018). Warming water temperatures can cause longer thermal stratification that can decrease primary production in large nutrient-poor lakes (Kraemer et al. 2017b). According to Kraemer et al. (2022), Chl-a concentrations decreased by about 56% of the lake area in 344 large lakes globally between 1997 to 2020 (Kraemer et al. 2022). These productivity reductions may not only be a response to climate change (Parmesan et al. 2022) but may also be due to anthropogenic activity (Kraemer et al. 2022). Climate change affects nutrient loading to lakes, leading to an increase in algal growth and resulting in changes in algal biomass (Kakouei et al. 2021). It is also recognised as one of the main factors leading to a rise in phytoplankton biomass and cyanobacteria abundance (Kakouei et al. 2021). A recent study by Kakouei et al. (2021) investigated the impacts of climate change and land use on phytoplankton and cyanobacteria as well as forecasted their future response in more than 1,500 lakes across Europe and North America. Their results highlighted that there will be a rise in phytoplankton and cyanobacteria biomass, however, this varied regionally (Kakouei et al. 2021). Nonetheless, any increase or decrease in algal biomass is not only a consequence of climate change but is also regulated by other changes in local weather conditions, land use and restoration, lake morphology, salinity and biotic interactions (Parmesan et al. 2022).

2.2. South American lakes

South America has an area of 17,870,218 km^2 (Llames and Zagarese 2009) (Fig. 2.2). This continent includes twelve countries, including Argentina, Bolivia, Brazil, Chile, Colombia, Ecuador, Guyana, Paraguay, Peru, Suriname, Uruguay, and Venezuela. There are four main geomorphologic areas: the Guiana and Brazilian Highlands, the interior lowlands, the

Cordillera and the Patagonia Steppe (Llames and Zagarese 2009). The continental shield of northeastern South America is formed by the Guiana and Brazilian Highlands (Llames and Zagarese 2009). Along the centre of the continent, lowlands spread southward from the Llanos del Norte to the Argentinean Pampa. The climate, vegetation and hydrology in these lowlands vary greatly (Llames and Zagarese 2009). The Cordillera extends along the Pacific coast from north to south. It consists of the Andes Mountain ranges as well as high intermountain basins and plateaus. The area is seismically active, with regular earthquakes (Llames and Zagarese 2009). Numerous volcanoes expand in the Andean Cordillera, although the majority of them are inactive. The Patagonia Steppe is located between east of the Andes and south of the Colorado River. The Patagonian commonly features tablelands (formed by erosion, smaller than plateaus, usually found at a lower elevation) (Llames and Zagarese 2009).



Figure 2.2. South American Map (Source: Rivas Martínez et al. 2011)

South America has a variety of climates and can be divided into three areas: equatorial and tropical, subtropical and extratropical. The climatic zones are influenced by the orographic presence, oceanic boundary conditions and large-scale phenomena, specifically the Pacific and

Atlantic Intertropical Convergence Zone, monsoon, South Atlantic Convergence Zone and the westerly wind belt (Garreaud et al. 2009). The equatorial climate mainly corresponds to the Amazon Basin (Jiminez and Oliver 2005). The tropical and subtropical areas have a distinct seasonal precipitation cycle, with a maximum north of the equator during austral winter, high precipitation from the southern Amazon Basin to northern Argentina during austral summer, and maximum precipitation steadily returns to northern South America during austral autumn. The climate is classified as monsoon-like in the central part of South America, as the low-level wind direction never reverses. The Intertropical Convergence Zone (the area near the equator where the trade winds of two Hemispheres come together), with convective precipitation near the equator, is a critical feature. The dry areas include the coastal desert in Peru and Chile (~ 30°S as far north as 5°S), the eastern tip of northeast Brazil and the extratropical plains east in the Andes (Garreaud et al. 2009). The extratropical lies along the west coast of southern South America and Patagonia (Jiminez and Oliver 2005). The extratropical climate is characterised by a year-round low-level westerly flow, accompanied by a reduction in pressure (Garreaud et al. 2009). Extratropical precipitation has pronounced zonal asymmetry, with extremely rainy (dry) weather to the west (east) of the Andes Cordillera (Garreaud et al. 2009). The arid diagonal area (below ~ 10^{o}S) runs from the Pacific coast in Peru and Chile to the Atlantic coast in Patagonia, southern Argentina (Llames and Zagarese 2009). This area is dry, lacks moisture, and has low precipitation (Llames and Zagarese 2009). Patagonia has a very dry condition due to the forced subsidence over the eastern Andes (Garreaud et al. 2009).

South America is under pressure of climate change such as increasing air temperatures (de Barros Soares et al. 2017; Dereczynski et al. 2020; Pabón-Caicedo et al. 2020), precipitation patterns shifting (Espinoza et al. 2019; Carvalho 2020; Giráldez et al. 2020), Andean glaciers retreating (Salzmann et al. 2013; Vuille et al. 2018; Masiokas et al. 2020) and a growing frequency of extreme events such as floods, droughts, and wildfires (Bennett et al. 2023; Cavazos et al. 2024; Feron et al. 2024). These impacts will be described in the following sections.

2.2.1. Climate change impacts in South America

2.2.1.1. Air temperature

Air temperature variability is influenced by latitudinal extent, topography (Garreaud et al. 2009; Espinoza et al. 2020; Arias et al. 2021) and the geography of South America, including the Andes Mountains, Amazon, and the southern regions. The annual mean air temperature is 21.1 ± 6.6°C and the mean annual precipitation is 1,503 mm in South America (Fick and Hijmans 2017). The coldest temperatures are recorded in the southernmost area of Chile, with a temperature of 8°C, whereas the highest temperatures are over the equatorial belt (~30°C) (Almazroui et al. 2021). The Andes play a considerable role in influencing temperature variations. At the equator, the Andes form distinct temperature patterns on the eastern and western slopes, with the eastern side regularly experiencing warmer weather due to the Amazon Basin (Garreaud et al. 2009). The Amazon Basin has consistent temperatures during the year, with mean annual temperatures ranging from 25°C to 27°C, while diurnal changes can be significant (Gloor et al. 2015). On the contrary, the southern parts of South America have stronger seasonal temperature changes. Countries like Argentina and Chile feature cold winters and warm summers, with mean annual temperatures ranging from 12°C to 18°C (Rusticucci and Barrucand 2004; Rusticucci and Tencer 2008). Air temperature had a warming trend of +0.23°C decade^{-1} from 1991 to 2021 in South America (World Meteorological Organization 2021). Temperature anomalies increased by +1°C - +2°C in 2021 relative to 1981-2010 in northeast and central Brazil, central and southern Argentina, central Chile and Colombia (World Meteorological Organization 2021). In other parts of South America, including Venezuela, Guyana, north of Bolivia, northeast Chile, north of Brazil and west of Uruguay, the temperature anomalies increased by +0.5°C in 2021 (World Meteorological Organization 2021).

The frequency and magnitude of warm temperature extremes will increase by the end of the 21st century (Margin et al. 2014). (Skansi et al. 2013) reported warming trends in both maximum and minimum temperatures since the middle of the 20th century, particularly in the Andean region and southeastern South America. Temperatures are expected to escalate by +2°C to +3°C and +3°C to +5°C by 2100 under the RCP 4.5 and RCP 8.5, respectively (Llopart et al. 2020), with the most significant warming in the Amazon basin and central Andes.

2.2.1.2. Solar radiation

South America is one of the three areas that have high radiation in the southern hemisphere (along with South Africa and Australia), spreading from latitude 10°S during the winter to 30°S during the summer with the highest values recorded at 750 gcal cm^{-2} day^{-1} (~ 363.2 W m^{-2}) (December and January) (Black 1956). There is high solar energy potential in all countries in South America, especially Chile and Brazil (Meisen and Krumpel 2009). High levels of solar radiation occur in the equatorial and tropical areas, such as northeast Brazil with the highest value of 6.5 kWh/m^2 (Martins et al. 2009). The northern area of Chile shows the highest levels of irradiation (Vargas Gil et al. 2020) because of the Atacama Desert, which has the highest long-term recorded solar irradiance of any place in the world (Rondanelli et al. 2015). The Cordillera Domeyko, is located in the west of Atacama, northern Chile (24°-25°S, along 69°W), has the highest downward solar radiation on Earth at a rate of 310 ± 15 W m^{-2} (Rondanelli et al. 2015). Northeast Brazil, northern Colombia, northern Argentina and the west coast of Peru also show substantial irradiation compared to other countries (Meisen and Krumpel 2009). Solar irradiation is moderate in much of the other parts of the continent and low in the Amazon rainforest (Vargas Gil et al. 2020). Due to the dense vegetation canopy and cloud cover, low incoming solar radiation occurs in the Amazon Forest (Martins et al. 2009). The Andes mountains have different solar radiation patterns between the east and west slopes. The eastern part of the Andes receives low levels of solar radiation because of greater cloud cover, whereas the western slopes experience higher radiation because of a clearer sky (Garreaud et al. 2009). This great potential of solar radiation has resulted in an increased interest in solar energy as a renewable energy resource in South American development (Martins et al. 2009).

Climate change affects solar radiation variability, potentially increasing it because of reduced cloud cover, but it might also cause reduction. The northern area of South America is expected to receive an increase of shortwave downward radiation at approximately +30 W m^{-2} in most regions, with a highest value of +64 W m^{-2} in northern Colombia by the end of the century in relation to the period of 1970-1999 under the RCP 2.6 (Narvaez et al. 2023). Nevertheless, shortwave downward radiation values are forecasted to decrease in some areas such as western Ecuador (-30 W m^{-2}), Bolivia (-42 W m^{-2}), and southern Peru (-112 W m^{-2}) by 2099 (Narvaez et al. 2023). The southern areas of the continent are unlikely to experience significant changes. Under the RCP 8.5 scenario, solar radiation is predicted to increase by

more than +30 W m^{-2} in the northern area with the highest value of +74 W m^{-2} in northern Colombia by the end of the 21st century (Narvaez et al. 2023). A reduction of solar radiation will likely happen in the coastal areas, including Ecuador (-30 W m^{-2}), and in southern Peru (-130 W m^{-2}) (Narvaez et al. 2023). There is an increase in solar radiation at the average rate of +11 W m^{-2} on the continent (Narvaez et al. 2023).

2.2.1.3. Humidity

The atmospheric conditions are also closely related to humidity. Approximately 80% of South America is located in the tropics, with most of the basins dominated by a warm and humid climate (Brêda et al. 2023). For example, the relative humidity (RH) was recorded from 46-62% in western Argentina, 60-80% in the Guajira Peninsula, Colombia or in Buenos Aires can be up to 90% (Eidt 1969). The Amazon Forest, which occupies 35% area of South America and 65% of the tropical area, is one of the most humid climates in the world (Satyamurty et al. 1998). On the contrary, the Atacama Desert in northern Chile and northeastern Brazil is one of the most arid areas due to the cold Humboldt Current and low precipitation (Satyamurty et al. 1998). Vicente-Serrano et al. (2018b) reported the changes in RH globally between 1979 and 2014 using the ERA-interim dataset. Their results showed that RH decreased in South America, except for northern South America (Vicente-Serrano et al. 2018b). A significant reduction was recorded in Peru, Bolivia and central Argentina with a rate from -5% $decade^{-1}$ to -10% $decade^{-1}$. This decrease was also observed in Specific Humidity (SH) trends, with a notable reduction in the Amazonia area and southern South America (from -1 to -2 g kg^{-1} $decade^{-1}$) (Vicente-Serrano et al. 2018b). Due to the changes in air temperature in the same period, these areas exhibited a water vapour decrease of about -2 g kg^{-1} $decade^{-1}$ to maintain steady RH levels (Vicente-Serrano et al. 2018b). The La Plata region reported a decrease of -6.6% $decade^{-1}$ in RH due to changes in land evapotranspiration and precipitation (Vicente-Serrano et al. 2018b). The study indicated that SH is the main factor which drives RH variability. As oceans warm at a slower rate than land, the SH of air from the ocean also increases slowly, resulting in a decrease in RH. This effect explains the decrease in RH in the Amazon, where limited moisture sources from the ocean contribute and air temperatures increase (Vicente-Serrano et al. 2018b). According to Fernandez-Duque et al. (2023), the annual mean RH was about 65% with a negative trend (-0.08% $decade^{-1}$) from 1950 to 2019 in Bolivia (Fernández-Duque et al. 2023). The reduction in RH was associated with an increase in air temperatures (Byrne and O'Gorman

2016; Byrne and O'Gorman 2018). This finding is aligned with the previous research from Caceres et al. (2007) regarding the humidity decrease in the Atacama Desert due to air temperatures increasing with extreme aridity conditions (Cáceres et al. 2007). Decreased RH limits convective formations and impacts precipitation (Brêda et al. 2023).

2.2.1.4. Wind speed

Wind plays an important role in South American weather patterns. The northeast trade wind, which blows from the northeast in the Northern Hemisphere along with the easterly component of the south, dominates in the north and shifts seasonally (Eidt 1969). The northeast trade wind reaches as far as 5°S in Brazil during January (Eidt 1969). Southeast trades influence the coast from 15°S to about 3°S during the summer, reaching northward during the winter (Eidt 1969). Strong and persistent westerlies dominate in the southern areas, also known as "Roaring Forties" (Eidt 1969). Westerlies advance to the coast between 40°S and 50°S. The Andes Mountain range prevents Pacific winds from entering the interior regions (Eidt 1969). Therefore, it creates two distinct climate regimes, including cold and dry weather on the western side and warm and moisture on the eastern part (Seluchi and Marengo 2000). The west coast of South America experiences a narrow northerly maximum wind speed in the lowest few kilometres of the atmosphere, known as the "South American Low Level Jet" (Stensrud 1996; Garreaud and Muñoz 2005). The "level" of South American Low Level Jet refers to the atmosphere vertical layer in which the wind current occurs. The "low level" means that the jet stream is situated within the first few kilometres above the Earth's surface. The South American Low Level Jet influences moisture transport, wind energy, and precipitation patterns in the region (Jones et al. 2023). In general, wind is low in most of the inner areas of South America (Gonzalez-Salazar and Poganietz 2021). However, wind is one of the popular resources for renewable energy in the continent such as Uruguay, Chile and Brazil (Vargas Gil et al. 2020).

Wind speed is projected to change in a range from -1.5 m s^{-1} to +1.3 m s^{-1} and from -1.3 m s^{-1} to +1.95 m s^{-1} by the end of the century under the RCP 2.6 and RCP 8.5, respectively (Narvaez et al. 2023). Venezuela, Colombia, northern Brazil and the centre of the Andes will experience an increase in wind speed at a rate of around +1.3 m s^{-1} under the RCP 2.6 (Narvaez et al. 2023). Under the RCP 8.5, Brazil shows a positive change in wind speed while Peru,

Bolivia and the centre of Argentina show a negative change in wind speed (Narvaez et al. 2023).

2.2.2. Climate change and anthropogenic impacts on South American lakes

South America encompasses a vast and diverse range of lake systems spread across its broad latitudinal and longitudinal extent (12°28'N–55°59'S; 30°W–80°W) (Nuñez-Hidalgo et al. 2023). Lakes, rivers, and wetlands are integral to the continent's hydrological cycle, serving as critical water sources for ecosystems, agriculture, and human populations (Hamilton et al. 2002; Junk 2013; Kandus et al. 2018; Siqueira et al. 2018; Fleischmann et al. 2021). South American lakes are spread out in different climates and geographic areas, from temperate to glacial lakes (Carabajal and Boy 2021). Lakes in South America are rather small compared to other lakes in the world such as the Great Lakes in North America or rift lakes in East Africa, however, their altitude and volumes are large enough to be visible in satellite observations (Carabajal and Boy 2021). The continent's lakes exhibit considerable variability in size, volume, and elevation. Surface areas range from small ponds measuring approximately 0.1 km^2 (Messager et al. 2016) to large water bodies such as Lake Titicaca, which spans 8,372 km^2 (Duquesne et al. 2021). Lake volumes vary between 0.0001 km^3 and 893 km^3 (Messager et al. 2016). Prominent systems include Amazon floodplain lakes, which experience dramatic seasonal water level fluctuations, and Andean glacial lakes, which are particularly sensitive to temperature changes and glacial melt.

Lakes across South America play critical roles in the hydrological cycle, serving as essential freshwater resources for agriculture, industry, hydropower generation, and drinking water supply. They also support rich biodiversity, including endemic and economically significant species, while holding cultural and societal importance for numerous communities (Llames and Zagarese 2009). However, South American freshwater resources are increasingly threatened by climate change and human activities (Buytaert and Breuer 2013; Junk 2013). Over recent decades, South America has experienced significant air temperature increases (World Meteorological Organization 2021). Warming trends are projected to continue and are likely to cause profound impacts on LSWT (Margin et al. 2014; Llopart et al. 2020). Despite the continent's ecological importance and vulnerability to climate change, research on LSWT dynamics and lake heatwaves across South America remains limited. Most studies have

focused on specific water bodies, particularly glacial lakes (Quade and Kaplan 2017; Wilson et al. 2018; Mergili et al. 2020; Hata et al. 2022) or on changes in lake water level (Zolá and Bengtsson 2006; Pasquini et al. 2008; Carabajal and Boy 2021). The relative scarcity of studies addressing LSWT trends and lake heatwave dynamics on a regional scale is partly due to limited in situ measurements, particularly in the Southern Hemisphere (Aranda et al. 2021). There is limited remote sensing validation and/or a lack of long-term lake temperature data. Consequently, knowledge gaps persist regarding how LSWT and lake heatwave characteristics are changing under climate change.

2.2.2.1. Lake surface water temperature

Despite these limitations, previous studies provide valuable insights into LSWT patterns across South America. LSWT in South America is varied because of the diverse climatic zones and topography. South America's tropical and subtropical areas such as the Amazon basin, consist of numerous floodplain lakes characterised by warm and steady surface water temperature across the year (Fleischmann et al. 2024). LSWTs of Amazon floodplain lakes are approximately 28-30°C (Caraballo et al. 2014). Lake Janauacá, located in the central Amazon floodplain, is an example of these patterns with LSWT variations between 27.5 and 35.5°C, reaching up to 40°C during the summer (Zhou et al. 2024). On the contrary, LSWTs in the Andean regions of Peru, Bolivia, Chile and Argentina show significant temperature changes in seasonal and daily because of their high elevation and distinct seasonal patterns. For example, Lake Titicaca, which is best known as the largest freshwater lake in South America, has LSWT typically ranging from 12-17^{o}C (Pillco Zolá et al. 2019; Duquesne et al. 2021) with mean diurnal changes of 4^{o}C (Duquesne et al. 2021). Lakes in southern Argentina and Chile show high seasonal temperature variability, ranging from 15-20°C during the summer and decreasing to 4-8°C during the winter (Geller et al. 1997). These lakes are affected by strong westerly winds, resulting in changes in lake mixing and thermal structure.

Lakes across South America have been influenced by climate change, with numerous lakes experiencing increasing temperatures over the last decades. According to Fleischmann et al. (2024), there was a warming LSWT trend with a rate of +0.6°C decade^{-1} recorded from 1990 to 2023 in 24 lakes in the Amazon (Fleischmann et al. 2024). Lake Cochrane, Lake Cardiel, Lake Buenos Aires and Lake Argentino in Patagonia experienced an increasing rate

of +0.38°C decade^{-1}, +0.42°C decade $^{-1}$, +0.34°C decade $^{-1}$, and +0.43°C decade $^{-1}$ in LSWT, respectively, from 2002 to 2022 (Zhao et al. 2025). These warming trends were influenced by climate forcings such as increasing air temperature and solar radiation (Zhao et al. 2025).

2.2.2.2. Lake water level/volume

Lake water levels in the Amazon Basin are characterised by seasonal fluctuations with annual amplitudes of up to 10 m in some regions (Junk et al. 2011). These fluctuations are influenced by seasonal precipitation patterns, with the rainy season starting from November-January to May-June, and the dry season occurring between July and November (Bonnet et al. 2008). The Andean lakes have more complex water level fluctuations and are driven by glacial melt, precipitation and evaporation (Moser et al. 2019). In Southern South America, especially in Patagonia, lake levels are mainly driven by glacial and snow melts from the Andes Mountains (Pasquini et al. 2008). Lake Mascadi, which is directly fed by glacial melt, showed a decreasing trend in water level during the summer due to the Manso Glacier retreat and declined meltwater supply (Pasquini et al. 2008). Increased temperatures and evaporation with high human water consumption also caused lake water storage to decrease (Yao et al. 2023). Lake water storage loss was reported in most of the South American continent, including Lake Mar Chiquita, Argentina (-0.75 ± 0.09 Gt year^{-1}), Lake Titicaca, Peru-Bolivia (-0.12 ± 0.08 Gt year^{-1}), between 1992 and 2020 (Yao et al. 2023).

2.2.2.3. Lake ice cover

Glacial lakes in South America are located mostly in the Andes Mountain Range (Wilson et al. 2018). Lake ice formation is rare and limited to small lakes at high altitudes of 3,500-4,500 m, where nighttime temperatures can decrease to below 0^{o}C in the tropical and subtropical Andes (Vuille et al. 2018). Seasonal lake ice cover is more common and plays an important role in lake ecosystem dynamics in the Southern Andes and Patagonia (Wilson et al. 2018). Ice duration in these areas varies (~ few weeks to several months) based on the latitude, elevation and weather conditions (Wilson et al. 2018). Lake ice regimes have been impacted by climate change. Climatological ice cover in this region was thin and had a short duration during the 20th century (Huang et al. 2022). Most lakes in the area are predicted to have ice cover only occasionally, while some are expected to lose ice permanently by the end of the 21st century

(Huang et al. 2022). For example, Lake Mascardi-Manso in Argentina recorded a decreasing trend in ice volume during the summer months between 1986 and 2016 (Pasquini et al. 2008). Ice formation was delayed due to the increase in temperatures observed in Lake Argentino during the period of 2010-2011 (Zhao et al. 2025). This decline is consistent with global trends in response to a warming climate (Huang et al. 2022). Such changes affect the lake's physical, chemical and biological processes (Sharma et al. 2020; Imrit and Sharma 2021; Sharma et al. 2021).

2.2.2.4. Lake mixing regimes

Shallow floodplain lakes in the Amazon basin are classified as polymictic or oligomictic (Tundisi et al. 1984). These lakes are characterised by strong patterns of diurnal stratification and mixing (Augusto-Silva et al. 2019). Most of the lakes in this region experience frequent mixing, while some deep lakes have stable stratification (Melack and Coe 2012). By examining hundreds of temperature profiles of floodplain lakes, vertical mixing patterns were revealed (MacIntyre and Melack 1984; MacIntyre and Melack 1988). Diel mixing from top to bottom was obtained at a depth of < 3-4 m. At depths > 5 m, a thermocline formed at 3 m and bottom mixing was intermittent. For depth > 8 m, mixing reached the bottom was rare (MacIntyre and Melack 2009). Most of the lakes in the Andes are classified as polymictic and have only a short period of thermal stratification, however, these patterns change in some cases because of climate change (Labaj et al. 2018). The duration of thermal stratification has been increasing in some lakes, such as in the Southern Sierra of Ecuador (Labaj et al. 2018). These lakes experienced thermal stratification from November to May when the air temperature was recorded highest and the lowest wind speed was observed. Air temperature is the main driver of stratification dynamics (Vincent 2009). Stratification changes will influence the chemical and biological processes in a lake. Increasing thermal stratification will affect primary production, phytoplankton and zooplankton assemblage composition shift (Labaj et al. 2018). Temperate lakes in Patagonia (southern Argentina, Chile) show warm monomictic or dimictic mixing regimes with seasonal stratification patterns influenced by seasonality and westerly winds (Geller et al. 1997; Diaz et al. 2000). Warming temperatures result in increasing vapour pressure gradients and evaporative heat loss, leading to escalating convective mixing frequency (Melack and Coe 2012). Some of the lakes in South America are expected to experience less frequency or no mixing by the end of the 21st century, specifically, continuous warm polymictic

can turn into discontinuous warm polymictic, and dimictic will become monomictic (Woolway and Merchant 2019).

2.2.2.5. Lake chemistry

Lakes in the Amazon basin have seasonal variations in water chemistry and are characterised by the mixing of river and local drainage basin (Forsberg et al. 1988). In this region, lakes have low conductivity, slightly acidic to neutral pH and high concentration of DOC (Forsberg et al. 1988). For example, more than 90% of lakes in the Lower Nhecolândia area (Brazil) have a pH ranging from 4.69 to 7.9 (Pereira et al. 2020). Floodplain lakes have distinct ecological characteristics (Junk and Howard-Williams 1984; Ríos-Villamizar et al. 2013). Whitewater lakes such as Lake Yahuarcaca, which are fed by rivers coming from the Andes, carry high amounts of sediments and nutrients (Jhon and Duque 2023). These waters are muddy or white because of the nutrient rich and therefore support higher photosynthesis biomass (Ríos-Villamizar et al. 2013). On the contrary, blackwater like Lake Pacatúa, is fed by rivers that flow through nutrient-poor soils (Jhon and Duque 2023). These waters are clear but darkly stained by dissolved organic matter, particularly tannins (Ríos-Villamizar et al. 2013). They are low in nutrients and hence have lower levels of plant growth (Ríos-Villamizar et al. 2013). However, both systems are important for sustaining food webs through carbon inputs from aquatic plants and periphyton (Ríos-Villamizar et al. 2013). The blackwater (e.g., Rio Negro) can have pH levels as low as 4.0 while whitewater has higher pH (6.5-7.0) (Ríos-Villamizar et al. 2013). The Andean lakes have unique chemical characteristics because of climatic variety and geography such as the volcanic influences. Volcanic eruption increases the trophic status of lakes and declines photoinhibition and releases phosphorus which influences the increase in phytoplankton biomass (Modenutti et al. 2013). Andean lakes often have high alkalinity and conductivity such as Lake Titicaca, which has a pH of ~8.5 with a high concentration of dissolved solids (Dejoux and Iltis 1992). Lakes at high elevations in the Andean region, such as Laguna Lejia and Laguna Verde, often have oligotrophic conditions, low nutrient levels and unique microbial communities (Runzheimer et al. 2024). Like Andean, most Patagonian lakes are oligotrophic with low nutrient concentrations and high water clarity (Villalobos et al. 2003). However, chemical compositions vary across the region based on geology, lake morphology, and weather patterns (Gerea et al. 2023). Lakes in the eastern Patagonian steppe have higher conductivity and alkalinity than those in more humid western areas (Gerea et al. 2023). Climate

change and human activities have significant impacts on the water quality. Extreme droughts caused the bloom of *Euglena sanguinea* in the Amazon lakes in 2023, which was potentially affecting the water quality and aquatic life through the production of a toxin called Euglenophycin (Mendes et al. 2024). Runoff from fertilisers, pesticides from agriculture and urbanisation activities can lead to contamination in lakes (Bashir et al. 2020). Industrial discharges, specifically mining activities, are threatening water quality (Machate et al. 2023). For example, due to untreated mining activities, industrial and domestic wastewater, heavy metals such as copper, lead, mercury, etc have been found in Lake Titicaca (Peru-Bolivia), Lake Uru-Uru (Bolivia), Lake San Martín (Ecuador), Lake Yahuarcaca (Colombia), Lake Nahuel Huapi and Lake Moreno (Argentina) (Rizzo et al. 2011; Archundia et al. 2017a; Archundia et al. 2017b; Achá et al. 2018; Sarret et al. 2019; Henao et al. 2020; García-Avila et al. 2023). These metals are not only degrading the water quality but also causing harmful algal blooms, resulting in massive fish deaths and affecting the freshwater biodiversity.

2.2.2.6. Lake biology

South American lakes have a diverse biology and ecology, ranging from microorganisms to fish (Reis et al. 2016). The freshwater fish population represents about one-third of freshwater species diversity in the world, with 5,160 species (Reis et al. 2016). The rich diversity is attributed by several factors such as low latitude regions that avoided mass extinctions, biotic shifts during the past climate cooling, a series of geological and climatic events and ecological characteristics such as altitude, water chemistry and temperature (Hoorn et al. 2010; Kristiansen et al. 2011). Amazon has more than 2,700 fish species and ~1,700 endemic to the basin (Reis et al. 2016; Dagosta and Pinna 2019). Despite its ecological importance, the Amazon face growing threats from deforestation, overfishing, extreme events like heatwaves, droughts, etc. During the heatwave in 2023, extreme temperatures caused more than 3,000 fish deaths, and 209 river dolphins and affected the farming of *Colossoma macropomum* in several lakes in the Amazon (Fleischmann et al. 2024). Recent warming trends are altering the ecological dynamics and physical properties of lakes in the Andes (Michelutti et al. 2015a). Increasing water temperature in the tropical Andes resulted in rising thermal stability in deep lakes and changes in diatom assemblages and production decline (Michelutti et al. 2015a; Michelutti et al. 2016; Labaj et al. 2018). The abrupt shifts in diatom assemblages have been recorded in hundreds of lakes in the world, but mostly with case studies in the Northern

Hemisphere (Michelutti et al. 2015b). In the Peruvian Andes, planktonic diatoms and *chrysophytes* have been increasing since the early 1900s due to the warming climate (Michelutti et al. 2015b). Similarly, the abrupt increase of *Cyclotella* taxa was also recorded in lakes from the southern Sierra of Ecuador (Michelutti et al. 2015b). Native fish species are relatively few compared to other areas in South America but include several endemic and highly specialised taxa (Pascual et al. 2007). For example, the *Percichthys genus* (Temperate perches), *Odontesthes* (Neotropical silversides), *Diplomystes* (Catfish), and the rare *Gymnocharacinus bergii* (Naked characin) are found in the Patagonian region (Pascual et al. 2007). However, they are facing threats from invasive salmonids from aquaculture activities (Habit and Cussac 2016).

2.2.3. Extreme events impact on South American climate and lakes

The frequency, length and intensity of extreme events such as heavy precipitation and snow, heatwaves, droughts, storms, etc, will increase (Margin et al. 2014), influencing the climate and lakes in South America. ENSO events influence the interannual variability of meteorological variables including temperatures, solar radiation, humidity and wind speed (Garreaud et al. 2009; Grimm and Tedeschi 2009; Watts et al. 2017; Muraria et al. 2020; Miranda et al. 2024).

During El Niño events, increasing cloud cover could result in a decrease in solar radiation in the tropical areas of the continent, such as in Brazil, Uruguay and northern Chile (Muraria et al. 2020). For example, lower solar radiation values were recorded mostly in November and December in the centre and northern Uruguay between 2010 and 2016 (Laguarda et al. 2020). During La Niña events, higher radiation can occur because of clearer skies (Muraria et al. 2020). El Niño events also influence wind speed patterns, decreasing wind speed in the centre of Chile (Watts et al. 2017) while increasing in the north of Chile (0.2 m s^{-1}) (Bianchi et al. 2017). In addition, the Antarctic Oscillation is one of the main factors that affect wind speed, especially during spring and summer. It has a negative correlation to wind speed in Paraguay, northern Patagonia, Argentinean and Uruguayan Pampas (Bianchi et al. 2017). Furthermore, El Niño events have significant impacts on humidity patterns in South America by increasing moisture and precipitation in the southeastern region while having drier conditions in the northern Amazon and northeast Brazil (Grimm and Tedeschi 2009).

ENSO events are expected to exacerbate the coastal risks in South America, including storm surges, sea level rise and erosion, particularly affecting Peru and Ecuador (Reguero et al. 2015; Wahl et al. 2017). Due to a reduction in precipitation and an increase in evapotranspiration, the drought will be more intensified in Amazonia and Northeast Brazil during the 21st century (Margin et al. 2014). According to the IPCC Sixth Assessment Report, the intensity and frequency of hot extremes are likely to escalate while cold extreme events will decline in South America (Intergovernmental Panel on Climate Change 2023). The areas which have historically been most affected by droughts are Chile and Paraná–La Plata Basin (south-eastern Bolivia, southern and central Brazil, Paraguay, Uruguay and northern Argentina) (World Meteorological Organization 2021). The most severe drought events were recorded during the years 1988-1989, 2008-2009, 2017-2018 and 2019-2023 (Rivera and Penalba 2014; Naumann et al. 2021; Naumann et al. 2023). During the El Niño events of 1982-1983 and 1991-1995, Lake Poopó water level was recorded at a low level of around 0.5 m (Zolá and Bengtsson 2006). Droughts had significant impacts on the economy, especially agriculture (production losses, animal health, etc) (Canedo Rosso et al. 2018; Poveda et al. 2020; Canedo-Rosso et al. 2021), for example, the 2008-2009 drought affected approximately 30% of agricultural land in Argentina (Naumann et al. 2019). There have been severe droughts since 2010 in central Chile, the subtropical Andes and western Argentina (Garreaud et al. 2021). Due to the drought of 2017-2018, Argentina estimated economic impacts of 4,600 million USD, which included 1,550 million USD losses for poor maize and soybean production (Bert et al. 2021). The mega-drought in central Chile has lasted for 13 years to the present day, causing a water crisis in the country, affecting the environment, economy and society (Garreaud et al. 2017). Extreme droughts in 2010 and 2016 exposed 16% and 46% of the Brazilian Amazon ecosystem, respectively (Anderson et al. 2018). Food security for indigenous and rural populations in the Amazon has been greatly impacted by these events, particularly for those who depend on small-scale agriculture and fishing (Camacho Guerreiro et al. 2016; Marengo and Espinoza 2016). The La Plata basin is the second largest river basin in South America, after the Amazon, covering approximately 17% of the South American area (Naumann et al. 2021). However, it has been impacted by droughts since 2019 (Naumann et al. 2021). This drought affected many sectors such as agriculture, hydropower, water supply, transportation, etc (Naumann et al. 2021).

Lake heatwave events are defined as similar to a marine heatwave, where LSWT surpasses the 90th percentile threshold compared to a baseline climatological average and lasts for five consecutive days or more (Hobday et al. 2016; Oliver et al. 2018). The concept of lake heatwave was introduced by Woolway et al. (2021), showing that lake heatwaves will increase more in duration and intensity as global temperature rises. Further research has confirmed the warming trends in lake heatwaves, which are observed from regional to global levels (Wang et al. 2023; Zhang and Yao 2023). Lake heatwaves will increase the risk of ecological and socioeconomic effects, including aquatic species loss, and harmful cyanobacteria spread, causing issues for drinking water safety (Ho et al. 2019; Till et al. 2019; Tassone et al. 2022). Increased air temperature leads to more frequency and intensity of heatwaves in the Andes (Vuille et al. 2018; Masiokas et al. 2020). Additionally, due to drought and heatwaves in 2023, five of ten lakes' temperatures in the Amazon were reported above 37ºC, causing widespread deaths of fish and river dolphins (Fleischmann et al. 2024). Tropical aquatic ecosystems are expected to experience temperatures that reach or surpass the thermal limits of aquatic organisms under the changing climate (Fleischmann et al. 2024).

On the contrary, heavy precipitation caused flooding and landslides that affected livelihood, infrastructure, and economy, in many countries such as Brazil, Venezuela, French Guyana, Peru, Bolivia, Argentina, and Colombia (World Meteorological Organization 2021). Flooding and landslides cause loss of life and impacts on the economy, infrastructure and environment. Due to the increase in precipitation and land use changes, the main rivers in Uruguay, Paraguay and Paraná in the La Plata basin have experienced an increase in flow rate and higher frequency of flooding since 1975 (Garcia and Vargas 1996; Barros et al. 2015). Every year, river floods affect approximately 1.1 million people and cause damages of 1.5 billion EUR in South America (Alfieri et al. 2017). The International Federation of Red Cross and Red Crescent Societies reported that the flood in August 2021 in Venezuela affected 10 states and more than 54,000 people, damaged 116 roads and 10 bridges and caused 40 landslides (IFRC 2021). The floods also affected approximately 40,000 people between April and September 2021 in Colombia (World Meteorological Organization 2021). Heavy precipitation caused floods at the end of May 2021 in Guyana, affecting more than 29,000 families and about 7,900 houses (Caring4others 2021). The frequency and duration of floods are projected to increase by the end of the 21st century in South America, except for southern South America (Hirabayashi et al. 2021). The South American population affected by floods

increased about 2-fold from the historical period (1971-2000) with 3°C warming (Hirabayashi et al. 2021).

In conclusion, climate change has been significantly affecting both atmospheric conditions and freshwater ecosystems across South America. Changes in meteorological variable patterns such as increasing air temperature, solar radiation fluctuations, wind speed changes, etc are influencing lake essential climate variables. Furthermore, increasing frequency and intensity of extreme events are particularly affecting LSWT. As LSWT responds to changes in climate forcing, it impacts lake processes such as thermal mixing, stratification, and changes in oxygen and nutrient levels, etc. These changes are affecting not only lake ecosystems but also local and regional livelihoods that depend on lakes (e.g., drinking water, agriculture, fisheries, tourism, etc). Despite the importance of understanding how lakes respond to climate change, there remains a lack of long-term in situ measurements of LSWT across South America. Additionally, limited validation of remote sensing data and insufficient regional-scale studies constrain the ability to analyse spatial and temporal LSWT trends and detect lake heatwaves. These knowledge gaps pose challenges for scientists and policymakers aiming to forecast future changes and develop mitigation and adaptation strategies. This study provides an overview of LSWT and lake heatwave variability in South America, identifies the main drivers and emphasizes the importance of improved in situ observation networks and regional cooperation. The findings are critical for developing water governance frameworks and supporting climate adaptation planning.

2.3. Lake Titicaca

While the previous section focuses on how climate change impacts lakes across South America, this section provides in detailed case study of Lake Titicaca. Lake Titicaca is located in a high plateau region referred to as the "Altiplano-Puna", in the Central/tropical Andes (15º47' S, 69º22' W) (Ruiz-Verdu et al. 2016; Bergmann et al. 2021) (Fig.2.3). As the largest freshwater lake in South America (Pillco Zolá et al. 2019; Duquesne et al. 2021), it covers a surface area of 8,372 km^2 (Duquesne et al. 2021). Additionally, it is one of the highest lakes in the world, situated at an elevation of 3,812 m above sea level (Duquesne et al. 2021) and has a maximum depth of 284 m (Ruiz-Verdu et al. 2016). It was formed approximately 3 million years ago and is considered one of the twenty ancient lakes on Earth (Lavenu 1992; Wirrmann et al. 1992; Hampton et al. 2018).

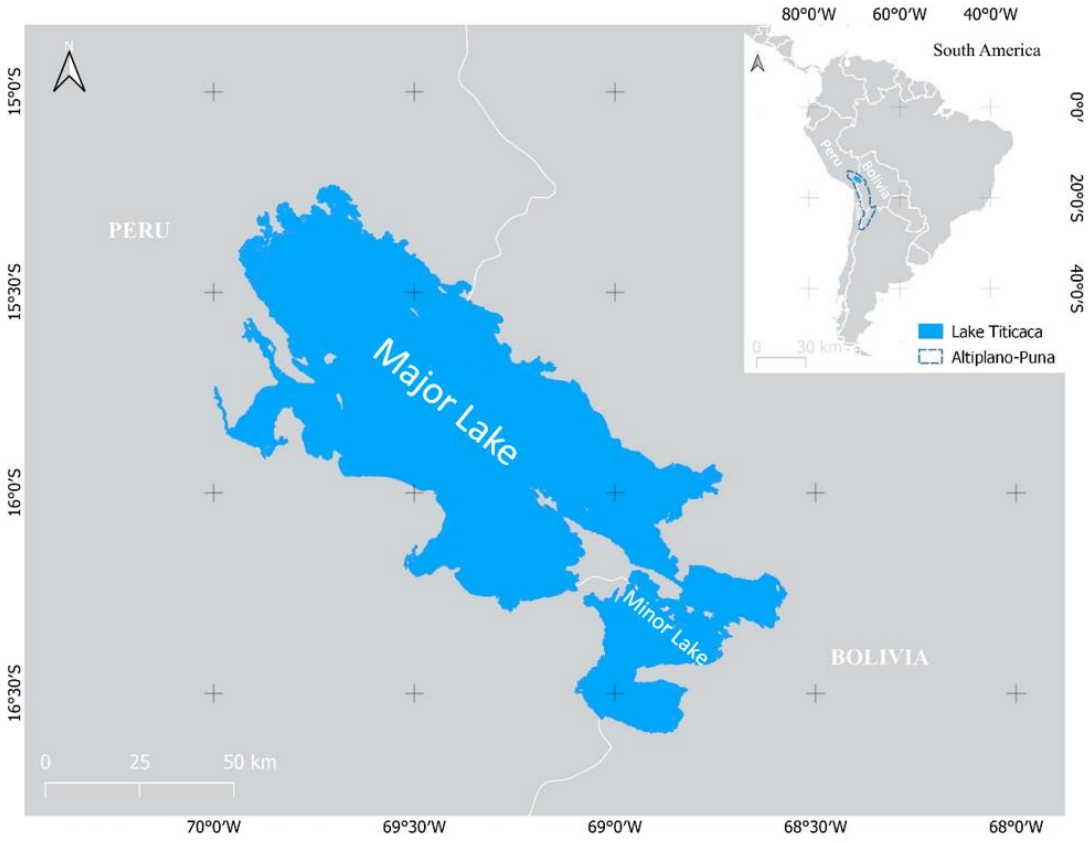


Figure 2.3. The location of the study site, Lake Titicaca (Peru-Bolivia)

Lake Titicaca is divided into two sub-basins: Lago Mayo (Major Lake or Lake Chuquito) (83.4% of the total surface) (Duquesne et al. 2021), with a mean depth of 135 m (Ruiz-Verdu et al. 2016) and Lago Menor (Minor Lake or Huiñaimarca) is located in the south, which is smaller (16.6% of the total surface) (Duquesne et al. 2021) and shallower at a mean depth of 9 m (Ruiz-Verdu et al. 2016) (Fig. 2.4).

Lake Titicaca supplies drinking water and food for 3 million people (Monroy et al. 2014; Loayza et al. 2022). The population in the catchment is mainly rural and indigenous, such as Aymara and Quechua (Monroy et al. 2014; Loayza et al. 2022). The lake has been an important source for Andean cultures, including the Tiwanaku civilization, and continues to play an essential role for the Aymara communities, supplying food, raw materials, and water resources for local populations (Pillco Zolá et al. 2019; Duquesne et al. 2021). The main economic activities in the area include agriculture, livestock herding (e.g., llamas, alpacas) and aquaculture (Trigoso 2007). Potatoes, oca, broad beans, barley, and quinoa are dominant crops in local agriculture, reflecting long-term adaptation to high altitude climate conditions (Richerson et al. 1977; Trigoso 2007). Fishing for native (e.g., *carachi*, *ispi*) or introduced

(e.g., rainbow trout) species is also vital for food and income, although overfishing and pollution have increasingly threatened these resources (Gammons et al. 2006; Biamont-Rojas et al. 2023). Lake Titicaca is also a great tourist attraction in South America, with millions of tourists visiting the lake each year (Duquesne et al. 2021). Besides its economic significance, the lake's catchment area exhibits socio-cultural traditions shaped by Inca and pre-Inca influences (Dejoux and Iltis 1992). Indigenous knowledge is deeply integrated into daily practices, including the use of natural resources like the Totora reed for crafting boats, houses, and floating islands, by the Uros people in Peru (Briefings 2023). Cultural identity continues to be maintained through language, ritual practices, and a shared history connected to the lake and its ecosystem (Dejoux and Iltis 1992).

Lake Titicaca feeds the downstream Desaguadero River and is the second largest and shallowest lake in Bolivia, Lake Poopó (Pillco Zolá et al. 2019). Lake Titicaca is managed by the Autonomous Binational Authority of Lake Titicaca, which was established by Peru and Bolivia in 1996 (Revollo 2001). This entity is responsible for the management, control and protection of the Lake Titicaca, Desaguadero River, and Lake Poopó basins (TDPS) system (Revollo 2001). It also manages the implementation of plans such as water use, pollution control and biodiversity protection, with support of international organizations (Revollo 2001). However, one of its main challenges is the lack of local stakeholders and public participation in the management process. Additionally, this issue has constrained its ability to effectively address problems from urban pollution, agricultural runoff, and climate variability.

This lake ecosystem is affected by both climate change and human activities (Duquesne et al. 2021). Numerous species are currently considered threatened according to the International Union for the Conservation of Nature (Monroy et al. 2014). Despite its importance, there are limited studies on Lake Titicaca's ECVs, specifically LSWT, due to the lack of in situ observations. This scarcity of measurements presents challenges for understanding the impacts of climate change on this lake. The following section investigates the impacts of climate change on the Lake Titicaca region overall and on the lake itself.

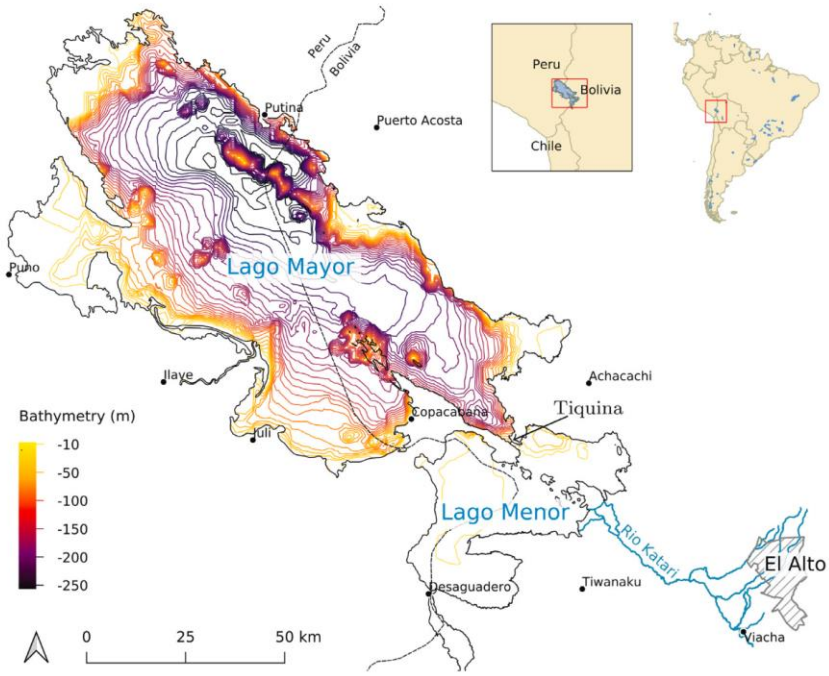


Figure 2.4. Lake Titicaca bathymetry map (Source: Duquesne et al. 2021).

2.3.1. Climate change and impacts on Lake Titicaca region

Several studies have shown that climate change has been affecting Lake Titicaca, especially in areas such as the Puno regions (Haylock et al. 2006; Trigoso 2007; Obregón et al. 2009; Bergmann et al. 2021) and Peruvian Altiplano (López-Moreno et al. 2016; Pabón-Caicedo et al. 2020; Zubieta et al. 2021).

2.3.1.1. Air temperature

Lake Titicaca is located in a semi-dry and cold area (Gonzales and Roncal 2007). The dry and cold season is between April and November and the wet and warm season is from December to March (Roche et al. 1992). The air temperature during the year, typically varies from 7°C to 12°C, occasionally reaching a low of -2°C in the winter (Gonzales and Roncal 2007) and a high of 20°C in the summer (Pillco Zolá et al. 2019). Warmer temperatures occur typically during the wet season and commonly in February, while cooler temperatures occur in July (Roche et al. 1992). The air temperature is higher in the north compared to the south of the lake due to its proximity to the equator (Gonzales and Roncal 2007). However, the region is also highly sensitive to the El Niño phenomena (Pillco Zolá et al. 2019). From 1966 to 2016,

measured air temperature at the Copacabana meteorological station was recorded higher than the mean daily temperature of 10°C and up to 20°C between 2015 and 2016 due to El Niño phenomena (Pillco Zolá et al. 2019).

Air temperature has been increasing in Peru over recent decades, however, this warming varies regionally (Vicente-Serrano et al. 2018a; Bergmann et al. 2021). It was reported that mean air temperature increased by +0.17°C decade^{-1} from 1964 to 2014 in Peru (Vicente-Serrano et al. 2018a). Air temperature is likely to continue to increase in Peru this century (Bergmann et al. 2021). More specifically, average temperatures in Peru are forecasted to warm by between +0.75-1.50°C and +1-1.75°C by mid-century and the end of the 21st century respectively based on the RCP 2.6 scenario. For the high-emissions scenario (RCP 8.5) it will escalate by +1.0-2.0°C by mid-century and +3.5-6.0°C by the end of the 21st century (Bergmann et al. 2021). Both scenarios were calculated based on the average of four Inter-Sectoral Impact Model Intercomparison Project (ISIMIP) models. Frost or freezing is a common occurrence throughout the TDPS system, however, its frequency varies greatly (Gonzales and Roncal 2007). During the winter (July to August), freezing regularly happens with more frequency (Gonzales and Roncal 2007). However, the lake and the region around it are the less impacted area in the freezing period because of the water regulating effects (Gonzales and Roncal 2007). The regions toward the border of Lake Titicaca basin have over 300 freezing days (freezing day happens when the mean daily temperature is below 0°C) per year whereas the regions surrounding the lake (lower valleys of Ilave, Coata, Ramis, Huancané and Huaycha rivers) and along Lake Titicaca coastline have below 150 freezing days and 100 freezing days per year respectively (Gonzales and Roncal 2007). A mass of cold air arriving from Antarctica enters Peru through the Titicaca plateau, called “friajes” (cold front). This atmospheric phenomenon causes decreasing in temperature for about 3-7 days and it occurs often from May to August. Due to the cold temperatures, people’s health, livestock, and crops in the highlands are affected (Bergmann et al. 2021).

2.3.1.2. Other meteorological variables

Monthly average humidity in the surrounding region of Lake Titicaca fluctuates from 52% to 68%, with a diurnal variation of 33% to 80% between 1966-2011 (Pillco Zolá et al. 2019).

Compared to the southern Altiplano, the Titicaca area has higher humidity (Pillco Zolá et al. 2019). Wind direction is from the northwest to southeast on the lake with a monthly average velocity of nearly 2 m s^{-1} and rarely up to 5 m s^{-1} daily (Pillco Zolá et al. 2019).

The annual sunshine close to Lake Titicaca is 3,000 hours per year in Puno and 2,915 hours per year at Belen (Roche et al. 1992). The minimum and maximum rates are 180 hours during the wet season and 296 hours during the dry season respectively (Roche et al. 1992). The average sunshine hours per day varies between 6 hours in January and 9.6 hours in July (Gonzales and Roncal 2007).

2.3.1.3. Extreme events

ENSO is the most prominent and consequential factor influencing climate variability in Peru (Bergmann et al. 2021). In the Lake Titicaca region, El Niño causes a reduction whereas La Niña leads to an increase in precipitation (Bergmann et al. 2021). According to IPCC (2019), extreme El Niño events will increase in frequency in both low and high-emission scenarios in Peru (Bergmann et al. 2021). Annual temperature change is associated with the ENSO events in the Peruvian Andes (Lavado Casimiro et al. 2012). During the recent decades, the number of warm days (percentage of days when daily maximum temperature is higher than the 90^{th} percentile from the reference period of 1971–2000) has increased by at least double over the period of December to February in northern South America (Feron et al. 2019). The temperature extremes are also associated with the warming trends in Peru (Bergmann et al. 2021). The total number of warm nights (percentage of days when minimum temperature is higher than the 90^{th} percentile from the reference period of 1971–2000) has been escalating while the total number of cold nights (percentage of days when minimum temperature is lower than the 10^{th} percentile from the reference period of 1971–2000) has been declining (Bergmann et al. 2021).

ENSO events also affect the intensity of drought. Severe drought associated with ENSO was recorded in Puno in 1982-1983 and 1997-1998 (Segura et al. 2016). The minimum total precipitation during the summer (December-January-February) in the Altiplano was 11 mm in 1982-1983 (Garreaud et al. 2003). There have been recurring droughts (in 1992 and 2004), floods and frost (in 2001) during the past years in Altiplano (Trigoso 2007). Some authors have

suggested that snow and ice cover might disappear due to global warming in high mountain areas (Hock et al. 2019). This would lead to the reduction of river flow and water availability (Hock et al. 2019). Drought caused losses in livestock, and crops and affected inhabitants. For example, research has provided evidence, that droughts were caused by the strong warm phase of ENSO in 2015-2016, causing losses in agricultural harvests and an increase in food insecurity in Altiplano (Canedo Rosso et al. 2018). The 1983 drought also caused damages of 500 million US$ two years afterwards and affected 1.5 million inhabitants, accounting for approximately 30% total loss of the whole country (Andrade 2018).

2.3.2. Climate change and anthropogenic impacts on Lake Titicaca

Lake Titicaca is used as a sentinel lake to understand climate change impacts by several studies (Cross et al. 2000; Baker et al. 2005). Several studies have investigated changes in lake physics (Aguilar-Lome et al. 2021; Lima-quispe et al. 2021), the effects of chemistry/heavy metal contamination in the area (Duwig et al. 2014; Archundia et al. 2017b; Guédron et al. 2017; Sarret et al. 2019), and the lake's ecosystem (Fritz et al. 2012; Achá et al. 2018).

2.3.2.1. Lake surface water temperature

LSWT in Lake Titicaca typically ranges from 12ºC (dry season) to 17ºC (wet season) (Pillco Zolá et al. 2019; Duquesne et al. 2021). The lake temperature below 40 m depth is constant (Pillco Zolá et al. 2019). The temperature on the surface is 17ºC while it is 12ºC at the bottom during the wet season (Duquesne et al. 2021). During the dry season, the surface water temperature decreases to 12ºC (Duquesne et al. 2021). The lowest temperature occurs in August while the highest temperature occurs in March (Dejoux and Iltis 1992).

Major Lake is warmer in winter and cooler in summer compared to Minor Lake (Dejoux and Iltis 1992). According to Dejoux and Iltis (1992), mean surface temperature in Major Lake was 1ºC lower in summer and 1.5ºC higher in winter than in Minor Lake from 1985 to 1987. Major LSWT ranges from 10.9ºC to 17ºC while the temperature ranges from 8.5ºC to 18.5ºC in Minor Lake (Dejoux and Iltis 1992). In Major Lake, the highest and lowest surface water temperatures are in April and August respectively (Aguilar-Lome et al. 2021). The highest

surface water temperature is in November and the lowest one is in July in Minor Lake (Aguilar-Lome et al. 2021). Minor Lake's surface temperature has a warming trend during winter and reacts to solar and atmospheric radiation faster than Major Lake (Aguilar-Lome et al. 2021). Lake water surface temperature ranges differently with depth and volume (Aguilar-Lome et al. 2021) and it is affected by air temperature and incident radiation (Dejoux and Iltis 1992). The air above the lake is unsteady (Pillco Zolá et al. 2019) as the lake water temperature is higher than the air temperature (Roche et al. 1992; Pillco Zolá et al. 2019). High solar irradiance and low atmospheric pressure result in a lower sensible and latent heat flux ratio than at sea level (Pillco Zolá et al. 2019).

There are still limited studies on Lake Titicaca water temperature and its variability (Roche et al. 1992; Ruiz-Verdu et al. 2016; Aguilar-Lome et al. 2021). Recent research by Aguilar-Llome et al. (2021), using MODIS satellite images, showed that there were increasing trends in Lake Titicaca LSWT in the winter (June-July-August) with a rate of 0.30^{o}C decade^{-1} (daytime) and 0.34^{o}C decade^{-1} (night time) during the period of 2000-2020. It also suggested that the change in air temperature might be the driver for the trends of LSWT. Bush et al. (2010) projected that Lake Titicaca's tipping point will occur between 2040 and 2050. A tipping point refers to a critical threshold in the lake system, beyond which the lake can no longer able to recover its previous state and will eventually disappear due to water volume reduction, loss in biodiversity and ecosystem services disruption. The tipping point requires a temperature rise of +1.5-2^{o}C over the present levels. As a consequence, the region will be irreversibly affected by the loss of the world's highest lake during the next 30 to 40 years (Bush et al. 2010).

2.3.2.2. Stratification and mixing regimes

The Major Lake basin of Titicaca is classified as a monomictic lake (mixing and only stratifying once per year) while the Minor Lake is a polymictic lake (frequently mixing and irregularly stratifying during the year) with seasonal variations (Dejoux and Iltis 1992). Stratification occurs from October to June and is rather weak (Fritz et al. 2012). During winter, mixing is inadequate, especially when the temperature increases (Fritz et al. 2012).

The thermocline primarily sits at a depth of 20-30 m (Duquesne et al. 2021). The temperature gap between the surface and the bottom reduces during the dry season (Duquesne

et al. 2021). A smooth thermal gradient appears and alters the clear thermocline because of the lake's thermal inertia (Duquesne et al. 2021). Thermal inertia helps cool down the water slowly, which keeps the temperature at a medium depth higher than near the surface. Because warmer and less dense water generally rises, temperature inversion drives vertical water movement (Duquesne et al. 2021).

2.3.2.3. Hydrology

Lake Titicaca belongs to the TDPS watershed system (Duquesne et al. 2021). Precipitation, river inflows and groundwater inflows are the major sources of water to Lake Titicaca, which accounted for 55%, 44% and 1% respectively (Gonzales and Roncal 2007). The major output is evaporation (95%) and outflow to the southeastern and feeds the Desaguadero River (5%) (Gonzales and Roncal 2007; Pillco Zolá et al. 2019).

The five major inflowing rivers to Lake Titicaca are Ramis, Coata, Ilave, Huancane and Suchez (Roche et al. 1992), which accounted for 68% of inflow rivers (Dejoux and Iltis 1992), flow directly to the Major Lake (Gonfiantini et al. 2002). Tiawanaku River flows into the Minor Lake from the southern area with an average discharge of 0.5 m^3/s (Gonfiantini et al. 2002). The annual river discharge is 878 mm (233 m^3/s) and happens mostly during the wet season (Lima-quispe et al. 2021). The total river inflow was estimated through a representative area approach based on the Ramis River discharge (Pillco Zolá et al. 2019). The annual discharge flow of Lake Titicaca to the downstream river is 86 mm (23 m^3/s) (Lima-quispe et al. 2021).

The mean precipitation rate is 650 mm/year with a maximum of 800-1,400 mm recorded at the centre of the lake (Gonzales and Roncal 2007). The wet season begins in December and lasts until March, with the wettest month in January (Pillco Zolá et al. 2019). The wet season contains 70% of the annual amount of precipitation (Roche et al. 1992; Delclaux et al. 2007), which is approximately 800 mm/year (Delclaux et al. 2007; Pillco Zolá et al. 2019). The precipitation is low between May and August (Gonzales and Roncal 2007) with the driest month in July (Pillco Zolá et al. 2019). The amount of precipitation is only around 250 mm during the dry season (Delclaux et al. 2007; Canedo et al. 2016). Because of Lake Titicaca's vast surface area and significant lake volume, it is easier to absorb solar radiation (Roche et al. 1992). Hence, the water temperature is higher than in surrounding

regions and it favours convection and causes more storms, especially in the lake centre with annual precipitation of 1,000 mm (Lima-quispe et al. 2021).

Lake water variations have significant implications for water resource management and planning (Mohammadi et al. 2020). Lake level changes depending on the season and on long time scales (Roche et al. 1992). Many climate factors influence lake level changes, including precipitation, evaporation, runoff and interactions between the lake and groundwater (Mohammadi et al. 2020). Climate factors account for about 80% while irrigation accounts for about 20% (Lima-quispe et al. 2021). A slight increase in evaporation or decline in precipitation may cause the lake to become a closed system without outflow (Pillco Zolá et al. 2019). According to Roche et al. (1992), the lowest water level is in December, before the wet season starts while the highest level is in April after the wet season ends and river discharge peaks. In alignment with Roche et al (1992), Chuchón et al (2017) also showed that the water level maximum and minimum levels are in April (~3,810.2 m) and in December (~3,809.5 m) respectively.

There are several studies have investigated water level changes in Lake Titicaca (Abbott et al. 1997; Cross et al. 2000; Abarca-Del-Rio et al. 2012; Chuchón and Pereira 2017; Mohammadi et al. 2020; Lima-quispe et al. 2021). Lake Titicaca's water level has declined below the outlet threshold during the past few years (Pillco Zolá et al. 2019). During the period of 1965-2011, the mean water level was 3,808.1 m, which is approximately 1 m higher than the outlet threshold (Pillco Zolá et al. 2019). Chuchón et al (2017) used meteorological data from 1914 to 2014 to analyze lake water level and the effects of precipitation, ENSO and PDO on the lake water level. Lake water peaked at 3,812.5 m (December 1986) during the rainy season between 1985 and 1986 (Chuchón and Pereira 2017). This event caused floods and disruptions in several areas around Lake Titicaca, prompting the Peruvian government to request international assistance (Chuchón and Pereira 2017). The lowest water level was recorded during the 1940s due to the recurring El Niño events from 1936 to 1943 (Chuchón and Pereira 2017). Lake water level declined by 6 m between 1933 and 1944 while it decreased by 4.2 m during the period 1986-1997 (Chuchón and Pereira 2017). Three periods of water level fluctuations associated with extremely high evaporation were March-December 1943, April 1963- December 1970 and April 1986-December 1996 (Chuchón and Pereira 2017). A study by Abarca-Del-Rio et al (2012) also analyzed Lake Titicaca's water level using different

satellite altimetry data from 2000 to 2009. Their results showed that Lake Titicaca's water level declined by 0.26 m/year between 2001 and 2004 (Abarca-Del-Rio et al. 2012). These changes in water level also affect the outflows to the Desaguadero River and Lake Poopó water level in downstream, which is sensitive to climate changes and Lake Titicaca input due to its shallowness (Lima-quispe et al. 2021).

A study by Rowe et al. (2004) highlighted that El Niño events result in less precipitation therefore it leads to lower lake levels (Rowe and Dunbar 2004). The positive (negative) phase of PDO has been associated with the Niño (La Niña) event, positive (negative) sea surface temperature anomalies and negative (positive) precipitation anomalies which resulted in the decline (rise) in Lake Titicaca water level (Ronchail et al. 2014; Chuchón and Pereira 2017). It was reported that the lowest water level happened in 1944 due to the consecutive years of El Niño events (Lima-quispe et al. 2021). Zola et al. (2019) emphasized that Lake Titicaca may turn to a closed system without outflow if the water level declines below the outlet threshold and evaporation rises or precipitation drops. From 1997 to 1998, the water level dropped below the Desaguadero River discharge in some months (Lima-quispe et al. 2021). As a result, it affected discharges to the Desaguadero River discharge and Lake Poopó water level and it posed a threat to water demand, especially for agriculture activities (Lima-quispe et al. 2021).

2.3.2.4. Lake chemistry and biology

Lake Titicaca has low seasonal variability in physical and chemical water properties and it has a stable lake environment (Dejoux and Iltis 1992). Except for the rainy season from December to March, and those areas near the mouths of the main tributaries (Ramis, Coata, and Ilave Rivers), the water chemistry is generally consistent throughout seasons and sites (Monroy et al. 2014). The pH values range from 8.55 to 8.65 and 8.3 to 8.6 in Minor Lake and Major Lake, respectively (Dejoux and Iltis 1992). The pH in Major Lake is slightly lower than in Minor Lake because of increased phytoplankton photosynthetic activity and the abundance of benthic macrophytes (Dejoux and Iltis 1992). Chloride, sulfate, and sodium ions are mainly found in lake water. Silica values range from 0 to 2.6 mg/l with a mean value of 1.8 mg/l (Dejoux and Iltis 1992), and the concentration is lower than the limitation for diatom growth (Fritz et al. 2012). Silica concentration is high with values between 0.2-1.8 mg/l in the first 5 m depth in

Minor Lake, while it remains low at a depth of less than 5 m (Dejoux and Iltis 1992). The lake is nitrogen-limited with a 3:1 ratio of dissolved inorganic nitrogen and soluble reactive phosphorus (Fritz et al. 2012). Nitrate (NO_3^-) and ammonia (NH_3) values were 3.5 µg/L and 2.5 µg/L, respectively, in Major Lake (Fritz et al. 2012). The ratio of dissolved inorganic nitrogen and soluble reactive phosphorus value was between 3 µg/L and 24 µg/L during the stratified period and deep mixing in Major Lake, respectively (Fritz et al. 2012). The trace elements of boron, iron, lead, chromium, manganese, aluminium, lithium and arsenic were also found in the lake (Dejoux and Iltis 1992).

Lake Titicaca has diverse fauna, including approximately 60 bird species (e.g., the Titicaca flightless grebe (*Rollandia microptera*), egrets, waterfowl) (Monroy et al. 2014), more than 20 species of fish (Miller et al. 2010; Monroy et al. 2014), and 18 amphibian species (e.g., the endemic Titicaca water frog *Telmatobius coleus*) (Monroy et al. 2014). Furthermore, lake water connects with a variety of streams and associated wetlands and is an ideal area for terrestrial vertebrates such as camelids, deer, and rodents (Miller et al. 2010). The current algal flora is mostly accounted for by chlorophytes (43-57%), cyanophytes (10-12%), and diatoms (27-39%) (Fritz et al. 2012). Diatom mainly occur during isothermal mixing, whereas biomass is significantly decreased when mixing is not as deep (Fritz et al. 2012). During the vertical mixing period, phytoplankton and zooplankton are both transferred to the surface (Duquesne et al. 2021), resulting in an increase in the phytoplankton concentration (Duquesne et al. 2021). There are 26 fish species that have been recorded in Lake Titicaca (Miller et al. 2010; Monroy et al. 2014). The killifish genus *Orestias* (> 20 species) and the catfish genus *Trichomycterus* (2 species) are dominant (Loayza et al. 2022). *Orestias* is a small species with a length < 5 cm, while *Trichomycterus* is bigger, with a length of 12-19 cm (Miller et al. 2010). *Orestias* has been observed consuming a diverse range of aquatic resources such as algae, macrophytes, zooplankton, amphipods, etc (Miller et al. 2010). *Orestias* can be caught along the high-altitude lakes and tributary streams in Peru, Chile and Bolivia (Gammons et al., 2006). *Trichomycterus* consumes organic remains as well as a variety of native benthic macroinvertebrates (Miller et al. 2010). *Trichomycterus* was reported near extinction, and the abundance is very scarce (Gammons et al., 2006). Two species of non-native and commercial fish, rainbow trout (*Salmo gairdneri*) and pejerrey (*Basilichthyes bonariensis*) were introduced to Lake Titicaca in 1942 and the 1950s, respectively. These non-native fishes consume insects, crustaceans, and small fish (Gammons et al. 2006). The rainbow trout population has plunged because of overfishing

and has migrated to other tributaries of Lake Titicaca (Gammons et al. 2006). On the contrary, pejerrey has grown sharply and become an essential food source for inhabitants and a famous food among tourists (Gammons et al. 2006). The pejerrey can be caught near the shore and open water of Lake Titicaca (Gammons et al. 2006).

Minor Lake has higher Chl-a concentrations compared to Major Lake (Ruiz-Verdu et al. 2016; Duquesne et al. 2021), with the highest values recorded nearest to the shoreline (Ruiz-Verdu et al. 2016). Mean Chl-a values derived from Landsat-8 in August 2013 for Major Lake and Minor Lake were 3.80 ± 0.24 µg/L and 4.80 ± 0.18 µg/L, respectively (Ruiz-Verdu et al. 2016). Duquesne et al (2021) mentioned that biomass levels were 5-36 times higher in Minor Lake than in Major Lake between 1985 and 1987. Macrophytes (mostly *Characeae spp.*) account for over 60% of the total biomass in Minor Lake and colonise one-third of its bottom (about 436 km^2) at depths ranging from 2 to 15 m (Guédron et al. 2017). Phytoplankton blooms happen during the rainy season with the supply of increased river nutrients (Ruiz-Verdu et al. 2016).

2.3.2.5. Extreme events

The magnitude and frequency of extreme events (heavy precipitation, drought) are projected to increase in the central Andes, especially in the Lake Titicaca region (Achá et al. 2018). During the wet season (December-March), there will be an increase in precipitation, whereas during the dry season, precipitation will decline (Achá et al. 2018). Heavy precipitation will move more nutrients, contaminants and organic matter from runoff (Achá et al. 2018). It may result in changes in phytoplankton communities and lead to harmful algal blooms, and carbon cycling (Achá et al. 2018).

The lake level is affected by extreme events such as drought or heavy rainfall (Lima-quispe et al. 2021). A strong increase in inflow to Lake Titicaca in the second half of the 1980s was due to heavy precipitation during several continuous years (Gonzales and Roncal 2007). Hence, the water level escalated gradually and inundated thousands of hectares in the floodplain area. For instance, in 1986, the heavy precipitation caused an inundation of 48,000 hectares (Gonzales and Roncal 2007). Heavy precipitation peaked in 1986-1987, resulting in

the highest recorded lake water level and causing floods along the Desaguadero River, Lake Uru-Uru and Lake Poopó (Gonzales and Roncal 2007).

Drought could also cause serious economic and social issues in the TDPS region, affecting agricultural activities and domestic water use. Historical records indicated that drought occurred in the region from 1982 to 1983 and from 1989 to 1990 (Gonzales and Roncal 2007).

2.3.2.6. Socio-economy impacts

There have been numerous studies to investigate Lake Titicaca water quality, some focusing on the influence of anthropogenic activities (Duwig et al. 2014; Archundia et al. 2017b) and others on heavy metal contamination (Gammons et al. 2006; Archundia et al. 2017a; Guédron et al. 2017; Achá et al. 2018; Sarret et al. 2019). Additionally, prior research reported water pollution in the Lake Titicaca areas, such as in the inner of Puno Bay (Rieckermann et al. 2006). The shallow areas of the lake have been the most polluted areas and those most subject to algal bloom in recent years (e.g., Puno Bay and the Major Lake). Specifically, due to the anthropogenic activities upstream, the southeastern section of Lake Titicaca is often impacted (Duquesne et al. 2021). Principal sources of contamination (mercury and heavy metals) in the lake are mining activities and wastewater discharges (Gammons et al. 2006; Guédron et al. 2017; Duwig et al. 2014). Gammons et al (2006) used different types of fish muscle tissues to analyse mercury (Hg) contamination in Lake Titicaca. Their results showed that Hg concentration surpassed the United States Environmental Protection Agency fish tissue-based water quality criterion level of 0.30 µg/g for pejerrey and Karachi fish. They concluded that mining activities upstream (Ramis River) could be the source of high Hg concentration in the lake (Gammons et al. 2006). Guédron et al. (2017), however, took a different approach and argued that Hg levels were not as serious as reported from previous studies and are in the lowest range when compared to other large lakes in the world. Mercury concentrations found in the fish muscle around the coastal areas of Major Lake are below the regulated health parameter values (Guédron et al. 2017). However, no prior studies have examined Hg contamination in the Minor Lake area, which is the most productive region and is also affected by anthropogenic impacts (wastewater discharges from agricultural, industrial and domestic activities) (Guédron et al. 2017). The level of Arsenic in the lake has also been found to exceed the World Health

Organization (WHO) drinking water limits (Duwig et al. 2014). Arsenic concentration and other metal concentrations (Cd, Zn and Ni) are also high in rivers upstream (Duwig et al. 2014).

The environmental pressures on the lake will probably increase in the future due to the human population rising around the lake area (Duquesne et al. 2021). Such contamination adversely affects the aquatic biota and the entire ecosystem of the lake (Duquesne et al. 2021). Many species have been affected due to these contaminations, especially some native species such as the iconic frog *Telmatobius coleus* (Duquesne et al. 2021). Therefore, the authorities should develop solutions to reduce the increase of emissions and the impacts of human activities to prevent the eutrophication and heavy metals input into the lake (Guédron et al. 2017).

In summary, understanding Lake Titicaca's LSWT variability is critical for assessing the environmental and ecological impacts of climate change on this lake.

2.4. Application of Satellite Earth Observations for LSWT Dynamics Analysis

To measure LSWT, researchers have traditionally relied on in situ observations. While these measurements may obtain temporal variability as well as provide information on decadal scale alterations in LSWT, they face challenges in spatial coverage and data consistency due to the limited number of in-situ data and in vast areas. Satellite Earth Observation (EO) data provides the ability to get over these limitations. Satellite EO data can provide both temporal and spatial coverage, especially in large and remote regions. Additionally, Satellite EO offers a grid of temperature data, each averaged over a certain area of the lake's surface (Hook et al. 2003; Oesch et al. 2005). Numerous available sensors for obtaining the LSWT data are Advanced Very High-Resolution Radiometer (AVHRR), Moderate Resolution Imaging Spectroradiometer (MODIS), ENVISAT/AATSR and Sentinel-3/SLSTR.

Gaps remain an issue in satellite images. These gaps can be caused by many factors, including cloud cover, errors in data transmission, or changes in the satellite sensors' orbits. Satellite image analysis might be distorted by missing data. Therefore, filling gaps is a fundamental step in processing satellite data. Several studies have implemented different gap-filling methods that can reconstruct satellite images, especially in marine satellite observations (sea surface temperature, Chlorophyll-a). Stock et al. (2020) compared ten different algorithms

to impute Chlorophyll-a satellite data in marine, showing that Data Interpolating Empirical Orthogonal Functions (DINEOF), ordinary Kinging and spatiotemporal Kriging algorithms reconstructed well across four study areas (Stock et al. 2020). Machine learning is also a common gap-filling method, such as Boosted regression tree (Kraemer et al. 2020) or Neural Networks (Ouala et al. 2018; Barth et al. 2022). The next chapter presents the evaluation of several gap-filling methods from classical methods, such as EOF-based techniques DINEOF, to more complex ones, such as machine learning algorithms, to reconstruct missing LSWT data in Lake Titicaca (Peru-Bolivia).

III. Evaluating gap-filling techniques for satellite-derived surface water temperature: A case study of Lake Titicaca[1]

3.1. Introduction

Lakes are essential components of the Earth system, playing significant roles in global hydrological and biogeochemical cycles (Busker et al. 2019; An et al. 2022). They provide essential ecosystem services, including fisheries, energy production, water supply, recreation, tourism, and biodiversity support (Schallenberg et al. 2013; Sterner et al. 2020). However, the resilience of lake ecosystems is increasingly threatened by climate change (Thayne et al. 2023; Han et al. 2024). Surface water temperature is among the key parameters influencing lakes. It affects, among other things, lake metabolism (Dillon et al. 2010; Kraemer et al. 2017b), carbon cycling (Tranvik et al. 2009; Åberg et al. 2010), and the balance and composition of aquatic species (Jeppesen et al. 2012; Dokulil et al. 2021). Additionally, lake surface water temperature (LSWT) is intricately linked to physical dynamics, including vertical mixing and thermal stratification (Wells and Troy 2022), which have profound implications for lake ecosystem health (Huot et al. 2019; Weyhenmeyer et al. 2024). LSWT also substantially influences regional weather patterns by regulating energy and mass exchange between a lake and the atmosphere (Balsamo et al. 2012; Thiery et al. 2014; Huang et al. 2019). Understanding energy exchange and the impacts of climate change on lakes thus requires a comprehensive understanding of LSWT, which has been designated as an Essential Climate Variable by the Global Climate Observing System (GCOS 2022).

LSWT is primarily driven by a combination of external factors, including solar radiation, air temperature, and wind speed (Edinger et al. 1968; Livingstone 2003; Magee et al. 2016; Schmid and Köster 2016). Solar radiation is often considered a dominant source of heat input, particularly in tropical systems, with its intensity and duration directly influencing the thermal dynamics of lake surfaces (Henderson-Sellers 1986; Livingstone and Imboden 1989; Fink et al. 2014; Schmid and Read 2022). Air temperature, closely linked to regional and global climate patterns, also plays a crucial role; higher air temperatures generally lead to increased lake surface temperatures (Livingstone and Lotter 1998; Austin and Colman 2007;

[1] The submitted article: *Dinh, D. A., McCarthy, V., Jennings, E., Jordan, S., Kraemer, B. M., Barth, A., Carrea, L., Simis, S., Liu, M., & Woolway, R. I. (2026). Evaluating Gap-Filling Techniques for Satellite-Derived Surface Water Temperature: A Case Study of Lake Titicaca* is based on this chapter. Dieu Anh Dinh is the first author and would like to thank all co-authors for their contributions.

O'Reilly et al. 2015; Niedrist et al. 2018). Wind patterns affect surface water temperature by promoting mixing and heat distribution within the lake (Horn et al. 1986; Desai et al. 2009), with stronger winds enhancing vertical mixing and potentially disrupting thermal stratification (Boehrer and Schultze 2008; Woolway et al. 2017b; Woolway et al. 2019). Precipitation and inflow from rivers and streams can also introduce cooler or warmer water into lakes, further influencing their thermal regime (Eyto et al. 2016; Rooney et al. 2018; Doubek et al. 2021). Additionally, water clarity significantly affects LSWT by determining the depth to which solar radiation can penetrate (Persson and Jones 2008; Heiskanen et al. 2015). Reduced water clarity, often caused by higher concentrations of chlorophyll-a (Chl-*a*) (e.g., due to algal blooms), is another important factor, which can lead to greater absorption of heat in the upper layers of the water column, increasing LSWT (Jones et al. 2005; Rinke et al. 2010). Warmer LSWT can also stimulate algal growth, which further reduces water clarity (Williamson et al. 2015; Rose et al. 2016), creating positive feedback (Paerl and Huisman 2008).

Conventional approaches to investigating LSWT have primarily relied on in situ observation (Livingstone and Dokulil 2001; Hampton et al. 2008; Leoni et al. 2019; Kangur et al. 2022). While these measurements can provide highly accurate data and the best opportunity to obtain depth-resolved temperature, their spatial coverage is often limited to point measurements (Lieberherr and Wunderle 2018; Carrea et al. 2023). Additionally, deploying and maintaining in situ sensors across large spatial scales is labour-intensive and costly, making it challenging to obtain comprehensive datasets for extensive regions (Pekel et al. 2016; Papenfus et al. 2020). Satellite Earth Observation (EO) offers a solution to these limitations by providing broad spatial coverage and frequent temporal observations (Schneider and Hook 2010; MacCallum and Merchant 2012; Tong et al. 2023; Korver et al. 2024). Recent studies have used satellite EO data to explore global lake thermal responses to climate change (Schneider and Hook 2010; Woolway and Merchant 2018; Maberly et al. 2020) and to examine intra-lake variations in surface water temperature (Mason et al. 2016; Woolway and Merchant 2018; Fichot et al. 2019). By leveraging satellite sensors, researchers can now gain a more complete and dynamic understanding of LSWT patterns and their implications for lake ecosystems and climate interactions (Piccolroaz et al. 2024).

Despite the advantages of satellite EO for observing LSWT, there are notable limitations. One significant constraint is that optical and thermal satellite EO data contain gaps, providing only a partial view of a lake at any given time (MacCallum and Merchant 2012).

Data gaps can arise due to various factors, including cloud cover, which obstructs the satellite view of the lake surface, sensor malfunctions, and orbital limitations that prevent full coverage (Sirjacobs et al. 2011). Cloud cover generally causes complete data loss for optical sensors but may result in partial attenuation, biases for thermal sensors and inaccurate atmospheric correction (Pekel et al. 2016). Additionally, high cloud frequency significantly limits the long-term changes in lake extent monitoring, as optical sensors maybe partially or entirely obstructed from detecting the target lakes (Feng et al. 2023). These limitations pose challenges for researchers conducting long-term and comprehensive studies of LSWT dynamics.

Efficient and accurate gap-filling is often a fundamental and an essential step in processing and analysing satellite-derived information on LSWT. Accurate gap-filling techniques need to ensure that the data are comprehensive and reliable, enabling researchers to better understand temporal trends and spatial patterns. Effective gap-filling is crucial for maximizing the utility of satellite-derived LSWT data. Various methods have been proposed to gap-fill satellite data, especially for the marine environment (Beckers and Rixen 2003; Hilborn and Costa 2018; Yan et al. 2023), including for sea surface temperature and Chl-*a* (Alvera-Azcárate et al. 2007; Stock et al. 2020; Barth et al. 2022). In the context of lakes, different approaches have also been applied, ranging from linear interpolation (Schwab et al. 1999) to the use of machine learning approaches (Kraemer et al. 2022). Linear interpolation achieved Root Mean Square Differences of 1.1-1.76^{o}C for LSWT in the Great Lakes (Schwab et al. 1999). Kraemer et al. (2022) applied Boosted Regression Tree method to reconstruct missing Chl-*a* data in lakes globally and resulted in the median predicted residual error sum of squares of 0.35 μg L^{-1}. The Data Interpolating Empirical Orthogonal Functions (DINEOF) has been employed to reconstruct LSWT data for a substantial number of lakes (MacCallum and Merchant 2012). DINEOF was used to fill data gaps for nighttime LSWT in Lake Malawi and Lake Winnipeg, resulting in the mean difference of 0.08 ± 0.28 K and 0.29 ± 0.55 K (with a maximum difference up to 2 K) respectively (MacCallum and Merchant 2012). However, despite these advancements, no study has yet systematically compared the different gap-filling approaches for lake temperature, which is crucial to identify the most effective methods for accurately reconstructing satellite EO-derived lake data.

In this study, we investigate and compare several gap-filling methods to reconstruct missing LSWT data. We explore classical techniques, including the Empirical Orthogonal Functions (EOF)-based method (Beckers and Rixen 2003; Alvera-Azcárate et al. 2005), as well

as machine learning algorithms such as Boosted Regression Trees. We implemented the Data Interpolating Convolutional Auto-Encoder (DINCAE) method, which has been previously applied to marine data (Barth et al. 2020; Barth et al. 2022) but has not yet been used for LSWT reconstruction. Additionally, we include in our assessment a multivariate DINCAE, which fills gaps in LSWT using both LSWT and Chl-*a* data, leveraging the correlation that oftentimes exist between surface temperature patterns and Chl-*a* in aquatic environments (Alvera-Azcárate et al. 2007; Kraemer et al. 2017a; Bouffard et al. 2018). This multivariate approach aims to enhance the reconstruction of LSWT by incorporating information from related variables. DINCAE univariate and multivariate reported RMSE of 0.55ºC and 0.54ºC respectively for reconstructing gaps in the Adriatic Sea (Barth et al. 2022). Here, we focus on LSWT observations from Lake Titicaca (Peru-Bolivia), the largest freshwater lake in South America, as a case study for our work. Lake Titicaca plays an important role in ecology, economy (agricultural and industrial activities, domestic water uses) and the environment (Pillco Zolá et al. 2019; Zubieta et al. 2021). Its unique high-elevation location makes it particularly sensitive to climate change, including shifts in both temperature and hydrology. The lake has highly sparse in situ data availability, emphasizing the necessity for precise remote sensing based estimates of surface properties. Using the new gap-filled data, we analyse changes in the temporal and spatial characteristics of LSWT in Lake Titicaca, contributing valuable insights to both scientific understanding and practical applications in lake monitoring and climate research. Our objective is to identify the most suitable and accurate reconstruction methods for LSWT, thereby improving the reliability and utility of satellite-derived LSWT data in similarly vulnerable aquatic ecosystems across the world.

3.2. Materials and Methods

3.2.1. Study site

(Please refer back to Chapter 2 section 2.3).

3.2.2. Materials

In this study, we analyse satellite EO data available from the European Space Agency Climate Change Initiative Lakes (ESA CCI) project v.2.0.1, which contains data on LSWT and Chl-*a*

concentrations for over 2000 lakes worldwide (Carrea et al. 2023). The satellite EO data are available at a daily temporal frequency and a spatial resolution of 1/120 degrees (~1 km^2 at the equator). Satellite-derived LSWT data are available from 1995 to 2020, and Chl-*a* data for Lake Titicaca are available between 2002 and 2020. LSWT was derived from several satellites including ERS-2, Envisat, Metop-A/B. MODIS-Terra and Sentinel-3A/B. Chl-*a* data was derived from three satellites, Envisat, MODIS-Aqua and Sentinel-3A/B. Due to the low density of observations from 1995 to 1999 (<10% of total observations) (Fig. A1; Fig. A2), we only analysed data available between 2000 and 2020 in this study; in total, there were 7671 daily LSWT observations for Lake Titicaca during this period. Additionally, Chl-*a* data from 2002 to 2020 was used as auxiliary data for the application of DINCAE multivariate method only (see details below). In post-processing the satellite EO data, a lake boundary mask for Lake Titicaca (CCI lake id = 20) was extracted from the dataset. Low-quality pixels in the LSWT dataset (defined by a quality flag ≤ 3) were removed as suggested by Carrea et al. (2023). This flag threshold indicates the level of data reliability and is commonly applied in remote sensing studies to ensure the use of reliable data for analysis. In addition to this flag, the quality control process for both LSWT and Chl-*a* data involved other standard measures, such as the removal of data affected by cloud cover, sensor errors, or extreme geographic location outliers. For the Chl-*a* data, pixels with uncertainty values > 60% were removed (Free et al. 2022). Additionally, Chl-*a* values outside the range of ±2 times the standard deviation from the mean Chl-*a* concentration were removed. The uncertainty of the Chl-*a* data varied spatially within the lake (Fig. A3). Several external factors such as sun angle, lighting conditions, and lake turbidity can also influence Chl-*a* measurement quality. These variables were not explicitly addressed in this study but represent important considerations for future work and potential preprocessing steps. The dataset was then resampled from a 1 km to 4 km spatial resolution using bilinear interpolation method (Zhang et al. 2021). This resampling was chosen to reduce processing time and minimise the memory usage. The workflow of our analysis is shown in Fig. A4.

3.2.3. Methods

The time series data was split as follows: 60% training data, 20% validation data and 20% test data. The training and validation data were used to tune and find the optimal hyperparameters. The clouds were added to the test dataset by applying cloud masks extracted from 50 images

into another 50 images. This test dataset was not involved in the model reconstruction process and was only used for evaluating the model performance.

3.2.3.1. Data Interpolating Empirical Orthogonal Functions (DINEOF)

The DINEOF optimized EOF-based technique was first introduced by Beckers and Rixen (2003). It uses EOF analysis, acquires the eigenvalues and eigenvectors, defines the optimal EOF modes for the dataset via a cross-validation process, and through an iteration procedure missing data is reconstructed (Yang et al. 2022). DINEOF can be used to reconstruct univariate data (e.g., Chl-*a* or surface water temperature) (Hilborn and Costa 2018; Han et al. 2020; Stock et al. 2020; Jiang et al. 2022; Lomelí-Huerta et al. 2022) and multivariate data (Chl-*a* and surface water temperature) (Alvera-Azcárate et al. 2007; Sirjacobs et al. 2011). DINEOF is commonly used in oceanography and has been applied to datasets at various timescales from < 1 year to > 10 years as well as with varying temporal frequencies (Hilborn and Costa 2018). This technique has been applied to fill LSWT gaps for 258 lakes from 1995 to 2009 and for a later version, an attempt was made for more than 1000 lakes with the European Space Agency ARC-Lake project (MacCallum and Merchant 2012).

DINEOF works with a two-dimensional matrix (mxn) where the spatial and temporal mean is removed from the data. The missing pixels are replaced by zero.

$$X = USV^T$$

where: X- two-dimensional matrix, U- the spatial pattern of EOFs, V- the temporal pattern of EOFs, S- the singular values.

The first EOF is computed by the singular value decomposition (SVD) method and used to replace the missing value. This procedure is repeated and continued with the second EOF, third EOF,….*p*EOFs until user-defined convergence. The missing data is then reconstructed by the truncated EOF modes.

$$X_r = U_p S_p V_p^T \quad (p=1 \ldots k)$$

where: X_r- reconstructed matrix, U_p- the mxp matrix with p columns containing the 1st p spatial EOFs, V_p- the nxp matrix with p columns containing the 1st p temporal EOFs, S_p- the pxp matrix containing the 1st p singular values.

The optimal number of EOFs is determined by cross-validation technique by checking with normally 3% of valid selected data at the beginning of the process. The root mean square of error (RMSE) between the original and reconstructed data is calculated in each EOF mode. The optimal EOFs for reconstruction are chosen with the lowest values of RMSE. The reconstruction will be performed again based on the optimal EOF mode until convergence is reached. We used the R package *sinkr* (Taylor et al. 2013) to apply the DINEOF method to our data. We also used the *rtsa* package in R (Filipponi et al. 2018) to process the data. LSWT was demeaned prior to applying DINEOF in order to improve DINEOF performance and avoid overfitting. After running DINEOF, mean LSWT was added back to the reconstructed data.

3.2.3.2. Multi-model gap-filling approach

Our multi-model gap-filling method, as detailed by Kraemer et al. (2020), integrates three distinct models: linear regression model, generalized additive model, and Boosted Regression Tree (BRT). This method follows a sequential approach, where the residuals from the simpler models, such as linear regression model, are fed as response variables into the subsequent, more complex models. Specifically, the residuals from the final model (BRT) are linearly interpolated over time for each combination of latitude and longitude pairs. The final gap-filled dataset is generated by combining the predicted values from each model with these interpolated residuals, resulting in a comprehensive and robust interpolated dataset.

The first model in our approach is the linear regression model, which serves as the baseline by capturing simple linear relationships between the predictors and the response variable. A simple linear regression model (LM) equation is as follows:

$$y=\alpha+\beta x+\varepsilon$$

where: y- the dependent variable values; α – intercept; x- the independent variable values; β – the coefficient for x; ε – the error term.

The lm() function in R is utilized to fit linear models. While linear regression model is effective for extrapolating straightforward relationships, it may not adequately capture more complex, nonlinear patterns in the data. To address these limitations, a generalized additive model is used next. Generalized additive model (GAM) equation is as follows:

$$y= \beta_0 + f(x_1) + \varepsilon \, , \, \varepsilon \sim N(0,\sigma^2)$$

where: y- the response variable; β_0- the intercept; $f(x_1)$- the smooth function of the predictor x_1; ε – the error term. This formula indicates that smooth function f now makes up the linear predictor's contribution.

Generalized additive model extends the traditional linear model by incorporating both parametric components and user-defined smooth functions of the predictors (Hastie 2023). This allows the generalized additive model to model nonlinear relationships while still retaining linear elements where applicable. GAM is an extension of the generalized linear model (GLM) where the linear predictor is composed of a traditional parametric component and user-defined smooth functions of the predictors (Hastie 2023). In R, the "gam" function in the *mgcv* package is commonly used to fit gam. GAM in *mgcv* uses penalized regression spline as a smooth function. Modelling complex relationships involving numerous predictors is mainly owing to the smooth terms in GAM, which can involve any number of covariates. The sum of all splines forms a GAM (Hastie 2023). To further refine the gap-filling process, we employ the BRT model as the final step in our sequence.

BRT, a member of the classification and regression tree family, utilizes boosting algorithms to iteratively enhance prediction accuracy. The BRT model grows decision trees in a stagewise manner, capturing complex interactions and nonlinear relationships that may not be adequately addressed by linear regression model and generalized additive model (Elith et al. 2008). BRT contains regression tree from classification, decision tree group of models and boosting algorithms. Decision tree is a statistical model that uses a set of rules to divide the predictor space into rectangles. The goal is to identify regions with comparable responses to predictors and give each region a constant value. The constant in regression trees represents the mean response, whereas it represents the most likely class in classification trees. Prediction errors are minimized through the selection of predictors and split points. Expanding the decision tree requires recursively applying binary partitions until a stopping criterion is satisfied. It is typical to first grow a large tree and then prune it by removing the weakest links, identified through cross-validation so that an effective decision tree can be created. Boosting is a type of "functional gradient descent" for regression issues. By adding a new tree that best decreases the loss function at each step, the numerical optimization technique known as "boosting" aims to minimise the loss function. The first regression tree maximally declined the loss function for the selected tree size. Each subsequent step focuses on the residuals, specifically the variation in the response (Elith et al. 2008).

The BRT model uses a stagewise approach for tree growth. A new tree is fitted to the residuals of the preceding tree in each step. Each additional tree may use a different set of variables and split points from the one before it. Each time a new tree is added, the model is updated, and the residuals for the revised model are computed. This procedure is repeated repetitively. The model grows without changing the existing trees. To account for the contribution of the newly added tree, only the fitted value for each observation is re-estimated at each step. The final BRT model was built by a linear combination of numerous trees which are numbered from hundreds to thousands. It can be thought of as a regression model in which each term is a tree (Elith et al. 2008).

LM and GAM are used first for the extrapolative parts of the interpolation function effectively. Nonlinear components and interactions are not adequately captured by LM and GAM, therefore, BRT is used as the final model. The multi-models result in a fine extrapolation performance of LM and GAM combined with fine details in the predicted and response variable interactions. BRT performance is influenced by several tuning parameters, including the bag fraction and tree complexity. The bag fraction, calculated based on the minimum number of data rows, helps mitigate the influence of outliers. While an increase in bag fraction results in more stable but potentially overfitted models, a decrease in bag fraction uses less data in each tree, making the model robust against outliers but possibly less stable. A tree complexity of 4 was chosen to account for strong interactions between variables. Higher tree complexity values can capture complex relationships but might overfit the data, lower values provide simpler models but might neglect significant variable interactions. The learning rate, bag fraction and tree complexity were optimized using the training and validation dataset. In this study, the generalized additive model and BRT models were implemented in R using the *mgcv v1.8* (Wood 2011) and *gbm v2.1.8.1* (Ridgeway 2007) packages, respectively.

3.2.3.3. Data Interpolating Convolutional Auto-Encoder (DINCAE)

The DINCAE algorithm, developed by Barth et al. (2020), was initially designed to reconstruct sea surface temperature observations by leveraging a convolutional neural network architecture. Unlike DINEOF, which relies on an EOF analysis, DINCAE is particularly adept at modelling non-linear spatial and temporal relationships within datasets, making it effective for reconstructing missing data (Yan et al. 2023). This approach is especially valuable for

filling gaps in incomplete satellite observations and estimating reconstruction errors, which require the optimization of a non-quadratic cost function (Han et al. 2020). DINCAE has been extensively applied in previous studies to address data gaps in satellite imagery (Han et al. 2020; Jung et al. 2022; Luo et al. 2022; Yan et al. 2023). The most recent iteration, DINCAE 2.0, was developed in the Julia programming language (Barth et al. 2022), allowing the use of non-gridded data as input. However, in the current study, we employed the earlier Python-based multivariate model as outlined by Han et al. (2020), as the features introduced in version 2.0 are not needed in this work. We used DINCAE to (i) reconstruct missing LSWT using available LSWT observations, and (ii) reconstruct LSWT from a multivariate perspective, integrating both LSWT and Chl-*a* data. We refer to this method as DINCAE multivariate. For this method, Chl-*a* concentrations were normalized using the natural logarithm (ln). It is important to note that, to our knowledge, the DINCAE algorithm has not previously been applied to reconstruct missing satellite data specifically for LSWT. This study, therefore, represents an initial exploration into the use of DINCAE for this purpose. DINCAE was implemented in Python (version 3.7) (Van Rossum and Drake Jr 1995).

The DINCAE process consists of three phases: data pre-processing phase, training phase, and reconstruction phase. During the data pre-processing phase, the input variables follow the implementation of Barth et al. (2020). The input data is a 4-dimensional tensor where different parameters are included in the so-called channel dimension (Table 3.1).

Table 3.1. List of input variables for DINCAE and DINCAE multivariate

No	Input parameters
1	LSWT anomalies scaled by the inverse of the error variance (the scaled anomaly is zero if the data is unavailable)
2	Inverse of the error variance (zero if the data is unavailable)
3-4	Scaled LSWT anomalies and inverse of error variance of the previous day
5-6	Scaled LSWT anomalies and inverse of error variance of the next day
7	Longitude (scaled linearly between −1 and 1)
8	Latitude (scaled linearly between −1 and 1)
9	Cosine of the day of the year divided by 365.25
10	Sine of the day of the year divided by 365.25

11	ln(Chl-*a*) anomalies scaled by the inverse of the error variance (the scaled anomaly is zero if the data is unavailable)*
12	Scaled ln(Chl-*a*) anomalies of the previous day*
13	Scaled ln(Chl-*a*) anomalies of the next day*

*used only in DINCAE multivariate

An encoder and a decoder are the two essential components of a convolutional auto-encoder model. A pooling layer (down-sampling layer) and a convolutional layer form the encoder. A convolutional layer and an upsampling layer form the decoder (Luo et al. 2022). For each minibatch, some valid data values are marked as missing in order to assess the training effect (test data) while the remaining data is used for training data. The structure of DINCAE contains five parts: input data, encoding layers, fully connected layers, decoding layers and an output (Han et al. 2020).

- Input data includes the training dataset and the test dataset.

- The encoding layers resemble the singular value decomposition (SVD) in DINEOF, which may lower the input data dimensions and reduce the computational complexity of neural networks. A convolutional layer's function is to extract the features from the input data; the depth of the convolutional layer, often referred to as the "convolution kernel size," determines the quantity and size of these features. The convolution kernel size used by DINCAE is 3x3. Pooling layers are used after convolutional stages to keep the average value of 2x2 boxes while reducing the size of the convolution layers.

- A fully connected layer functions is similar to a hidden layer in an auto-encoder, allowing a nonlinear combination of extracted features. In this algorithm, N/5 (rounded to the closest integer) and N, where N is the number of neurons in the final pooling layer.

- The decoding layer comprises of convolutional and nearest neighbour interpolation layers. In order to capture small-scale features that are lost in the encoding layers and fully connected layers, the interpolation layers are skip-connected to the pooling layer output.

- Output data consists of the mean and standard deviation of the Gaussian probability distribution function of the reconstructed data and the average input data used to calculate anomalies.

The Gaussian probability distribution function was added to optimize the model. Two dropout layers, which randomly deactivate the neural units in fully connected layers (take out 30% of neurons) to avoid overfitting. This approach, like Gaussian distribution function, was only employed in the training phase and was deactivated during the reconstruction phase (Yan et al. 2023). Regularization and activation techniques are also applied in DINCAE algorithm to avoid overfitting. The Adam optimizer contains a regularization algorithm. The regularization adds a weighting factor to the loss function to minimize model complexity and overfitting (Han et al. 2020). The activation function, which is used to improve the model's nonlinear fitting ability, is commonly utilized after the fully connected layer and convolution layer (Yan et al. 2023). The leaky rectified linear unit (RELU) is defined as:

$$f(x) = max(x, \alpha x)$$

where α=0.2. This function can help the gradients decrease too quickly.

During the training phase, the input dataset was randomly mixed (across the time dimension) and separated into mini batches of 50 images, resulting in an array size of 10 x 55 x 83 x 7671 and 13 x 55 x 83 x 7671 (number of inputs x longitude x latitude x time steps) for DINCAE and DINCAE multivariate respectively. The entire time series was divided into 153 mini batches of 50 images each and one final minibatch of only 21 images. The inverse of the error variance value is either 0 (for missing data) or a constant. Because this constant will be multiplied by a weight matrix, which will be enhanced through network training, its exact value is not essential. The hyperparameters used to train DINCAE in this study remain the same as the setup of DINCAE. For training the model, grid search was used to tune the hyperparameters. DINCAE runs a total of 100-300 iterations (hereafter referred to as "epochs"), resulting in a reconstructed dataset every 10 epochs. The drop-out rate ranges from 0.1-0.3 with the learning rate of 1×10^{-4}, 1×10^{-3}, 1×10^{-2}. The optimal hyperparameters for DINCAE are epochs= 200, dropout rate= 0.3 and learning rate= 1×10^{-3} and for DINCAE multivariate are epochs= 300, dropout rate= 0.3 and learning rate= 1×10^{-3}. The result was averaged for the final reconstruction output.

3.2.3.4. Validation and analysis

To estimate the accuracy of the gap-filling methods described above, the correlation coefficient (r), bias, Root Mean Square Error (RMSE) and Mean Absolute Error (MAE) were used. This

evaluation was used to calculate the reconstructed pixel values (i.e., only for the pixels where artificial gaps were introduced) and the corresponding true pixel values from the original images. A lower RMSE, MAE, bias and higher r indicate the closer the reconstructed method resembles the original values.

$$r = \frac{\sum(Xori,i - \bar{X}ori)\,(Xrec,i - \bar{X}rec)}{\sqrt{\sum(Xori,i - \bar{X}ori)^2}\,\sqrt{\sum(Xrec,i - \bar{X}rec)^2}} ; \bar{X}ori = \frac{\sum_{i=1}^{n} Xori,i}{n} ; \bar{X}rec = \frac{\sum_{i=1}^{n} Xrec,i}{n}$$

$$\text{Bias (K)} = \sum_{i=1}^{n} \frac{(Xrec,i - Xori,i)}{n}$$

$$\text{RMSE (K)} = \sqrt{\frac{\sum_{i}^{n}(Xrec,i - Xori,i)^2}{n}}$$

$$\text{MAE (K)} = \frac{1}{n}\sum_{i=1}^{n} |\,Xrec,i - Xori,i|$$

where n is the number of samples, $X_{ori,i}$ and $X_{rec,i}$ are the values of the original images at index i and the reconstructed images at index i respectively.

The validation was performed in Python. In this study, trends were calculated using Sen's slope to estimate the slope and the Mann-Kendall test to determine *p*-values, implemented using the *trend v1.1.4* package (Pohlert 2023a) in R (version 4.2) (R Core 2022).

3.3. Results

3.3.1. Satellite-derived observations of LSWT and Chl-*a*

Satellite-derived LSWTs from Lake Titicaca were often incomplete, containing substantial gaps during the period of 2000-2020 (Fig. 3.1). The availability of LSWT data varied widely throughout the study period, with the highest annual coverage observed in 2015, where about 45% of the lake's surface had available data. In contrast, 2001 had the lowest coverage, with data available for only 10% of the lake's surface. Notably, between 2013 and 2016, LSWT data were available for approximately 40% of the lake surface, but coverage was particularly sparse between 2000 and 2006, with less than 20% of the lake's surface observed. In contrast, satellite-derived Chl-*a* data, available from 2002 onward, exhibited greater data sparsity. The lowest coverage occurred in 2003, with only 8% of the lake surface observed. The year 2019 had the most comprehensive Chl-*a* observations, covering about 30% of the lake surface. The period from 2016 to 2020 had the highest density of Chl-*a* observations, with coverage exceeding

20%. However, a substantial gap in Chl-*a* data occurred between 2012 and 2015, due to the absence of optical satellite data (MERIS and OLCI).

Spatially, the LSWT dataset reached a maximum observation count of approximately 3,000 observations per cell, which represents less than half of the potential maximum (n = 7,671) over the study period. The availability of Chl-*a* data, with around 2,000 observations per cell, was more limited. Observation density also varied across the lake surface, with higher concentrations in open-water regions and fewer observations near the shore. Chl-*a* observations were also more frequent in Minor Lake compared to Major Lake (Fig. 3.1).

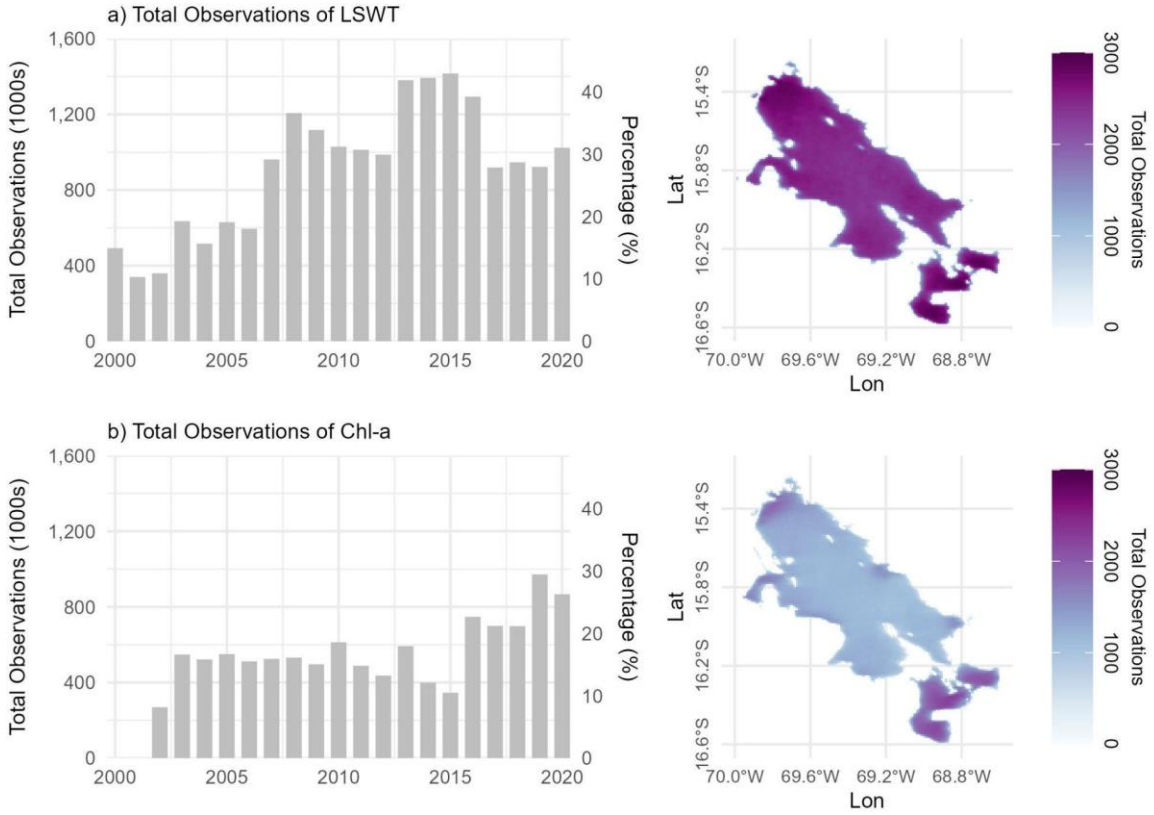


Figure 3.1. Total number of annual (a) LSWT and (b) Chl-*a* observations, both temporally and spatially in Lake Titicaca during the study period (2000-2020). The percentage was calculated based on the ratio of observed or available pixels to the total potentially available pixels over 365 days in percentage.

Temporal analysis further highlighted the variations in data availability. LSWT observations peaked at about 400 per month from April to September (Fig. 3.2), whereas Chl-*a* observations reached a maximum of 300 per month from May to August (Fig. A5). Both

datasets showed a decrease in observations from October to March, with LSWT data decreasing from 250 to 100 and Chl-*a* data remaining below 150 during these months. Additionally, there was a clear seasonal pattern, with more observations during the dry (April-November) than the wet (December-March) season (Fig. A6). The highest LSWT observation counts were around 3,000 in the dry season and 500 in the wet season, while Chl-*a* counts were 1,900 and 400, respectively.

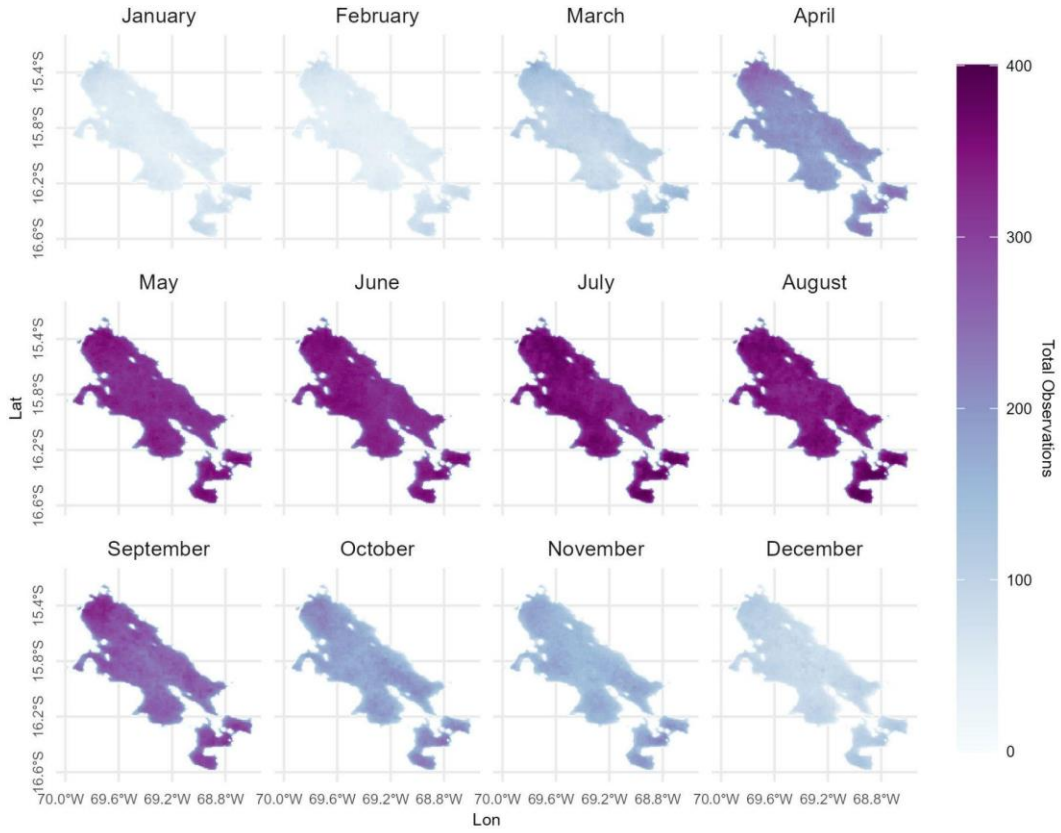


Figure 3.2. Monthly observations, per 4 km^2 pixel, of LSWT from 2000 to 2020 in Lake Titicaca. Observation counts ranged between 0 and 400 per cell monthly.

It is important to note that Chl-*a* data was primarily used as auxiliary information in the DINCAE multivariate approach. Specifically, during periods when LSWT observations were missing, Chl-*a* data helped supplement the gap-filling process (Fig. A7-A9). The observed discrepancy between the gaps in LSWT and Chl-*a* data arises due to differences in the sensors and retrieval algorithms used for each variable. Furthermore, the data processing and quality control protocols differ for each dataset.

3.3.2. Comparison of gap-filling methods

We applied each of our gap-filling methods to the test dataset and evaluated which gap-filling method provides optimum performance. An example, a mostly cloud-free day (21/04/2017), with artificial gaps, as well as the reconstructed images, are shown in Fig. 3.3a-f. BRT showed overfitting artefacts while DINEOF, DINCAE univariate and multivariate resulted in smooth images. DINCAE univariate and multivariate performed well and clearly detected land and water pixels as it effectively depicted the islands in the northwest of the lake, including Amantani and Taquile and Isla del Sol in the east.

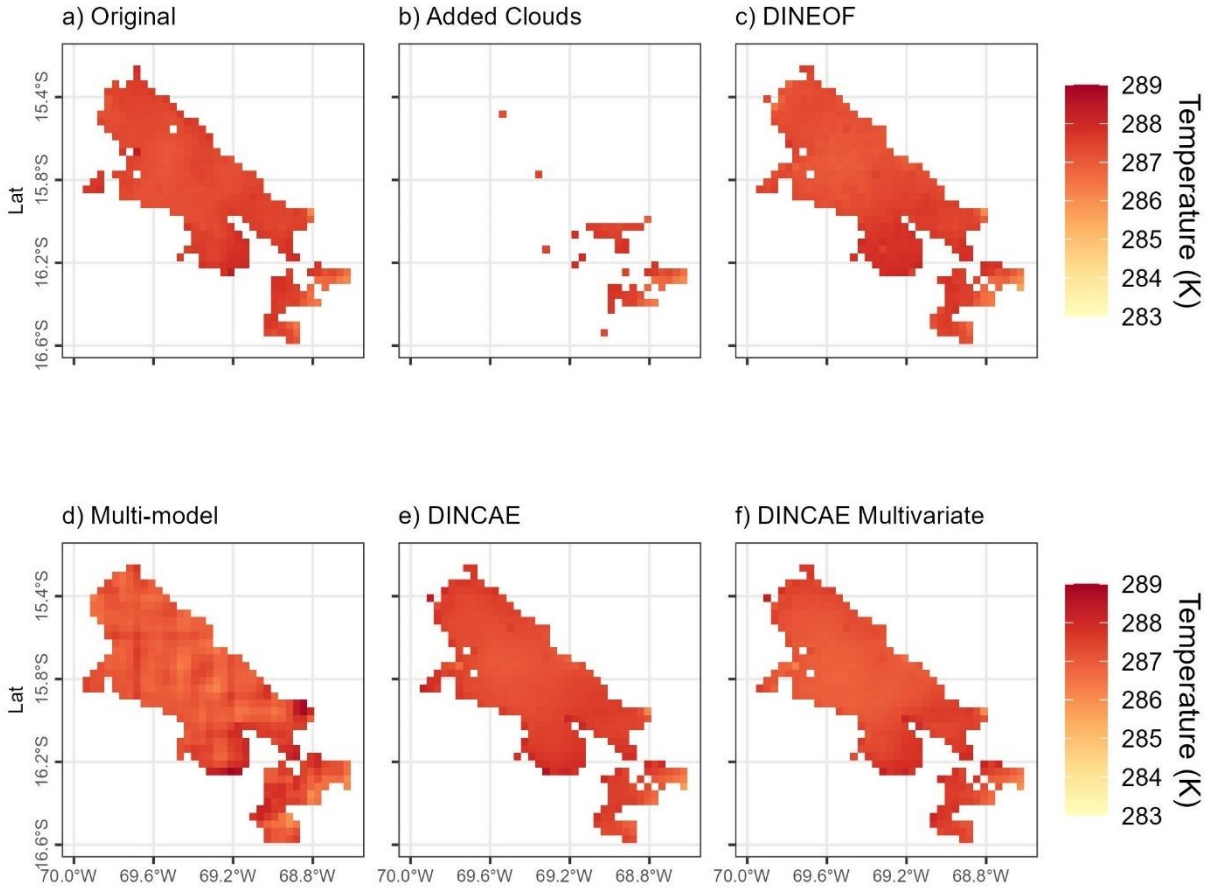


Figure 3.3. Examples of a) Original, b) Added clouds, as well as the reconstructed images (c-f).

Among the gap-filling methods tested, the DINEOF method had the highest RMSE of 0.57 K, MAE of 0.34 K, with low correlation r = 0.81 and high bias of -0.09 K (Fig. 3.4a). The multi-model method had lower RMSE, MAE, higher r and lower bias than those of the DINEOF (RMSE = 0.36 K, MAE = 0.26 K, r = 0.91, bias = -0.04 K) (Fig. 3.4b). DINCAE multivariate and DINCAE univariate performed best and most consistently among the different

gap-filling algorithms tested (Fig. 3.4c-d). DINCAE multivariate recorded a slightly lower RMSE of 0.25 K compared to DINCAE with RMSE of 0.27 K. Both DINCAE methods had the same MAE of 0.19 K and r = 0.95. Thus, our analysis indicates that there was a minor improvement when using the DINCAE multivariate method, i.e., which also considered spatial patterns in Chl-*a* when reconstructing LSWT. This improvement can be attributed to the relationship between LSWT and Chl-*a*, particularly in certain months of the year (Fig. A10 and Fig. A11).

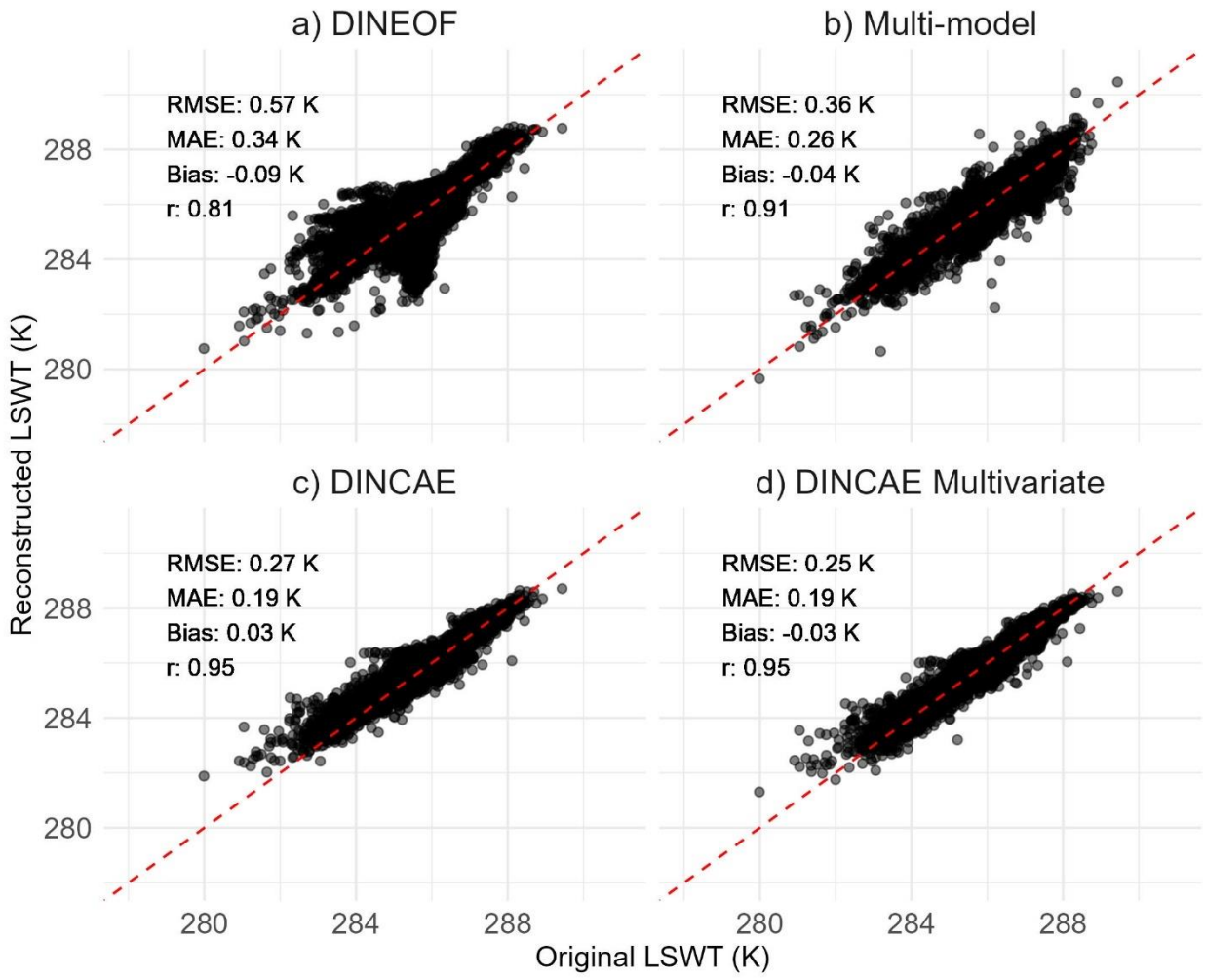


Figure 3.4. Comparison of the tested gap-filling algorithms in reconstructing LSWT in Lake Titicaca, shown in scatter plots of observed and predicted LSWTs. The red lines denoted the 1:1 line.

3.3.3. Spatial and temporal variations in LSWT

The annual LSWT pixel-wise variability in Lake Titicaca derived from the gap-filled data varied from 284.9 K to 289.1 K from 2000 to 2020 (Fig. 3.5a). The range in LSWT in the wet season (Fig. 3.5b) was 286.8 K to 289.1 K, being higher than the LSWT during the dry season (Fig. 3.5c), which ranged from 284.9 K to 286.9 K. In terms of Lake Titicaca's monthly thermal characteristics (Fig. 3.5d), LSWT was lowest (around 285 K) during the Southern Hemisphere winter (June-August) and highest during Southern Hemisphere summer (December-February), with a LSWT of around 287.8 K. Using the gap-filled data, we also calculated the inter-annual variability of LSWT between 2000 and 2020 (Fig. 3.5e). The annual average lake-mean (i.e., averaged across the lake surface) LSWT ranged from 286.6 to 286.9 K. Annual LSWTs peaked at approximately 287 K in 2010 and 2016. Interannual LSWT variations showed notable differences between the dry and wet seasons. LSWT during the wet season (287.6 K to 288.1 K) was higher than LSWT during the dry season (286.1 K to 286.4 K). On average, annual average LSWT increased at a rate of +0.04 K decade^{-1} ($p > 0.05$), while LSWTs during the wet and dry season increased at rates of +0.02 K decade^{-1} and +0.05 K decade^{-1} ($p > 0.05$), respectively.

Annual pixel-wise LSWT trends ranged from -0.05 to +0.12 K decade^{-1} across the lake surface, but with the majority of lake pixels (98.9%) experiencing a warming trend during the study period (Fig. 3.5f-h). Warming trends calculated in 4.3 percent of lake pixels were statistically significant (Fig. A12). LSWT trends calculated during the wet season were between -0.02 to +0.12 K decade^{-1} (Fig. 3.5g) while the dry season trend ranged from -0.04 to 0.09 K decade^{-1} (Fig. 3.5h). Warming trends calculated in 1.1 and 21.9 percent of lake pixels during the wet and dry seasons, respectively, were statistically significant (Fig. A12).

Our analysis also suggested that in Major Lake, there was an upward trend in LSWT annually and during the dry season, except for the northwestern area during the wet season. The northwestern region of the Major Lake showed contrasting seasonal LSWT trends. During the wet season, this area showed a cooling trend with a rate of around -0.03 K decade^{-1}, however, this same region experienced a warming trend during the dry season of +0.11 K decade^{-1}. The eastern area of the Major Lake followed a more pronounced warming pattern during the wet season compared to the dry season. In Minor Lake, the western area showed a warming trend while the eastern area showed a cooling trend, except in the wet season.

Statistically significant trends ($p < 0.05$) were mainly observed along the lake shorelines and in the northern areas of the open water during the dry season.

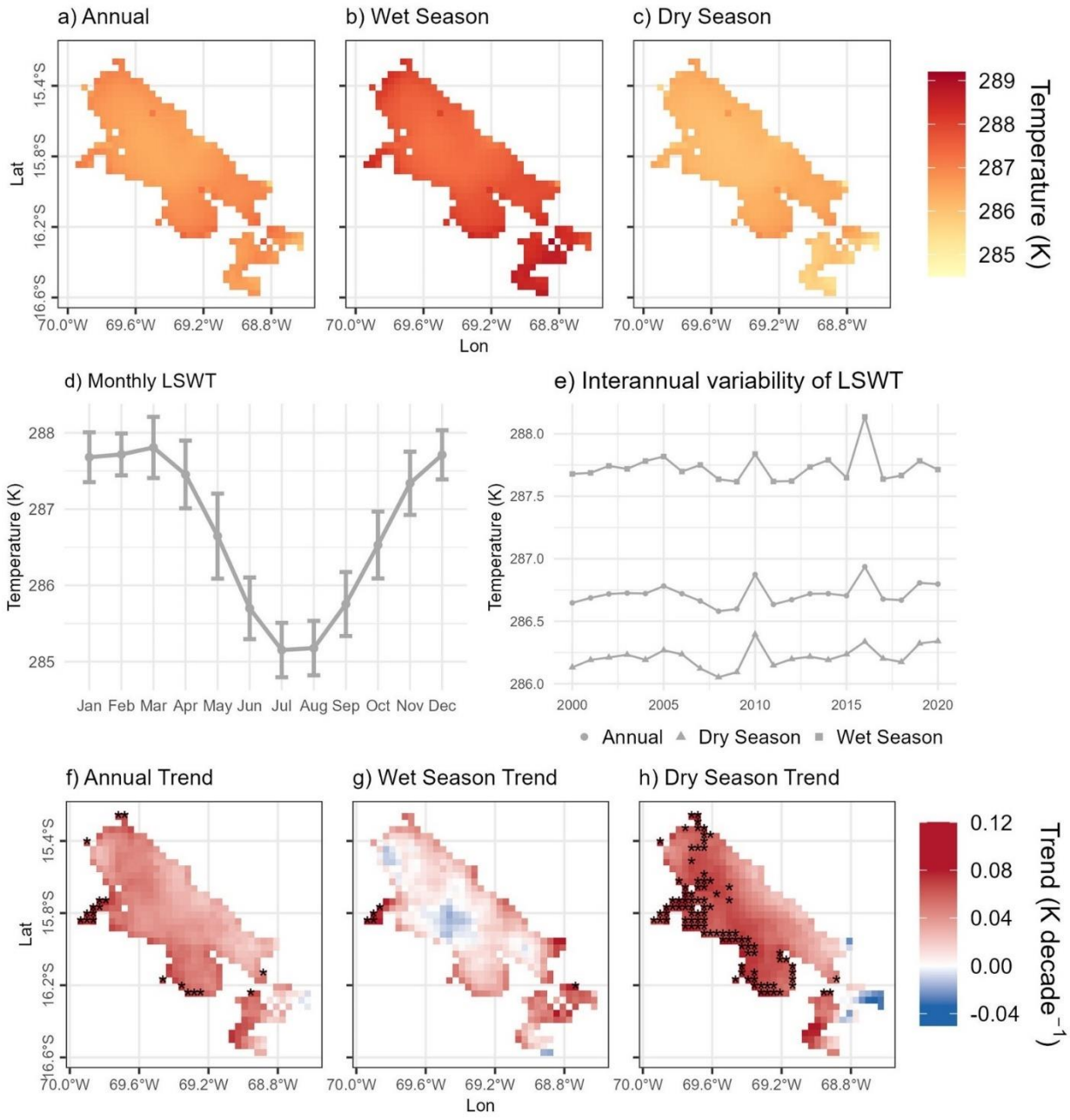


Figure 3.5. Annual, seasonal, and monthly gap-filled LSWTs in Lake Titicaca (2000 to 2020). Shown are the average (a) annual and (b, c) wet/dry season LSWTs throughout the study period, (d) monthly LSWT variations (error bars represent the standard deviation), and (e) the interannual variability in LSWT. Also shown are the LSWT trends, calculated (f) annually and (g, h) during the wet/dry season. The asterisk (*) shows statistically significant trends with $p <$

0.05. The LSWT data used in this analysis are those reconstructed using the DINCAE multivariate algorithm.

3.4. Discussion

Satellite EO data is becoming increasingly used for monitoring and assessing various environmental phenomena, including the impacts of climate change on lakes. These data are especially valuable where in situ monitoring is limited or nonexistent, either due to resource issues or the remoteness of sites. However, satellite images still contain data gaps due to factors such as cloud cover and other atmospheric interference, and the orbit functions and swath width of the satellites involved, which may limit their utility. Filling these gaps is essential in many modelling frameworks used in environmental assessments and decision-making. The key finding of our study of Lake Titicaca is that the DINCAE algorithm, particularly in the multivariate version proposed here, which incorporates Chl-*a* data, outperformed other methods. Specifically, our results indicate that the multivariate DINCAE approach, which accounts for intra-lake variations in both LSWT and Chl-*a*, demonstrates superior accuracy and consistency compared to the other gap-filling algorithms tested for the studied lake. This multivariate approach leveraged the oftentimes correlated dynamics between LSWT and Chl-*a*, enhancing the model ability to reconstruct missing temperature data. The superior performance of DINCAE, particularly when using a multivariate approach, highlights the potential of incorporating auxiliary variables that capture the ecological and physical processes within a lake. By integrating Chl-*a* data in our application, which is indicative of phytoplankton biomass and can influence thermal properties, DINCAE is better equipped to model the complex interactions and variations within the lake environment. Our findings underscore the potential of advanced machine learning techniques, such as DINCAE, in improving the quality of satellite-derived environmental datasets. The enhanced accuracy and consistency achieved by these methods can significantly advance our understanding of lake dynamics, support more robust climate change impact assessments, and inform effective lake management and conservation strategies.

The relationship between LSWT and Chl-*a* concentrations has been widely discussed in the scientific literature (Gerten and Adrian 2002; Boyce et al. 2010; Vasseur et al. 2014; Dokulil et al. 2021) and highlights the interconnectedness of thermal and biological processes

in aquatic environments. Namely, LSWT influences the growth and distribution of phytoplankton (Berger et al. 2007; Rasconi et al. 2015), as warmer temperatures can enhance metabolic rates and promote algal blooms (Paerl and Huisman 2008; Carey et al. 2012; Visser et al. 2016). Conversely, high concentrations of Chl-*a*, indicative of substantial phytoplankton biomass (Kasprzak et al. 2008), can affect the thermal properties of the water column through processes such as shading and the absorption of sunlight (Jones et al. 2005; Rinke et al. 2010). This relationship means that variations in Chl-*a* can provide valuable insights into the spatial and temporal patterns of LSWT (Kong et al. 2021; Thayne et al. 2023). However, it should also be noted that Chl-*a* can sometimes have opposing effects on water temperature in lakes. For example, increased Chl-*a* levels can lead to higher lake temperatures by absorbing more sunlight and heating the water surface (Jones et al. 2005; Rinke et al. 2010). This surface warming can, in turn, contribute to a strengthening of thermal stratification, which can limit the mixing of warmer surface waters with cooler deep waters, potentially leading to higher surface temperatures. Additionally, thermal stratification can limit the upwelling of nutrients from bottom waters (Berger et al. 2010), which can reduce nutrient availability for phytoplankton and consequently lower concentrations of Chl-*a* (Engel and Fischer 2017). Furthermore, darker surface waters, which can arise due to algal blooms (and higher Chl-*a* levels), can lead to greater heat loss at the surface due to increased atmospheric heat exchange (Hocking and Straškraba 1999; Heiskanen et al. 2015). These opposing effects might balance each other out over long time scales, resulting in no noticeable direct relationship between LSWT and Chl-*a* (Bouffard et al. 2018). By incorporating satellite-derived Chl-*a* data, the multivariate DINCAE algorithm can leverage these complex and potentially offsetting correlations to more accurately reconstruct missing temperature data for Lake Titicaca. The algorithm's ability to consider the co-variability of LSWT and Chl-*a* allows it to reconstruct the lake's thermal dynamics more comprehensively, capturing both the direct and indirect effects of phytoplankton on water temperature. This integrative approach is particularly beneficial in addressing the complex environmental processes that drive temperature fluctuations, thereby enhancing the overall quality of the reconstructed LSWT time series. The low correlation between LSWT and Chl-*a* in Lake Titicaca ($r = 0.2$) suggests that incorporating Chl-*a* data into the DINCAE multivariate results only marginal improvements in gap-filling, as evidenced by the small change in our RMSE values. Also, correlation measures only linear relationships, and a linear model is not able to account for the various effects mentioned above.

The correlation of LSWT and Chl-*a* was higher during the wet season compared to the dry season, suggesting that DINCAE multivariate may outperform the univariate DINCAE algorithm during this time of year. However, the statistical significance showed an opposite trend, with higher significance in the dry season and lower significance in the wet season, which may be attributed by cloud cover during the wet season.

One potential limitation of our approach was the exclusion of Chl-*a* observations with high uncertainty, which may have introduced spatial bias and increased gaps in the input series, because the Chl-*a* estimation framework used in the European Space Agency Lakes Climate Change Initiative dataset is based on a priori identification of optical water types, some of which cannot be assessed with the same confidence as others. There is, therefore, a trade-off to consider between allowing data with lower confidence into the reconstruction model to enhance the number of observations and reduce spatial bias, or to strengthen the contribution of the Chl-*a* input variable to the model by selecting results with higher confidence. To maintain the robustness of our analysis, we retained only the data with the lowest uncertainty. However, this fixed thresholding method may have limitations, particularly when data characteristics vary seasonally or across different lake regions. In future work, more adaptive strategies such as using interquartile range (IQR)-based filters or percentile-based thresholds could be explored to better accommodate spatial and temporal variability in Chl-*a* concentrations. These approaches may provide more flexible and context-specific ways to identify and handle outliers. Additionally, the uncertainty threshold could be assessed to determine whether including more uncertain Chl-*a* data may, in fact, improve algorithm performance in terms of representativeness of the reconstructed model. This will require studies to be carried out in the presence of more reference observations across multiple lakes.

By analysing a gap-filled satellite-derived LSWT dataset, we calculated the temporal (annual, seasonal) variations and spatial patterns of LSWT. The annual and seasonal LSWT trends showed variability across different regions of Lake Titicaca. Annual LSWT calculated in our study ranged from 285–289 K, approximately one degree lower than the values reported in the previous study by Pillco Zolá et al. (2019), which likely represent measurements from specific locations within Lake Titicaca, rather than capturing the entire lake. Our results are based on spatially averaged LSWT and this process can reduce peak temperature values and limit extreme variability. Additionally, resampling data to a coarser resolution may have contributed to lower LSWT estimates by averaging out the extremes. Spatial resolution can

impact the accuracy of the reconstructed data, particularly in regions with significant spatial variation, such as lake edges. The resolution may affect the representation of fine-scale features and small-scale processes. It is recommended to investigate the smoothing effect of the resampling and the impact of spatial resolution on model performance in future work. Our findings on wet/dry seasonal temperatures demonstrate that LSWT in the wet season is higher than compared to the annual and dry season LSWT. This can be explained because the wet season aligns with the warmest time of year i.e., when air temperature and solar radiation are highest (Pillco Zolá et al. 2019). In Lake Titicaca, lake-mean LSWT fluctuated between 2000 and 2020, however, we found no statistically significant increasing trend during this period. Our findings on seasonal temperature variations show some differences when compared to earlier studies (Dejoux and Iltis 1992). While our results align with their findings that March experiences the highest temperatures, we observed the lowest temperatures in July and not in August as indicated in their study. However, our results also correspond with other studies, which have shown July to be the driest month (Pillco Zolá et al. 2019; Lima-quispe et al. 2021). As a result, LSWTs in August were only 0.02 K higher than in July. Given that the study periods are different and the variations in the observed periods, this could potentially explain the shift in the lowest temperature month. LSWT trends showed variability across seasons and in different areas of Lake Titicaca. Annual pixel-wise LSWT trends indicated both warming and cooling trends, ranging from -0.04 to 0.12 K decade^{-1}. The observed trends are not statistically significant and may be influenced by reconstruction uncertainty or data variability. Seasonal changes were most noticeable, with the wet season showing a negative trend and the dry season experiencing a strong positive trend in Major Lake. The cooling trend in the wet season could be attributed to an increase in precipitation and/or cloud cover, resulting in a decrease in surface air temperature, solar radiation and cooler LSWT (Rooney et al. 2018). In contrast, specific areas of Minor Lake showed the opposite, with a cooling trend during the dry season and a warming trend during the wet season. The distinct trends found between Major Lake and Minor Lake can be due to their physical characteristics. Major Lake, a monomictic system with a mean depth of 135 m (Dejoux and Iltis 1992), has higher thermal inertia, resulting in more consistent warming trends. Minor Lake, a polymictic system, is shallower with a mean depth of 9 m (Dejoux and Iltis 1992). This shallower part is more sensitive to atmospheric temperature fluctuations and seasonal variations, which results in more variable patterns, such as a cooling trend during the dry season and a warming trend in the wet season. Shallow parts

have a lower thermal inertia due to their smaller volume. The mixing of upper layers brings warm water to the surface, where it loses heat to the cooler air above, resulting in a cooler temperature.

While our study addresses a notable gap in knowledge of gap-filling LSWT data, we emphasize that the optimal gap-filling algorithm may vary depending on several factors, including the specific characteristics of the study area, the intended purpose of the gap-filling, the period covered, and the available data. In this study, we focused on Lake Titicaca, whose unique attributes, such as its considerable size, might influence the efficacy of different gap-filling methods. Consequently, our findings might not be universally applicable. Future research should extend the testing of these gap-filling methods to a variety of lake environments to ensure broader applicability. Smaller lakes, in particular, pose unique challenges due to their limited data availability, necessitating tailored approaches to gap-filling. Furthermore, it is essential to evaluate these methods in lakes with differing trophic states, such as more eutrophic systems, to determine if the gap-filling techniques maintain their accuracy and reliability, and particularly to test the performance of the multivariate gap-filling technique. Eutrophic lakes could pose a notable challenge due to their higher biological productivity and potential for larger temperature variations within the lake. Investigating how gap-filling algorithms perform in these environments will be crucial for a comprehensive understanding and broader application. Additionally, incorporating auxiliary data sources, such as meteorological data (e.g., wind speed), into the gap-filling process holds promise for further enhancing accuracy and applicability across diverse lake ecosystems. The impact of seasonal and interannual variations in LSWT on the effectiveness of gap-filling methods also warrants further investigation. Such variations can significantly influence the thermal dynamics of lakes, and understanding their effects on gap-filling accuracy is crucial for developing robust methodologies. The DINCAE algorithm effectively reconstructs missing observations by leveraging spatial and temporal correlations, which helps mitigate gaps resulting from persistent cloud cover. However, prolonged periods of missing data during high-cloud seasons could introduce biases, particularly if the reconstruction relies heavily on temporal interpolation. Future improvements could involve integrating additional data sources or enhancing the model's ability to handle long-duration gaps. In addition, future studies could consider implementing space-time cross-validation, especially when applying the methodology to other lakes or across broader spatial domains. The integration of advanced remote sensing

technologies and the use of higher-resolution satellite data hold great potential for enhancing the quality of gap-filled LSWT datasets.

3.5. Conclusions

Missing data in satellite EO products can introduce uncertainties and inaccuracies in calculating changes in LSWT. However, the application of gap-filling techniques, such as the DINCAE multivariate method, can help reduce these errors. Although our study did not find a significant correlation between Chl-*a* and LSWT, we demonstrated that the multivariate DINCAE method outperformed other gap-filling approaches for Lake Titicaca, offering marginal improvements over the univariate DINCAE technique. The adaptability of DINCAE methods makes them applicable to a range of lake environments. Expanding the scope of this research to include other geographical regions, such as glacial or shoreline lakes, could provide further validation of these methods. Our findings indicated that LSWT for Lake Titicaca fluctuated between 285 K and 289 K from 2000 to 2020, with a spatially increasing trend over the past 21 years. Spatial and temporal variability in LSWT trends ranged from -0.04 to +0.12 K decade^{-1}, which could be attributed to the specific study period, the lake's physical characteristics, and other meteorological drivers. Further research is needed to investigate additional drivers of LSWT variability, which could provide valuable insights into the dynamics of this critical ecosystem. Understanding these factors will aid in the effective management and conservation of Lake Titicaca and other similar lake environments.

IV. The current and future warming of Lake Titicaca[2]

4.1. Introduction

Lakes are vital global water resources, holding 87% of the Earth's liquid surface fresh water and serving as critical indicators of climate change (Adrian et al. 2009; Verpoorter et al. 2014; Woolway et al. 2020b). Among their numerous attributes, lake surface water temperature (LSWT) is especially important due to the profound impact it has on physical, chemical, and biological processes within lakes (Magnuson et al. 1979; Benson and Krause 1980; Boehrer and Schultze 2008). Changes in LSWT affect lake stratification, gas solubility, and biological productivity, making it a crucial variable for assessing climate impacts (Kraemer et al. 2021; Woolway et al. 2022c). As a result, LSWT is classified as an Essential Climate Variable (ECV) by the Global Climate Observing System (GCOS 2022).

LSWT is influenced by a variety of meteorological factors, including air temperature, solar radiation, wind speed, and humidity (Edinger et al. 1968; Schmid and Read 2022). From 1981 to 2020, global LSWTs have risen at an average rate of 0.24°C per decade, largely reflecting the parallel increase in air temperature (Tong et al. 2023). Solar radiation has also been a significant driver of mean LSWT increases in some lakes (O'Reilly et al. 2015; Schmid and Köster 2016), while wind speed and humidity also contribute greatly to variations in surface water temperature (Andrew et al. 2008; Dias and Vissotto 2017; Woolway et al. 2019). Additionally, LSWT is affected by water colour and clarity; lakes with lower clarity, often associated with higher levels of dissolved organic carbon, typically have higher temperatures (Snucins and Gunn 2000; Edmundson and Mazumder 2002; Persson and Jones 2008). Other physical characteristics of lakes, such as their surface area, depth, and volume (Hostetler 1995; Butcher et al. 2015; Kraemer et al. 2015), as well as their geographical location (e.g., altitude), also influence LSWT variability (Woolway et al. 2017a; Sabás et al. 2021; Vinnå et al. 2021).

In addition to long-term trends in LSWT, lake heatwaves - defined as when LSWTs exceed a seasonally varying 90th percentile threshold relative to a baseline climatological average for a sustained period (Hobday et al. 2016; Oliver et al. 2018)- have also shown notable

[2] The published article: *Dinh, D. A., Tong, Y., Feng, L., McCarthy, V., Jennings, E., Jordan, S., Shi, K., & Woolway, R. I. (2026). The current and future warming of Lake Titicaca. Journal of Great Lakes Research, 102752. https://doi.org/10.1016/j.jglr.2026.102752* is based on this chapter. Dieu Anh Dinh is the first author and would like to thank all co-authors for their contributions.

changes in recent decades (Woolway et al. 2021b; Wang et al. 2023; Wang et al. 2024). As global temperatures rise, the duration and intensity of lake heatwaves have increased (Wang et al. 2023; Zhang and Yao 2023), amplifying the risk of ecological and socioeconomic impacts. These include aquatic species loss and the spread of harmful cyanobacteria, which can compromise drinking water safety (Ho et al. 2019; Till et al. 2019; Tassone et al. 2022; Feng et al. 2024). Given these implications, understanding the historic and future trajectories of lake heatwaves is critically important for mitigating their impacts.

Lakes at lower latitudes, which typically have higher average temperatures (MacCallum and Merchant 2012; Tong et al. 2023; Korver et al. 2024), are particularly sensitive to climatic warming, in terms of not only their thermal stratification characteristics (Kraemer et al. 2015), but also on the impact of climate change on aquatic species (Kraemer et al. 2017a) and biogeochemical cycles (Jansen et al. 2022). Despite experiencing slower rates of surface temperature increase (Schneider and Hook 2010; O'Reilly et al. 2015; Tong et al. 2023), these lakes have shown the most substantial changes in stratification patterns in recent decades (Kraemer et al. 2015; Woolway and Merchant 2019), arising largely from the nonlinear relationship between water density and temperature (Boehrer and Schultze 2008). Additionally, the low seasonality of LSWT in low-latitude lakes means that their surface temperatures can more frequently reach extreme levels, as suggested by the higher frequency of lake heatwave events during the historic periods (Woolway et al. 2022c), which is also projected in the future (Woolway et al. 2021b). Moreover, warmer tropical lakes typically have a lower level of background natural variability, meaning that they can encounter novel thermal conditions earlier, compared to other lakes worldwide (Huang et al. 2024). In turn, low-latitude lakes are considered sensitive indicators of climate change, offering early warnings of the broader impacts of global warming on the ecology of aquatic ecosystems (Kraemer et al. 2017a).

Lake Titicaca, located in the Altiplano region, is recognized as a sentinel lake for studying climate change due to its profound ecological, economic, and environmental significance (Cross et al. 2000; Hampton et al. 2018; Zubieta et al. 2021). The lake has been subjected to substantial nutrient inflows (Monroy et al. 2014; Archundia et al. 2017b; Guédron et al. 2017; Sarret et al. 2019), making water temperature a critical factor affecting its water quality. As the climate warms, local communities are increasingly vulnerable to threats to water security (Duquesne et al. 2021). Comprehensive local research is essential to thoroughly assess these challenges, elucidate the lake's ecological and cultural values, and examine how rising

water temperatures could exacerbate issues that jeopardize community well-being. While recent research has examined historical trends in LSWT and water levels (Abarca-Del-Rio et al. 2012; Aguilar-Lome et al. 2021), there remains a gap in understanding the detailed patterns of LSWT variability and future projections as well as extreme thermal conditions (i.e., heatwave) for this water body. This study seeks to address these gaps by analyzing historical (1981-2020) changes in LSWT and project future LSWT changes from 2021 to 2099 under several climate change scenarios. This research will enhance our understanding of the lake's physical processes and provide critical information for water governance.

4.2. Study Area

(Please refer back to Chapter 2, section 2.3).

4.3. Data and Methods

4.3.1. Data

4.3.1.1. GLAST Dataset

The Global LAke Surface water Temperature (GLAST) dataset was used in this study to investigate the impact of climate change on the surface temperature of Lake Titicaca. This dataset contains LSWT data for 92,245 lakes worldwide from 1981 to 2099 (Tong et al. 2023). The GLAST dataset was derived from Landsat satellite data and numerical modelling in a workflow that was composed of four steps (Tong et al. 2023). The first was to determine the lake centres (defined as the point that lies farthest from the permanent water's shoreline) by using the lake boundaries from the HydroLAKES dataset (v1.0) and water occurrence from the global surface water occurrence dataset (Pekel et al. 2016). Landsat satellite images were then used to retrieve lake surface temperature observations for the lakes based on a statistical mono-window algorithm. The Landsat observations (including Landsat 4, 5, 7, and 8 with a spatial resolution of 60-120 m between 1982 and 2020) were obtained and then used to calibrate the Freshwater Lake model (FLake) (Mironov et al. 2010). Specifically, the calibration dataset (38 years of Landsat data) was used to select optimal model settings at an hourly scale for each lake; the calibrated model was then used to generate daily LSWT (Tong et al. 2023). The European Centre for Medium-Range Weather Forecasts (ECMWF) Re-Analysis v5-Land

(ERA5-Land) hourly dataset (Hersbach et al. 2020) (1981-2020) with a spatial resolution of 0.1^{o} x 0.1^{o} were used as forcing data. The ERA5-Land meteorological variables included air temperature at 2 m (K), shortwave and longwave solar radiation (W m^{-2}), wind speed at 10 m (m s^{-1}), surface pressure (Pa) and specific humidity (kg kg^{-1}). Daily simulated LSWT values were generated for individual lakes. The historical GLAST dataset (1980-2020) was validated using various in situ datasets (LSWT, surface heat flux, evaporation and ice phenology) for several lake types, resulting in an overall median absolute error value at the daily scale of 1.16°C (Tong et al. 2023).

The model was then used to project future LSWTs (2006-2099) for each lake for three Representative Concentration Pathway (RCP) scenarios: RCP 2.6 (low emissions), RCP 6.0 (medium emissions) and RCP 8.5 (high emissions). The future climate forcing data were selected from the Inter-Sectoral Impact Model Intercomparison Project (ISIMIP2b) (Frieler et al. 2017) with four different Global Climate Models (GCMs): GFDL ESM2M, IPSL-CM5A-LR, HadGEM2-ES and MIROC5. The ISIMIP2b dataset had a spatial resolution of 0.5^{o} and a daily temporal resolution (Frieler et al. 2017). The variables of ISIMIP2b used for the future simulation include 2 m air temperature, surface solar and thermal radiation, 10 m wind speed and specific humidity. The historical and future GLAST dataset is freely accessible at https://zenodo.org/records/8322038. In this study, we demonstrate LSWT changes as anomalies, calculated relative to 1981-2006. A positive anomaly represents warmer conditions relative to the reference period, while a negative anomaly indicates cooler conditions.

4.3.1.2. Satellite-derived lake surface water temperature

The European Space Agency Climate Change Initiative (ESA CCI) developed multi-decadal satellite Earth Observation (EO) products for Lake ECVs at a global scale (https://climate.esa.int/en/projects/lakes/). The dataset provides LSWT for over 2000 lakes worldwide from 1995 to 2020 (Carrea et al. 2023) at a spatial resolution of 1/120 degrees grid and a daily temporal resolution. In this study, we used this dataset (2000-2020) to compare with the results from the model-derived GLAST dataset. When analysing the satellite EO data we only included days with high quality levels (shown as quality level 4 and 5). The satellite data was then resampled from a spatial resolution of 1 to 4 km using a bilinear interpolation method and any gaps in the data were reconstructed using the Data-Interpolating Convolutional

Auto-Encoder (DINCAE) method (Barth et al. 2020). This method was recommended by a previous study, which compared various gap-filling methods applied to LSWTs of Lake Titicaca (Dinh et al., personal communication, 2025). We used the gap-filled LSWT data, specifically the lake-mean time series, in this study to validate the LSWT data available from GLAST. We estimated the difference between the satellite data and GLAST data based on the RMSE, MAE, bias and r. These analyses were performed in R (version 4.2). Comparisons between the ESA CCI Lakes and GLAST data are shown in Figs. B1-B3.

The time series of LSWT anomalies from the GLAST dataset (1981-2020) were similar to those derived from gap-filled satellite data (2000-2020) (Fig. B1a-c). The RMSE and MAE between GLAST and satellite-derived data were 0.12 K and 0.10 K, respectively.

4.3.2. Methods

4.3.2.1. Bias correction for future projections of GLAST

The discrepancies between future climate model data and reanalysis data lead to temporal inconsistency between simulated historical results and future projections (Teutschbein and Seibert 2012). To address this issue, we employed five bias correction methods to adjust the future simulations in GLAST dataset, aiming to minimize the model bias by reducing discrepancies during the common period (i.e., 2006-2020). Specifically, five methods were selected, ranging from simple Linear Scaling (LS) to advanced ones including Quantile Mapping (QM), Quantile Delta Mapping (QDM), Scale Distribution Mapping (SDM) and ISIMIP3BASD (more details in Appendix B; Text B1). LS is a simple bias correction technique that uses mean values to adjust modelled data (Maraun 2016). Correction values are calculated based on the difference between the monthly mean of observed and historical climate model data in the same baseline period, then the future climate model values are subtracted by the difference (Maraun 2016). QM adjusts the distributions of observed and climate modelled data (Cannon et al. 2015). QDM and SDM are based on QM and retain the advantages of QM while taking into account the variations of the Cumulative Distribution Function (CDF) across different time intervals. QDM considers the variation between the historical and future simulations. As a result, QDM not only maintains quantile changes but also corrects biases in future simulations by using the CDF (Cannon et al. 2015). SDM is a trend-preserving method, similar to QDM, SDM scaled CDF based on expected absolute changes. Simultaneously, it

modifies the return intervals before the mapping process to change the likelihood of certain events (Switanek et al. 2017). ISIMIP3BASD is a semi-parametric, trend-preserved method based on quantile mapping (Lange 2019; Lange 2021). It creates "pseudo future observations" by adding climate change trends from climate models into observed data using additive or multiplicative approaches (Lange 2019; Lange 2021). ISIMIP used a running window to account for seasonality (Lange 2019; Lange 2021). Both observed and climate modelled data were detrended prior to running ISIMIP3BASD, ensuring that the focus was on bias correction rather than trend adjustment (Lange 2019; Lange 2021).

We evaluated the performance of different bias correction methods over the calibration period (2006-2012) applied to the observed/historical and future projection data, and adjusted the biases for the validation period (2013-2020). Several statistical indices were calculated based on the observations and bias corrected values for the validation period (2013-2020) including Root Mean Square Error (RMSE), Mean Absolute Error (MAE), correlation coefficient (r), and percentage bias (PBIAS). The lower the RMSE, MAE (close to 0) and the higher the r values are, the better the bias correction method. PBIAS was calculated based on the relative volume difference between the future and observed volumes. A positive BIAS value represents over prediction while a negative PBIAS value represents under prediction. These indices are calculated as follows:

$$\text{RMSE} = \sqrt{\frac{\sum_i^n (F_i - O_i)^2}{n}} \qquad (1)$$

$$\text{MAE} = \sqrt{\frac{\sum_i^n |F_i - O_i|}{n}} \qquad (2)$$

$$\text{PBIAS} = 100*\left(\frac{\sum_i^n (F_i - O_i)}{\sum_i^n O_i}\right) \qquad (3)$$

$$\text{r} = \frac{cov(F,O)}{\sqrt{var(F)}var(O)'} \qquad (4)$$

where F and O are the future projected and observed values respectively

The results of the bias correction methods are shown in Appendix B; Table B1. Based on the evaluation, QDM which had the lowest RMSE and MAE, and highest r and PBIAS ~ 0 compared to other methods, was applied to the future projection (2021-2099) with the base historical period of 1981-2020. The bias was obtained on daily values and was implemented in Python using the *ibicus* package (v1.0.1) (Spuler et al. 2023).

4.3.2.2. Attribution analysis

The relative contributions of meteorological variables (surface air temperature, shortwave and longwave downward radiation, specific humidity and wind speed) to historical LSWT trends were quantified using the FLake model. To calculate these contributions, six simulations were performed: one reference simulation that maintained trends across all meteorological variables, and five control simulations where one variable was kept with its long-term trend, while the others were detrended. The detrending process involved replicating the 1981 data over the following 40 years. This approach was used in previous studies (Woolway et al. 2017b; Li et al. 2019; Tong et al. 2023). Detailed model setting information on these simulations is provided in Table B2.

4.3.2.3. Lake heatwaves

Using daily LSWT from GLAST, we identified lake heatwaves following the methods outlined in Woolway et al. (2021) (Schlegel and Smit 2018). Specifically, the heatwave analysis followed these steps: (1) For each calendar day, we calculated the climatological mean and 90th percentile temperature threshold across all years within a climatological period (1991–2020), using an 11-day window centred on each date and smoothing with a 31-day moving average. (2) A lake heatwave was defined as any period during which daily lake surface temperatures exceeded this local, seasonally adjusted 90th percentile for a minimum of five consecutive days. Events separated by fewer than two days were merged as a single heatwave event. For heatwaves spanning two or more calendar years, events were segmented on December 31, setting a maximum duration of 366 days per event. (3) For each heatwave event, we calculated the duration (in days), average intensity (K), and cumulative intensity (K x days), where average and cumulative intensity represent the mean and total temperature anomalies above the climatological mean, respectively. To characterize annual heatwave activity, we aggregated these metrics, including total heatwave days, average duration, average intensity, and cumulative intensity. Annual total days reflect the summed duration of all heatwave events within a year, while annual averages for duration, intensity, and cumulative intensity were computed across all heatwave events for each year.

4.3.2.4. Statistical analysis

The LSWT anomaly for each observation was calculated by subtracting the long-term mean LSWT from the observed temperature, thereby isolating deviations from the average condition. Sen's slope was applied to calculate the magnitude of the LSWT anomaly trend over the study period. This method estimates the slope as the median of all possible slopes calculated between pairs of points, providing a robust measure of the trend. The resulting slope represents the rate of change in LSWT anomalies over time, allowing for the estimation of the overall warming or cooling trend. The non-parametric Mann-Kendall test was used to determine the significance of the trends. Sen's slope estimation and Mann-Kendall test were performed using *trend* package (Pohlert 2023) in R.

4.4. Results

4.4.1. Historical to contemporary temperature changes in Lake Titicaca

LSWT anomalies between 1981 and 2020 fluctuated from -1 K to +1 K, with negative anomalies (cooler conditions) most common between 1981 and 2000, and positive anomalies (warmer conditions) dominant from 2000 to 2020, reflecting the long-term warming trend (Fig. 4.1). LSWT anomalies during the wet season were higher compared to those in the dry season (Fig. 4.1). LSWT anomalies peaked at 0.9 K in the wet season in 1998 while during the dry season, they peaked at 0.5 K (Fig. 4.1). LSWT anomalies increased significantly ($p < 0.01$), both annually (+0.15 K decade^{-1}) and seasonally, with a rate of +0.14 K decade^{-1} during the dry season and +0.16 K decade^{-1} during the wet season. Due to the decrease in annual range, there was a slight change in LSWT variability between the wet and dry seasons (Fig. B5). A comparison of the GLAST and satellite-derived data at monthly and seasonal timescales are shown in Fig. B2 and B3.

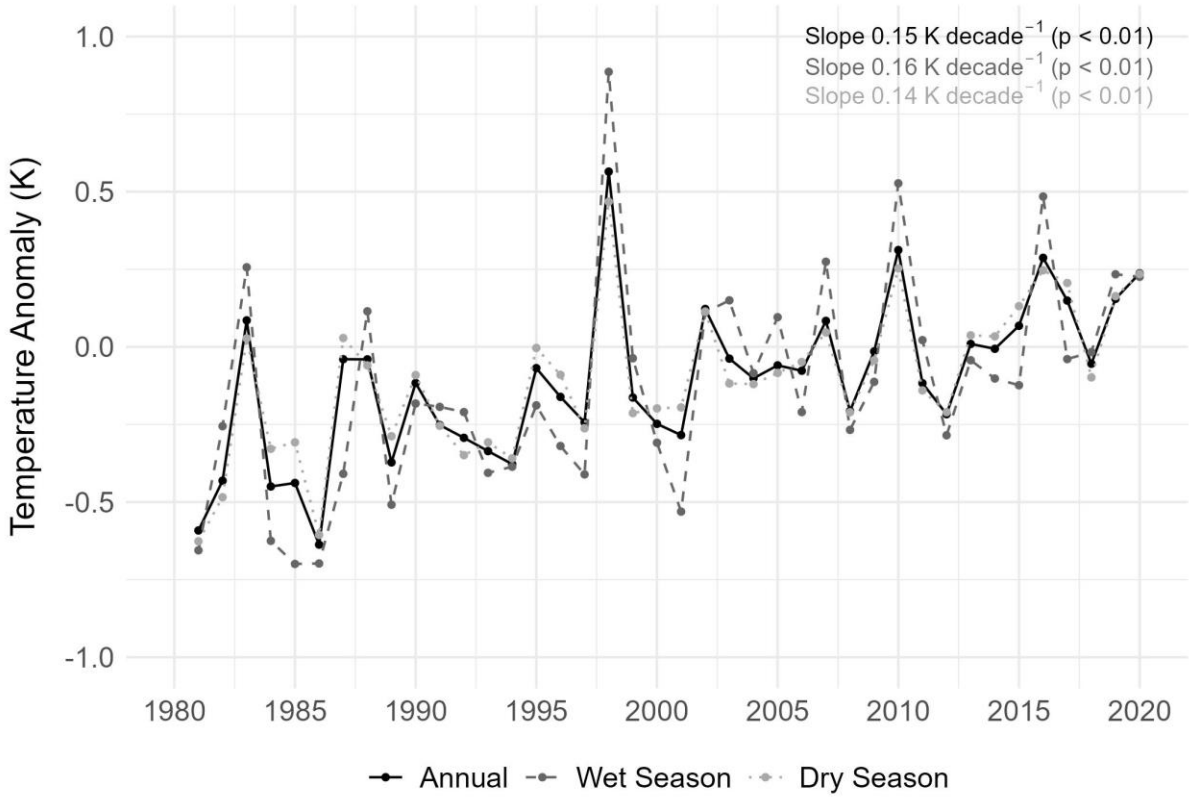


Figure 4.1. Annual temperature (black), wet season temperature (dashed dark grey), dry season temperature (dotted grey) derived from GLAST data from 1981 to 2020, with the trends respectively on the top right.

4.4.2. Contributions of meteorological drivers to LSWT trends

Surface air temperature (SAT) and shortwave downward radiation (SWdown) showed similar contributions among the meteorological variables investigated in this study, to the long-term change in LSWT (Fig. 4.2a). Both drivers contributed +0.06 K decade^{-1} of the simulated change in LSWT (Fig. 4.2a) with the increase in SAT (+0.24 K decade^{-1}) and SWdown (+1.86 Wm^{-2} decade^{-1}) (Fig. B4). Significant contributions were also attributed to changes in specific humidity (SH) (+0.03 K decade^{-1}) and longwave radiation (LWdown) (+0.005 K decade^{-1}) (Fig. 4.2a). In contrast, wind speed (WindSpeed), which had increased in the study region during the historic period (+0.04 ms^{-1} decade^{-1}) (Fig. B4), had a cooling effect on LSWT (-0.02 K decade^{-1}) (Fig. 4.2a).

The main driver of LSWT during the dry season was SWdown, which contributed +0.07 K decade^{-1} to the LSWT trends (Fig. 4.2b). SAT and SH were also attributed +0.06 K decade^{-1} and +0.03 K decade^{-1} respectively to the long-term changes in LSWT (Fig. 4.2b). In contrast to the dry season, SAT was the main factor influencing the LSWT trends during the wet season, contributing +0.07 K decade^{-1} (Fig. 4.2c). SWdown also contributed to increasing LSWT trends (+0.05 K decade^{-1}) along with SH (+0.04 K decade^{-1}) and LWdown (+0.01 K decade^{-1}) during the wet season (Fig. 4.2c). Similar to the annual long-term change in LSWT, wind speed had a negative influence in both dry and wet seasons (-0.01 K decade^{-1} and -0.02 K decade^{-1} respectively).

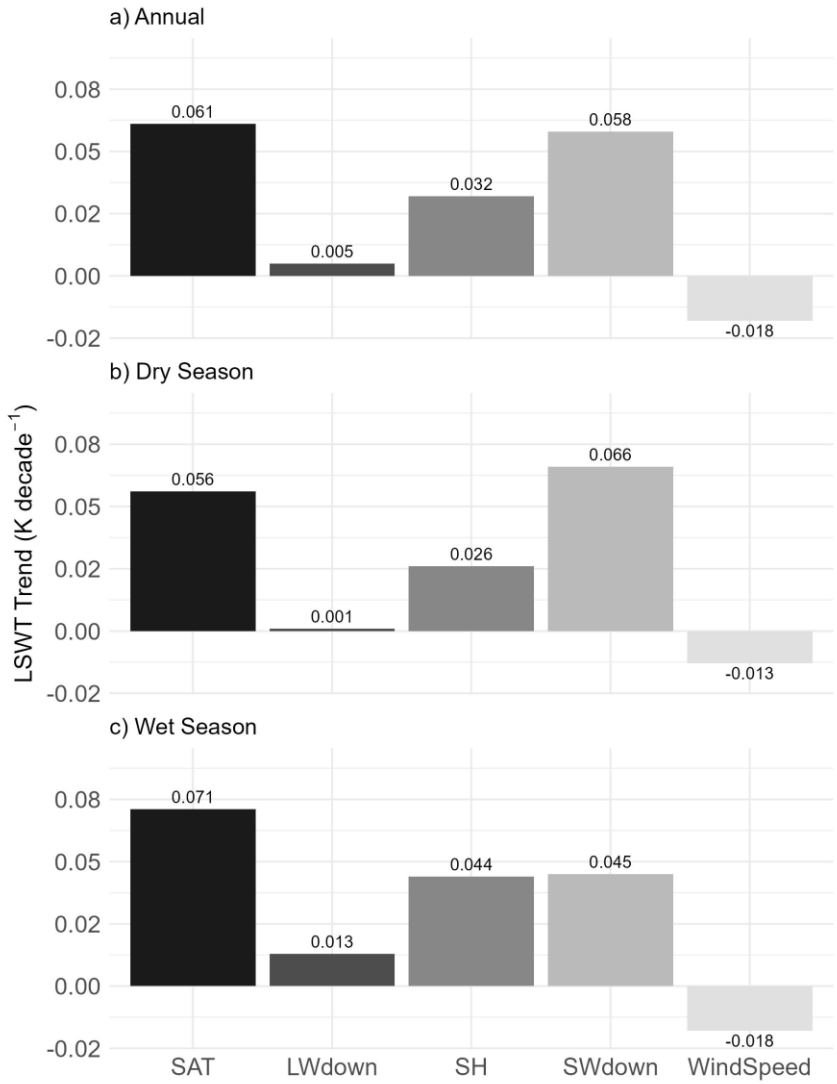


Figure 4.2. Contributions of meteorological variables (SAT- Surface Air Temperature, LWdown- Longwave Downward Radiation, SH- Specific Humidity, SWdown- Shortwave

Downward Radiation, WindSpeed- Wind Speed) in driving lake surface water temperature changes in a) Annual; b) Dry Season and c) Wet Season.

4.4.3. Future warming of Lake Titicaca

Climate projections indicate significant warming of Lake Titicaca under all RCP (Representative Concentration Pathways) scenarios by the end of the 21st century. The projected mean temperature anomalies relative to the reference period are 1.0 ± 0.1 K under RCP 2.6, 1.6 ± 0.5 K under RCP 6.0, and 2.4 ± 1.0 K under RCP 8.5 (Fig. 4.3). The warming trends are statistically significant ($p < 0.01$) across all scenarios, with rates of +0.02 K decade^{-1} (RCP 2.6), +0.23 K decade^{-1} (RCP 6.0), and +0.44 K decade^{-1} (RCP 8.5) (Fig. 4.3a). Seasonal warming patterns vary across scenarios. Under RCP 6.0, dry season and annual warming rates are similar, at a rate of +0.23 K decade^{-1}, while wet season increasing rate is slightly higher at 0.24 K decade^{-1} (Fig. 4.3b-c). This seasonal similarity suggests an increase in the annual temperature range (Fig. B5). In contrast, RCP 2.6 and RCP 8.5 show more uniform trends across seasonal and annual timescales. Future projections of LSWT at monthly and seasonal timescales are shown in Fig. B6 and Fig. B7.

By the late 21st century (2080–2099), the projected mean annual temperature anomalies will reach 1.0 ± 0.1 K (RCP 2.6), 2.4 ± 0.1 K (RCP 6.0), and 3.7 ± 0.2 K (RCP 8.5). Seasonal analyses suggest slightly higher temperature anomalies during the wet season compared to annual averages, with expected increases of 1.1 ± 0.1 K (RCP 2.6), 1.8 ± 0.6 K (RCP 6.0), and 2.5 ± 1.0 K (RCP 8.5) (Fig. 4.3b). Corresponding warming trends for the wet season are +0.02 K decade^{-1} (RCP 2.6), +0.24 K decade^{-1} (RCP 6.0), and +0.44 K decade^{-1} (RCP 8.5). By 2080–2099, wet season anomalies are projected to reach 1.2 ± 0.1 K (RCP 2.6), 2.5 ± 0.1 K (RCP 6.0), and 3.8 ± 0.3 K (RCP 8.5). Similarly, during the dry season, projected mean temperature anomalies are 1.0 ± 0.1 K (RCP 2.6), 1.6 ± 0.5 K (RCP 6.0), and 2.3 ± 1.0 K (RCP 8.5) (Fig. 4.3c). Dry season warming trends are consistent with the annual trends. By the end of the century, dry season anomalies will rise to 1.0 ± 0.1 K (RCP 2.6), 2.3 ± 0.1 K (RCP 6.0), and 3.6 ± 0.2 K (RCP 8.5). These projections indicate a persistent warming trend across all scenarios, with potentially significant implications for lake hydrology, evaporation rates, and regional climate interactions.

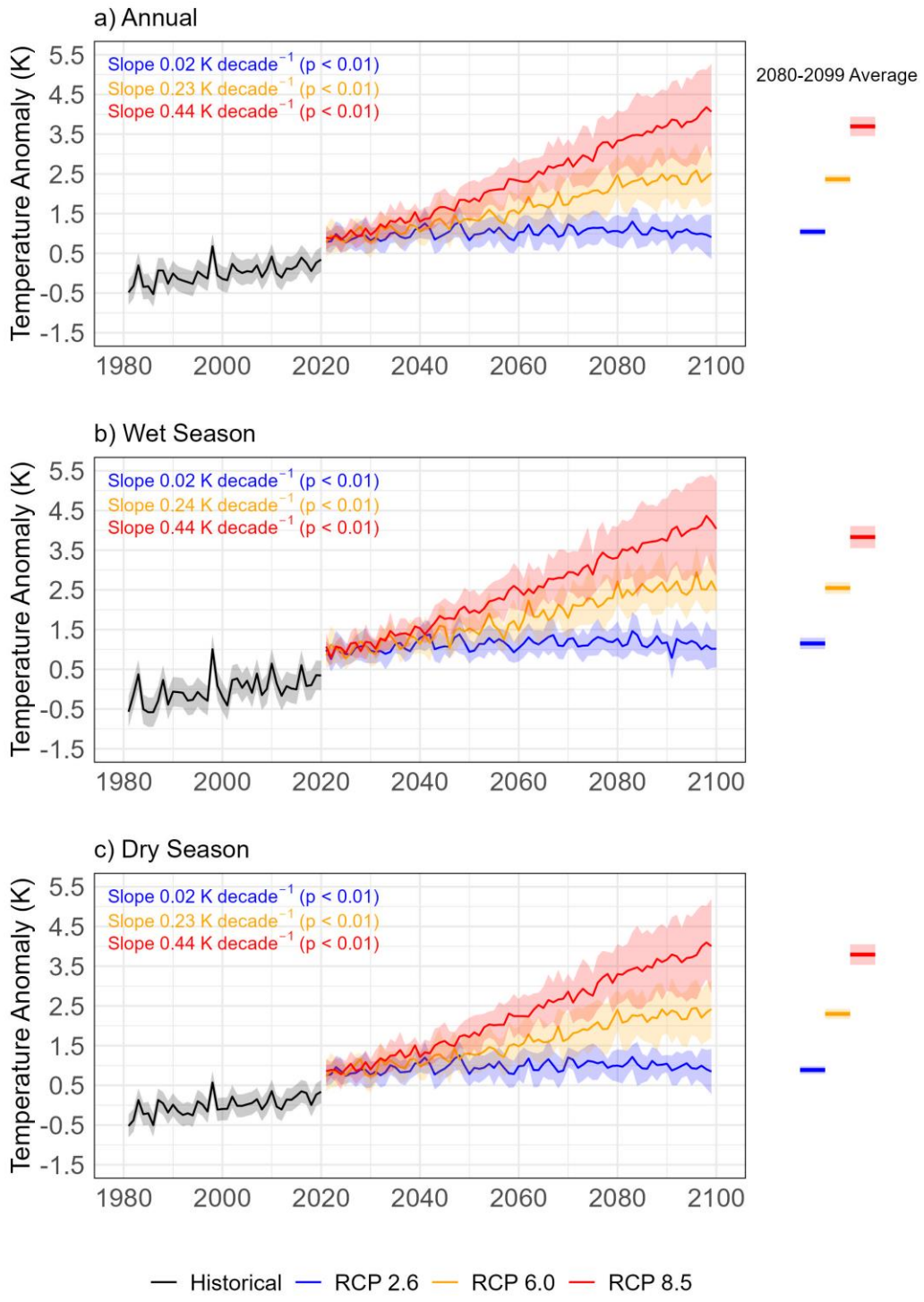


Figure 4.3. Historical and future projections of temperature anomalies under different RCPs in a) Annual, b) Wet season, c) Dry season. The thick lines represent mean temperature anomalies and the shaded areas show the standard deviation across the multi-model ensemble. The historical temperature anomalies (black) from 1981 to 2020, the projections under RCP

2.6 (blue), RCP 6.0 (orange), RCP 8.5 (red) scenarios from 2021 to 2099. The three bars represent the mean temperature (central lines) from 2080-2099 and its standard deviation.

4.4.4. Persistence of extreme temperatures this century

During the historic period, there were 52 annual lake heatwave days in Lake Titicaca. Lake heatwaves lasted, on average, for 22 days, had an average intensity of 0.5 K and a cumulative intensity of 13.3 K days (Fig. 4.4a-d). From 2021 to 2099, the average number of lake heatwave days increased to 267 ± 36 days, 327 ± 49 days and 349 ± 36 days under RCP 2.6, RCP 6.0 and RCP 8.5, respectively (Fig. 4.4a). The average duration, intensity, and cumulative intensity of lake heatwaves are also projected to increase this century, but will vary according to the RCP scenario. Under RCP 2.6, the average duration of lake heatwaves is expected to increase to 140 ± 52 days with an intensity of 0.7 ± 0.1 K and cumulative intensity of 115.7 ± 53.8 K days. The average intensity, duration and cumulative intensity will increase to 1.3 ± 0.2 K, 255 ± 62 days and 388.8 ± 86.9 K days respectively under RCP 6.0. Under the high emission RCP 8.5, lake heatwave duration is projected to increase to 308 ± 60 days with an intensity of 2.0 ± 0.3 K and cumulative intensity of 679.6 ± 100.7 K days.

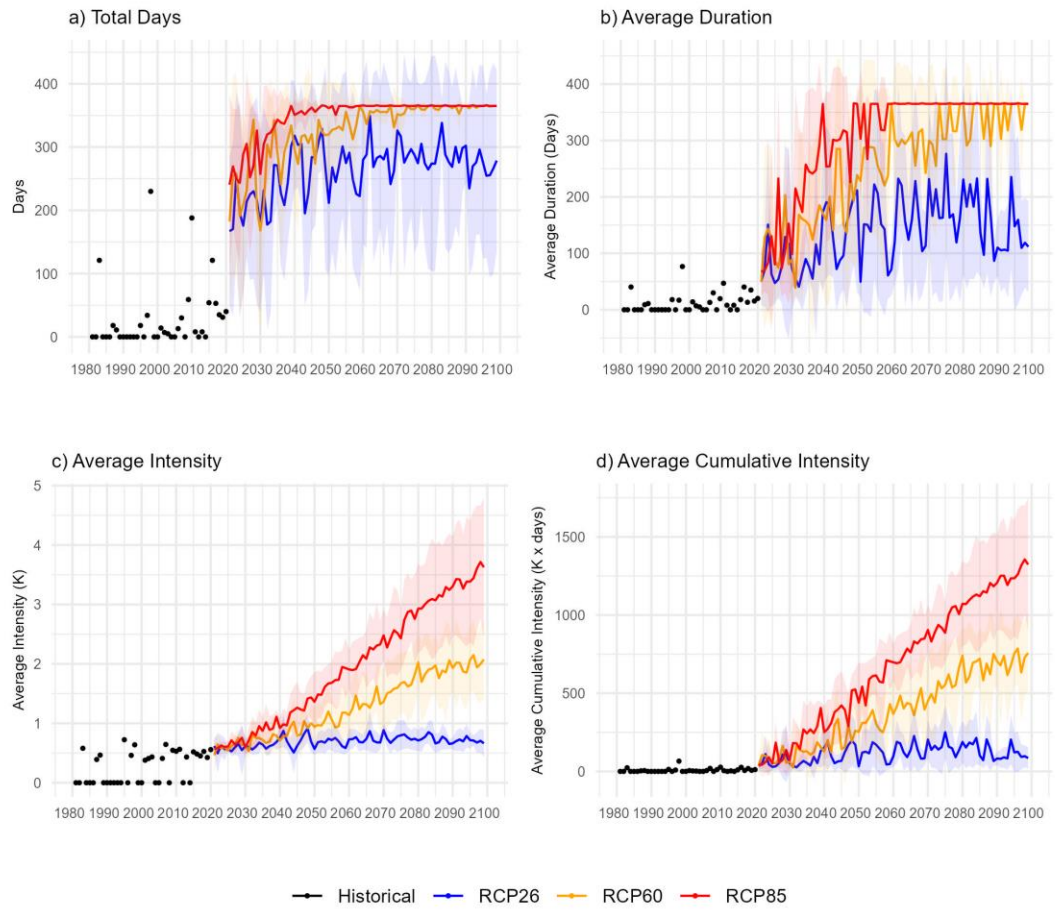


Figure 4.4. Historical and future projections of extreme temperatures driven under different RCPs of a) Total days; b) Average duration; c) Average intensity; and d) Average Cumulative Intensity. The thick lines represent mean values, and the shaded areas show the standard deviation. The historical temperature anomalies (black) from 1981 to 2020, the projections under RCP 2.6 (blue), RCP 6.0 (orange), and RCP 8.5 (red) scenarios from 2021 to 2099.

By the end of the 21st century (2080-2099), we project a considerable increase in each of the heatwave metrics calculated (Fig. 4.5a-e). Under RCP 2.6, our simulations suggest that the total number of heatwave days will reach 280 ± 22 days with an average duration of 154 ± 53 days (seven times higher compared to the historical period), an average intensity of 0.7±0.1 K and a cumulative intensity of 128.3 ± 50.6 K days. For RCP 8.5, the total number of heatwave days per year will increase to 365 ± 0.4 days with a duration of 365 ± 0.4 days, i.e., likely reaching a permanent heatwave state, an intensity of 3.3 ± 0.2 K and a cumulative intensity of 1196.1 ± 83.3 K days. Our simulations suggest that Lake Titicaca will likely experience a

permanent heatwave state (i.e., lasting 365 days) from as early as 2058 under RCP 8.5 (Fig. 4.5b). Moreover, Lake Titicaca will experience permanent heatwaves for 13 years and 20 years during 2080-2099, under the RCP 6.0 and RCP 8.5 respectively.

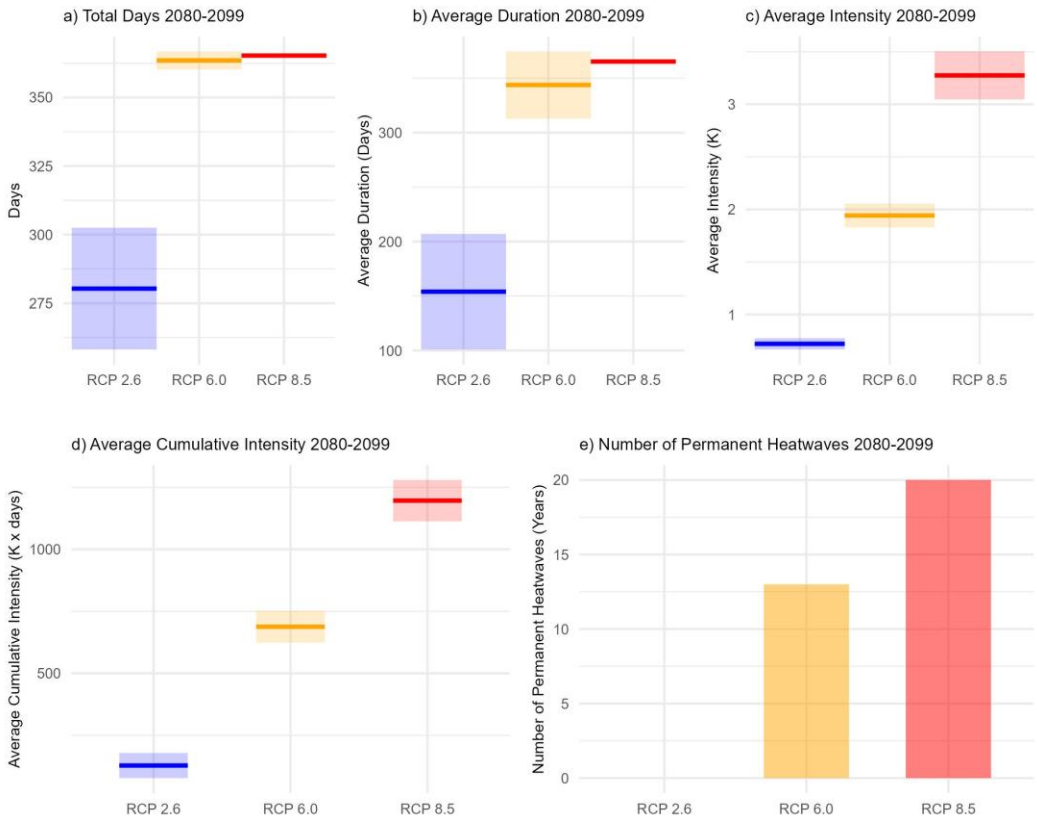


Figure 4.5. Boxplots represent the mean temperature (central lines) from 2080-2099 and its standard deviation of a) Total days; b) Average duration; c) Average intensity and d) Average Cumulative Intensity; Barplot of d) Total permanent heatwaves from 2080-2099.

4.5. Discussion

This study represents the first comprehensive assessment of LSWT changes in Lake Titicaca, covering both the historical (1981-2020) and future (2021-2099) periods. Understanding LSWT variations is critical for assessing how climate change is influencing lakes, with implications for physical, chemical and biological processes. Although some previous studies have documented the variability in the surface temperature of Lake Titicaca (Aguilar-Lome et al. 2021), analysing the Altiplano region remains challenging due to the limited availability of

long-term hydrological and climatological data, which are hindered by substantial gaps in historical records (Canedo et al. 2016). In the present study, we aimed to fill this gap by analysing satellite EO and model-derived LSWT simulations. Our analysis suggests that LSWT in Lake Titicaca has increased gradually (+0.15 K decade^{-1}), with a significant trend over the last 40 years. The major factors influencing LSWT are solar radiation and air temperature. Both of these factors have considerable impacts on the thermal structure and stratification patterns of lakes (Wetzel 2001), thereby contributing to changes in LSWT (Arvola et al. 2009; Fink et al. 2014). Specifically, air temperature and solar radiation have been described as contributing up to 60% and 40%, respectively, to the increase in LSWT of some lakes during the historic period (Schmid and Köster 2016b). Globally, LSWT has been suggested to increase by 70-85% of the increase in air temperature (Schmid et al. 2014). Thus, as local air temperature increases, LSWTs are expected to change accordingly (O'Reilly et al. 2015; Tong et al. 2023). Temperature changes in lakes, particularly in South America, are further influenced by the El Niño-Southern Oscillation (ENSO), which is the most prominent and consequential natural climate variability factor in Peru (Bergmann et al. 2021). In our study, we found substantially warmer LSWTs in 1983, 1998 and 2016, coinciding with ENSO events observed in the Puno region during 1982-1983, 1997-1998 (Segura et al. 2016) and in 2015-2016 (NOAA 2025) (Fig. B8). Similar impacts of El Niño on LSWT have been observed in other lakes around the world. For example, LSWTs in the Laurentian Great Lakes increased considerably due to the strong El Niño of 1997/1998 (Assel 1998), which also resulted in a regime shift in ice cover and water temperature in Lake Superior (Van Cleave et al. 2014).

Our analysis quantified changes in LSWT under different climate change scenarios that reflect the influence of different emission trajectories. Previous research has demonstrated that global lake surface water temperatures are expected to increase by 1 to 4 K by 2100 due to anthropogenic climate change (Grant et al. 2021). Our findings revealed that the wet season will likely experience the highest warming rates compared to the dry season and annual averages. Specifically, our projections show that LSWT in Lake Titicaca will warm most rapidly during spring and summer (Fig. B7), consistent with broader studies that report higher warming trends in summer relative to winter (Woolway and Maberly 2020). The anticipated increase in LSWT will likely have profound implications for the physical and biochemical processes within Lake Titicaca's ecosystem. Changes in thermal stratification, shifts in mixing regimes, reductions in gas solubility and dissolved oxygen, and variability in aquatic species

distribution and abundance are all likely outcomes of rising water temperatures (Wang et al. 2023). These findings highlight the critical need for further research to understand and mitigate the ecological impacts of warming in this unique and vital lake system.

Our study suggested that lake heatwave events have occurred in Lake Titicaca during the historical period, with a mean intensity of 0.5 K and an average duration of 22 days. These events coincided with El Niño episodes observed in 1983, 1998, 2010, and 2016, which explain the peaks in lake heatwave characteristics during these years compared to other historical periods (Fig. B8). Moving forward, our analyses indicate a significant increase in the frequency, duration, and intensity of lake heatwaves under various future climate scenarios. Critically, under a high-emission scenario, a permanent heatwave state may be reached as early as 2058 in Lake Titicaca, with profound implications for the ecosystem. The consequences of lake heatwaves on aquatic ecosystems and lake physical dynamics have been documented in some previous studies, but the full-scale of these impacts is yet underexplored. For instance, lake heatwaves can induce regime shifts by strengthening thermal stratification and reducing vertical mixing (Bartosiewicz et al. 2016). This process enhances water-column stability, leading to stronger oxygen depletion in the hypolimnion of large, deep lakes (Jankowski et al. 2006). Strong thermal stratification may also promote phytoplankton blooms in eutrophic lakes, potentially increasing carbon uptake (Bartosiewicz et al. 2016). For example, cyanobacterial blooms, particularly by *Microcystis*, were intensified specifically in growth and abundance by surface warming during an atmospheric heatwave event in Lake Nieuwe Meer, the Netherlands (Jöhnk et al. 2008). Harmful algal blooms driven by lake heatwaves have been similarly observed in Lake Dianchi, China, where 141 heatwave events occurred between 1951 and 2020 (Duan et al. 2024). In addition to algal blooms, lake heatwaves can directly impact aquatic fauna. For instance, fish die-offs during extreme heat have been reported in North Temperate Lakes (Till et al. 2019). Similarly, a summer heatwave in 2003 led to inhibited reproduction in the freshwater mussel *Dreissena polymorpha* due to hypoxia in a shallow eutrophic lake (Wilhelm and Adrian 2008). Recent events in 2023 provide strong evidence of the impacts of extreme heat on Amazonian lakes, where temperatures exceeding 41°C in Tefé Lake caused widespread fish and river dolphin mortality (Fleischmann et al. 2024). These diverse and severe impacts underscore the need for a deeper understanding of lake heatwaves and the development of effective mitigation strategies under a warming climate. For Lake

Titicaca, proactive measures to monitor and manage these events will be critical to preserving its ecological integrity and the services it provides.

Our study advances understanding of the historical and future LSWT trends in Lake Titicaca, highlighting the profound impacts of climate change and extreme events on this vital ecosystem. As climate projections indicate increases in the frequency, intensity, and duration of such events in the Altiplano region (Zubieta et al. 2021), the ecological and cultural significance of Lake Titicaca becomes increasingly vulnerable. The lake has been a cornerstone for Andean cultures, including the Tiwanaku civilization, and remains essential to the Aymara tribes, providing food, raw materials, and water resources for local communities (Pillco Zolá et al. 2019; Duquesne et al. 2021). Given its critical ecological and socio-economic roles, there is an urgent need to investigate ongoing warming trends and develop long-term records of climate variability. The findings of this study contribute to the growing body of knowledge necessary to inform strategies for mitigating climate impacts and guiding lake management and conservation efforts. By providing insights into historical patterns and future scenarios, this research lays the groundwork for preserving the resilience and sustainability of Lake Titicaca and its dependent communities.

4.6. Conclusions

This study provides the first comprehensive assessment of Lake Titicaca's surface water temperature over a historical period and in terms of future forecasts. Our results suggest an increase in LSWT at a rate of +0.15 K decade^{-1} between 1981 and 2020. Depending on the climate change scenario, LSWT is projected to increase between 1.0 and 3.7 K by the end of the 21st century. Accompanying this long-term warming trend, our study suggested that lake heatwaves will become warmer and longer by the end of the 21st century, with an average intensity of 2.0 ± 0.3 K and a duration of 308 ± 60 days under the high emission scenario. Moreover, our simulations suggest that there will be 13- and 20-year permanent heatwaves in Lake Titicaca by the end of the century under RCPs 6.0 and 8.5, respectively. These findings will serve as a base for future studies estimating and forecasting the impact of climate change on Lake Titicaca's ecosystem as well as the lake's physical, biogeochemical and ecological processes, and will aid both practitioners and policy-makers in understanding and mitigating the negative effects of climate change on Lake Titicaca's natural resources.

V. Emerging changes in lake temperature extremes and variability in South America[3]

5.1. Introduction

Lakes are widely recognized as sentinels of climate change, responding rapidly to atmospheric and hydrological shifts (Adrian et al. 2009). Changes in lake surface water temperature (LSWT), ice cover, and water levels serve as notable early warning indicators of broader climatic transformations (Castendyk et al. 2016; Vinnå et al. 2021; Zhang and Duan 2021). Among these indicators, LSWT is particularly critical due to its role in regulating heat balance and moisture exchange between lakes and their surroundings (Schmid and Read 2022). It also influences essential physical, chemical, and biological processes, including thermal stratification, oxygen dynamics, and ecosystem productivity (Schmid et al. 2014; Jane et al. 2021; Kraemer et al. 2021). Therefore, understanding long-term LSWT variations is essential for assessing how lake ecosystems respond to climate change.

Global LSWT trends are primarily driven by rising air temperatures, with consistent evidence of warming across diverse geographical regions (Schneider and Hook 2010; O'Reilly et al. 2015; Tong et al. 2023; Piccolroaz et al. 2024). However, LSWT patterns exhibit considerable regional variability, influenced by climatic drivers such as solar radiation (Schmid and Köster 2016) and wind speed (Woolway et al. 2019), as well as intrinsic lake characteristics like surface area and depth (Kraemer et al. 2015; Augusto-Silva et al. 2019; Zhou et al. 2024). In addition to long-term warming, extreme events such as lake heatwaves, defined as prolonged periods of anomalously high surface water temperatures, are becoming more frequent (Woolway et al. 2021b; Woolway et al. 2022a; Wang et al. 2023; Wang et al. 2024). These extreme events can intensify thermal stratification (Woolway et al. 2020a), exacerbate hypoxia in deeper layers, and disrupt metabolic and microbial processes, thereby altering nutrient cycling and oxygen dynamics (Jankowski et al. 2006; North et al. 2014). Such disruptions may trigger harmful algal blooms and mass mortality events among aquatic species (Ho et al. 2019; Till et al. 2019; Fleischmann et al. 2024; Mendes et al. 2024). With ongoing global warming,

[3] The published article: *Dinh, D. A., Tong, Y., Feng, L., Fleischmann, A., McCarthy, V., Jennings, E., Jordan, S., & Woolway, R. I. (2026). Emerging changes in lake temperature extremes and variability in South America. Climatic Change, 179, 41.* https://doi.org/10.1007/s10584-026-04137-0 is based on this chapter. Dieu Anh Dinh is the first author and would like to thank all co-authors for their contributions.

lake heatwaves are projected to increase in frequency, duration, and intensity throughout the 21st century (Woolway et al. 2021b; Wang et al. 2023; Zhang and Yao 2023).

South America hosts some of the world's most diverse and expansive freshwater systems, including the Amazon River, the largest river system by discharge, and numerous high-altitude lakes along the Andes, the longest continental mountain range (Buytaert and Breuer 2013). Lakes, rivers, and wetlands are integral to the continent's hydrological cycle, serving as critical water sources for ecosystems, agriculture, and human populations (Hamilton et al. 2002; Junk 2013; Kandus et al. 2018; Siqueira et al. 2018; Fleischmann et al. 2021). However, South American freshwater resources are increasingly threatened by climate change and human activities (Buytaert and Breuer 2013; Junk 2013). Over recent decades, South America has experienced significant air temperature increases (World Meteorological Organization 2021), a trend projected to continue and likely to cause profound impacts on LSWT (Margin et al. 2014; Llopart et al. 2020). Despite the continent's ecological importance and vulnerability to climate change, research on LSWT dynamics and lake heatwaves across South America remains limited. Most studies have focused on specific water bodies, particularly glacial lakes (Quade and Kaplan 2017; Wilson et al. 2018; Mergili et al. 2020; Hata et al. 2022) or on changes in lake water level (Zolá and Bengtsson 2006; Pasquini et al. 2008; Carabajal and Boy 2021). The relative scarcity of studies addressing LSWT trends and lake heatwave dynamics on a regional scale is partly due to limited *in situ* measurements, particularly in the Southern Hemisphere (Aranda et al. 2021). This results in major knowledge gaps in understanding how LSWT and thermal extremes are evolving across different regions and lake types.

To address these gaps, this study investigates historical (1981–2020) and projected future (2021–2099) changes in LSWT and lake heatwave patterns across South America using satellite-derived and modelled data (Tong et al. 2023). We examine LSWT trends, lake heatwave characteristics (duration, intensity, and cumulative intensity), and the role of meteorological drivers, including air temperature, solar and longwave radiation, wind speed, and humidity. In addition to long-term trends, this study explores short- and medium-term thermal variability by introducing a novel typology of lake responses based on diurnal and seasonal temperature range (DTR and STR, respectively). DTR captures short-term fluctuations within a 24-hour cycle, while STR reflects annual-scale thermal variability. Together, they provide complementary insights into how lakes respond to atmospheric forcing.

By classifying lakes according to combinations of DTR and STR, we identify distinct thermal response types, offering a new framework for assessing lake sensitivity to climate change across multiple timescales.

5.2. Study area

(Please refer back to Chapter 2, section 2.2).

5.3. Data and Methods

5.3.1. GLAST dataset

The GLAST dataset provides LSWT data for 92,245 lakes worldwide from 1981 to 2020 (Tong et al. 2023). It was generated using a combination of satellite earth observation data and numerical modeling in four key steps: (i) Lake Selection: Lakes were identified based on permanent water bodies in the HydroLAKES database (Messager et al. 2016); (ii) Temperature Retrieval: LSWT was derived from Landsat satellite data using a statistical mono-window algorithm. With a spatial resolution of 60–120 m, temperatures were measured at least three pixels away from the shoreline to ensure accuracy; (iii) Model Calibration: The Freshwater Lake (FLake) model (Mironov et al. 2010) was calibrated using the Landsat-derived LSWT data (1981–2020). The model was fine-tuned for hourly temperature predictions using meteorological variables - including air temperature, wind speed, longwave and shortwave downward radiation, and specific humidity - obtained from ERA5-Land reanalysis dataset (Hersbach et al. 2020) at a grid resolution of 0.1° × 0.1°; (iv) Simulation and Validation: the calibrated FLake model was used to simulate hourly LSWT for each lake, with validation against *in situ* measurements resulting in a median absolute error of 1.16°C (Tong et al. 2023). Using the hourly simulations, we estimated the DTR in the studied lakes, calculated as the difference between daytime and nighttime LSWT, as well as the seasonal and inter-annual variations in LSWT.

Future LSWT projections (2021–2099) were generated using an optimized lake-specific FLake model for each lake (i.e., relative to the satellite-derived LSWTs), forced by four Global Climate Models (GCM, including IPSL-CM5A-LR, GFDL-ESM2M, MIROC5, and HadGEM2-ES) under three greenhouse gas emission scenarios: RCP 2.6 (low), RCP 6.0

(intermediate), and RCP 8.5 (high) (Tong et al. 2023). FLake simulations were conducted for each GCM, and the mean and standard deviation were estimated. In this study, LSWT anomalies were computed relative to the 1981–2006 baseline. Future LSWTs were also bias-corrected using a Quantile Delta Mapping (QDM) approach, which has been demonstrated as an effective method in a previous study on Lake Titicaca, South America (Dinh et al. In Review). As the GCM input data were only available at daily intervals, our future projections do not resolve diurnal temperature ranges.

5.3.2. Lake Heatwaves

The GLAST dataset was used to calculate lake heatwaves, defined as periods in which surface water temperatures increase higher than the seasonal 90th percentile for at least five consecutive days(Woolway et al. 2021c). Lake heatwave frequency was calculated during the ice-free season using the package "*heatwaveR*" in R (Schlegel and Smit 2018). Lake heatwave data were generated using three steps: (1) annual climatological mean and 90th percentile temperature threshold were calculated over the period of 1991–2020. An 11-day window centred on each date was used, followed by smoothing with a 31-day moving average; (2) Lake heatwaves were then calculated as defined above. If two events were separated by < 2 days, they were combined into a single event. These thresholds also indicate ecological limits for lakes. If heatwaves extended to 2 or more calendar years, they were split on December 31, with a maximum length of 366 days per event; (3) We focused on four heatwave metrics including the total number of heatwave days (days), duration (days), intensity (the anomalies above the climatological mean; K) and cumulative intensity (K x days). These metrics were then aggregated annually to estimate heatwave trends.

5.3.3. Lake classification

Lake data from GLAST was classified into different thermal regions following the methods of Maberly et al. (2020). Maberly et al. (2020) used satellite observations of LSWT from 732 lakes globally between 1996 and 2011 to categorise distinct lake regions. Firstly, mean LSWT of individual lakes were calculated (Maberly et al. 2020). Secondly, a saturated b-spline based statistical modelling (de Boor 1980) was used to smooth out the LSWT of each lake over time (Maberly et al. 2020). If ice was detected, the temperature under ice cover was set to 0^{o}C and

the smooth function was adjusted accordingly (Maberly et al. 2020). Thirdly, K-means clustering was used to group the lakes based on their temperature temporal patterns (seasonal patterns, mean temperature and long-term changes) (Maberly et al. 2020). Finally, nine thermal regions were classified using gap statistics (Tibshirani et al. 2002). These lake groups were also compared with other classification schemes (global climate and terrestrial ecoregions). Lakes were divided into 11 groups using the Koppen-Geiger climate classification (Peel et al. 2007). For the terrestrial ecoregions, lakes were classified into 13 groups (Olson et al. 2001). Furthermore, lake groups were compared with the air temperature clusters derived from bi-monthly temperature for the same number of LSWT from 1995 to 2012 (Harris et al. 2014). The air temperature clusters matched the LSWT clusters, grouped into nine classifications that corresponded as nearly as possible to lake thermal regions (Maberly et al. 2020). Following this approach, 2406 lakes from the GLAST dataset were categorised into five lake thermal regions (Northern Hot [n = 17], Tropical Hot [n = 660], Southern Hot [n = 414], Southern Warm [n = 613] and Southern Temperate [n = 702]) (Fig. 6.1a; Fig. 6.1c).

5.3.4. Diurnal to seasonal lake temperature typology

In this study, we developed a typology of lake thermal responses by classifying lakes according to their diurnal and seasonal temperature range (i.e., DTR and STR, respectively). The DTR was computed as the average difference between daytime and nighttime surface water temperatures across the observation period, capturing short-term thermal variability within a 24-hour cycle. In contrast, STR was defined as the difference between the annual maximum and minimum surface water temperatures, reflecting long-term seasonal thermal variability. To categorize lakes based on these metrics, we used percentile-based thresholds derived from the distribution of DTR, STR, and the DTR/STR ratio across all lakes in South America included in our dataset. Specifically, values below the 25th percentile were considered low, while those above the 75th percentile were considered high. These thresholds allowed us to systematically identify distinct thermal response patterns among lakes. Based on combinations of high and low values of DTR and STR, as well as their ratio, we defined four thermal typologies of lakes: (i) Diurnally Volatile Lakes (High DTR, Low STR): Lakes exhibiting strong diurnal thermal fluctuations but relatively stable temperatures across seasons; (ii) Seasonally Stable Lakes (Low DTR, High STR): Lakes with muted diurnal variability but pronounced seasonal changes in temperature; (iii) Thermally Extreme Lakes (High DTR, High STR): Lakes that experience

large temperature variations both diurnally and seasonally; (iv) Thermally Buffered Lakes (Low DTR, Low STR): Lakes that remain relatively stable in temperature over both daily and seasonal timescales. This classification framework provides new insight into how lakes respond to thermal forcing on different timescales, facilitating comparative analyses of thermal dynamics and their potential ecological implications.

5.3.5. Data analysis

To assess the relative impacts of climate forcings - such as surface air temperature, longwave and shortwave downward radiation, specific humidity, and wind speed - on LSWT and DTR trends, the FLake model, as used in generating the GLAST dataset, was employed. Six simulations were conducted: one reference simulation that preserved the trends of all meteorological variables, and five control simulations in which each variable was individually maintained while the others were detrended. The detrending process involved repeating the 1981 input forcing for the subsequent 40 years, following methods used in previous studies (Li et al. 2019; Tong et al. 2023). Trends of LSWTs and DTR were estimated using Sen's slope and Mann Kendall test using *trend* package (Pohlert 2023a) in R (version 4.4) (R Core Team 2025).

5.4. Results

5.4.1. Historic patterns of change in LSWT, lake heatwaves and diurnal-seasonal variability

Between 1981 and 2020, mean annual LSWTs across South American lakes ranged from 273 K to 304 K, exhibiting substantial spatial variability (Fig. 5.1b). Warmer lakes were concentrated in the Tropical Hot (TH), Northern Hot (NH), and Southern Hot (SH) regions, while cooler lakes predominated in the Southern Temperate (ST) and Southern Warm (SW) zones (Figs. 5.1b, 5.1d). The TH region recorded the highest average LSWT at approximately 301 K. During this period, LSWT anomalies generally fluctuated between –1 K and +1 K, with notable deviations in the TH and SH regions (Fig. 5.1e). A strong warming trend was observed in 97.0% of the lakes (n = 2,333), averaging +0.11 K decade^{-1} (Fig. 5.1g), whereas only 3.0% (n = 73) exhibited marginal cooling at a rate of -0.02 K decade^{-1}. Regionally, TH warmed the

fastest (+0.15 K decade^{-1}), followed by NH and SH (each +0.13 K decade^{-1}; $p < 0.05$). Warming in ST and SW was lower, at +0.05 K decade^{-1} (not significant) and +0.07 K decade^{-1} ($p < 0.05$), respectively (Fig. 5.1f). Air temperature was identified as the primary driver of LSWT trends in most lakes (52.7%; n = 1,269). In contrast, shortwave downward radiation was the dominant driver in the SW region, affecting 30.8% of lakes (n = 741) (Fig. 5.1h; Fig. 5.2- 5.3; Fig. C1). Other contributing variables included longwave radiation (7.2%), specific humidity (7.6%), and wind speed (1.6%).

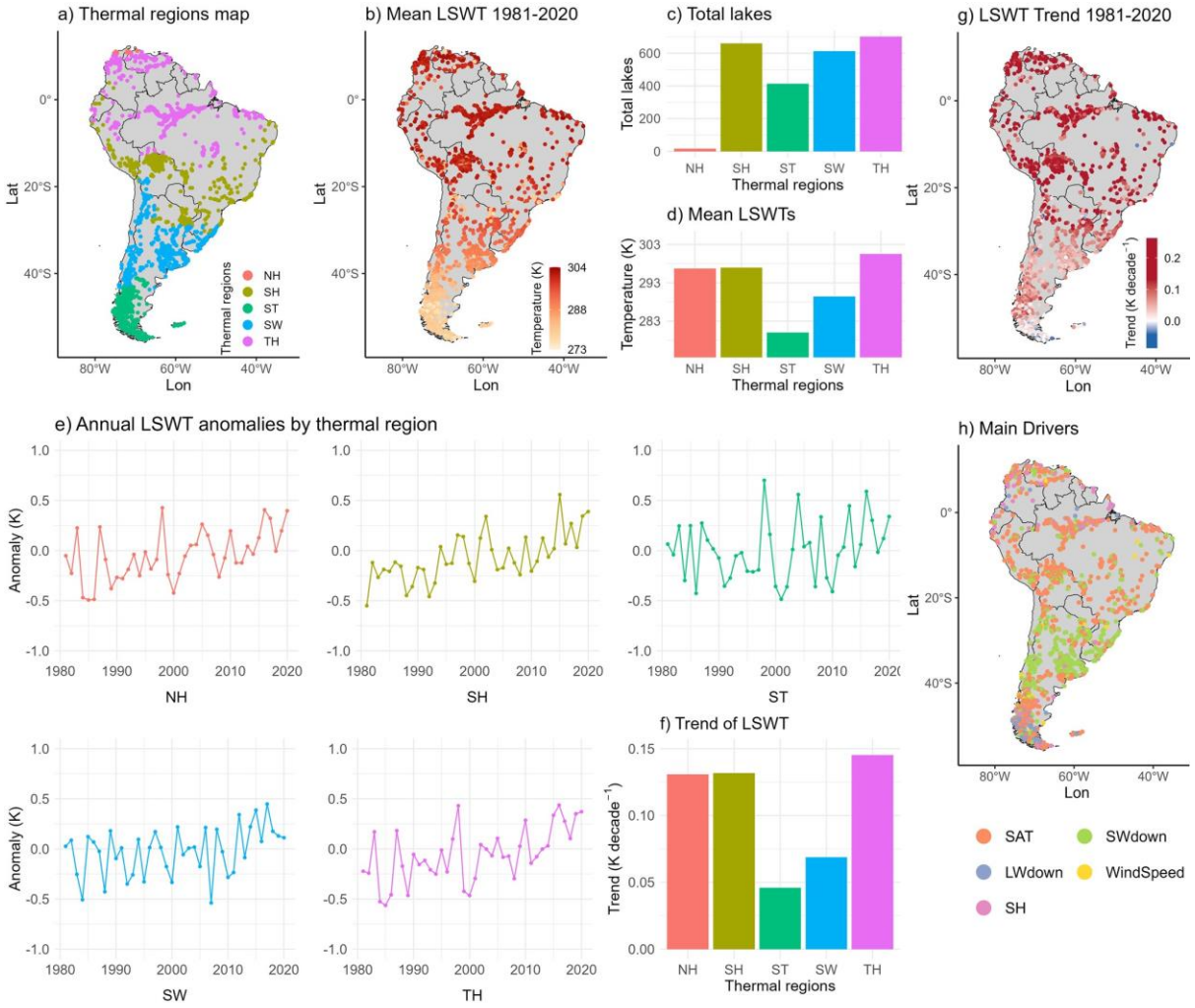


Figure 5.1. Temporal and spatial pattern of LSWTs during the historical period (1981-2020). (a) Maps of thermal regions in South America (NH- Northern Hot, SH- Southern Hot, ST- Southern Temperate, SW- Southern Warm, TH- Tropical Hot); (b) Average LSWT of each lake map; (c) Total number of lakes per thermal region; (d) Average LSWT per thermal region; (e) Annual LSWT anomaly per thermal region; (f) LSWT Trends per thermal region; (g) LSWT trend per lake; (h) Contribution of meteorological variables to LSWT trend map (SAT- Surface

Air Temperature, SH- Specific Humidity, WindSpeed- Wind Speed, LWdown- Longwave downward radiation, SWdown- Shortwave downward radiation).

Annual mean and trends of daily meteorological variables are shown in Fig. 5.2 and 5.3 respectively. Air temperature ranged between 269 and 302 K (Fig. 5.2) and generally warmed across the continent with the rates up to 0.5 K decade^{-1} (Fig. 5.3). Longwave radiation was higher in the southern regions. The highest shortwave radiation occurred in the Atacama Desert with the rate above 285 Wm^{-2} (Fig. 5.2). Both longwave radiation and shortwave radiation increased, except for the southernmost areas (Fig. 5.3). Specific humidity was higher in the north (~10-20 g/kg) compared to the south (~0-10 g/kg) (Fig 5.2) and recorded a cooling trend. Wind speeds were generally low in northern regions (~0-6 m/s) (Fig. 5.2) but increased in most of the southern areas (Fig. 5.3).

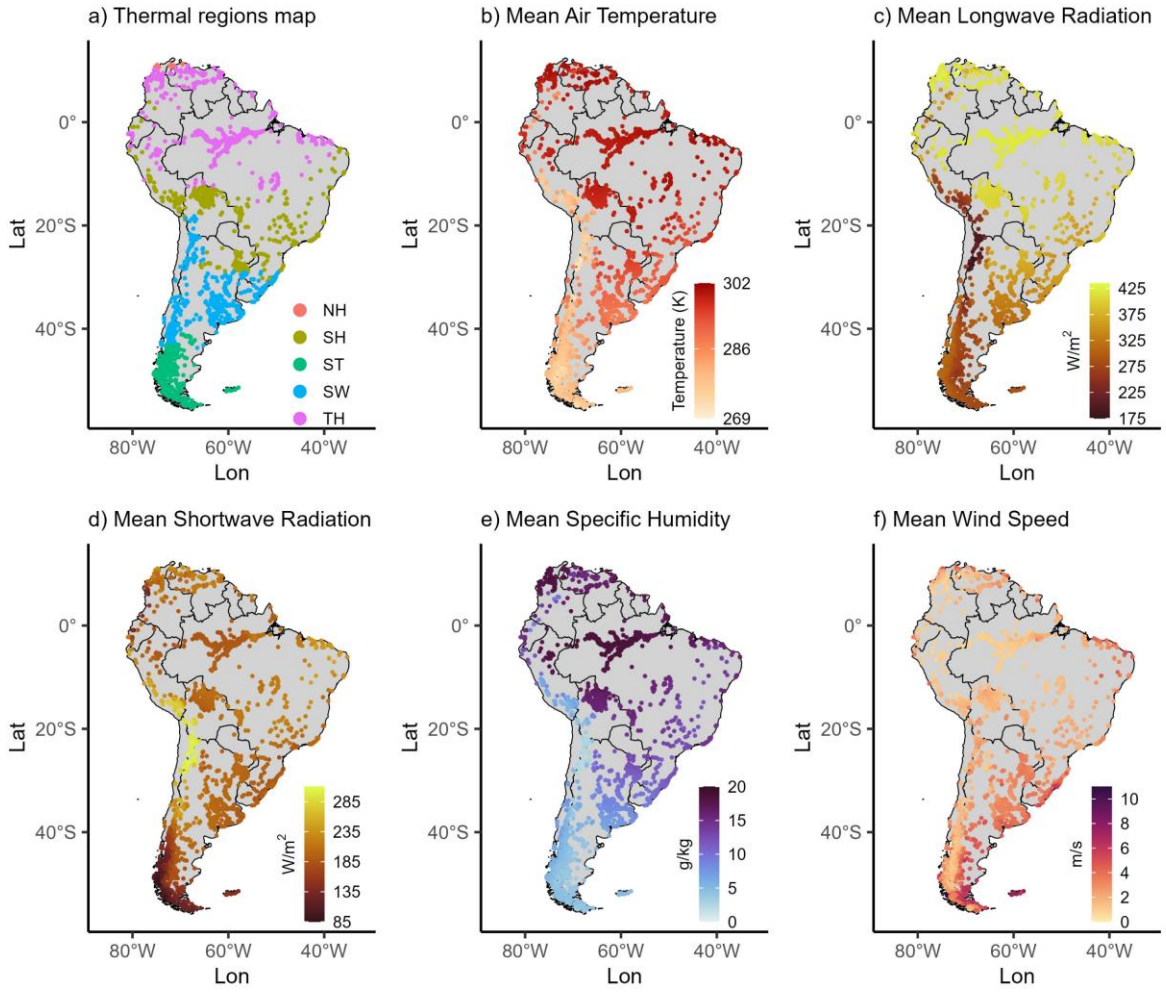


Figure 5.2. Mean daily meteorological variables from 1981 to 2020- (b) air temperature, (c) longwave downward radiation, (d) shortwave downward radiation, (e) specific humidity, (f) wind speed.

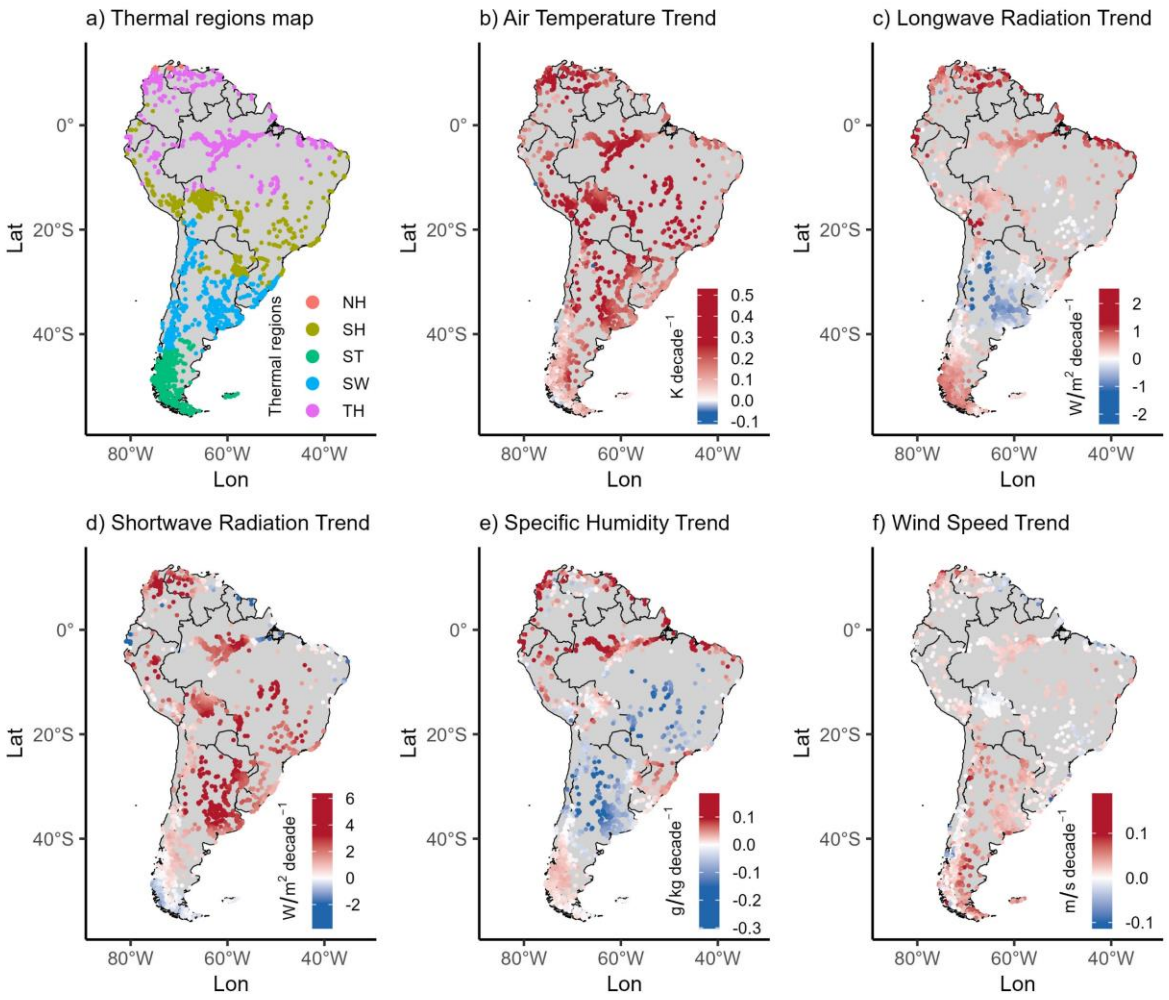


Figure 5.3. Trends in daily meteorological variables from 1981 to 2020- (a) Maps of thermal regions in South America (NH- Northern Hot, SH- Southern Hot, ST- Southern Temperate, SW- Southern Warm, TH- Tropical Hot); (b) air temperature, (c) longwave downward radiation, (d) shortwave downward radiation, (e) specific humidity, (f)-wind speed.

The DTR varied from ~0 to 5 K across lakes during the study period (Fig. 5.4a). The SH region exhibited the highest average DTR (1.9 K), followed by SW (1.6 K), TH (1.1 K), NH (0.7 K), and ST (0.6 K) (Fig. 5.4c). Most lakes (86.2%, n = 2,074) experienced increasing DTR trends, averaging +0.02 K decade^{-1}, while the remainder (13.8%, n = 332) showed a modest decline of -0.03 K decade^{-1} (Fig. 5.4e). Although overall changes were small, regional trends were considerable. NH exhibited a notable decline (-0.05 K decade^{-1}; $p < 0.05$), whereas other regions showed slight positive trends ranging from +0.01 K to +0.02 K decade^{-1} (Figs. 5.4b, 5.4d). Shortwave downward radiation was the dominant driver of DTR variability,

influencing 66.8% of the lakes (n = 1,530) (Fig. 5.4f; Fig. 5.5-5.6; Fig. C2). Longwave radiation (13.4%) and air temperature (12.5%) also played important roles, with wind speed (5.8%) and specific humidity (4.7%) contributing to a lesser extent.

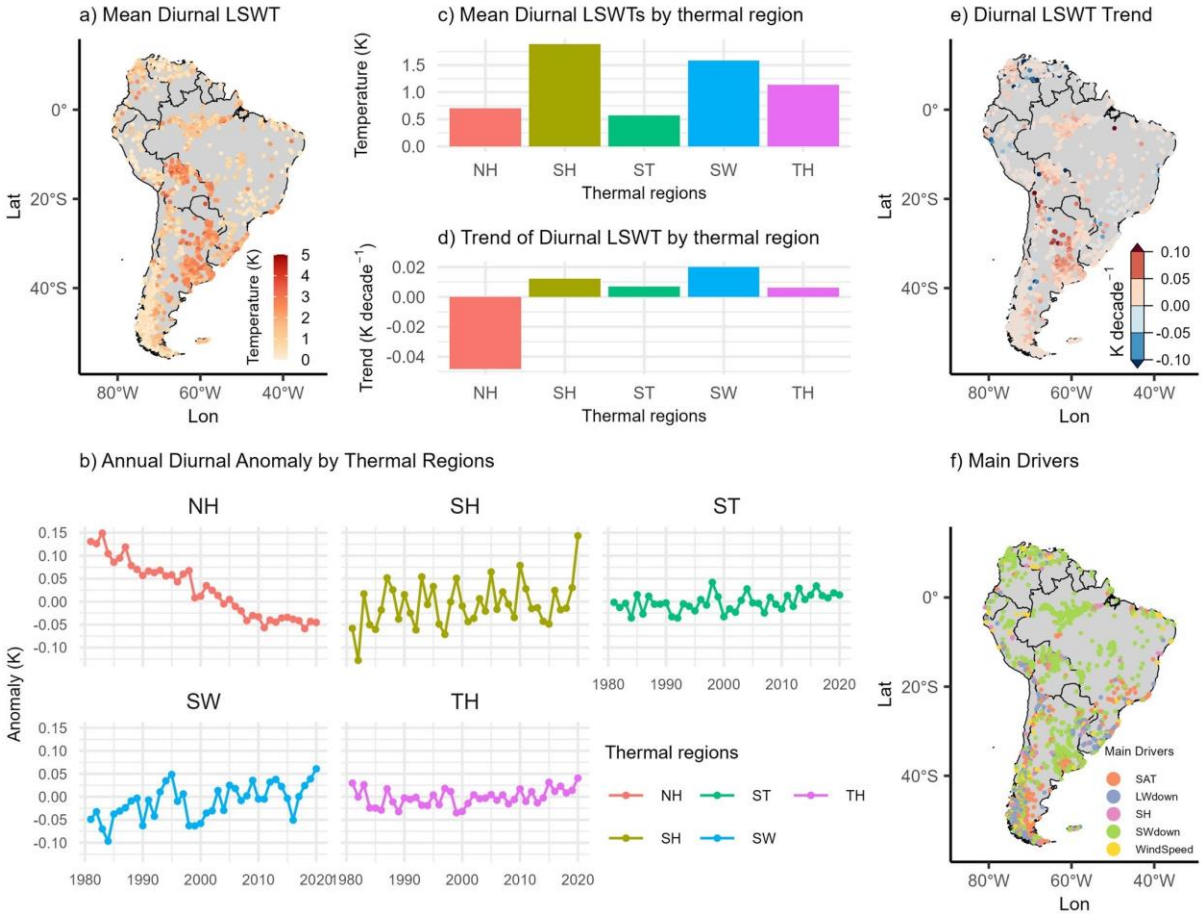


Figure 5.4. Temporal and spatial pattern of diurnal LSWTs during the historical period (1981-2020). (a) Average diurnal LSWT of each lake map; (b) Annual diurnal LSWT anomaly per thermal region; (c) Average diurnal LSWT per thermal region; (d) Diurnal LSWT Trends per thermal region; (e) Diurnal LSWT Trends map; (f) Contribution of meteorological variables to diurnal LSWT trend map.

Annual mean and trends of diurnal meteorological variables are illustrated in Fig. 5.5 and 5.6 respectively. Diurnal air temperature ranged between 2 and 17 K (Fig. 5.5) and generally warmed in most areas of South America with the rates up to 0.5 K decade^{-1} (Fig. 5.6). Diurnal shortwave radiation was higher in the northern regions with a range of 15-45 Wm^{-2}. The highest diurnal shortwave radiation occurred in the Atacama Desert with the rate above 45

Wm^{-2} (Fig. 5.6). Diurnal shortwave radiation generally increased, while diurnal longwave showed cooling trends in some of the areas (Fig. 5.7). Diurnal specific humidity ranged between 0-4 g/kg (Fig. 5.6) and recorded an increasing trend. Diurnal wind speeds were generally low (Fig. 5.6) but increased in most of the southern areas (Fig. 5.7).

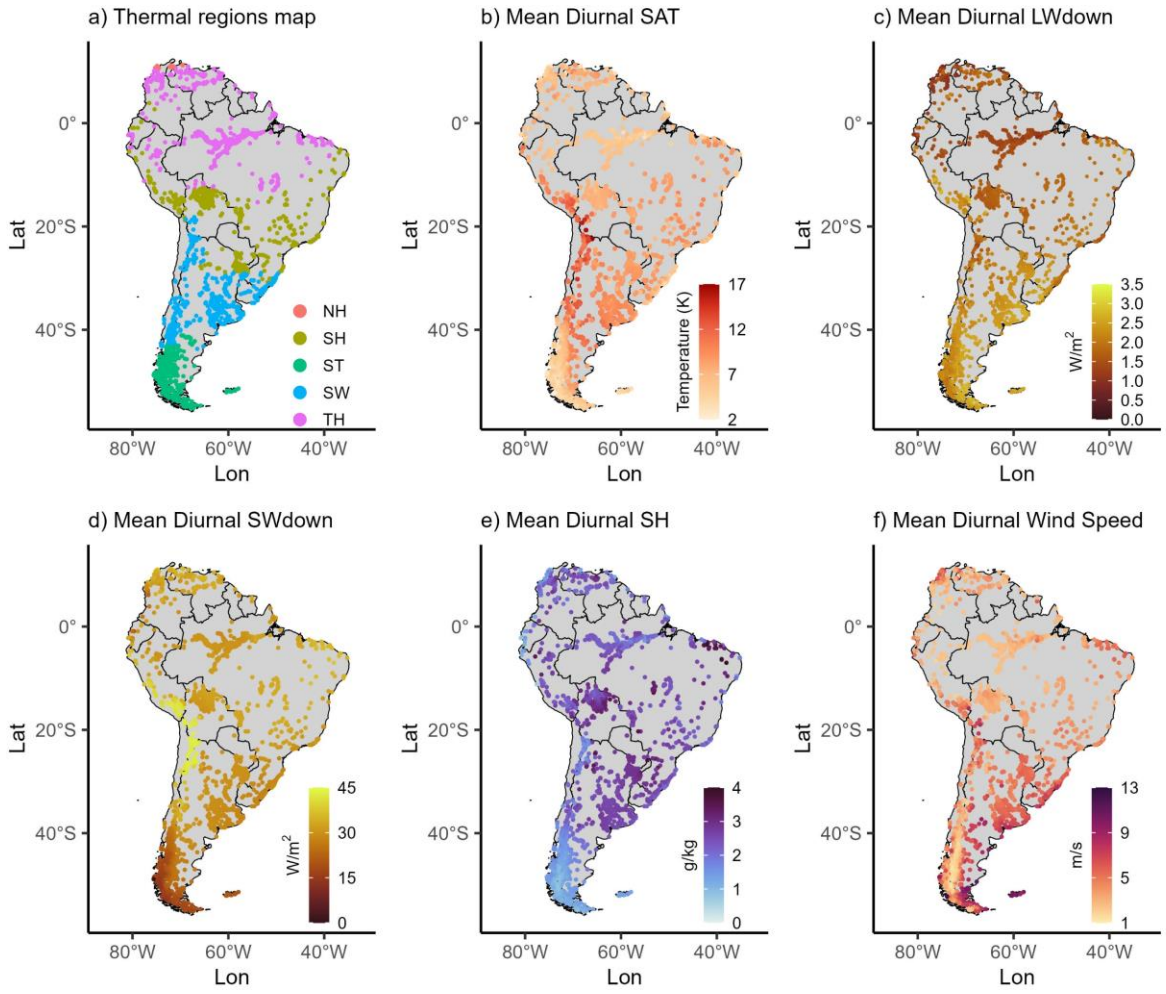


Figure 5. 5. Mean diurnal meteorological variables from 1981 to 2020- (b) air temperature, (c) longwave downward radiation, (d) shortwave downward radiation, (e) specific humidity, (f)- wind speed.

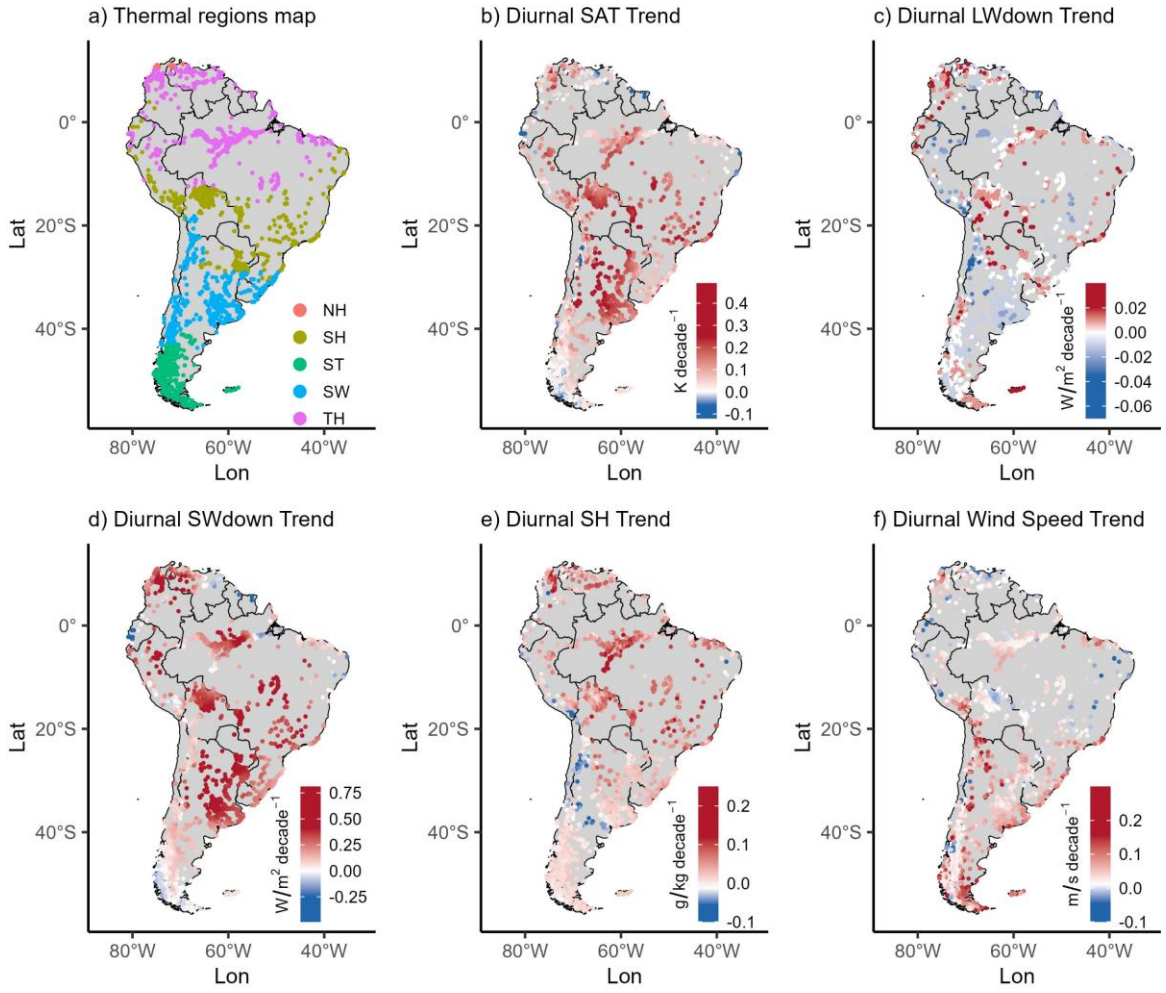


Figure 5.6. Trends in diurnal meteorological variables from 1981 to 2020- (b) surface air temperature, (c) longwave downward radiation, (d) shortwave downward radiation, (e) specific humidity, (f)-wind speed.

Historic lake heatwaves ranged in duration from 5 to 116 days, with average intensities between 0.4 K and 6.3 K and cumulative intensities from 6 to 131 K x days (Fig. 5.7a–c). The SH and SW regions exhibited the highest heatwave intensities. Trends in lake heatwave characteristics were pronounced. A majority of lakes (79.5%, n = 1,912) showed increasing duration trends, and nearly half (47.8%, n = 1,151) experienced rising intensity trends at approximately +0.1 K decade^{-1} (Fig. 6.7d–f). Cumulative heatwave intensity increased in 63.0% of lakes (n = 1,516). Across the continent, the number of heatwave days showed a significant positive trend (+0.3 days decade^{-1}), while changes in intensity were minor and not statistically significant (-3.7 × 10^{-4} K decade^{-1}) (Fig. 5.9a-d).

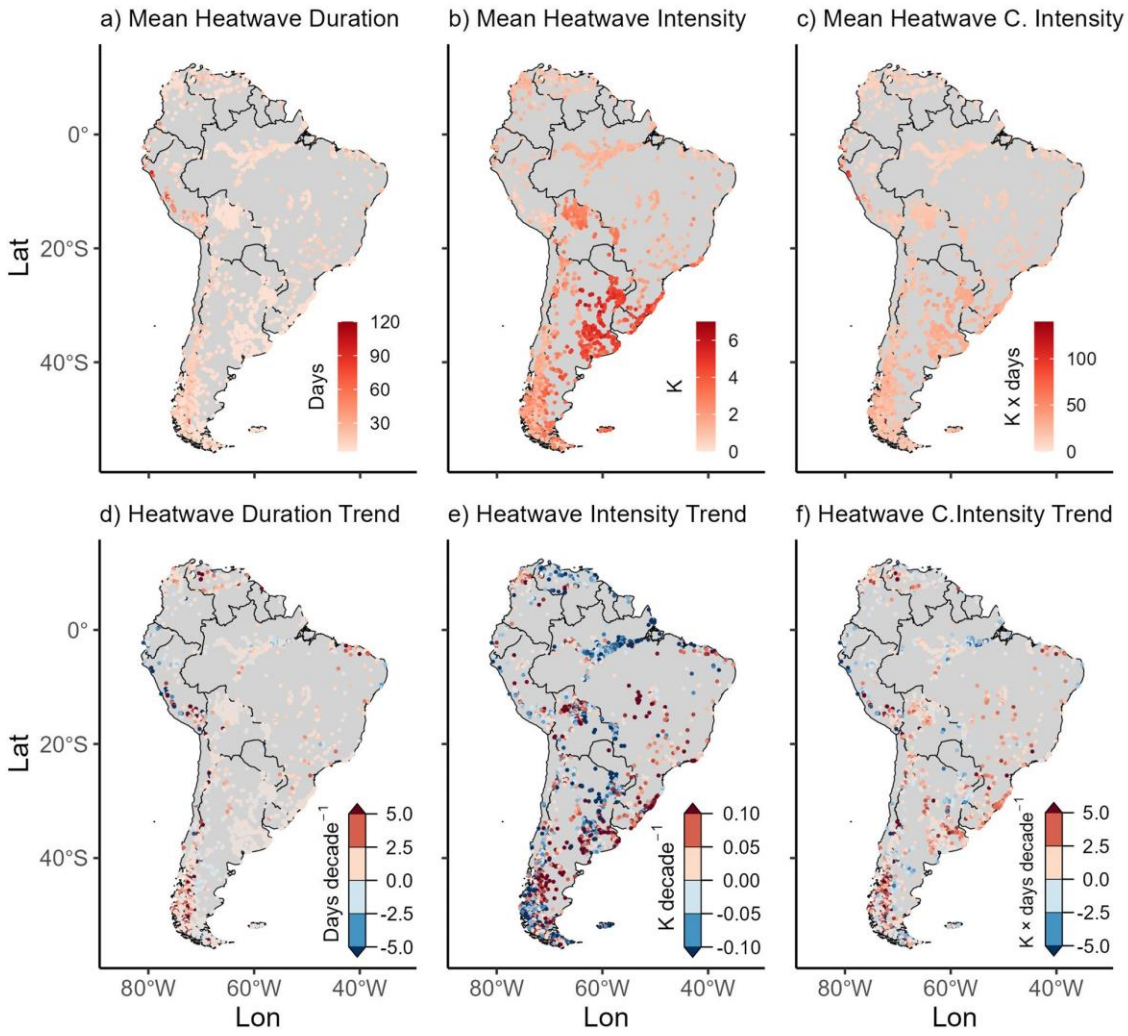


Figure 5.7. Historical mean heatwave (HW) and trend maps (1981-2020); (a) Mean HW duration, (b) Mean HW Intensity, (c) Mean HW Cumulative Intensity, (d) HW Duration Trend, (e) HW Intensity Trend and (f) HW Cumulative Intensity Trend.

Lakes were further categorized in this study based on the ratio of DTR to STR, revealing distinct spatial patterns. Approximately 50% of lakes (n = 1,202) exhibited a mid-range DTR/STR ratio, while high and low ratio lakes each accounted for 25% (n = 602) (Fig. 5.8a). High-ratio lakes were concentrated in the Amazon and northern South America, mid-range lakes in the southeast, and low-ratio lakes in the Andes. Although DTR/STR trends ranged from -0.1 to +0.3 decade^{-1}, most values clustered around ±0.005 decade^{-1} (Fig. 6.8b). Lakes in the north and east generally showed decreasing trends, while central South America exhibited the most prominent increases (>0.005 decade^{-1}). Using DTR, STR, and their ratio, lakes were classified into four thermal response types: Thermally Extreme (n = 258), Thermally Buffered

(n = 113), Seasonally Stable (n = 69), and Diurnally Volatile (n = 52), with the remainder (n = 1,914) categorized as "Others" (Fig. 5.8c). Thermally Extreme lakes were mostly in south-eastern South America, Diurnally Volatile and Thermally Buffered lakes occurred mainly in the north (~12°N-20°S), and Seasonally Stable lakes were found primarily in the Patagonian Andes.

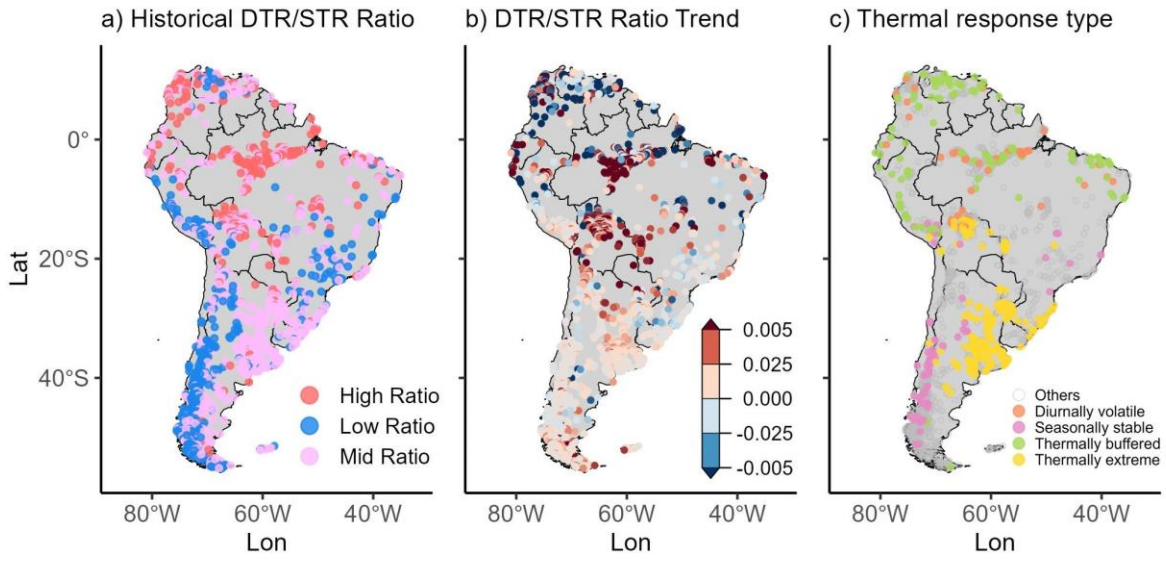


Figure 5.8. Diurnal-seasonal variability during the historical period (1981-2020): (a) Historical DTR/STR ratio; (b) DTR/STR trend per decade, and (c) Thermal response type (grey circle defined as “Others” type).

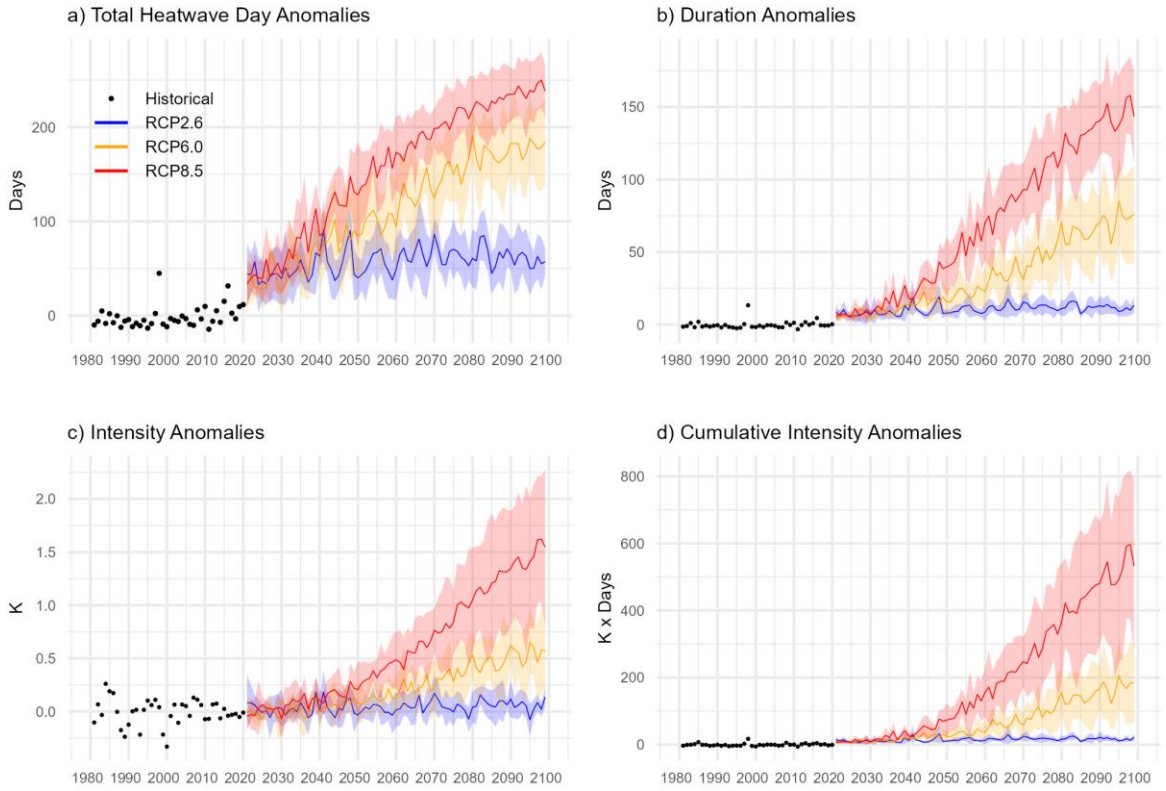


Figure 5.9. Historical and future projections of lake heatwave anomalies in the studied lakes under different RCPs, including (a) Total heatwave days, (b) Heatwave duration, (c) Heatwave intensity, and (d) Heatwave cumulative intensity. The black points represent anomaly values during the historical period from 1981 to 2020. The thick lines represent heatwave anomalies and the shaded areas show the standard deviation across the multi-model ensemble. The projections under RCP 2.6 (blue), RCP 6.0 (orange), and RCP 8.5 (red) scenarios from 2021 to 2099.

5.4.2. Future changes during the 21st century

By the late 21st century (2080-2099), LSWTs across South America are projected to increase substantially under all emission scenarios, with pronounced regional differences (Fig. 5.10a-f). Under the low-emission scenario (RCP 2.6), LSWTs are projected to increase by between 0.3 ± 0.1 K and 1.0 ± 0.1 K across the lake thermal regions. LSWT warming is projected to intensify further under the moderate-emission scenario (RCP 6.0), with projected increases ranging from 1.0 ± 0.1 K to 2.2 ± 0.1 K by 2080-2099 across thermal regions. Projections under

the high-emission scenario (RCP 8.5) suggest the greatest warming, with temperature increases ranging from 1.8 ± 0.3 K in the ST region to 3.6 ± 0.2 K in the TH region. Overall, the TH region is projected to experience the greatest temperature increases across all scenarios, while the ST region consistently exhibits the lowest warming rates.

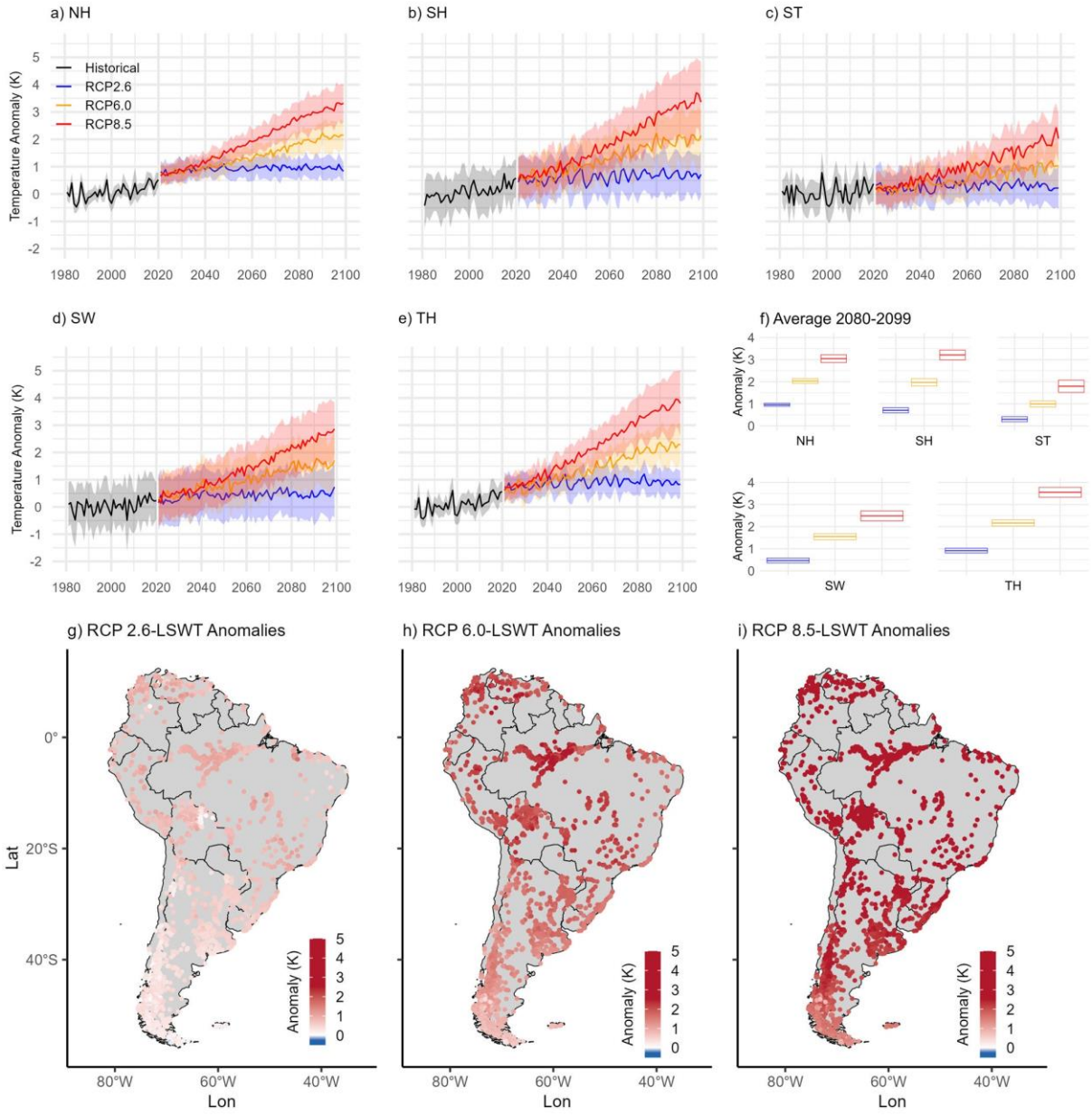


Figure 5.10. Historical and future projections of LSWT anomalies under different RCPs per thermal region: (a) NH, (b) SH, (c) ST, (d) SW and (e) TH. The thick lines represent mean temperature anomalies and the shaded areas show the standard deviation across the multi-model ensemble. The historical temperature anomalies (black) from 1981 to 2020, the

projections under RCP 2.6 (blue), RCP 6.0 (orange), RCP 8.5 (red) scenarios from 2021 to 2099. (f) Average LSWT during the period of 2080-2099 per thermal region. (g-i) LSWT anomalies from 2080 to 2099 under RCP 2.6, RCP 6.0 and RCP 8.5, respectively.

Future projections under various emission scenarios suggest substantial increases in heatwave intensity, frequency, and duration (Fig. 5.9a-d; Fig. C3-C6). Under RCP 2.6, relative to the 1981–2006 baseline, average heatwave intensity is projected to increase by 0.04 ± 0.06 K, with an increase in average duration of 11 ± 3 days, a total increase in heatwave days of 57 ± 14 days and a cumulative intensity of 15 ± 6 K x days. Under RCP 6.0, heatwave intensity is projected to increase by 0.2 ± 0.2 K, with a cumulative intensity increase of 69 ± 59 K x days. Additionally, the total number of heatwave days is projected to increase by 114 ± 51 days, and the average duration is expected to extend by 34 ± 24 days. The projections under RCP 8.5 suggest the most drastic changes. Under this scenario, heatwave intensity is anticipated to increase by 0.6 ± 0.5 K, average duration by 71 ± 50 days, total heatwave days by 157 ± 67 days and a cumulative intensity of 205 ± 185 K x days by the end of this century.

Spatial variability across the continent is notable, with northern regions, including the Amazon, and areas along the western Andes, experiencing the most substantial increases in heatwave frequency and intensity (Fig. 5.11a-l). Conversely, the southeastern region consistently exhibits smaller changes and, in some cases, even negative trends under some future scenarios. For example, under RCP 2.6, the total number of heatwave days ranges from a maximum decrease of 69 days to a maximum increase of 276 days by 2080-2099. Moreover, changes in heatwave duration vary from a decrease of 79 days to an increase of 214 days, while intensity changes range from a decrease of 2.0 K to an increase of 1.1 K. Under RCP 6.0, the projected increases are more pronounced, with total heatwave days ranging from 7 to 343 days, duration changes from -18 to 329 days, intensity variations between -1 and 1.6 K, and cumulative intensity ranging from -53 to 871 K x days across the continent. The high-emission scenario (RCP 8.5) projects the most severe impacts, with the maximum change in total heatwave days extending by up to 355 days, duration increasing up to 358 days, intensity changes increasing up to 3.4 K, and cumulative intensity reaching a maximum of 1,721 K x days.

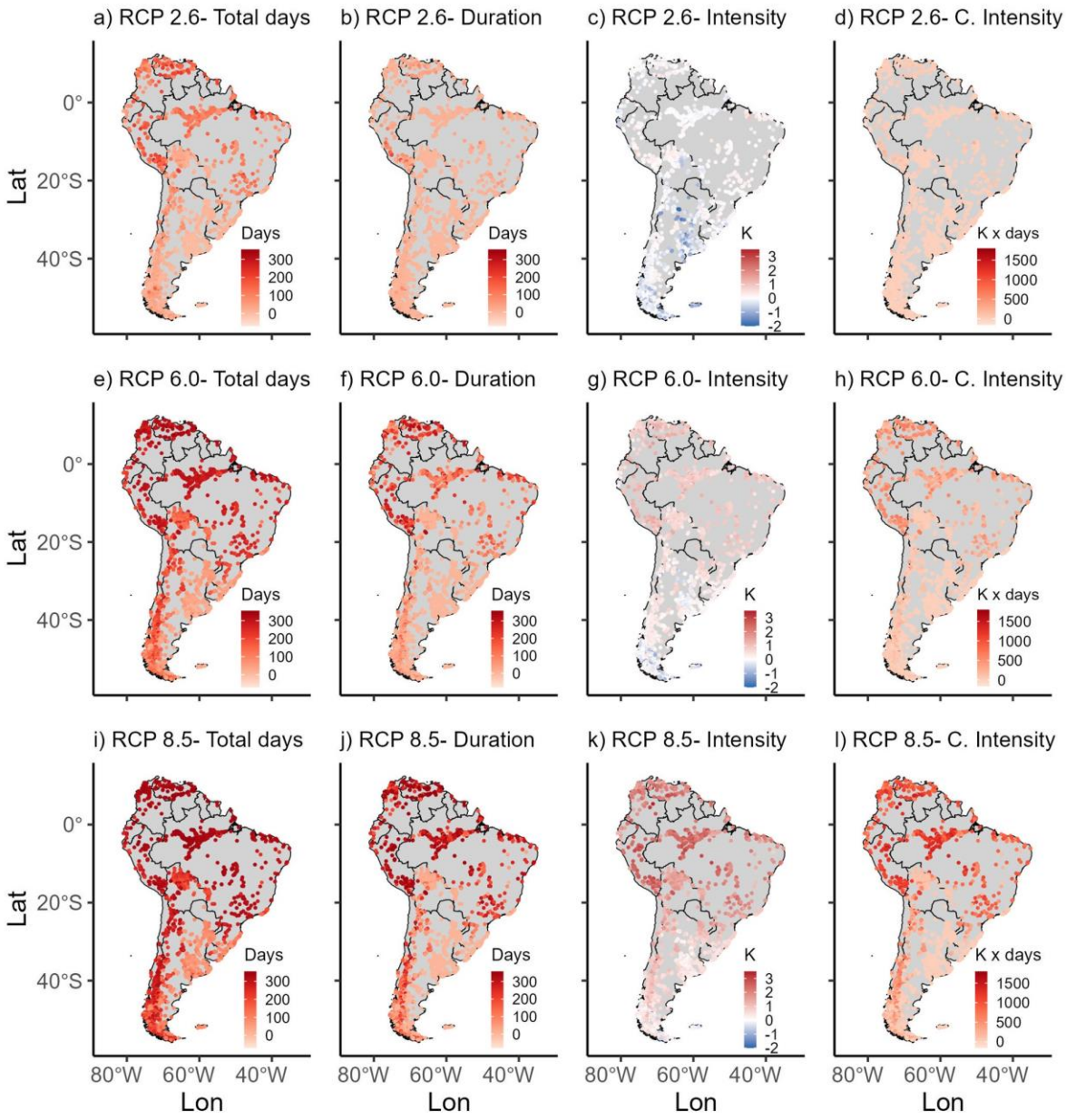


Figure 5.11. Future projections of lake heatwave anomalies (from left to right: total heatwave days, heatwave duration, heatwave intensity and cumulative intensity) of each studied lake under (a-d) RCP 2.6; (e-h) RCP 6.0; (i-l) RCP 8.5 scenarios between 2080 and 2099.

5.5. Discussion

This study provides the first comprehensive evaluation of LSWT dynamics across South America, spanning both historical (1981–2020) and projected future periods (2021–2099). Our results indicate that rising air temperatures and associated changes in surface energy fluxes are

driving significant LSWT increases across the continent. Under a high-emission scenario (RCP 8.5), LSWT anomalies could rise by an average of 2.8 ± 0.2 K by the end of the century, with the TH region projected to warm most rapidly (+3.6 ± 0.2 K). These trends are consistent with global projections of lake warming (Grant et al. 2021) and align with regional climate forecasts predicting increases of +3°C to +5°C in South American air temperatures (Llopart et al. 2020). Historical observations already show increased warming, more frequent heat extremes, and reduced precipitation, especially in the Amazon and Andes (Seneviratne et al. 2021).

The ecological implications of rising LSWTs are profound. Warmer water temperatures can extend stratification periods, reduce vertical mixing, and accelerate oxygen depletion in deeper layers, leading to hypoxic or anoxic conditions that compromise aquatic life (Wagner and Adrian 2009; Jane et al. 2021). These conditions also favour harmful algal blooms, which degrade water quality and alter species composition, posing major risks to biodiversity, particularly in South America's highly diverse freshwater ecosystems (Reis et al. 2016; Campos et al. 2021). Our findings also highlight a significant intensification of lake heatwaves across most of South America. By 2099, lake heatwaves are projected to become more frequent, longer, and more intense, especially in the NH, SH, and TH regions. This trend reflects broader climate extremes and mirrors warming patterns observed globally (Woolway et al. 2021b; Wang et al. 2024). These events pose risks not only to aquatic ecosystems but also to water-dependent livelihoods, such as fisheries and aquaculture. The 2023 Amazon heatwave, which caused mass mortality of fish and dolphins and triggered harmful microalgal blooms (Fleischmann et al. 2024; Mendes et al. 2024), underscores the urgency of addressing these threats. Projections suggest northern South America and coastal areas will be particularly vulnerable, demanding adaptive management that considers both ecological sensitivity and social vulnerability (Feron et al. 2019; Ramarao et al. 2024).

A key contribution of this study is the introduction of a diurnal–seasonal thermal typology, which provides a novel lens through which to assess lake thermal responsiveness. By classifying lakes based on their DTR, STR, and the DTR/STR ratio, we identified four distinct thermal response types: Thermally Extreme, Thermally Buffered, Seasonally Stable, and Diurnally Volatile. These categories reflect differences in the amplitude and timing of lake thermal variability and offer new insights into how lakes may respond to future climate stressors on different timescales. Thermally Extreme lakes, characterized by high variability at both diurnal and seasonal scales, were concentrated in southeastern South America and are

likely to be the most vulnerable to both short-term heat events and long-term warming. Conversely, Thermally Buffered lakes, mainly located in the north, exhibited low variability and may be more resistant to abrupt thermal shocks. Seasonally Stable lakes, which fluctuate over the year but show limited diurnal variation, were primarily observed in high-altitude regions like the Andes. These distinctions are ecologically significant: for instance, strong DTRs can increase stress on temperature-sensitive organisms, while high STRs may alter phenological cues. Moreover, the spatial patterns in DTR/STR ratios suggest that lake thermal regimes are shaped not only by climate but also by geography, elevation, and basin morphometry. Understanding these typologies can improve predictions of ecosystem responses and help prioritize lakes for targeted conservation or management interventions under future climate scenarios.

Our driver analysis identified air temperature and shortwave radiation as the dominant controls of both LSWT and DTR trends, consistent with previous studies in both tropical and temperate systems (Livingstone and Dokulil 2001; O'Reilly et al. 2015; Schmid and Köster 2016b). In particular, the influence of solar radiation was most pronounced in regions with minimal cloud cover, such as the SH region, which includes the Atacama Desert. Conversely, in the NH region near the Equator, the Intertropical Convergence Zone (ITCZ) likely dampens diurnal heating by increasing humidity and cloud cover, leading to observed declines in DTR. In addition to atmospheric drivers, lake-specific factors such as morphometry, elevation, and geographic setting strongly modulate thermal behaviour. High-altitude and deep lakes often buffer against short-term thermal fluctuations, while shallow and exposed lakes respond more acutely to atmospheric forcing (Gunkel and Casallas 2002; Augusto-Silva et al. 2019). These findings emphasize the value of integrating lake attributes with climate variables to explain LSWT variability.

Our results underscore the urgency of improving lake monitoring systems in South America, particularly given the limited availability of in situ data in many regions. The FLake model and satellite-derived datasets used in this study offer a scalable alternative, but their accuracy, especially for tropical lakes, remains constrained by sparse validation data. Expanding high-frequency temperature monitoring and improving data sharing networks would enhance model calibration and deepen our understanding of lake-climate interactions. Finally, the introduction of a diurnal–seasonal typology provides a valuable framework for future lake research globally. Applying this classification across other continents could help

identify generalizable patterns of lake thermal sensitivity and inform adaptive water management in the face of accelerating climate change.

5.6. Conclusions

This study provides the first continent-wide assessment of historical and projected LSWT dynamics across South America, incorporating both diurnal and seasonal thermal patterns from 1981 to 2099. We found that 97.0% of lakes exhibited a significant long-term warming trend, averaging +0.11 K decade^{-1}, while 86.2% showed increasing diurnal variability (+0.02 K decade^{-1}) over the past four decades. Air temperature and solar radiation emerged as the dominant drivers of these trends, with solar radiation particularly influencing short-term (diurnal) fluctuations. Projections under different greenhouse gas scenarios indicate that LSWTs will continue to rise across all thermal regions, with warming rates ranging from +0.02–0.03 K decade^{-1} under RCP 2.6 to +0.3–0.4 K decade^{-1} under RCP 8.5 by the end of the 21st century. Correspondingly, lake heatwaves are expected to become significantly more severe. Under the high-emission scenario, heatwave durations could extend by up to 358 days and intensities may increase by as much as 3.4 K. Importantly, this study introduces a new typology of lake thermal responses based on diurnal and seasonal temperature ranges (DTR and STR). This framework reveals distinct lake types, such as Thermally Extreme, Thermally Buffered, Seasonally Stable, and Diurnally Volatile, which reflect different sensitivities to atmospheric forcing. These classifications offer a valuable tool for identifying lakes most vulnerable to climate change and for prioritizing future monitoring and management efforts. Altogether, this work enhances our understanding of how South American lakes are responding to a changing climate and underscores the need for targeted, region-specific adaptation strategies. Continued integration of high-resolution modelling, satellite data, and improved in situ observations will be critical for safeguarding freshwater ecosystems and resources in the decades ahead.

Data availability

The GLAST dataset is available at https://zenodo.org/records/8322038.

VI. Conclusion and Future Perspectives

6.1. Summary of findings

Lakes are vital components in the global water cycle, playing an important role in regulating hydrology, climate and biodiversity (Lehner and Döll 2004; Messager et al. 2016). LSWT is one of the lake essential climate variables, as it influences chemical, physical and biological processes (Benson and Krause 1980; Boehrer and Schultze 2008; Sharma et al. 2015). LSWT has been increasingly affected by climate change and human activities (Pekel et al. 2016; Yao et al. 2023). Traditional methods like in situ observations can provide highly accurate measurements of lake conditions (Livingstone and Dokulil 2001; Hampton et al. 2008) but are limited in spatial coverage and only provide data at specific locations of the lake (Lieberherr and Wunderle 2018; Carrea et al. 2023). To complement in situ observations, satellite EO can be used to provide high spatial and temporal resolution data (MacCallum and Merchant 2012; Tong et al. 2023; Korver et al. 2024). However, satellite EO is often impacted by cloud cover, resulting in missing data (Sirjacobs et al. 2011; Feng et al. 2023). While various gap-filling methods have been applied successfully in marine data (Beckers and Rixen 2003; Hilborn and Costa 2018; Stock et al. 2020), their application to lake environments is less common (MacCallum and Merchant 2011). This study highlights the importance of identifying and evaluating the most suitable reconstruction method for satellite-derived lake data.

Although LSWT has been studied globally (O'Reilly et al. 2015; Schneider et al. 2019; Tong et al. 2023; Korver et al. 2024), research focused on LSWT variability in the Southern Hemisphere (e.g., South America) is underrepresented. Notably, Lake Titicaca, the largest lake in South America and the world's highest navigable lake (Pillco Zolá et al. 2019; Duquesne et al. 2021), has not been studied for long-term LSWT variability and lake heatwave occurrence. Freshwater lakes are important water resources in South America (Buytaert and Breuer 2013). Previous studies mainly focused on glacial lakes, while individual lakes were often limited to specific regions (Moser et al. 2019; Veettil and Kamp 2021; Zhao et al. 2025). Given these research gaps, it is crucial to investigate LSWT changes under the current warming climate and to project future LSWT variability. This research aims to (1) evaluate the suitable gap-filling methods for satellite-derived lake temperature data and (2) provide a comprehensive understanding of LSWT variability and lake heatwaves in Lake Titicaca, while also extending these findings to lakes across South America.

The first result chapter focuses on identifying the most suitable gap-filling method for satellite EO data, using the ESA CCI dataset (Carrea et al. 2023) and Lake Titicaca as a case study. As the largest lake in South America and a critically important water resource in Peru and Bolivia, Lake Titicaca is among the most susceptible lakes to climate change impacts (Canedo et al. 2016; Ruiz-Verdu et al. 2016; Pillco Zolá et al. 2019). Satellite EO offers long-term LSWT observations, however, cloud cover remains a significant challenge (Sirjacobs et al. 2011). Several gap-filling methods were assessed, including DINEOF (Beckers and Rixen 2003; Taylor et al. 2013), and machine learning algorithms such as Boosted Regression Tree (Kraemer et al. 2020) and DINCAE (Barth et al. 2020). DINCAE multivariate performed best compared to the other reconstruction methods. It was subsequently utilised for analysing LSWT variability at various timescales (annual, seasonal). Our findings showed that annual LSWT derived from DINCAE multivariate ranged from 285-289 K between 2000 and 2020, with higher temperatures observed during the wet season compared to the dry season. These findings highlight the importance of robust gap-filling methods and comprehensive spatial-temporal analysis of LSWT dynamics in large lakes like Lake Titicaca.

The second result chapter compared the DINCAE-derived data with the daily Global LAke Surface water Temperature (GLAST) dataset (Tong et al. 2023). The results showed that there were slight differences between the satellite-derived data and the GLAST dataset. The GLAST data was then used to analyse the LSWT and lake heatwave variability for both historical and future periods. Over the past 40 years, LSWT of Lake Titicaca exhibited an annual warming trend, with shortwave radiation and air temperature being the dominant drivers. LSWT is projected to experience warming trends, with the magnitude varying across different RCP scenarios. Additionally, heatwave metrics such as the average number of heatwave days, duration, intensity, and cumulative intensity are expected to increase significantly in this century.

The third result chapter expands the analysis to a broader set of lakes across South America, where limited in situ measurements have restricted LSWT research. The GLAST dataset was used to investigate the interannual and diurnal LSWT trends and heatwave events variability in South America. Additionally, the short-term and medium-term thermal variability were explored using new lake thermal responses based on the diurnal-seasonal temperature range. The results revealed that most of the studied lakes showed warming trends of LSWT and diurnal LSWT over the past 40 years. Air temperature was the primary driver for LSWT

increase in northern (10°N-20°S) and southern (40°S-50°S) regions, while shortwave radiation was the main influencing factor in central South America (20°S-40°S). Across South America, shortwave radiation was the dominant driver in diurnal LSWT variations. LSWT will likely increase by the end of the 21st century. Other research at the global scale also reported the changes in LSWT at a similar rate (Grant et al. 2021). Lake heatwave frequency and intensity are projected to increase in the future. The increase in LSWT and lake heatwaves can disrupt the ecological balance and therefore influence the aquatic ecosystems. Such impacts have already been observed in several South American lakes, including the Amazon, where heatwaves resulted in mass fish mortality and affected aquaculture. Additionally, these phenomena pose challenges to local communities, especially indigenous populations and tourism activities. This research highlights the rapid warming of LSWT in South America and suggests urgent attention and mitigation efforts to protect lake ecosystems under climate change on this continent.

6.2. Synthesis of contributions

The systematic evaluation and comparison of gap-filling methods for satellite EO data for lakes is one of the main contributions of this dissertation. While gap-filling techniques are widely used in marine satellite EO data (Beckers and Rixen 2003; Alvera-Azcárate et al. 2005; Barth et al. 2020), there has been a notable gap in their application and performance for inland waters (MacCallum and Merchant 2011). This research is the first study applying and rigorously comparing advanced machine learning algorithms, such as multi-model BRT or DINCAE for reconstructing missing data in lakes. In addition, using multivariate input (e.g., Chl-a) represents a novel approach which enhances the reconstruction accuracy by incorporating additional variables. The comparative analysis not only identified the most effective reconstruction method for Lake Titicaca but also for lakes globally. These results can be applied to regions where in situ data are limited and satellite EO data are obstructed by atmospheric conditions.

Another key contribution of this dissertation is its focus on the understudied region of South America. Although there are growing studies on LSWT variability globally, a large number of lake studies have focused on the Northern Hemisphere (e.g., North America and Europe) (Michelutti et al. 2015a; Aranda et al. 2021). Consequently, there is limited

understanding of LSWT changes under a changing climate in the Southern Hemisphere, such as South America. Additionally, in situ observations and long-term measurements are scarce in this region. By providing a comprehensive analysis of LSWT and lake heatwave as well as diurnal-seasonal variability in South America, with a particular emphasis on Lake Titicaca, the dissertation addresses this knowledge gap. The research used both historical and future GLAST datasets to investigate the temporal LSWT trends along with the frequency and intensity of lake heatwaves. This study offers valuable insights into climate change impacts on freshwater lakes across the continent.

Furthermore, it also advances the knowledge of meteorological variables influencing LSWT variability in South America. The findings revealed that solar radiation and air temperature are the main drivers, which are consistent with other studies conducted in different regions across the world (Schneider and Hook 2010; Toffolon et al. 2014; Schmid and Köster 2016). A novel aspect of Chapter 6 is the lake thermal response classification based on diurnal-seasonal variability. By analysing lake DTR, STR, and the DTR/STR ratio, four thermal response types are classified as Thermally Extreme, Thermally Buffered, Seasonally Stable, and Diurnally Volatile. Lakes with high DTR can impose significant stress on temperature sensitive aquatic species by disrupting metabolic functions. High STR might interfere with phenological cues, affecting life cycle events (e.g., migration). This classification provides insights for assessing lake vulnerability and resilience under climate stressors.

The findings of this dissertation have important implications for the lake ecosystem and water resource management. Increasing LSWT and frequent lake heatwaves are likely to pose significant risks to aquatic species and community livelihoods that depend on these lakes. Mass fish mortality and aquaculture disruption due to lake heatwaves in South America highlight the need for urgent monitoring and adaptive management.

6.3. Limitations and uncertainties

Satellite EO data play an important role in assessing inland water quantity and quality. However, these satellite images often contain missing pixels due to clouds, shadows, etc, which limit their applicability. Gap filling in satellite datasets is essential to ensure the continuity, reliability and more complete time series data.

DINCAE multivariate is the most appropriate method for filling missing data with the lowest RMSE. The classical interpolation method, such as DINEOF, has simple computation, is less complex and running time than other methods. However, DINCAE required a specific setup and a Graphics Processing Unit (GPU) processor. DINCAE 1.0 only works with Python (version 3.6/3.7) and uses the specific packages *Tensorflow* (version 1.15), *netcdf4* (version 1.4.2) and *numpy* (version 1.15.4). For high-performance computers, it could be a challenge to install the older version of these Python packages. The latest version of DINCAE 2.0 is now written in the Julia programming language and is freely accessible at https://github.com/gher-uliege/DINCAE.jl. It is also advised to adjust parameters such as reducing the mini-batch size, changing the number of filter layers, or using lower resolution data to reduce memory and processing time. However, parameter optimisation depends on the study area and data availability (temporal coverage).

DINEOF method has specific considerations that must be addressed. The maximum number of EOFs is not defined before the reconstruction in the DINEOF method, but it is defined using the iterative process. Therefore, it can take a long time to determine the optimal number of EOFs (Ping et al. 2016). DINEOF does not work well for reconstructing a small amount of satellite image data because the reconstructed values can be close to the mean values of the original data. When each temporal slice of data (daily timestep) includes valid data of a minimum of 5% of the potential pixels, EOF-based reconstruction performs best (Alvera-Azcárate et al. 2007). Because of the smoothing effect from DINEOF, some extreme events contribute little variance that might not be clearly represented in the reconstructed data (Wang and Liu 2014). Overall, the rigorous assessment of the gap-filling methods gave confidence in the use of DINCAE in the current work.

The impact of spatial resolution on the analysis results was not assessed in this study, as the main objective was to compare gap-filling methods. However, the choice of spatial resolution can impact the accuracy of the reconstructed data, particularly in regions with significant spatial variation, such as lake edges. The resolution may affect the representation of fine-scale features and small-scale processes. Due to computational constraints related to processing large datasets, evaluating higher-resolution data (1 km) was beyond the scope of this study. Evaluating the influence of different spatial resolutions on model performance is an important aspect and should be considered in future work.

Auxiliary variables, particularly Chl-a and meteorological variables such as wind speed, could indeed enhance the reconstruction of LSWT. However, these data have their limitations. For example, filtering pixels with uncertainty values > 60% for Chl-a data was used to mitigate limitations inherent in aquatic remote sensing due to sensor limitations, data processing or algorithm assumptions (Merchant et al. 2017). The filtering process was suggested by Free et al. (2022), who used the same dataset and established this threshold to ensure that only data with a high level of confidence were included in the analysis. Meteorological data availability was constrained in the case of Lake Titicaca. In situ meteorological data (e.g., wind speed) are not consistently available, and satellite or reanalysis alternatives (e.g., ERA5 or ERA5-Land) have spatial resolutions (0.25° and 0.09°, respectively) that are too coarse relative to the spatial detail of the satellite-derived LSWT data used in this study. Moreover, validation of reanalysis wind products over large tropical lakes remains limited, introducing additional uncertainty. Therefore, this study focused on evaluating the performance of different gap-filling methods using available satellite-derived variables. Such variables could be considered when higher-resolution or validated datasets become available for Lake Titicaca or other well-instrumented lakes.

One of the challenges in this study is the limited availability of in situ data across South American lakes, which constrains the calibration and validation processes of the model-derived and satellite-derived data. While these data offer valuable and scalable solutions for monitoring LSWT, uncertainties can still exist, and limited accuracy remains in freshwater lakes. By expanding in situ monitoring networks and enhancing regional collaboration, these issues would significantly improve model-derived and satellite-derived data reliability and accuracy.

6.4. Implications for water management

Warming surface water temperature will cause changes in the physical and biochemical processes in the lake ecosystem, such as thermal stratification changes, shifting mixing regimes, gas solubility and dissolved oxygen reduction and aquatic species distribution and abundance variability, etc (Wang et al. 2023). These changes influence agriculture, aquaculture, and domestic water use in this area. Lake Titicaca is one of the most valuable natural resources in the region as it has historically been critical in forming the Andean cultures, such as the Tiwanaku and continues to give the Aymara tribes food and raw materials

(Duquesne et al. 2021) and provides water supply for the inhabitants (Pillco Zolá et al. 2019). The lake is also considered an internationally important wetland because of its ecological, zoological and botanical diversity (Zubieta et al. 2021). However, this lake has experienced severe water deficits in recent years, for example, it was fully dried out in December 2015 (Pillco Zolá et al. 2019) and most recently in 2023 due to El Niño (Briefings 2023). The continuous drop in water level not only affects the indigenous people (Uros, Aymara, Quechua) whose livelihoods depend on agriculture (fishing, farming, etc) and tourism, but also the ecosystem (Briefings 2023). For example, the aquatic plant "totora" (*Schoenoplectus californicus*), important to the socioeconomic of the Uros, is diminishing (Briefings 2023).

Similar to Lake Titicaca, other lakes in South America have also been affected by warming temperatures and lake heatwaves, resulting in a decline of freshwater fish populations (Campos et al. 2021). For example, due to the 2023 heatwave, mass fish death was recorded in lakes in the Amazon (Fleischmann et al. 2024). Aquaculture production will also decrease in the near future (Fleischmann et al. 2024). Lake heatwaves caused oxygen depletion, increased eutrophication and harmful algal bloom formation, causing water quality issues (Jankowski et al. 2006; Jöhnk et al. 2008; Woolway et al. 2021c). Mendes et al (2024) reported that heatwaves with extreme drought caused a bloom of harmful microalgae in Amazon lakes (Mendes et al. 2024). This event directly affected the aquatic ecosystem as well as the water supply of hundreds of thousands of people in the Amazon River and nearby urban areas (Mendes et al. 2024). Lake heatwaves, along with increased lake surface temperature, will threaten fish productivity, water availability, and ecosystem health, which directly affect livelihoods, food security, and cultural activities connected to lake systems. Decreased water quality and fisheries productivity may lead to poverty and migration pressures to urban areas. Existing policies and legislative frameworks, such as the Autonomous Binational Authority of Lake Titicaca and national water governance laws in Peru, Bolivia, Chile, etc, provide a foundation for cooperative lake management. However, these policies often lack mechanisms to integrate climate change adaptation, community participation, and social equity. Climate-resilient water management, strengthened transboundary cooperation, and the inclusion of indigenous knowledge and local engagement should be prioritized. As warming LSWT and extreme events like lake heatwaves are expected to increase in frequency, intensity and duration, investigating current trends and long-term monitoring of climate fluctuations are critical for developing adaptation and water management plans. This current study can support strategies and policy-

makers for the development of early warning systems for aquatic system management by developing real-time lake temperature and heatwave monitoring tools.

6.5. Future research

This study presented the advantages of using gap-filling methods to reconstruct missing data in satellite EO data for lake research. In addition, it highlights the importance of investigating the current LSWT and lake heatwave variability and projecting their future trends in South American lakes. However, parts of this research can be improved and addressed in future work. Due to the computational cost, the gap-filling methods were operated on a Central Processing Unit (CPU) computer. It would be beneficial to run the algorithms on a GPU processor to decrease the processing time and process bulk and high-resolution data.

Reconstruction methods were applied in Lake Titicaca as a first case study; however, these algorithms can be extended to other lakes in South America. Applying and validating the gap-filling techniques for lakes in diverse climates and geographic regions would help to assess the robustness of these methods. Meteorological variables such as wind speed, humidity and/or solar radiation can be added to the model to increase the accuracy of the algorithms, where LSWT dynamics are mainly influenced by atmospheric conditions. However, such data requires long-term and high-resolution monitoring, which is limited for lakes in this area.

Several factors, such as sun angle, lighting conditions, and lake turbidity, can affect the quality of Chl-a data and contribute to variability in the measurements. However, these factors were not specifically accounted for in this study's quality control process. Future work could explore how these variables influence Chl-a data and consider integrating additional pre-processing steps to correct for such influences. Additionally, more adaptive approaches such as robust statistical methods (e.g., the interquartile range (IQR) method or percentile-based thresholds) or methods that account for seasonal and spatial variability in Chl-a concentrations could be explored.

Future assessment can also extend beyond physical parameters by including the socio-economic and ecological impacts. Collaborating with stakeholders and engaging with local communities, such as the indigenous people, will provide insights into the consequences of warming LSWT. An interdisciplinary approach that combines ecology, social and climate research will be beneficial for adaptation and management plans.

6.6. Final remarks

This dissertation provides a comprehensive understanding of LSWT and lake heatwave dynamics in Lake Titicaca and at a broader continental scale of South America. By evaluating and comparing various gap-filling methods, including machine learning, this study addresses the challenge of missing data in satellite EO and the scarcity of in situ observations in the region. A novel lake thermal typology was introduced, offering insights into lake vulnerability and resilience under climate change. The research highlights the ecological and socio-economic risks posed by warming LSWT and frequent lake heatwaves. Freshwater biodiversity, ecosystems and community well-being that mostly depend on lake resources for their livelihoods are threatened by these extreme events. These findings emphasise the importance of continuous lake monitoring systems, improved regional scientific collaboration and implementation of environmental policy to protect critical lake ecosystems and support local communities under the warming climate.

References

Abarca-Del-Rio, R., Crétaux, J.F., Berge-Nguyen, M. and Maisongrande, P. 2012. Does Lake Titicaca still control the Lake Poopó system water levels? An investigation using satellite altimetry and MODIS data (2000–2009). *Remote Sensing Letters* 3(8), pp. 707–714. doi: 10.1080/01431161.2012.667884.

Abbott, M.B., Binford, M.W., Brenner, M. and Kelts, K.R. 1997. A 3500 14 C yr High-Resolution Record of Water-Level Changes in Lake Titicaca, Bolivia/Peru. *Quaternary Research* 47(2), pp. 169–180. doi: 10.1006/qres.1997.1881.

Åberg, J., Jansson, M. and Jonsson, A. 2010. Importance of water temperature and thermal stratification dynamics for temporal variation of surface water CO2 in a boreal lake. *Journal of Geophysical Research: Biogeosciences* 115(G2). Available at: https://doi.org/10.1029/2009JG001085.

Abrahams, C. et al. 2013. The impact of extreme events on freshwater ecosystems. *Ecological Issues*, p. 68.

Achá, D., Guédron, S., Amouroux, D., Point, D., Lazzaro, X., Fernandez, P.E. and Sarret, G. 2018. Algal bloom exacerbates hydrogen sulfide and methylmercury contamination in the emblematic high-altitude lake titicaca. *Geosciences (Switzerland)* 8(12). doi: 10.3390/geosciences8120438.

Adrian, R. et al. 2009. Lakes as sentinels of climate change. *Limnology and Oceanography* 54(6 PART 2), pp. 2283–2297. doi: 10.4319/lo.2009.54.6_part_2.2283.

Adrian, R. et al. 2016. Environmental Impacts—Lake Ecosystems. In: *Hydrobiologia*. pp. 315–340. doi: 10.1007/978-3-319-39745-0_10.

Aguilar-Lome, J., Soca-Flores, R. and Diego, G. 2021. Journal of South American Earth Sciences Evaluation of the Lake Titicaca's surface water temperature using LST MODIS time series (2000 – 2020). 112(October). doi: 10.1016/j.jsames.2021.103609.

Alfieri, L. et al. 2017. Global projections of river flood risk in a warmer world. *Earth's Future* 5(2), pp. 171–182. doi: https://doi.org/10.1002/2016EF000485.

Almazroui, M. et al. 2021. Assessment of CMIP6 Performance and Projected Temperature and Precipitation Changes Over South America. *Earth Systems and Environment* 5(2), pp. 155–183. doi: 10.1007/s41748-021-00233-6.

Alvera-Azcárate, A., Barth, A., Beckers, J.M. and Weisberg, R.H. 2007. Multivariate reconstruction of missing data in sea surface temperature, chlorophyll, and wind satellite fields. *Journal of Geophysical Research: Oceans* 112(3), pp. 1–11. doi: 10.1029/2006JC003660.

Alvera-Azcárate, A., Barth, A., Rixen, M. and Beckers, J.M. 2005. Reconstruction of incomplete oceanographic data sets using empirical orthogonal functions: application to the Adriatic Sea surface temperature. *Ocean Modelling* 9(4), pp. 325–346. doi: https://doi.org/10.1016/j.ocemod.2004.08.001.

An, C., Zhang, F., Chan, N.W., Johnson, V.C. and Shi, J. 2022. A review on the research progress of lake water volume estimation methods. *Journal of Environmental Management* 314(November 2021), p. 115057. doi: 10.1016/j.jenvman.2022.115057.

Anderson, L.O. et al. 2018. Vulnerability of Amazonian forests to repeated droughts. *Philosophical Transactions of the Royal Society B: Biological Sciences* 373(1760), p. 20170411. doi: 10.1098/rstb.2017.0411.

Andrade, M. 2018. *Atlas - Clima y eventos extremos del Altiplano Central perú-boliviano / Climate and extreme events from the Central Altiplano of Peru and Bolivia 1981-2010.* doi: 10.4480/GB2018.N01.

Andrew, T. et al. 2008. Cooling lakes while the world warms: Effects of forest regrowth and increased dissolved organic matter on the thermal regime of a temperate, urban lake. *Limnology and Oceanography* 53(1), pp. 404–410. doi: 10.4319/lo.2008.53.1.0404.

Anushka, B.A. and Mishra, A. 2022. Effects of dissolved oxygen concentration on freshwater fish: A review. *International Journal of Fisheries and Aquatic Studies* 10(4), pp. 113–127. doi: 10.22271/fish.2022.v10.i4b.2693.

Aranda, A.C. et al. 2021. Evidence of climate change based on lake surface temperature trends in south central Chile. *Remote Sensing* 13(22). doi: 10.3390/rs13224535.

Archundia, D. et al. 2017a. Antibiotic pollution in the Katari subcatchment of the Titicaca Lake: Major transformation products and occurrence of resistance genes. *Science of the Total Environment* 576, pp. 671–682. doi: 10.1016/j.scitotenv.2016.10.129.

Archundia, D. et al. 2017b. How Uncontrolled Urban Expansion Increases the Contamination of the Titicaca Lake Basin (El Alto, La Paz, Bolivia). *Water, Air, and Soil Pollution* 228(1). doi: 10.1007/s11270-016-3217-0.

Arias, P.A. et al. 2021. Hydroclimate of the Andes Part II: Hydroclimate Variability and Sub-Continental Patterns. *Frontiers in Earth Science* 8(February), pp. 1–25. doi: 10.3389/feart.2020.505467.

Armstrong, J.B. et al. 2021. The importance of warm habitat to the growth regime of cold-water fishes. *Nature Climate Change* 11(4), pp. 354–361. doi: 10.1038/s41558-021-00994-y.

Arvola, L. et al. 2009. The Impact of the Changing Climate on the Thermal Characteristics of Lakes. pp. 85–101. doi: 10.1007/978-90-481-2945-4_6.

Assel, R.A. 1998. The 1997 ENSO event and implication for North American Laurentian Great Lakes winter severity and ice cover. *Geophysical Research Letters* 25(7), pp. 1031–1033. doi: 10.1029/98GL00720.

Augusto-Silva, P.B., MacIntyre, S., de Moraes Rudorff, C., Cortés, A. and Melack, J.M. 2019. Stratification and mixing in large floodplain lakes along the lower Amazon River. *Journal of Great Lakes Research* 45(1), pp. 61–72. doi: 10.1016/j.jglr.2018.11.001.

Austin, J.A. and Colman, S.M. 2007. Lake Superior summer water temperatures are increasing more rapidly than regional temperatures: A positive ice-albedo feedback. *Geophysical Research Letters* 34(6), pp. 1–5. doi: 10.1029/2006GL029021.

Baker, P.A., Fritz, S.C., Garland, J. and Ekdahl, E. 2005. Holocene hydrologic variation at Lake Titicaca, Bolivia/Peru, and its relationship to North Atlantic climate variation. *Journal of Quaternary Science* 20(7–8), pp. 655–662. doi: 10.1002/jqs.987.

Balsamo, G., Salgado, R., Dutra, E., Boussetta, S., Stockdale, T. and Potes, M. 2012. On the contribution of lakes in predicting near-surface temperature in a global weather forecasting

model. *Tellus A: Dynamic Meteorology and Oceanography* 64(1), p. 15829. doi: 10.3402/tellusa.v64i0.15829.

de Barros Soares, D., Lee, H., Loikith, P.C., Barkhordarian, A. and Mechoso, C.R. 2017. Can significant trends be detected in surface air temperature and precipitation over South America in recent decades? *International Journal of Climatology* 37(3), pp. 1483–1493. doi: 10.1002/joc.4792.

Barros, V.R., Boninsegna, J.A., Camilloni, I.A., Chidiak, M., Magrín, G.O. and Rusticucci, M. 2015. Climate change in Argentina: trends, projections, impacts and adaptation. *WIREs Climate Change* 6(2), pp. 151–169. doi: https://doi.org/10.1002/wcc.316.

Barth, A., Alvera-Azcárate, A., Licer, M. and Beckers, J.M. 2020. DINCAE 1.0: A convolutional neural network with error estimates to reconstruct sea surface temperature satellite observations. *Geoscientific Model Development* 13(3), pp. 1609–1622. doi: 10.5194/gmd-13-1609-2020.

Barth, A., Alvera-Azcárate, A., Troupin, C. and Beckers, J.M. 2022. DINCAE 2.0: multivariate convolutional neural network with error estimates to reconstruct sea surface temperature satellite and altimetry observations. *Geoscientific Model Development* 15(5), pp. 2183–2196. doi: 10.5194/gmd-15-2183-2022.

Bartosiewicz, M., Laurion, I., Clayer, F. and Maranger, R. 2016. Heat-Wave Effects on Oxygen, Nutrients, and Phytoplankton Can Alter Global Warming Potential of Gases Emitted from a Small Shallow Lake. *Environmental Science and Technology* 50(12), pp. 6267–6275. doi: 10.1021/acs.est.5b06312.

Bashir, I., Lone, F.A., Bhat, R.A., Mir, S.A., Dar, Z.A. and Dar, S.A. 2020. Concerns and Threats of Contamination on Aquatic Ecosystems. In: Hakeem, K. R., Bhat, R. A., and Qadri, H. eds. *Bioremediation and Biotechnology: Sustainable Approaches to Pollution Degradation*. Cham: Springer International Publishing, pp. 1–26. doi: 10.1007/978-3-030-35691-0_1.

Beckers, J.M. and Rixen, M. 2003. EOF calculations and data filling from incomplete oceanographic datasets. *Journal of Atmospheric and Oceanic Technology* 20(12), pp. 1839–1856. doi: 10.1175/1520-0426(2003)020<1839:ECADFF>2.0.CO;2.

Bennett, A.C. et al. 2023. Sensitivity of South American tropical forests to an extreme climate anomaly. *Nature Climate Change* 13(9), pp. 967–974. doi: 10.1038/s41558-023-01776-4.

Benson, B.B. and Krause, D. 1980. The concentration and isotopic fractionation of gases dissolved in freshwater in equilibrium with the atmosphere. 1. Oxygen. *Limnology and Oceanography* 25(4), pp. 662–671. doi: 10.4319/lo.1980.25.4.0662.

Berger, S.A. et al. 2007. Water temperature and mixing depth affect timing and magnitude of events during spring succession of the plankton. *Oecologia* 150(4), pp. 643–654. doi: 10.1007/s00442-006-0550-9.

Berger, S.A., Diehl, S., Stibor, H., Trommer, G. and Ruhenstroth, M. 2010. Water temperature and stratification depth independently shift cardinal events during plankton spring succession. *Global Change Biology* 16(7), pp. 1954–1965. doi: 10.1111/j.1365-2486.2009.02134.x.

Bergmann, J. et al. 2021. *Assessing the Evidence: Climate Change and Migration in Peru.* Potsdam Institute for Climate Impact Research (PIK), Potsdam, and International Organization for Migration (IOM), Geneva.

Bergström, A.K., Jonsson, A., Isles, P.D.F., Creed, I.F. and Lau, D.C.P. 2020. Changes in nutritional quality and nutrient limitation regimes of phytoplankton in response to declining N deposition in mountain lakes. *Aquatic Sciences* 82(2). doi: 10.1007/s00027-020-0697-1.

Bert, F., Estrada, M. De, Naumann, G., Negri, R. and Podestá, G. 2021. The 2017-18 drought in the Argentine Pampas – Impacts on Agriculture Key points. *GAR Special Report on Drought 2021* 2, pp. 1–24.

Bianchi, E., Solarte, A. and Guozden, T.M. 2017. Large scale climate drivers for wind resource in Southern South America. *Renewable Energy* 114, pp. 708–715. doi: 10.1016/j.renene.2017.07.075.

Biamont-Rojas, I.E., Cardoso-Silva, S., Figueira, R.C.L., Kim, B.S.M., Alfaro-Tapia, R. and Pompêo, M. 2023. Spatial distribution of arsenic and metals suggest a high ecotoxicological potential in Puno Bay, Lake Titicaca, Peru. Science of the Total Environment 871(April 2022). doi: 10.1016/j.scitotenv.2023.162051.

Black, J.N. 1956. The distribution of solar radiation over the Earth's surface. *Archiv für Meteorologie, Geophysik und Bioklimatologie Serie B* 7(2), pp. 165–189. doi: 10.1007/BF02243320.

Boehrer, B. and Schultze, M. 2008. Stratification of lakes. *Reviews of Geophysics* 46(2), pp. 1–27. doi: 10.1029/2006RG000210.

Bonacina, L., Fasano, F., Mezzanotte, V. and Fornaroli, R. 2023. Effects of water temperature on freshwater macroinvertebrates: a systematic review. *Biological Reviews* 98(1), pp. 191–221. doi: 10.1111/brv.12903.

Bonnet, M.P. et al. 2008. Floodplain hydrology in an Amazon floodplain lake (Lago Grande de Curuaí). *Journal of Hydrology* 349(1), pp. 18–30. doi: https://doi.org/10.1016/j.jhydrol.2007.10.055.

de Boor, C. 1980. A Practical Guide to Splines. *Mathematics of Computation* 34(149), p. 325. doi: 10.2307/2006241.

Bouffard, D., Kiefer, I., Wüest, A., Wunderle, S. and Odermatt, D. 2018. Are surface temperature and chlorophyll in a large deep lake related? An analysis based on satellite observations in synergy with hydrodynamic modelling and in-situ data. *Remote Sensing of Environment* 209(August 2017), pp. 510–523. doi: 10.1016/j.rse.2018.02.056.

Boyce, D.G., Lewis, M.R. and Worm, B. 2010. Global phytoplankton decline over the past century. *Nature* 466(7306), pp. 591–596. doi: 10.1038/nature09268.

Brêda, J.P.L.F., Cauduro Dias de Paiva, R., Siqueira, V.A. and Collischonn, W. 2023. Assessing climate change impact on flood discharge in South America and the influence of its main drivers. *Journal of Hydrology* 619, p. 129284. doi: https://doi.org/10.1016/j.jhydrol.2023.129284.

Briefings, E. 2023. *Titicaca drought hits local Peru-Bolivia economy*. doi: 10.1108/OXAN-DB282037.

Brown, L. and Duguay, C. 2010. The response and role of ice cover in lake-climate interactions. *Progress in Physical Geography: Earth and Environment* 34(5), pp. 671–704. doi: 10.1177/0309133310375653.

Brown, L.C. and Duguay, C.R. 2022. *Lake Ice*. doi: https://doi.org/10.25923/1v84-vt30.

Bush, M.B., Hanselman, J.A. and Gosling, W.D. 2010. Nonlinear climate change and Andean feedbacks: an imminent turning point? *Global Change Biology* 16(12), pp. 3223–3232. doi: 10.1111/j.1365-2486.2010.02203.x.

Busker, T. et al. 2019. A global lake and reservoir volume analysis using a surface water dataset and satellite altimetry. *Hydrology and Earth System Sciences* 23(2), pp. 669–690. doi: 10.5194/hess-23-669-2019.

Butcher, J.B., Nover, D., Johnson, T.E. and Clark, C.M. 2015. Sensitivity of lake thermal and mixing dynamics to climate change. *Climatic Change* 129(1), pp. 295–305. doi: 10.1007/s10584-015-1326-1.

Buytaert, W. and Breuer, L. 2013. Water resources in South America: Sources and supply, pollutants and perspectives. *IAHS-AISH Proceedings and Reports* 361(July), pp. 106–113.

Byrne, M.P. and O'Gorman, P.A. 2016. Understanding Decreases in Land Relative Humidity with Global Warming: Conceptual Model and GCM Simulations. *Journal of Climate* 29(24), pp. 9045–9061. doi: 10.1175/JCLI-D-16-0351.1.

Byrne, M.P. and O'Gorman, P.A. 2018. Trends in continental temperature and humidity directly linked to ocean warming. *Proceedings of the National Academy of Sciences* 115(19), pp. 4863–4868. doi: 10.1073/pnas.1722312115.

Cáceres, L., Gómez-Silva, B., Garró, X., Rodríguez, V., Monardes, V. and McKay, C.P. 2007. Relative humidity patterns and fog water precipitation in the Atacama Desert and biological implications. *Journal of Geophysical Research: Biogeosciences* 112(G4). doi: https://doi.org/10.1029/2006JG000344.

Camacho Guerreiro, A.I., Ladle, R.J. and da Silva Batista, V. 2016. Riverine fishers' knowledge of extreme climatic events in the Brazilian Amazonia. *Journal of Ethnobiology and Ethnomedicine* 12(1), p. 50. doi: 10.1186/s13002-016-0123-x.

Campos, D.F., Amanajás, R.D., Almeida-Val, V.M.F. and Val, A.L. 2021. Climate vulnerability of South American freshwater fish: Thermal tolerance and acclimation. *Journal of Experimental Zoology Part A: Ecological and Integrative Physiology* 335(9–10), pp. 723–734. doi: 10.1002/jez.2452.

Canedo, C., Zolá, R.P. and Berndtsson, R. 2016. Role of hydrological studies for the development of the TDPS system. *Water (Switzerland)* 8(4), pp. 1–14. doi: 10.3390/w8040144.

Canedo Rosso, C., Hochrainer-Stigler, S., Pflug, G., Condori, B. and Berndtsson, R. 2018. Early warning and drought risk assessment for the Bolivian Altiplano agriculture using high resolution satellite imagery data. *Natural Hazards and Earth System Sciences Discussions* (May), pp. 1–23. doi: https://doi.org/10.5194/nhess-2018-133.

Canedo-Rosso, C., Hochrainer-Stigler, S., Pflug, G., Condori, B. and Berndtsson, R. 2021. Drought impact in the Bolivian Altiplano agriculture associated with the El Niño–Southern Oscillation using satellite imagery data. *Natural Hazards and Earth System Sciences* 21(3), pp. 995–1010. doi: 10.5194/nhess-21-995-2021.

Cannon, A.J., Sobie, S.R. and Murdock, T.Q. 2015. Bias correction of GCM precipitation by quantile mapping: How well do methods preserve changes in quantiles and extremes? *Journal of Climate* 28(17), pp. 6938–6959. doi: 10.1175/JCLI-D-14-00754.1.

Carabajal, C.C. and Boy, J.P. 2021. Lake and reservoir volume variations in South America from radar altimetry, ICESat laser altimetry, and GRACE time-variable gravity. *Advances in Space Research* 68(2), pp. 652–671. doi: 10.1016/j.asr.2020.04.022.

Caraballo, P., Forsberg, B.R., de Almeida, F.F. and Leite, R.G. 2014. Comportamento diário da temperatura, Condutividade e oxigênio dissolvido em um lago de inundação Amazônico: Descrição de um fenômeno de friagem. *Acta Limnologica Brasiliensia* 26(3), pp. 318–331. doi: 10.1590/S2179-975X2014000300011.

Caretta, M.A. et al. 2022. *IPCC 2022: Chapter 4*. Cambridge University Press, Cambridge, UK and New York, NY, USA. doi: 10.1017/9781009325844.006.

Carey, C.C., Ibelings, B.W., Hoffmann, E.P., Hamilton, D.P. and Brookes, J.D. 2012. Eco-physiological adaptations that favour freshwater cyanobacteria in a changing climate. *Water Research* 46(5), pp. 1394–1407. doi: 10.1016/j.watres.2011.12.016.

Caring4others. 2021. *Flooding Crisis in Guyana, June 2021*. Available at: https://caring4others.org/flooding-crisis-in-guyana-june-2021/ [Accessed: 11 December 2023].

Carrea, L. et al. 2023. Satellite-derived multivariate world-wide lake physical variable timeseries for climate studies. *Scientific Data* 10(1), pp. 1–28. doi: 10.1038/s41597-022-01889-z.

Carvalho, L.M. V. 2020. Assessing precipitation trends in the Americas with historical data: A review. *WIREs Climate Change* 11(2), p. e627. doi: https://doi.org/10.1002/wcc.627.

Castendyk, D.N., Obryk, M.K., Leidman, S.Z., Gooseff, M. and Hawes, I. 2016. Lake Vanda: A sentinel for climate change in the McMurdo Sound Region of Antarctica. *Global and Planetary Change* 144, pp. 213–227. doi: 10.1016/j.gloplacha.2016.06.007.

Cavazos, T. et al. 2024. Challenges for climate change adaptation in Latin America and the Caribbean region. *Frontiers in Climate* 6(April), pp. 1–17. doi: 10.3389/fclim.2024.1392033.

Choiński, A. and Strzelczak, A. 2018. Variability of Short-Term Diel Water Temperature Amplitudes in a Mountain Lake. *Water* 10(795), pp. 1–18. doi: https://doi.org/10.3390/w10060795.

Chuchón, E. and Pereira, A. 2017. Analysis of the variability of water levels of Titicaca. In: *Sciforum Electronic Conference Series*. pp. 12–16.

Van Cleave, K., Lenters, J.D., Wang, J. and Verhamme, E.M. 2014. A regime shift in lake superior ice cover, Evaporation, And water temperature following the warm el niño winter of 1997–1998. *Limnology and Oceanography* 59(6), pp. 1889–1898. doi: 10.4319/lo.2014.59.6.1889.

Coppens, J., Trolle, D., Jeppesen, E. and Beklioğlu, M. 2020. The impact of climate change on a Mediterranean shallow lake: insights based on catchment and lake modelling. *Regional Environmental Change* 20(2). doi: 10.1007/s10113-020-01641-6.

Cretaux, J.-F., Letolle, R. and Bergé-Nguyen, M. 2013. History of Aral Sea level variability and current scientific debates. *Global and Planetary Change* 110, pp. 99–113. doi: https://doi.org/10.1016/j.gloplacha.2013.05.006.

Cross, S.L., Baker, P.A., Seltzer, G.O., Fritz, S.C. and Dunbar, R.B. 2000. A new estimate of the Holocene lowstand level of Lake Titicaca, central Andes, and implications for tropical palaeohydrology. *Holocene* 10(1), pp. 21–32. doi: 10.1191/095968300671452546.

Dagosta, F.C.P. and Pinna, M. De. 2019. The Fishes of the Amazon: Distribution and Biogeographical Patterns, with a Comprehensive List of Species. *Bulletin of the American Museum of Natural History* 2019(431), pp. 1–163. doi: 10.1206/0003-0090.431.1.1.

Dejoux, C. and Iltis, A. 1992. *Lake Titicaca: A Synthesis of Limnological Knowledge*.

Delclaux, F., Coudrain, A. and Condom, T. 2007. Evaporation estimation on Lake Titicaca: a synthesis review and modelling. *Hydrological Processes* 21(13), pp. 1664–1677. doi: 10.1002/hyp.6360.

Dereczynski, C. et al. 2020. Downscaling of climate extremes over South America – Part I: Model evaluation in the reference climate. *Weather and Climate Extremes* 29, p. 100273. doi: https://doi.org/10.1016/j.wace.2020.100273.

Desai, A.R., Austin, J.A., Bennington, V. and McKinley, G.A. 2009. Stronger winds over a large lake in response to weakening air-to-lake temperature gradient. *Nature Geoscience* 2(12), pp. 855–858. Available at: https://doi.org/10.1038/ngeo693.

Desgué-itier, O. et al. 2022. Past and future climate change effects on thermal regime and oxygen solubility of four peri-alpine lakes. 1(June), pp. 1–34. doi: 10.5194/egusphere-2022-260.

Dias, N.L. and Vissotto, D. 2017. The effect of temperature-humidity similarity on Bowen ratios, dimensionless standard deviations, and mass transfer coefficients over a lake. *Hydrological Processes* 31(2), pp. 256–269. doi: 10.1002/hyp.10925.

Diaz, M., Pedrozo, F. and Baccala, N. 2000. Summer classification of Southern Hemisphere temperate lakes (Patagonia, Argentina). *Lakes & Reservoirs: Science, Policy and Management for Sustainable Use* 5(4), pp. 213–229. doi: 10.1046/j.1440-1770.2000.00118.x.

Dillon, M.E., Wang, G. and Huey, R.B. 2010. Global metabolic impacts of recent climate warming. *Nature* 467(7316), pp. 704–706. doi: 10.1038/nature09407.

Dokulil, M.T. 2014. Impact of climate warming on European inland waters. *Inland Waters* 4(1), pp. 27–40. doi: 10.5268/IW-4.1.705.

Dokulil, M.T., de Eyto, E., Maberly, S.C., May, L., Weyhenmeyer, G.A. and Woolway, R.I. 2021. Increasing maximum lake surface temperature under climate change. *Climatic Change* 165(3–4), pp. 1–17. doi: 10.1007/s10584-021-03085-1.

Doubek, J.P. et al. 2021. The extent and variability of storm-induced temperature changes in lakes measured with long-term and high-frequency data. *Limnology and Oceanography* 66(5), pp. 1979–1992. doi: https://doi.org/10.1002/lno.11739.

Duan, Z., Gao, W., Cheng, G., Zhang, Y. and Chang, X. 2024. Warming surface and Lake heatwaves as key drivers to harmful algal Blooms: A case study of Lake Dianchi, China. *Journal of Hydrology* 632(February), p. 130971. doi: 10.1016/j.jhydrol.2024.130971.

Duquesne, F., Vallaeys, V., Vidaurre, P.J. and Hanert, E. 2021. A coupled ecohydrodynamic model to predict algal blooms in Lake Titicaca. *Ecological Modelling* 440(October 2020), p. 109418. doi: 10.1016/j.ecolmodel.2020.109418.

Duwig, C. et al. 2014. Impacts of Anthropogenic Activities on the Contamination of a Sub Watershed of Lake Titicaca. Are Antibiotics a Concern in the Bolivian Altiplano? *Procedia Earth and Planetary Science* 10, pp. 370–375. doi: 10.1016/j.proeps.2014.08.062.

Edinger, J.E., Duttweiler, D.W. and Geyer, J.C. 1968. The Response of Water Temperatures to Meteorological Conditions. *Water Resources Research* 4(5), pp. 1137–1143. doi: 10.1029/WR004i005p01137.

Edmundson, J.A. and Mazumder, A. 2002. Regional and hierarchical perspectives of thermal regimes in subarctic, Alaskan lakes. *Freshwater Biology* 47(1), pp. 1–17. doi: 10.1046/j.1365-2427.2002.00775.x.

Eidt, R.C. 1969. The Climatology of South America. In: *Biogeography and Ecology in South America*. Dordrecht: Springer Netherlands, pp. 54–81. doi: 10.1007/978-94-011-9731-1_3.

Elith, J., Leathwick, J.R. and Hastie, T. 2008. A working guide to boosted regression trees. *Journal of Animal Ecology* 77(4), pp. 802–813. doi: 10.1111/j.1365-2656.2008.01390.x.

Engel, F. and Fischer, H. 2017. Effect of Thermal Stratification on Phytoplankton and Nutrient Dynamics in a Regulated River (Saar, Germany). *River Research and Applications* 33(1), pp. 135–146. doi: 10.1002/rra.3071.

Espinoza, J.C. et al. 2020. Hydroclimate of the Andes Part I: Main Climatic Features. *Frontiers in Earth Science* 8(March), pp. 1–20. doi: 10.3389/feart.2020.00064.

Espinoza, J.C., Ronchail, J., Marengo, J.A. and Segura, H. 2019. Contrasting North–South changes in Amazon wet-day and dry-day frequency and related atmospheric features (1981–2017). *Climate Dynamics* 52(9), pp. 5413–5430. doi: 10.1007/s00382-018-4462-2.

Eyto, E. de, Jennings, E., Ryder, E., Sparber, K., Dillane, M., Dalton, C. and Poole, R. 2016. Response of a humic lake ecosystem to an extreme precipitation event: Physical, chemical, and biological implications. *Inland Waters* 6(4), pp. 483–498. doi: 10.5268/IW-6.4.875.

Feng, L. et al. 2024. Harmful algal blooms in inland waters. *Nature Reviews Earth and Environment* 5(9), pp. 631–644. doi: 10.1038/s43017-024-00578-2.

Feng, L., Pi, X., Luo, Q. and Li, W. 2023. Reconstruction of long-term high-resolution lake variability: Algorithm improvement and applications in China. *Remote Sensing of Environment* 297, p. 113775. doi: https://doi.org/10.1016/j.rse.2023.113775.

Feng, Y. et al. 2022. Decadal Lake Volume Changes (2003–2020) and Driving Forces at a Global Scale. *Remote Sensing* 14(4), pp. 1–20. doi: 10.3390/rs14041032.

Fernández-Duque, B. et al. 2023. Long-term observed changes of air temperature, relative humidity and vapour pressure deficit in Bolivia, 1950–2019. *International Journal of Climatology* 43(14), pp. 6484–6504. doi: 10.1002/joc.8226.

Feron, S. et al. 2019. Observations and Projections of Heat Waves in South America. *Scientific Reports* 9(1), pp. 1–15. doi: 10.1038/s41598-019-44614-4.

Feron, S. et al. 2024. South America is becoming warmer, drier, and more flammable. *Communications Earth and Environment* 5(1), pp. 1–10. doi: 10.1038/s43247-024-01654-7.

Fichot, C.G., Matsumoto, K., Holt, B., Gierach, M.M. and Tokos, K.S. 2019. Assessing change in the overturning behavior of the Laurentian Great Lakes using remotely sensed lake surface water temperatures. *Remote Sensing of Environment* 235, p. 111427. doi: https://doi.org/10.1016/j.rse.2019.111427.

Fick, S.E. and Hijmans, R.J. 2017. WorldClim 2: new 1-km spatial resolution climate surfaces for global land areas. *International Journal of Climatology* 37(12), pp. 4302–4315. doi: 10.1002/joc.5086.

Ficker, H., Luger, M. and Gassner, H. 2017. From dimictic to monomictic: Empirical evidence of thermal regime transitions in three deep alpine lakes in Austria induced by climate change. *Freshwater Biology* 62(8), pp. 1335–1345. doi: 10.1111/fwb.12946.

Filipponi, F., Valentini, E., Xuan, A.N., Guerra, C.A., Wolf, F., Andrzejak, M. and Taramelli, A. 2018. Global MODIS fraction of green vegetation cover for monitoring abrupt and gradual vegetation changes. *Remote Sensing* 10(4). doi: 10.3390/rs10040653.

Fink, G., Schmid, M. and Wüest, A. 2014. Large lakes as sources and sinks of anthropogenic heat: Capacities and limits. *Water Resources Research* 50(9), pp. 7285–7301. doi: 10.1002/2014WR015509.

Fleischmann, A. et al. 2024. Extreme warming of Amazon waters in a changing climate. *Science* (July). doi: 10.31223/X56D9T.

Fleischmann, A.S., Fialho Brêda, J.P., Rudorff, C., Dias de Paiva, R.C., Collischonn, W., Papa, F. and Ravanello, M.M. 2021. Chapter 4 - River Flood Modeling and Remote Sensing Across Scales: Lessons from Brazil. In: Schumann, G. J.-P. ed. *Earth Observation for Flood Applications*. Earth Observation. Elsevier, pp. 61–103. doi: https://doi.org/10.1016/B978-0-12-819412-6.00004-3.

Forsberg, B.R., Devol, A.H., Richey, J.E., Martinelli, L.A. and dos Santos, H. 1988. Factors controlling nutrient concentrations in Amazon floodplain lakes. *Limnology and Oceanography* 33(1), pp. 41–56. doi: 10.4319/lo.1988.33.1.0041.

Free, G. et al. 2022. Shorter blooms expected with longer warm periods under climate change: an example from a shallow meso-eutrophic Mediterranean lake. *Hydrobiologia* 849(17–18), pp. 3963–3978. doi: 10.1007/s10750-021-04773-w.

Frieler, K. et al. 2017. Assessing the impacts of 1.5 °C global warming – simulation protocol of the Inter-Sectoral Impact Model Intercomparison Project (ISIMIP2b). *Geoscientific Model Development* 10(12), pp. 4321–4345. doi: 10.5194/gmd-10-4321-2017.

Fritz, S.C., Baker, P.A., Tapia, P., Spanbauer, T. and Westover, K. 2012. Evolution of the Lake Titicaca basin and its diatom flora over the last ~370,000 years. *Palaeogeography, Palaeoclimatology, Palaeoecology* 317–318, pp. 93–103. doi: 10.1016/j.palaeo.2011.12.013.

Fuente, S. La et al. 2024. Title : Ensemble modeling of global lake evaporation under climate change Affiliations : *Journal of Hydrology*, p. 130647. doi: 10.1016/j.jhydrol.2024.130647.

Gammons, C.H. et al. 2006. Mercury concentrations of fish, river water, and sediment in the Río Ramis-Lake Titicaca watershed, Peru. *Science of The Total Environment* 368(2–3), pp. 637–648. doi: 10.1016/j.scitotenv.2005.09.076.

Garcia, N.O. and Vargas, W.M. 1996. The spatial variability of runoff and precipitation in the Rio de la Plata basin. *Hydrological Sciences Journal* 41(3), pp. 279–299. doi: 10.1080/02626669609491503.

García-Avila, F., Loja-Suco, P., Siguenza-Jeton, C., Jiménez-Ordoñez, M., Valdiviezo-Gonzales, L., Cabello-Torres, R. and Aviles-Añazco, A. 2023. Evaluation of the water quality of a high Andean lake using different quantitative approaches. *Ecological Indicators* 154, p. 110924. doi: https://doi.org/10.1016/j.ecolind.2023.110924.

Garreaud, R. et al. 2017. The 2010-2015 megadrought in central Chile: Impacts on regional hydroclimate and vegetation. *Hydrology and Earth System Sciences* 21(12), pp. 6307–6327. doi: 10.5194/hess-21-6307-2017.

Garreaud, R., Clem, K. and Veloso, J.V. 2021. The south pacific pressure trend dipole and the southern blob. *Journal of Climate* 34(18), pp. 7661–7676. doi: 10.1175/JCLI-D-20-0886.1.

Garreaud, R., Vuille, M. and Clement, A.C. 2003. The climate of the Altiplano: Observed current conditions and mechanisms of past changes. *Palaeogeography, Palaeoclimatology, Palaeoecology* 194(1–3), pp. 5–22. doi: 10.1016/S0031-0182(03)00269-4.

Garreaud, R., Vuille, M., Compagnucci, R. and Marengo, J. 2009. Present-day South American climate. *Palaeogeography, Palaeoclimatology, Palaeoecology* 281(3–4), pp. 180–195. doi: 10.1016/j.palaeo.2007.10.032.

Garreaud, R.D. and Muñoz, R.C. 2005. Dynamics of the low-level jet off the west coast of subtropical South America. *Monthly Weather Review* 133(12), pp. 3661–3677. doi: 10.1175/MWR3074.1.

GCOS. 2022. The 2022 GCOS ECVs Requirements (GCOS-245). pp. 1–244.

Geller, W., Hannappel, S. and Campos, H. 1997. Temperature and stratification of southern hemisphere temperate lakes in Patagonia (Chile, Argentina). *SIL Proceedings, 1922-2010* 26(2), pp. 243–247. doi: 10.1080/03680770.1995.11900709.

George, G., Järvinen, M., Nõges, T., Blenckner, T. and Moore, K. 2010. The Impact of the Changing Climate on the Supply and Recycling of Nitrate BT - The Impact of Climate Change on European Lakes. In: George, G. ed. Dordrecht: Springer Netherlands, pp. 161–178. doi: 10.1007/978-90-481-2945-4_10.

Gerea, M., Soto Cárdenas, C., Garcia, P.E., Quiroga, M.V. and Queimaliños, C. 2023. Contrasting dissolved organic matter biodegradation and bacterial cytometric features in oligotrophic and ultraoligotrophic Patagonian lakes. *Journal of Plankton Research* 45(5), pp. 716–731. doi: 10.1093/plankt/fbad033.

Gerten, D. and Adrian, R. 2002. Effects of climate warming, North Atlantic Oscillation, and El Niño-Southern Oscillation on thermal conditions and plankton dynamics in northern hemispheric lakes. *TheScientificWorldJournal* 2, pp. 586–606. doi: 10.1100/tsw.2002.141.

Giráldez, L., Silva, Y., Zubieta, R. and Sulca, J. 2020. Change of the Rainfall Seasonality Over Central Peruvian Andes: Onset, End, Duration and Its Relationship With Large-Scale Atmospheric Circulation. *Climate* 8(2). doi: 10.3390/cli8020023.

Gloor, M. et al. 2015. Recent Amazon climate as background for possible ongoing and future changes of Amazon humid forests. *Global Biogeochemical Cycles* 29(9), pp. 1384–1399. doi: 10.1002/2014GB005080.

Gonfiantini, R., Cioni, R. and Paredes, M. 2002. Hydrochemical and isotope study of Lake Titicaca. International Atomic Energy Agency, Vienna (Austria); United Nations

Educational, Scientific and Cultural Organization, Paris (France); Japan Science and Technology Corporation (Japan), pp. 231–242.

Gonzales, I.M. and Roncal, R.Z. 2007. *Co-operation on the Lake Titicaca*.

Gonzalez-Salazar, M. and Poganietz, W.R. 2021. Evaluating the complementarity of solar, wind and hydropower to mitigate the impact of El Niño Southern Oscillation in Latin America. *Renewable Energy* 174, pp. 453–467. doi: 10.1016/j.renene.2021.04.048.

Grant, L. et al. 2021. Attribution of global lake systems change to anthropogenic forcing. *Nature Geoscience* 14(11), pp. 849–854. doi: 10.1038/s41561-021-00833-x.

Grimm, A.M. and Tedeschi, R.G. 2009. ENSO and extreme rainfall events in South America. *Journal of Climate* 22(7), pp. 1589–1609. doi: 10.1175/2008JCLI2429.1.

Gronewold, A.D. and Stow, C.A. 2014. Water Loss from the Great Lakes. *Science* 343(6175), pp. 1084–1085. doi: 10.1126/science.1249978.

Guédron, S. et al. 2017. Mercury contamination level and speciation inventory in Lakes Titicaca & Uru-Uru (Bolivia): Current status and future trends. *Environmental Pollution* 231, pp. 262–270. doi: 10.1016/j.envpol.2017.08.009.

Gunkel, G. and Casallas, J. 2002. Limnology of an equatorial high mountain lake - Lago San Pablo, Ecuador: The significance of deep diurnal mixing for lake productivity. *Limnologica* 32(1), pp. 33–43. doi: 10.1016/S0075-9511(02)80015-9.

Habit, E. and Cussac, V. 2016. Conservation of the freshwater fauna of Patagonia: an alert to the urgent need for integrative management and sustainable development. *Journal of Fish Biology* 89(1), pp. 369–370. doi: 10.1111/jfb.12882.

Hamilton, S.K., Sippel, S.J. and Melack, J.M. 2002. Comparison of inundation patterns among major South American floodplains. *Journal of Geophysical Research Atmospheres* 107(20), p. LBA 5-1-LBA 5-14. doi: 10.1029/2000JD000306.

Hampton, S.E. et al. 2018. Recent ecological change in ancient lakes. *Limnology and Oceanography* 63(5), pp. 2277–2304. doi: 10.1002/lno.10938.

Hampton, S.E., Izmest'eva, L.R., Moore, M. V., Katz, S.L., Dennis, B. and Silow, E.A. 2008. Sixty years of environmental change in the world's largest freshwater lake - Lake Baikal, Siberia. *Global Change Biology* 14(8), pp. 1947–1958. doi: 10.1111/j.1365-2486.2008.01616.x.

Han, Y., Lin, Q., Huang, S., Du, C., Shen, J. and Zhang, K. 2024. Human Impacts Dominate Global Loss of Lake Ecosystem Resilience. *Geophysical Research Letters* 51(11). doi: 10.1029/2024GL109298.

Han, Z., He, Y., Liu, G. and Perrie, W. 2020. Application of DINCAE to reconstruct the gaps in chlorophyll-a satellite observations in the South China sea and West Philippine Sea. *Remote Sensing* 12(3), pp. 1–25. doi: 10.3390/rs12030480.

Harris, I., Jones, P.D., Osborn, T.J. and Lister, D.H. 2014. Updated high-resolution grids of monthly climatic observations – the CRU TS3.10 Dataset. *International Journal of Climatology* 34(3), pp. 623–642. doi: https://doi.org/10.1002/joc.3711.

Hastie, T. 2023. *_gam: Generalized Additive Models_. R package version 1.22-2*.

Hata, S., Sugiyama, S. and Heki, K. 2022. Abrupt drainage of Lago Greve, a large proglacial lake in Chilean Patagonia, observed by satellite in 2020. *Communications Earth and Environment* 3(1), pp. 1–8. doi: 10.1038/s43247-022-00531-5.

Haylock, M.R. et al. 2006. Trends in total and extreme South American rainfall in 1960-2000 and links with sea surface temperature. *Journal of Climate* 19(8), pp. 1490–1512. doi: 10.1175/JCLI3695.1.

Hebért, M.P., Beisner, B.E., Rautio, M. and Fussmann, G.F. 2021. Warming winters in lakes: Later ice onset promotes consumer overwintering and shapes springtime planktonic food webs. *Proceedings of the National Academy of Sciences of the United States of America* 118(48), pp. 1–9. doi: 10.1073/pnas.2114840118.

Heiskanen, J.J. et al. 2015. Effects of water clarity on lake stratification and lake-atmosphere heat exchange. *Journal of Geophysical Research: Atmospheres* 120(15), pp. 7412–7428. doi: 10.1002/2014JD022938.

Henao, E., Cantera, J.R. and Rzymski, P. 2020. Conserving the Amazon River Basin: The case study of the Yahuarcaca Lakes System in Colombia. *Science of The Total Environment* 724, p. 138186. doi: https://doi.org/10.1016/j.scitotenv.2020.138186.

Henderson-Sellers, B. 1986. Calculating the surface energy balance for lake and reservoir modeling: A review. *Reviews of Geophysics* 24(3), pp. 625–649. doi: 10.1029/RG024i003p00625.

Hersbach, H. et al. 2020. The ERA5 global reanalysis. *Quarterly Journal of the Royal Meteorological Society* 146(730), pp. 1999–2049. doi: 10.1002/qj.3803.

Hilborn, A. and Costa, M. 2018. Applications of DINEOF to satellite-derived chlorophyll-a from a productive coastal region. *Remote Sensing* 10(9), pp. 11–13. doi: 10.3390/rs10091449.

Hirabayashi, Y., Tanoue, M., Sasaki, O., Zhou, X. and Yamazaki, D. 2021. Global exposure to flooding from the new CMIP6 climate model projections. *Scientific Reports* 11(1), p. 3740. doi: 10.1038/s41598-021-83279-w.

Ho, J.C., Michalak, A.M. and Pahlevan, N. 2019. Widespread global increase in intense lake phytoplankton blooms since the 1980s. *Nature* 574(7780), pp. 667–670. doi: 10.1038/s41586-019-1648-7.

Hobday, A.J. et al. 2016. A hierarchical approach to defining marine heatwaves. *Progress in Oceanography* 141, pp. 227–238. doi: 10.1016/j.pocean.2015.12.014.

Hock, R. et al. 2019. High Mountain Areas. In: IPCC Special Report on the Ocean and Cryosphere in a Changing Climate. In: *The Ocean and Cryosphere in a Changing Climate*. Cambridge University Press, pp. 131–202. doi: 10.1017/9781009157964.004.

Hocking, G.C. and Straškraba, M. 1999. The Effect of Light Extinction on Thermal Stratification in Reservoirs and Lakes. *International Review of Hydrobiology* 84(6), pp. 535–556. doi: 10.1002/iroh.199900046.

Hook, S.J., Prata, F.J., Alley, R.E., Abtahi, A., Richards, R.C., Schladow, S.G. and Pálmarsson, S.Ó. 2003. Retrieval of Lake Bulk and skin temperatures using along-track scanning radiometer (ATSR-2) data: A case study using Lake Tahoe, California. *Journal of Atmospheric and Oceanic Technology* 20(4), pp. 534–548. doi: 10.1175/1520-0426(2003)20<534:ROLBAS>2.0.CO;2.

Hoorn, C. et al. 2010. Amazonia Through Time: Andean Uplift, Climate Change, Landscape Evolution, and Biodiversity. *Science* 330(6006), pp. 927–931. doi: 10.1126/science.1194585.

Horn, W., Mortimer, C.H. and Schwab, D.J. 1986. Wind-induced internal seiches in Lake Zurich observed and modeled. *Limnology and Oceanography* 31(6), pp. 1232–1254. doi: 10.4319/lo.1986.31.6.1232.

Hossain, K., Yadav, S., Quaik, S., Pant, G., Maruthi, A.Y. and Ismail, N. 2017. Vulnerabilities of macrophytes distribution due to climate change. *Theoretical and Applied Climatology* 129(3–4), pp. 1123–1132. doi: 10.1007/s00704-016-1837-3.

Hostetler, S.W. 1995. Hydrological and Thermal Response of Lakes to Climate: Description and Modeling. In: Lerman, A., Imboden, D. M., and Gat, J. R. eds. *Physics and Chemistry of Lakes*. Berlin, Heidelberg: Springer Berlin Heidelberg, pp. 63–82. doi: 10.1007/978-3-642-85132-2_3.

Huang, A. et al. 2019. Evaluating and Improving the Performance of Three 1-D Lake Models in a Large Deep Lake of the Central Tibetan Plateau. *Journal of Geophysical Research: Atmospheres* 124(6), pp. 3143–3167. doi: 10.1029/2018JD029610.

Huang, L., Timmermann, A., Lee, S.-S., Rodgers, K.B., Yamaguchi, R. and Chung, E.-S. 2022. Emerging unprecedented lake ice loss in climate change projections. *Nature Communications* 13(1), p. 5798. doi: 10.1038/s41467-022-33495-3.

Huang, L., Woolway, R.I., Timmermann, A., Lee, S.-S., Rodgers, K.B. and Yamaguchi, R. 2024. Emergence of lake conditions that exceed natural temperature variability. *Nature Geoscience* 17(8), pp. 763–769. doi: 10.1038/s41561-024-01491-5.

Huot, Y. et al. 2019. The NSERC Canadian Lake Pulse Network: A national assessment of lake health providing science for water management in a changing climate. *Science of the Total Environment* 695, p. 133668. doi: 10.1016/j.scitotenv.2019.133668.

IFRC. 2021. DREF Plan of Action Venezuela: Floods. (August), pp. 1–24.

Imrit, M.A. and Sharma, S. 2021. Climate Change is Contributing to Faster Rates of Lake Ice Loss in Lakes Around the Northern Hemisphere. *Journal of Geophysical Research: Biogeosciences* 126(7), pp. 1–13. doi: 10.1029/2020JG006134.

Intergovernmental Panel on Climate Change. 2023. *Climate Change 2021 – The Physical Science Basis*. doi: 10.1017/9781009157896.

IPCC. 2022. *Future Climate Changes, Risks and Impacts*. Available at: https://ar5-syr.ipcc.ch/topic_futurechanges.php [Accessed: 26 December 2022].

Jane, S.F. et al. 2021. Widespread deoxygenation of temperate lakes. *Nature* 594(7861), pp. 66–70. doi: 10.1038/s41586-021-03550-y.

Jankowski, T., Livingstone, D.M., Bührer, H., Forster, R. and Niederhauser, P. 2006. Consequences of the 2003 European heat wave for lake temperature profiles, thermal stability, and hypolimnetic oxygen depletion: Implications for a warmer world. *Limnology and Oceanography* 51(2), pp. 815–819. doi: https://doi.org/10.4319/lo.2006.51.2.0815.

Jansen, J. et al. 2022. Global increase in methane production under future warming of lake bottom waters. *Global Change Biology* 28(18), pp. 5427–5440. doi: 10.1111/gcb.16298.

Jennings, E. et al. 2012. Effects of weather-related episodic events in lakes: an analysis based on high-frequency data. *Freshwater Biology* 57(3), pp. 589–601. doi: 10.1111/j.1365-2427.2011.02729.x.

Jensen, O.P., Benson, B.J., Magnuson, J.J., Card, V.M., Futter, M.N., Soranno, P.A. and Stewart, K.M. 2007. Spatial analysis of ice phenology trends across the Laurentian Great Lakes region during a recent warming period. *Limnology and Oceanography* 52(5), pp. 2013–2026. doi: 10.4319/lo.2007.52.5.2013.

Jeppesen, E. et al. 2009. Climate Change Effects on Runoff, Catchment Phosphorus Loading and Lake Ecological State, and Potential Adaptations. *Journal of Environmental Quality* 38(5), pp. 1930–1941. doi: 10.2134/jeq2008.0113.

Jeppesen, E. et al. 2012. Impacts of climate warming on the long-term dynamics of key fish species in 24 European lakes. *Hydrobiologia* 694(1), pp. 1–39. doi: 10.1007/s10750-012-1182-1.

Jeppesen, E. et al. 2014. Climate change impacts on lakes: An integrated ecological perspective based on a multi-faceted approach, with special focus on shallow lakes. *Journal of Limnology* 73(1 SUPPL), pp. 88–111. doi: 10.4081/jlimnol.2014.844.

Jhon, C. and Duque, S.R. 2023. Littoral areas of Amazonian floodplain lakes : a biological reserve to biodiversity loss. 42(1), pp. 85–99. doi: 10.23818/limn.42.07.

Jiang, Y., Gao, Z., He, J., Wu, J. and Christakos, G. 2022. Application and Analysis of XCO2 Data from OCO Satellite Using a Synthetic DINEOF–BME Spatiotemporal Interpolation Framework. *Remote Sensing* 14(17). doi: 10.3390/rs14174422.

Jiminez, N. and Oliver, J.E. 2005. South America, Climate of. In: *Encyclopedia of World Climatology*. Springer Netherlands, pp. 673–679. doi: 10.1007/1-4020-3266-8_193.

Jöhnk, K.D., Huisman, J., Sharples, J., Sommeijer, B., Visser, P.M. and Stroom, J.M. 2008. Summer heatwaves promote blooms of harmful cyanobacteria. *Global Change Biology* 14(3), pp. 495–512. doi: 10.1111/j.1365-2486.2007.01510.x.

Jones, C., Mu, Y., Carvalho, L.M.V. and Ding, Q. 2023. The South America Low-Level Jet: form, variability and large-scale forcings. *npj Climate and Atmospheric Science* 6(1). doi: 10.1038/s41612-023-00501-4.

Jones, I., George, G. and Reynolds, C. 2005. Quantifying effects of phytoplankton on the heat budgets of two large limnetic enclosures. *Freshwater Biology* 50(7), pp. 1239–1247. doi: 10.1111/j.1365-2427.2005.01397.x.

Jung, S., Yoo, C. and Im, J. 2022. High-Resolution Seamless Daily Sea Surface Temperature Based on Satellite Data Fusion and Machine Learning over Kuroshio Extension. *Remote Sensing* 14(3). doi: 10.3390/rs14030575.

Junk, W.J. 2013. Current state of knowledge regarding South America wetlands and their future under global climate change. *Aquatic Sciences* 75(1), pp. 113–131. doi: 10.1007/s00027-012-0253-8.

Junk, W.J. and Howard-Williams, C. 1984. Ecology of aquatic macrophytes in Amazonia. In: Sioli, H. ed. *The Amazon: Limnology and landscape ecology of a mighty tropical river and its basin*. Dordrecht: Springer Netherlands, pp. 269–293. doi: 10.1007/978-94-009-6542-3_10.

Junk, W.J., Piedade, M.T.F., Schöngart, J., Cohn-Haft, M., Adeney, J.M. and Wittmann, F. 2011. A classification of major naturally-occurring amazonian lowland wetlands. *Wetlands* 31(4), pp. 623–640. doi: 10.1007/s13157-011-0190-7.

Kakouei, K. et al. 2021. Phytoplankton and cyanobacteria abundances in mid-21st century lakes depend strongly on future land use and climate projections. *Global Change Biology* 27(24), pp. 6409–6422. doi: 10.1111/gcb.15866.

Kandus, P. et al. 2018. Remote sensing of wetlands in South America: status and challenges. *International Journal of Remote Sensing* 39(4), pp. 993–1016. doi: 10.1080/01431161.2017.1395971.

Kangur, K., Tammiksaar, E. and Pauly, D. 2022. Using the "mean temperature of the catch" to assess fish community responses to warming in a temperate lake. *Environmental Biology of Fishes* 105(10), pp. 1405–1413. doi: 10.1007/s10641-021-01114-7.

Kasprzak, P., Padisák, J., Koschel, R., Krienitz, L. and Gervais, F. 2008. Chlorophyll a concentration across a trophic gradient of lakes: An estimator of phytoplankton biomass? *Limnologica* 38(3–4), pp. 327–338. doi: 10.1016/j.limno.2008.07.002.

Kong, X. et al. 2021. Unravelling winter diatom blooms in temperate lakes using high frequency data and ecological modeling. *Water Research* 190, p. 116681. doi: 10.1016/j.watres.2020.116681.

Korver, M.C., Lehner, B., Cardille, J.A. and Carrea, L. 2024. Surface water temperature observations and ice phenology estimations for 1.4 million lakes globally. *Remote Sensing of Environment* 308(April), p. 114164. doi: 10.1016/j.rse.2024.114164.

Kraemer, B.M. et al. 2015. Morphometry and average temperature affect lake stratification responses to climate change. *Geophysical Research Letters* 42(12), pp. 4981–4988. doi: 10.1002/2015GL064097.

Kraemer, B.M. et al. 2017a. Global patterns in lake ecosystem responses to warming based on the temperature dependence of metabolism. *Global Change Biology* 23(5), pp. 1881–1890. doi: 10.1111/gcb.13459.

Kraemer, B.M. et al. 2021. Climate change drives widespread shifts in lake thermal habitat. *Nature Climate Change* 11(6), pp. 521–529. doi: 10.1038/s41558-021-01060-3.

Kraemer, B.M., Kakouei, K., Munteanu, C., Thayne, M.W. and Adrian, R. 2022. Worldwide moderate-resolution mapping of lake surface chl-a reveals variable responses to global change (1997–2020). *PLOS Water* 1(10), p. e0000051. doi: 10.1371/journal.pwat.0000051.

Kraemer, B.M., Mehner, T. and Adrian, R. 2017b. Reconciling the opposing effects of warming on phytoplankton biomass in 188 large lakes. *Scientific Reports* 7(1), pp. 1–7. doi: 10.1038/s41598-017-11167-3.

Kraemer, B.M., Seimon, A., Adrian, R. and McIntyre, P.B. 2020. Worldwide lake level trends and responses to background climate variation. *Hydrology and Earth System Sciences* 24(5), pp. 2593–2608. doi: 10.5194/hess-24-2593-2020.

Kristiansen, T., Svenning, J.-C., Pedersen, D., Eiserhardt, W.L., Grández, C. and Balslev, H. 2011. Local and regional palm (Arecaceae) species richness patterns and their cross-scale determinants in the western Amazon. *Journal of Ecology* 99(4), pp. 1001–1015. doi: https://doi.org/10.1111/j.1365-2745.2011.01834.x.

Labaj, A.L., Michelutti, N. and Smol, J.P. 2018. Annual stratification patterns in tropical mountain lakes reflect altered thermal regimes in response to climate change. *Fundamental and Applied Limnology* 191(4), pp. 267–275. doi: 10.1127/fal/2018/1151.

Laguarda, A., Alonso-Suárez, R. and Terra, R. 2020. Solar irradiation regionalization in Uruguay: Understanding the interannual variability and its relation to El Niño climatic phenomena. *Renewable Energy* 158, pp. 444–452. doi: 10.1016/j.renene.2020.05.083.

Lange, S. 2019. Trend-preserving bias adjustment and statistical downscaling with ISIMIP3BASD (v1.0). *Geoscientific Model Development* 12(7), pp. 3055–3070. doi: 10.5194/gmd-12-3055-2019.

Lange, S. 2021. ISIMIP3b bias adjustment fact sheet. (2019), p. 39.

Lavado Casimiro, W.S., Labat, D., Ronchail, J., Espinoza, J.C. and Guyot, J.L. 2012. Trends in rainfall and temperature in the Peruvian Amazon-Andes basin over the last 40 years (1965-2007). *Hydrological Processes* 27(20), p. n/a-n/a. doi: 10.1002/hyp.9418.

Lavenu, A. 1992. Origins. In: Dejoux, C. and Iltis, A. eds. *Lake Titicaca: A Synthesis of Limnological Knowledge*. Dordrecht: Springer Netherlands, pp. 3–15. doi: 10.1007/978-94-011-2406-5_1.

Lehner, B. and Döll, P. 2004. Development and validation of a global database of lakes, reservoirs and wetlands. *Journal of Hydrology* 296(1), pp. 1–22. doi: https://doi.org/10.1016/j.jhydrol.2004.03.028.

Leoni, B., Spreafico, M., Patelli, M., Soler, V., Garibaldi, L. and Nava, V. 2019. Long-term studies for evaluating the impacts of natural and anthropic stressors on limnological features and the ecosystem quality of Lake Iseo. *Advances in Oceanography and Limnology* 10(2), pp. 81–93. doi: 10.4081/aiol.2019.8622.

Li, X., Peng, S., Deng, X., Su, M. and Zeng, H. 2019. Attribution of Lake Warming in Four Shallow Lakes in the Middle and Lower Yangtze River Basin. *Environmental science & technology* 53(21), pp. 12548–12555. doi: 10.1021/acs.est.9b03098.

Lieberherr, G. and Wunderle, S. 2018. Lake surface water temperature derived from 35 years of AVHRR sensor data for European lakes. *Remote Sensing* 10(7). doi: 10.3390/rs10070990.

Lima-quispe, N., Escobar, M., Wickel, A.J., Kaenel, M. Von and Purkey, D. 2021. Journal of Hydrology : Regional Studies management on water levels in Lakes Titicaca and Poop o. *Journal of Hydrology: Regional Studies* 37(September), p. 100927. doi: 10.1016/j.ejrh.2021.100927.

Liu, C. et al. 2023. Combined influence of ENSO and North Atlantic Oscillation (NAO) on Eurasian Steppe during 1982–2018. *Science of the Total Environment* 892(March), p. 164735. doi: 10.1016/j.scitotenv.2023.164735.

Livingstone, D.M. 2003. Impact of Secular Climate Change on the Thermal Structure of a Large Temperate Central European Lake. *Climatic Change* 57(1–2), pp. 205–225. Available at: https://link.springer.com/10.1023/A:1022119503144.

Livingstone, D.M. and Dokulil, M.T. 2001. Eighty years of spatially coherent Austrian lake surface temperatures and their relationship to regional air temperature and the North Atlantic Oscillation. *Limnology and Oceanography* 46(5), pp. 1220–1227. doi: https://doi.org/10.4319/lo.2001.46.5.1220.

Livingstone, D.M. and Imboden, D.M. 1989. Annual heat balance and equilibrium temperature of Lake Aegeri, Switzerland. *Aquatic Sciences* 51(4), pp. 351–369. doi: 10.1007/BF00877177.

Livingstone, D.M. and Lotter, F. 1998. The relationship between air and water temperatures in lakes of the Swiss Plateau. *Journal of Paleolimnology* 19, pp. 181–198.

Llames, M.E. and Zagarese, H.E. 2009. Lakes and Reservoirs of South America. In: *Encyclopedia of Inland Waters*. Elsevier, pp. 533–543. doi: 10.1016/B978-012370626-3.00034-X.

Llopart, M., Simões Reboita, M. and Porfírio da Rocha, R. 2020. Assessment of multi-model climate projections of water resources over South America CORDEX domain. *Climate Dynamics* 54(1–2), pp. 99–116. doi: 10.1007/s00382-019-04990-z.

Loayza, E., Trigoso Barrientos, A.C. and Janssens, G.P.J. 2022. Evidence of microplastics in water and commercial fish from a high-altitude mountain lake (Lake Titicaca). *PeerJ* 10, p. e14112. doi: 10.7717/peerj.14112.

Lomelí-Huerta, J.R., Rivera-Caicedo, J.P., De-la-Torre, M., Acevedo-Juárez, B., Cepeda-Morales, J. and Avila-George, H. 2022. An approach to fill in missing data from satellite imagery using data-intensive computing and DINEOF. *PeerJ Computer Science* 8, pp. 1–21. doi: 10.7717/peerj-cs.979.

López-Moreno, J.I. et al. 2016. Recent temperature variability and change in the Altiplano of Bolivia and Peru. *International Journal of Climatology* 36(4), pp. 1773–1796. doi: 10.1002/joc.4459.

Luo, X., Song, J., Guo, J., Fu, Y., Wang, L. and Cai, Y. 2022. Reconstruction of chlorophyll-a satellite data in Bohai and Yellow sea based on DINCAE method. *International Journal of Remote Sensing* 43(9), pp. 3336–3358. doi: 10.1080/01431161.2022.2090872.

Maberly, S.C. et al. 2020. Global lake thermal regions shift under climate change. *Nature Communications* 11(1), pp. 1–9. doi: 10.1038/s41467-020-15108-z.

MacCallum, P. and Merchant, C. 2011. ATSR Reprocessing for Climate Lake Surface Water Temperature: ARC-Lake: Algorithm Theoretical Basis Document. *October*, pp. 1–60.

MacCallum, S.N. and Merchant, C.J. 2012. Surface water temperature observations of large lakes by optimal estimation. *Canadian Journal of Remote Sensing* 38(1), pp. 25–45. doi: 10.5589/m12-010.

Machate, O., Schmeller, D.S., Schulze, T. and Brack, W. 2023. Review: mountain lakes as freshwater resources at risk from chemical pollution. *Environmental Sciences Europe* 35(1), p. 3. doi: 10.1186/s12302-022-00710-3.

MacIntyre, S. and Melack, J.M. 1984. Vertical mixing in Amazon floodplain lakes. *SIL Proceedings, 1922-2010* 22(2), pp. 1283–1287. doi: 10.1080/03680770.1983.11897486.

MacIntyre, S. and Melack, J.M. 1988. Frequency and depth of vertical mixing in an Amazon floodplain lake (L. Calado, Brazil). *SIL Proceedings, 1922-2010* 23(1), pp. 80–85. doi: 10.1080/03680770.1987.11897906.

MacIntyre, S. and Melack, J.M. 2009. Mixing Dynamics in Lakes Across Climatic Zones. In: Likens, G. E. ed. *Encyclopedia of Inland Waters*. Oxford: Academic Press, pp. 603–612. doi: https://doi.org/10.1016/B978-012370626-3.00040-5.

Magee, M.R., Wu, C.H., Robertson, D.M., Lathrop, R.C. and Hamilton, D.P. 2016. Trends and abrupt changes in 104 years of ice cover and water temperature in a dimictic lake in response to air temperature, wind speed, and water clarity drivers. *Hydrology and Earth System Sciences* 20(5), pp. 1681–1702. doi: 10.5194/hess-20-1681-2016.

Magnuson, J.J. et al. 2000. Historical trends in lake and river ice cover in the northern hemisphere. *Science (New York, N.Y.)* 289(5485), pp. 1743–1746. doi: 10.1126/science.289.5485.1743.

Magnuson, J.J., Crowder, L.B. and Medvick, P.A. 1979. Temperature as an ecological resource. *Integrative and Comparative Biology* 19(1), pp. 331–343. doi: 10.1093/icb/19.1.331.

Mantua, N.J., Hare, S.R., Zhang, Y., Wallace, J.M. and Francis, R.C. 1997. A Pacific Interdecadal Climate Oscillation with Impacts on Salmon Production. *Bulletin of the American Meteorological Society* 78(6), pp. 1069–1079. doi: 10.1175/1520-0477(1997)078<1069:APICOW>2.0.CO;2.

Maraun, D. 2016. Bias Correcting Climate Change Simulations - a Critical Review. *Current Climate Change Reports* 2(4), pp. 211–220. doi: 10.1007/s40641-016-0050-x.

Marengo, J.A. and Espinoza, J.C. 2016. Extreme seasonal droughts and floods in Amazonia: Causes, trends and impacts. *International Journal of Climatology* 36(3), pp. 1033–1050. doi: 10.1002/joc.4420.

Margin, G. et al. 2014. *Central and South America. In: Climate Change 2014: Impacts, Adaptation, and Vulnerability. Part B: Regional Aspects. Contribution of Working Group II to the Fifth Assessment Report of the Intergovernmental Panel on Climate Change*. Barros, V.R., C.B. Field, D.J. Dokken, M.D. Mastrandrea, K.J. Mach, T.E. Bilir, M. Chatterjee, K.L. Ebi, Y.O. Estrada, R.C. Genova, B. Girma, E.S. Kissel, A.N. Levy, S. MacCracken, P.R. Mastrandrea, and L.L. White (eds.)] C.B. Field, D.J. D, and L. L. W. (eds ed. Cambridge University Press, Cambridge, United Kingdom and New York, NY, USA.

Martins, F.R., Pereira, E., Abreu, S.L. and Colle, S. 2009. Brazilian Atlas for Solar Energy Resource: Swera Results. *Proceedings of ISES World Congress 2007 (Vol. I – Vol. V)* (May 2014), pp. 3–7. doi: 10.1007/978-3-540-75997-3.

Masiokas, M.H. et al. 2020. A Review of the Current State and Recent Changes of the Andean Cryosphere. *Frontiers in Earth Science* 8(June), pp. 1–27. doi: 10.3389/feart.2020.00099.

Mason, L.A. et al. 2016. Fine-scale spatial variation in ice cover and surface temperature trends across the surface of the Laurentian Great Lakes. *Climatic Change* 138(1–2), pp. 71–83. doi: 10.1007/s10584-016-1721-2.

Meisen, P. and Krumpel, S. 2009. Renewable Energy Potential of Latin America. *Environmental Earth Sciences* 70(8), pp. 3875–3893.

Melack, J.M. and Coe, M.T. 2012. Climate Change and the Floodplain Lakes of the Amazon Basin. *Climatic Change and Global Warming of Inland Waters: Impacts and Mitigation for Ecosystems and Societies*, pp. 295–310. doi: 10.1002/9781118470596.ch17.

Mendes, R.C. et al. 2024. Extreme Drought Leads to First Record of Euglena sanguinea Ehrenberg Blooms in Amazon Lakes Extreme Drought Leads to First Record of Euglena

sanguinea Ehrenberg Blooms in Amazon Lakes. pp. 0–14. doi: 10.20944/preprints202411.1322.v1.

Merchant, C.J. et al. 2017. Uncertainty information in climate data records from Earth observation. *Earth System Science Data* 9(2), pp. 511–527. doi: 10.5194/essd-9-511-2017.

Mergili, M., Pudasaini, S.P., Emmer, A., Fischer, J.T., Cochachin, A. and Frey, H. 2020. Reconstruction of the 1941 GLOF process chain at Lake Palcacocha (Cordillera Blanca, Peru). *Hydrology and Earth System Sciences* 24(1), pp. 93–114. doi: 10.5194/hess-24-93-2020.

Messager, M.L., Lehner, B., Grill, G., Nedeva, I. and Schmitt, O. 2016. Estimating the volume and age of water stored in global lakes using a geo-statistical approach. *Nature Communications* 7, pp. 1–11. doi: 10.1038/ncomms13603.

Michelutti, N., Cooke, C.A., Hobbs, W.O. and Smol, J.P. 2015a. Climate-driven changes in lakes from the Peruvian Andes. *Journal of Paleolimnology* 54(1), pp. 153–160. doi: 10.1007/s10933-015-9843-5.

Michelutti, N., Labaj, A.L., Grooms, C. and Smol, J.P. 2016. Equatorial mountain lakes show extended periods of thermal stratification with recent climate change. *Journal of Limnology* 75(2), pp. 403–408. doi: 10.4081/jlimnol.2015.1444.

Michelutti, N., Wolfe, A.P., Cooke, C.A., Hobbs, W.O., Vuille, M. and Smol, J.P. 2015b. Climate change forces new ecological states in tropical Andean lakes. *PLoS ONE* 10(2), pp. 1–10. doi: 10.1371/journal.pone.0115338.

Miller, M.J., Capriles, J.M. and Hastorf, C.A. 2010a. The fish of Lake Titicaca: implications for archaeology and changing ecology through stable isotope analysis. *Journal of Archaeological Science* 37(2), pp. 317–327. doi: 10.1016/j.jas.2009.09.043.

Miller, M.J., Capriles, J.M. and Hastorf, C.A. 2010b. The fish of Lake Titicaca: implications for archaeology and changing ecology through stable isotope analysis. *Journal of Archaeological Science* 37(2), pp. 317–327. doi: 10.1016/j.jas.2009.09.043.

Miranda, V.F.V.V. et al. 2024. Heat stress in South America over the last four decades: a bioclimatic analysis. *Theoretical and Applied Climatology* 155(2), pp. 911–928. doi: 10.1007/s00704-023-04668-x.

Mironov, D., Heise, E., Kourzeneva, E., Ritter, B., Schneider, N. and Terzhevik, A. 2010. Implementation of the lake parameterisation scheme FLake into the numerical weather prediction model COSMO. *Boreal Environment Research* 15(2), pp. 218–230.

Modenutti, B.E. et al. 2013. Effect of volcanic eruption on nutrients, light, and phytoplankton in oligotrophic lakes. *Limnology and Oceanography* 58(4), pp. 1165–1175. doi: 10.4319/lo.2013.58.4.1165.

Moe, S.J., Hobæk, A., Persson, J., Skjelbred, B. and Løvik, J.E. 2021. Shifted dynamics of plankton communities in a restored lake: exploring the effects of climate change on phenology through four decades. *Climate Research* 86, pp. 125–143. doi: 10.3354/cr01654.

Mohammadi, B., Guan, Y., Aghelpour, P., Emamgholizadeh, S., Pillco Zolá, R. and Zhang, D. 2020. Simulation of Titicaca Lake Water Level Fluctuations Using Hybrid Machine Learning Technique Integrated with Grey Wolf Optimizer Algorithm. *Water* 12(11), p. 3015. doi: 10.3390/w12113015.

Monroy, M., Maceda-Veiga, A. and de Sostoa, A. 2014. Metal concentration in water, sediment and four fish species from Lake Titicaca reveals a large-scale environmental concern. *Science of the Total Environment* 487(1), pp. 233–244. doi: 10.1016/j.scitotenv.2014.03.134.

Moser, K.A. et al. 2019. Mountain lakes: Eyes on global environmental change. *Global and Planetary Change* 178(April), pp. 77–95. doi: 10.1016/j.gloplacha.2019.04.001.

Muraria, T.B., Nascimento Filho, A.S., Moret, M.A., Pitombo, S. and Santos, A.A.B. 2020. How Does ENSO Impact the Solar Radiation Forecast in South America? The Self-affinity Analysis Approach. *arXiv*.

Narvaez, G., Bressan, M., Pantoja, A. and Giraldo, L.F. 2023. Climate change impact on photovoltaic power potential in South America. *Environmental Research Communications* 5(8). doi: 10.1088/2515-7620/acf02e.

Naumann, G., Vargas, W.M., Barbosa, P., Blauhut, V., Spinoni, J. and Vogt, J. V. 2019. Dynamics of Socioeconomic Exposure, Vulnerability and Impacts of Recent Droughts in Argentina. *Geosciences* 9(1). doi: 10.3390/geosciences9010039.

Naumann, Gustavo. et al. 2021. *The 2019-2021 extreme drought episode in La Plata Basin*. doi: 10.2760/773.

Naumann, Gustavo. et al. 2023. *Extreme and long-term drought in the La Plata Basin: event evolution and impact assessment until September 2022*. doi: 10.2760/62557.

Niedrist, G.H., Psenner, R. and Sommaruga, R. 2018. Climate warming increases vertical and seasonal water temperature differences and inter-annual variability in a mountain lake. *Climatic Change* 151(3–4), pp. 473–490. doi: 10.1007/s10584-018-2328-6.

NOAA. 2025. *Oceanic Niño Index*. Available at: https://www.cpc.ncep.noaa.gov/data/indices/oni.ascii.txt [Accessed: 11 June 2023].

Nõges, P. and Nõges, T. 2014. Weak trends in ice phenology of Estonian large lakes despite significant warming trends. *Hydrobiologia* 731(1), pp. 5–18. doi: 10.1007/s10750-013-1572-z.

North, R.P., North, R.L., Livingstone, D.M., Köster, O. and Kipfer, R. 2014. Long-term changes in hypoxia and soluble reactive phosphorus in the hypolimnion of a large temperate lake: consequences of a climate regime shift. *Global Change Biology* 20(3), pp. 811–823. doi: https://doi.org/10.1111/gcb.12371.

Nuñez-Hidalgo, I., Meseguer-Ruiz, O., Serrano-Notivoli, R. and Sarricolea, P. 2023. Population dynamics shifts by climate change: High-resolution future mid-century trends for South America. *Global and Planetary Change* 226(March). doi: 10.1016/j.gloplacha.2023.104155.

Obregón, G. et al. 2009. *CLIMATE SCENARIOS FOR PERU TO 2030*.

Oesch, D.C., Jaquet, J.M., Hauser, A. and Wunderle, S. 2005. Lake surface water temperature retrieval using advanced very high resolution radiometer and Moderate Resolution Imaging Spectroradiometer data: Validation and feasibility study. *Journal of Geophysical Research: Oceans* 110(12), pp. 1–17. doi: 10.1029/2004JC002857.

Oliver, E.C.J. et al. 2018. Longer and more frequent marine heatwaves over the past century. *Nature Communications* 9(1), p. 1324. doi: 10.1038/s41467-018-03732-9.

Olson, D.M. et al. 2001. Terrestrial Ecoregions of the World: A New Map of Life on Earth: A new global map of terrestrial ecoregions provides an innovative tool for conserving biodiversity. *BioScience* 51(11), pp. 933–938. doi: 10.1641/0006-3568(2001)051[0933:TEOTWA]2.0.CO;2.

O'Reilly, C.M., Rowley, R.J., Schneider, P., Lenters, J.D., Mcintyre, P.B. and Kraemer, B.M. 2015. Rapid and highly variable warming of lake surface waters around the globe. Geophysical Research Letters, 42: 1-9. *Geophysical Research Letters*, pp. 1–9. doi: 10.1002/2015GL066235.

Ouala, S., Fablet, R., Herzet, C., Chapron, B., Pascual, A., Collard, F. and Gaultier, L. 2018. Neural network based Kalman filters for the spatio-temporal interpolation of satellite-derived sea surface temperature. *Remote Sensing* 10(12), pp. 1–16. doi: 10.3390/rs10121864.

Pabón-Caicedo, J.D. et al. 2020. Observed and Projected Hydroclimate Changes in the Andes. *Frontiers in Earth Science* 8(March), pp. 1–29. doi: 10.3389/feart.2020.00061.

Paerl, H.W. and Huisman, J. 2008. Climate: Blooms like it hot. *Science* 320(5872), pp. 57–58. doi: 10.1126/science.1155398.

Papenfus, M., Schaeffer, B., Pollard, A.I. and Loftin, K. 2020. Exploring the potential value of satellite remote sensing to monitor chlorophyll-a for US lakes and reservoirs. *Environmental Monitoring and Assessment* 192(12). doi: 10.1007/s10661-020-08631-5.

Parmesan, C. et al. 2022. *Chapter 2: Terrestrial and Freshwater Ecosystems and their Services*. doi: 10.1017/9781009325844.004.198.

Pascual, M., Cussac, V., Dyer, B., Soto, D., Vigliano, P., Ortubay, S. and Macchi, P. 2007. Freshwater fishes of Patagonia in the 21st Century after a hundred years of human settlement, species introductions, and environmental change. *Aquatic Ecosystem Health & Management* 10, pp. 212–227. doi: 10.1080/14634980701351361.

Pasquini, A.I., Lecomte, K.L. and Depetris, P.J. 2008. Climate change and recent water level variability in Patagonian proglacial lakes, Argentina. *Global and Planetary Change* 63(4), pp. 290–298. doi: 10.1016/j.gloplacha.2008.07.001.

Pauly, D. and Dimarchopoulou, D. 2022. Introduction: Fishes in a warming and deoxygenating world. *Environmental Biology of Fishes* 105(10), pp. 1261–1267. doi: 10.1007/s10641-022-01357-y.

Peel, M.C., Finlayson, B.L. and McMahon, T.A. 2007. Updated world map of the Köppen-Geiger climate classification. *Hydrology and Earth System Sciences* 11(5), pp. 1633–1644. doi: 10.5194/hess-11-1633-2007.

Pekel, J.-F., Cottam, A., Gorelick, N. and Belward, A.S. 2016. High-resolution mapping of global surface water and its long-term changes. *Nature* 540, p. 418.

Pereira, O.J.R., Merino, E.R., Montes, C.R., Barbiero, L., Rezende-Filho, A.T., Lucas, Y. and Melfi, A.J. 2020. Estimating Water pH Using Cloud-Based Landsat Images for a New Classification of the Nhecolândia Lakes (Brazilian Pantanal). *Remote Sensing* 12(7). doi: 10.3390/rs12071090.

Persson, I. and Jones, I.D. 2008. The effect of water colour on lake hydrodynamics: A modelling study. *Freshwater Biology* 53(12), pp. 2345–2355. doi: 10.1111/j.1365-2427.2008.02049.x.

Piccolroaz, S. et al. 2024. Lake Water Temperature Modeling in an Era of Climate Change: Data Sources, Models, and Future Prospects. *Reviews of Geophysics* 62(1). doi: 10.1029/2023RG000816.

Piccolroaz, S., Woolway, R.I. and Merchant, C.J. 2020. Global reconstruction of twentieth century lake surface water temperature reveals different warming trends depending on the climatic zone. *Climatic Change* 160(3), pp. 427–442. doi: 10.1007/s10584-020-02663-z.

Pillai, P.A., Kiran, V.G. and Suneeth, K. V. 2023. The strengthened role of new predictors of Indian Ocean Dipole (IOD) during the recent decades of weakened ENSO-IOD relationship. *Dynamics of Atmospheres and Oceans* 106(July 2023), p. 101432. doi: 10.1016/j.dynatmoce.2023.101432.

Pillco Zolá, R. et al. 2019. Modelling Lake Titicaca's daily and monthly evaporation. *Hydrology and Earth System Sciences* 23(2), pp. 657–668. doi: 10.5194/hess-23-657-2019.

Ping, B., Su, F. and Meng, Y. 2016. An improved DINEOF algorithm for filling missing values in spatio-temporal sea surface temperature data. *PLoS ONE* 11(5), pp. 1–12. doi: 10.1371/journal.pone.0155928.

Pohlert, T. 2023a. trend: Non-Parametric Trend Tests and Change-Point Detection.

Pohlert, T. 2023b. trend: Non-Parametric Trend Tests and Change-Point Detection. Available at: https://cran.r-project.org/package=trend.

Poveda, G., Espinoza, J.C., Zuluaga, M.D., Solman, S.A., Garreaud, R. and van Oevelen, P.J. 2020. High Impact Weather Events in the Andes. *Frontiers in Earth Science* 8(May), pp. 1–32. doi: 10.3389/feart.2020.00162.

Quade, J. and Kaplan, M.R. 2017. Lake-level stratigraphy and geochronology revisited at Lago (Lake) Cardiel, Argentina, and changes in the Southern Hemispheric Westerlies over the last 25 ka. *Quaternary Science Reviews* 177, pp. 173–188. doi: 10.1016/j.quascirev.2017.10.006.

R Core, T. 2022. R: A language and environment for statistical computing. R Foundation for Statistical Computing, Vienna, Austria.

R Core Team. 2025. R: A Language and Environment for Statistical Computing.

Ramarao, M.V.S. et al. 2024. Projected changes in heatwaves over Central and South America using high-resolution regional climate simulations. *Scientific reports* 14(1), p. 23145. doi: 10.1038/s41598-024-73521-6.

Rasconi, S., Gall, A., Winter, K. and Kainz, M.J. 2015. Increasing water temperature triggers dominance of small freshwater plankton. *PLoS ONE* 10(10), pp. 1–17. doi: 10.1371/journal.pone.0140449.

Rathore, S.S., Chandravanshi, P., Chandravanshi, A. and Jaiswal, K. 2016. Eutrophication: Impacts of Excess Nutrient Inputs on Aquatic Ecosystem. *IOSR Journal of Agriculture and Veterinary Science* 09(10), pp. 89–96. doi: 10.9790/2380-0910018996.

Richerson, P.J., Widmer, C. and Kittel, T. 1977. The Limnology of Lake Titicaca (Peru-Bolivia), A large, High Altitude Tropical Lake. Institute of Ecology Publication 14, p. 43.

Reguero, B.G., Losada, I.J., Díaz-Simal, P., Méndez, F.J. and Beck, M.W. 2015. Effects of Climate Change on Exposure to Coastal Flooding in Latin America and the Caribbean. *PLOS ONE* 10(7), pp. 1–19. doi: 10.1371/journal.pone.0133409.

Reis, R.E., Albert, J.S., Di Dario, F., Mincarone, M.M., Petry, P. and Rocha, L.A. 2016. Fish biodiversity and conservation in South America. *Journal of Fish Biology* 89(1), pp. 12–47. doi: https://doi.org/10.1111/jfb.13016.

Reitsema, R.E., Meire, P. and Schoelynck, J. 2018. The future of freshwater macrophytes in a changing world: Dissolved organic carbon quantity and quality and its interactions with macrophytes. *Frontiers in Plant Science* 9(May), pp. 1–15. doi: 10.3389/fpls.2018.00629.

Revollo, M.M. 2001. Management issues in the Lake Titicaca and Lake Poopo system: Importance of developing a water budget. *Lakes and Reservoirs: Research and Management* 6(3), pp. 225–229. doi: 10.1046/j.1440-1770.2001.00151.x.

Ridgeway, G. 2007. Generalized Boosted Models: A guide to the gbm package.package 'gbm', version 1.5-7. *Update* 1(1), pp. 1–15.

Rieckermann, J., Daebel, H., Ronteltap, M. and Bernauer, T. 2006. Assessing the performance of international water management at Lake Titicaca. 68, pp. 502–516. doi: 10.1007/s00027-006-0863-0.

Rinke, K., Yeates, P. and Rothhaupt, K.-O.O. 2010. A simulation study of the feedback of phytoplankton on thermal structure via light extinction. *Freshwater Biology* 55(8), pp. 1674–1693. doi: https://doi.org/10.1111/j.1365-2427.2010.02401.x.

Ríos-Villamizar, E., Piedade, M.T., Costa, J., Adeney, J. and Junk, W. 2013. Chemistry of different Amazonian water types for river classification: A preliminary review. In: *WIT Transactions on Ecology and the Environment*. pp. 17–28. doi: 10.2495/WS130021.

Rivas Martínez, S., Navarro Sánchez, G., Penas Merino, Á. and Costa Talens, M. 2011. Biogeographic Map of South America. An initial advance. *International Journal of Geobotanical Research* 1(1), pp. 21–40. doi: 10.5616/ijgr110002.

Rivera, J.A. and Penalba, O.C. 2014. Trends and Spatial Patterns of Drought Affected Area in Southern South America. *Climate* 2(4), pp. 264–278. doi: 10.3390/cli2040264.

Rizzo, A., Arcagni, M., Arribére, M.A., Bubach, D. and Guevara, S.R. 2011. Mercury in the biotic compartments of Northwest Patagonia lakes, Argentina. *Chemosphere* 84(1), pp. 70–79. doi: https://doi.org/10.1016/j.chemosphere.2011.02.052.

Roche, M.A., Bourges, J.C. and Mattos, R. 1992. Climatology and hydrology of the Lake Titicaca basin. *Lake Titicaca: A Synthesis of Limnological Knowledge.*, pp. 63–83.

Ronchail, J., Espinoza, J., Labat, D., Lavado, W. and Callede, J. 2014. EVOLUCION DEL NIVEL DEL LAGO TITICACA DURANTE EL SIGLO 20 EVOLUTION OF THE TITICACA LAKE LEVEL DURING THE 20 TH CENTURY.

Rondanelli, R., Molina, A. and Falvey, M. 2015. The Atacama surface solar maximum. *Bulletin of the American Meteorological Society* 96(3), pp. 405–418. doi: 10.1175/BAMS-D-13-00175.1.

Rooney, G.G., van Lipzig, N. and Thiery, W. 2018. Estimating the effect of rainfall on the surface temperature of a tropical lake. *Hydrology and Earth System Sciences* 22(12), pp. 6357–6369. doi: 10.5194/hess-22-6357-2018.

Rose, K.C. et al. 2023. Indicators of the effects of climate change on freshwater ecosystems. *Climatic Change* 176(3), pp. 1–20. doi: 10.1007/s10584-022-03457-1.

Rose, K.C., Winslow, L.A., Read, J.S. and Hansen, G.J.A. 2016. Climate-induced warming of lakes can be either amplified or suppressed by trends in water clarity. *Limnology And Oceanography Letters* 1(1), pp. 44–53. doi: 10.1002/lol2.10027.

Van Rossum, G. and Drake Jr, F.L. 1995. *Python reference manual*. Centrum voor Wiskunde en Informatica Amsterdam.

Rowe, H.D. and Dunbar, R.B. 2004. Hydrologic-energy balance constraints on the Holocene lake-level history of lake Titicaca, South America. *Climate Dynamics* 23(3–4), pp. 439–454. doi: 10.1007/s00382-004-0451-8.

Ruiz-Verdu, A. et al. 2016. Comparison of MODIS and Landsat-8 retrievals of Chlorophyll-a and water temperature over Lake Titicaca. In: *2016 IEEE International Geoscience and Remote Sensing Symposium (IGARSS)*. IEEE, pp. 7643–7646. doi: 10.1109/IGARSS.2016.7730993.

Runzheimer, K. et al. 2024. Exploring Andean High-Altitude Lake Extremophiles through Advanced Proteotyping. *Journal of Proteome Research* 23(3), pp. 891–904. doi: 10.1021/acs.jproteome.3c00538.

Rusticucci, M. and Barrucand, M. 2004. Observed Trends and Changes in Temperature Extremes over Argentina. *Journal of Climate* 17(20), pp. 4099–4107. doi: 10.1175/1520-0442(2004)017<4099:OTACIT>2.0.CO;2.

Rusticucci, M. and Tencer, B. 2008. Observed changes in return values of annual temperature extremes over Argentina. *Journal of Climate* 21(21), pp. 5455–5467. doi: 10.1175/2008JCLI2190.1.

Sabás, I., Miró, A., Piera, J., Catalan, J., Camarero, L., Buchaca, T. and Ventura, M. 2021. Factors of surface thermal variation in high-mountain lakes of the Pyrenees. *PLoS ONE* 16(8 August), pp. 1–19. doi: 10.1371/journal.pone.0254702.

Salzmann, N., Huggel, C., Rohrer, M., Silverio, W., Mark, B.G., Burns, P. and Portocarrero, C. 2013. Glacier changes and climate trends derived from multiple sources in the data scarce Cordillera Vilcanota region, southern Peruvian Andes. *Cryosphere* 7(1), pp. 103–118. doi: 10.5194/tc-7-103-2013.

Sarret, G. et al. 2019. Extreme Arsenic Bioaccumulation Factor Variability in Lake Titicaca, Bolivia. *Scientific Reports* 9(1), pp. 1–12. doi: 10.1038/s41598-019-47183-8.

Satyamurty, P., Nobre, C. and Dias, P.L.S. 1998. Chapter 3C South America. *Meteorological Monographs* (Hastenrath 1991), pp. 119–139.

Schallenberg, M., De Winton, M.D., Verburg, P., Kelly, D.J., Hamill, K.D. and Hamilton, D.P. 2013. Ecosystem Services of Lakes. *Ecosystem services in New Zealand - Conditions and trends*, pp. 203–225.

Schindler, D.W. et al. 1990. Effects of Climatic Warming on Lakes of the Central Boreal Forest. *Science* 250(4983), pp. 967–970. doi: 10.1126/science.250.4983.967.

Schlegel, R. and Smit, A. 2018. heatwaveR: A central algorithm for the detection of heatwaves and cold-spells. *Journal of Open Source Software* 3(27), p. 821. doi: 10.21105/joss.00821.

Schmid, M., Hunziker, S. and Wüest, A. 2014. Lake surface temperatures in a changing climate: A global sensitivity analysis. *Climatic Change* 124(1–2), pp. 301–315. doi: 10.1007/s10584-014-1087-2.

Schmid, M. and Köster, O. 2016. Excess warming of a Central European lake driven by solar brightening. *Water Resources Research* 52(10), pp. 8103–8116. Available at: http://doi.wiley.com/10.1002/2016WR018651.

Schmid, M. and Read, J. 2022. *Heat Budget of Lakes*. 2nd ed. Elsevier Inc. doi: 10.1016/B978-0-12-819166-8.00011-6.

Schneider, P., Healey, N.C., Hulley, G.C. and Hook, S.J. 2019. Lake Surface Temperature. *Taking the Temperature of the Earth* (January 2019), pp. 129–150. doi: 10.1016/b978-0-12-814458-9.00004-6.

Schneider, P. and Hook, S.J. 2010. Space observations of inland water bodies show rapid surface warming since 1985. *Geophysical Research Letters* 37(22), pp. 1–5. doi: 10.1029/2010GL045059.

Schwab, D.J., Leshkevich, G.A. and Muhr, G.C. 1999. Automated mapping of surface water temperature in the Great Lakes. *Journal of Great Lakes Research* 25(3), pp. 468–481. doi: 10.1016/S0380-1330(99)70755-0.

Schwefel, R., Gaudard, A., Wüest, A. and Bouffard, D. 2016. Effects of climate change on deepwater oxygen and winter mixing in a deep lake (Lake Geneva): Comparing observational findings and modeling. *Water Resources Research* 52(11), pp. 8811–8826. doi: 10.1002/2016WR019194.

Segura, H., Espinoza, J.C., Junquas, C. and Takahashi, K. 2016. Evidencing decadal and interdecadal hydroclimatic variability over the Central Andes. *Environmental Research Letters* 11(9). doi: 10.1088/1748-9326/11/9/094016.

Seluchi, M.E. and Marengo, J.A. 2000. Tropical–midlatitude exchange of air masses during summer and winter in South America: Climatic aspects and examples of intense events. 20, pp. 1167–1190.

Seneviratne, S.I. et al. 2021. *Weather and Climate Extreme Events in a Changing Climate. In Climate Change 2021: The Physical Science Basis. Contribution of Working Group I to the Sixth Assessment Report of the Intergovernmental Panel on Climate Change*. doi: 10.1017/9781009157896.013.1514.

Sepulveda-Jauregui, A., Hoyos-Santillan, J., Martinez-Cruz, K., Walter Anthony, K.M., Casper, P., Belmonte-Izquierdo, Y. and Thalasso, F. 2018. Eutrophication exacerbates the impact of climate warming on lake methane emission. *The Science of the total environment* 636, pp. 411–419. doi: 10.1016/j.scitotenv.2018.04.283.

Sharma, S. et al. 2015. A global database of lake surface temperatures collected by in situ and satellite methods from 1985-2009. *Scientific Data* 2, pp. 1–19. doi: 10.1038/sdata.2015.8.

Sharma, S. et al. 2019. Widespread loss of lake ice around the Northern Hemisphere in a warming world. *Nature Climate Change* 9(3), pp. 227–231. doi: 10.1038/s41558-018-0393-5.

Sharma, S. et al. 2020. Integrating Perspectives to Understand Lake Ice Dynamics in a Changing World. *Journal of Geophysical Research: Biogeosciences* 125(8), pp. 1–18. doi: 10.1029/2020JG005799.

Sharma, S. et al. 2021. Loss of Ice Cover, Shifting Phenology, and More Extreme Events in Northern Hemisphere Lakes. *Journal of Geophysical Research: Biogeosciences* 126(10), pp. 1–12. doi: 10.1029/2021JG006348.

Shatwell, T., Thiery, W. and Kirillin, G. 2019. Future projections of temperature and mixing regime of European temperate lakes. *Hydrology and Earth System Sciences* 23(3), pp. 1533–1551. doi: 10.5194/hess-23-1533-2019.

Siqueira, V.A. et al. 2018. Toward continental hydrologic–hydrodynamic modeling in South America. *Hydrology and Earth System Sciences* 22(9), pp. 4815–4842. doi: 10.5194/hess-22-4815-2018.

Sirjacobs, D. et al. 2011. Cloud filling of ocean colour and sea surface temperature remote sensing products over the Southern North Sea by the Data Interpolating Empirical Orthogonal Functions methodology. *Journal of Sea Research* 65(1), pp. 114–130. doi: 10.1016/j.seares.2010.08.002.

Skansi, M. de los M. et al. 2013. Warming and wetting signals emerging from analysis of changes in climate extreme indices over South America. *Global and Planetary Change* 100, pp. 295–307. doi: 10.1016/j.gloplacha.2012.11.004.

Snucins, E. and Gunn, J. 2000. Interannual variation in the thermal structure of clear and colored lakes. *Limnology and Oceanography* 45(7), pp. 1639–1646. doi: 10.4319/lo.2000.45.7.1639.

Spuler, F., Wessel, J., Comyn-platt, E., Varndell, J. and Cagnazzo, C. 2023. ibicus : a new open-source Python package and comprehensive interface for statistical bias adjustment and evaluation in climate modelling (v1 . 0 . 1). (August), pp. 1–27.

Stensrud, D.J. 1996. Importance of Low-Level Jets to Climate: A Review. *Journal of Climate* 9(8), pp. 1698–1711. doi: 10.1175/1520-0442(1996)009<1698:IOLLJT>2.0.CO;2.

Sterner, R.W., Keeler, B., Polasky, S., Poudel, R., Rhude, K. and Rogers, M. 2020. Ecosystem services of Earth's largest freshwater lakes. *Ecosystem Services* 41(October 2019), p. 101046. doi: 10.1016/j.ecoser.2019.101046.

Stock, A. et al. 2020. Comparison of cloud-filling algorithms for marine satellite data. *Remote Sensing* 12(20), pp. 1–25. doi: 10.3390/rs12203313.

Switanek, B.M., Troch, A.P., Castro, L.C., Leuprecht, A., Chang, H.I., Mukherjee, R. and Demaria, M.C.E. 2017. Scaled distribution mapping: A bias correction method that preserves raw climate model projected changes. *Hydrology and Earth System Sciences* 21(6), pp. 2649–2666. doi: 10.5194/hess-21-2649-2017.

Tassone, S.J., Besterman, A.F., Buelo, C.D., Walter, J.A. and Pace, M.L. 2022. Co-occurrence of Aquatic Heatwaves with Atmospheric Heatwaves, Low Dissolved Oxygen, and Low pH Events in Estuarine Ecosystems. *Estuaries and Coasts* 45(3), pp. 707–720. doi: 10.1007/s12237-021-01009-x.

Taylor, M.H., Losch, M., Wenzel, M. and Schröter, J. 2013. On the sensitivity of field reconstruction and prediction using empirical orthogonal functions derived from Gappy data. *Journal of Climate* 26(22), pp. 9194–9205. doi: 10.1175/JCLI-D-13-00089.1.

Teutschbein, C. and Seibert, J. 2012. Bias correction of regional climate model simulations for hydrological climate-change impact studies : Review and evaluation of different methods. *Journal of Hydrology* 456–457, pp. 12–29. doi: 10.1016/j.jhydrol.2012.05.052.

Thayne, M.W. et al. 2023. Lake surface water temperature and oxygen saturation resistance and resilience following extreme storms: chlorophyll a shapes resistance to storms. *Inland Waters* 0(0), pp. 1–23. doi: 10.1080/20442041.2023.2242081.

Thiery, W., Martynov, A., Darchambeau, F., Descy, J.P., Plisnier, P.D., Sushama, L. and Van Lipzig, N.P.M. 2014. Understanding the performance of the FLake model over two African Great Lakes. *Geoscientific Model Development* 7(1), pp. 317–337. doi: 10.5194/gmd-7-317-2014.

Tibshirani, R., Walther, G. and Hastie, T. 2002. Estimating the Number of Clusters in a Data Set Via the Gap Statistic. *Journal of the Royal Statistical Society Series B: Statistical Methodology* 63(2), pp. 411–423. doi: 10.1111/1467-9868.00293.

Till, A., Rypel, A.L., Bray, A. and Fey, S.B. 2019. Fish die-offs are concurrent with thermal extremes in north temperate lakes. *Nature Climate Change* 9(8), pp. 637–641. doi: 10.1038/s41558-019-0520-y.

Toffolon, M., Piccolroaz, S., Majone, B., Soja, A.M., Peeters, F., Schmid, M. and Wüest, A. 2014. Prediction of surface temperature in lakes with different morphology using air temperature. *Limnology and Oceanography* 59(6), pp. 2185–2202. doi: 10.4319/lo.2014.59.6.2185.

Tong, Y., Feng, L., Wang, X., Pi, X., Xu, W. and Woolway, R.I. 2023. Global lakes are warming slower than surface air temperature due to accelerated evaporation. pp. 6–8. doi: 10.1038/s44221-023-00148-8.

Tong, Y., Huang, Z., Janssen, A.B.G., Wishart, M., He, W., Wang, X. and Zhao, Y. 2022. Influence of social and environmental drivers on nutrient concentrations and ratios in lakes: A comparison between China and Europe. *Water Research* 227(November), p. 119347. doi: 10.1016/j.watres.2022.119347.

Tranvik, L.J. et al. 2009. Lakes and reservoirs as regulators of carbon cycling and climate. *Limnology and Oceanography* 54(6 PART 2), pp. 2298–2314. doi: 10.4319/lo.2009.54.6_part_2.2298.

Trenberth, K.E. 1997. The Definition of El Niño. *Bulletin of the American Meteorological Society* 78(12), pp. 2771–2777. doi: 10.1175/1520-0477(1997)078<2771:TDOENO>2.0.CO;2.

Trigoso, E. 2007. Climate Change Impacts and Adaptation in Peru: The Case of Puno and Piura. *Human Development*, p. 15.

Tundisi, J.G. et al. 1984. Mixing patterns in Amazon lakes. *Hydrobiologia* 108(1), pp. 3–15. doi: 10.1007/bf00028177.

Vargas Gil, G.M., Bittencourt Aguiar Cunha, R., Giuseppe Di Santo, S., Machado Monaro, R., Fragoso Costa, F. and Sguarezi Filho, A.J. 2020. Photovoltaic energy in South America: Current state and grid regulation for large-scale and distributed photovoltaic systems. *Renewable Energy* 162, pp. 1307–1320. doi: 10.1016/j.renene.2020.08.022.

Vasseur, D.A. et al. 2014. Increased temperature variation poses a greater risk to species than climate warming. *Proceedings of the Royal Society B: Biological Sciences* 281(1779). doi: 10.1098/rspb.2013.2612.

Veettil, B.K. and Kamp, U. 2021. Glacial Lakes in the Andes under a Changing Climate: A Review. *Journal of Earth Science* 32(6), pp. 1575–1593. doi: 10.1007/s12583-020-1118-z.

Verpoorter, C., Kutser, T., Seekell, D.A. and Tranvik, L.J. 2014. A global inventory of lakes based on high-resolution satellite imagery. *Geophysical Research Letters* 41(18), pp. 6396–6402. doi: 10.1002/2014GL060641.

Vicente-Serrano, S.M. et al. 2018a. Recent changes in monthly surface air temperature over Peru, 1964–2014. *International Journal of Climatology* 38(1), pp. 283–306. doi: 10.1002/joc.5176.

Vicente-Serrano, S.M. et al. 2018b. Recent changes of relative humidity: Regional connections with land and ocean processes. *Earth System Dynamics* 9(2), pp. 915–937. doi: 10.5194/esd-9-915-2018.

Villalobos, L., Woelfl, S., Parra, O. and Campos, H. 2003. Lake Chapo: a baseline study of a deep, oligotrophic North Patagonian lake prior to its use for hydroelectricity generation: II. Biological properties. *Hydrobiologia* 510, pp. 225–237. doi: 10.1023/B:HYDR.0000008647.51685.4d.

Vincent, W.F. 2009. Effects of Climate Change on Lakes. *Encyclopedia of Inland Waters*, pp. 55–60. doi: 10.1016/B978-012370626-3.00233-7.

Vinnå, L.R., Medhaug, I., Schmid, M. and Bouffard, D. 2021. The vulnerability of lakes to climate change along an altitudinal gradient. *Communications Earth and Environment* 2(1), pp. 2–11. doi: 10.1038/s43247-021-00106-w.

Visser, P.M. et al. 2016. How rising CO2 and global warming may stimulate harmful cyanobacterial blooms. *Harmful Algae* 54, pp. 145–159. doi: 10.1016/j.hal.2015.12.006.

Vuille, M. et al. 2018. Rapid decline of snow and ice in the tropical Andes – Impacts, uncertainties and challenges ahead. *Earth-Science Reviews* 176(May 2017), pp. 195–213. doi: 10.1016/j.earscirev.2017.09.019.

Wagner, C. and Adrian, R. 2009. Cyanobacteria dominance: Quantifying the effects of climate change. *Limnology and Oceanography* 54(6part2), pp. 2460–2468. doi: https://doi.org/10.4319/lo.2009.54.6_part_2.2460.

Wahl, T., Haigh, I.D., Nicholls, R.J., Arns, A., Dangendorf, S., Hinkel, J. and Slangen, A.B.A. 2017. Understanding extreme sea levels for broad-scale coastal impact and adaptation analysis. *Nature Communications* 8(1), p. 16075. doi: 10.1038/ncomms16075.

Walsh, S.E., Vavrus, S.J., Foley, J.A., Fisher, V.A., Wynne, R.H. and Lenters, J.D. 1998. Global patterns of lake ice phenology and climate: Model simulations and observations. *Journal of Geophysical Research Atmospheres* 103(D22), pp. 28825–28837. doi: 10.1029/98JD02275.

Wang, J. et al. 2018a. Recent global decline in endorheic basin water storages. *Nature Geoscience* 11(12), pp. 926–932. doi: 10.1038/s41561-018-0265-7.

Wang, W. et al. 2018b. Global lake evaporation accelerated by changes in surface energy allocation in a warmer climate. *Nature Geoscience* 11(6), pp. 410–414. doi: 10.1038/s41561-018-0114-8.

Wang, W., Shi, K., Wang, X., Zhang, Y., Qin, B., Zhang, Y. and Woolway, R.I. 2024. The impact of extreme heat on lake warming in China. *Nature Communications* 15(1), p. 70. doi: 10.1038/s41467-023-44404-7.

Wang, X. et al. 2022. Continuous Loss of Global Lake Ice Across Two Centuries Revealed by Satellite Observations and Numerical Modeling. *Geophysical Research Letters* 49(12), pp. 1–9. doi: 10.1029/2022GL099022.

Wang, X. et al. 2023. Climate change drives rapid warming and increasing heatwaves of lakes. *Science Bulletin* 68(14), pp. 1574–1584. doi: 10.1016/j.scib.2023.06.028.

Wang, Y. and Liu, D. 2014. Reconstruction of satellite chlorophyll-a data using a modified DINEOF method: A case study in the Bohai and Yellow seas, China. *International Journal of Remote Sensing* 35(1), pp. 204–217. doi: 10.1080/01431161.2013.866290.

Watts, D., Durán, P. and Flores, Y. 2017. How does El Niño Southern Oscillation impact the wind resource in Chile? A techno-economical assessment of the influence of El Niño and La Niña on the wind power. *Renewable Energy* 103, pp. 128–142. doi: 10.1016/j.renene.2016.10.031.

Wells, M.G. and Troy, C.D. 2022. Surface Mixed Layers in Lakes. *Encyclopedia of Inland Waters, Second Edition* 1, pp. 546–561. doi: 10.1016/B978-0-12-819166-8.00126-2.

Wetzel, R.G. 2001. LIGHT IN INLAND WATERS. In: Wetzel, R. ed. *Limnology*. Third Edit. San Diego: Elsevier, pp. 49–69. doi: 10.1016/B978-0-08-057439-4.50009-5.

Weyhenmeyer, G.A. et al. 2024. Global Lake Health in the Anthropocene: Societal Implications and Treatment Strategies. *Earth's Future* 12(4), pp. 1–24. doi: 10.1029/2023EF004387.

Wilcock, R.J., Nagels, J.W., McBride, G.B., Collier, K.J., Wilson, B.T. and Huser, B.A. 1998. Characterisation of lowland streams using a single-station diurnal curve analysis model with continuous monitoring data for dissolved oxygen and temperature. *New Zealand Journal of Marine and Freshwater Research* 32(1), pp. 67–79. doi: 10.1080/00288330.1998.9516806.

Wilhelm, S. and Adrian, Ri. 2008. Impact of summer warming on the thermal characteristics of a polymictic lake and consequences for oxygen, nutrients and phytoplankton. *Freshwater Biology* 53(2), pp. 226–237. doi: https://doi.org/10.1111/j.1365-2427.2007.01887.x.

Williamson, C.E. et al. 2015. Ecological consequences of long-term browning in lakes. *Scientific Reports* 5(July), pp. 1–10. doi: 10.1038/srep18666.

Wilson, R., Glasser, N.F., Reynolds, J.M., Harrison, S., Anacona, P.I., Schaefer, M. and Shannon, S. 2018. Glacial lakes of the Central and Patagonian Andes. *Global and Planetary Change* 162(January), pp. 275–291. doi: 10.1016/j.gloplacha.2018.01.004.

Wirrmann, D., Ybert, J.-P., Mourguiart, P. and Ybert, J.-P. 1992. Paleohydrology. In: Dejoux, C. and Iltis, A. eds. *Lake Titicaca: A Synthesis of Limnological Knowledge*. Dordrecht: Springer Netherlands, pp. 40–62. doi: 10.1007/978-94-011-2406-5_3.

Wood, S.N. 2011. Fast stable restricted maximum likelihood and marginal likelihood estimation of semiparametric generalized linear models. *Journal of the Royal Statistical Society: Series B (Statistical Methodology)* 73(1), pp. 3–36. doi: https://doi.org/10.1111/j.1467-9868.2010.00749.x.

Woolway, R.I. et al. 2017a. Latitude and lake size are important predictors of over-lake atmospheric stability. *Geophysical Research Letters* 44(17), pp. 8875–8883. doi: 10.1002/2017GL073941.

Woolway, R.I. et al. 2019. Northern Hemisphere Atmospheric Stilling Accelerates Lake Thermal Responses to a Warming World. *Geophysical Research Letters* 46(21), pp. 11983–11992. doi: 10.1029/2019GL082752.

Woolway, R.I. et al. 2021a. Phenological shifts in lake stratification under climate change. *Nature Communications* 12(1), pp. 1–11. doi: 10.1038/s41467-021-22657-4.

Woolway, R.I., Albergel, C., Frölicher, T.L. and Perroud, M. 2022a. Severe Lake Heatwaves Attributable to Human-Induced Global Warming. *Geophysical Research Letters* 49(4), pp. 1–10. doi: 10.1029/2021GL097031.

Woolway, R.I., Anderson, E.J. and Albergel, C. 2021b. Rapidly expanding lake heatwaves under climate change. *Environmental Research Letters* 16(9). doi: 10.1088/1748-9326/ac1a3a.

Woolway, R.I., Huang, L., Sharma, S., Lee, S.S., Rodgers, K.B. and Timmermann, A. 2022b. Lake Ice Will Be Less Safe for Recreation and Transportation Under Future Warming. *Earth's Future* 10(10), pp. 1–15. doi: 10.1029/2022EF002907.

Woolway, R.I., Jennings, E. and Carrea, L. 2020a. Impact of the 2018 European heatwave on lake surface water temperature. *Inland Waters* 10(3), pp. 322–332. doi: 10.1080/20442041.2020.1712180.

Woolway, R.I., Jennings, E., Shatwell, T., Golub, M., Pierson, D.C. and Maberly, S.C. 2021c. Lake heatwaves under climate change. *Nature* 589(7842), pp. 402–407. doi: 10.1038/s41586-020-03119-1.

Woolway, R.I., Jones, I.D., Maberly, S.C. and French, J.R. 2016. Diel Surface Temperature Range Scales with Lake Size. pp. 1–14. doi: 10.1371/journal.pone.0152466.

Woolway, R.I., Kraemer, B.M., Lenters, J.D., Merchant, C.J., O'Reilly, C.M. and Sharma, S. 2020b. Global lake responses to climate change. *Nature Reviews Earth and Environment* 1(8), pp. 388–403. doi: 10.1038/s43017-020-0067-5.

Woolway, R.I., Livingstone, D.M. and Kernan, M. 2015. Altitudinal dependence of a statistically significant diel temperature cycle in Scottish lochs. *Inland Waters* 5(4), pp. 311–316. doi: 10.5268/IW-5.4.854.

Woolway, R.I. and Maberly, S.C. 2020. Climate velocity in inland standing waters. *Nature Climate Change* 10(12), pp. 1124–1129. doi: 10.1038/s41558-020-0889-7.

Woolway, R.I., Meinson, P., Nõges, P., Jones, I.D. and Laas, A. 2017b. Atmospheric stilling leads to prolonged thermal stratification in a large shallow polymictic lake. *Climatic Change* 141(4), pp. 759–773. doi: 10.1007/s10584-017-1909-0.

Woolway, R.I. and Merchant, C.J. 2018. Intralake Heterogeneity of Thermal Responses to Climate Change: A Study of Large Northern Hemisphere Lakes. *Journal of Geophysical Research: Atmospheres* 123(6), pp. 3087–3098. doi: https://doi.org/10.1002/2017JD027661.

Woolway, R.I. and Merchant, C.J. 2019. Worldwide alteration of lake mixing regimes in response to climate change. *Nature Geoscience* 12(4), pp. 271–276. doi: 10.1038/s41561-019-0322-x.

Woolway, R.I., Sharma, S. and Smol, J.P. 2022c. Lakes in Hot Water: The Impacts of a Changing Climate on Aquatic Ecosystems. *BioScience* XX(Xx), pp. 1–12. doi: 10.1093/biosci/biac052.

World Meteorological Organization. 2021. *State of the Climate in Latin America and the Caribbean*.

Wu, Z. et al. 2022. Imbalance of global nutrient cycles exacerbated by the greater retention of phosphorus over nitrogen in lakes. *Nature Geoscience* 15(6), pp. 464–468. doi: 10.1038/s41561-022-00958-7.

Wüest, A. and Lorke, A. 2003. SMALL-SCALE HYDRODYNAMICS IN LAKES. *Annual Review of Fluid Mechanics* 35(1), pp. 373–412. doi: 10.1146/annurev.fluid.35.101101.161220.

Wurtsbaugh, W.A. et al. 2017. Decline of the world's saline lakes. *Nature Geoscience* 10(11), pp. 816–821. doi: 10.1038/ngeo3052.

Yan, X., Gao, Z., Jiang, Y., He, J., Yin, J. and Wu, J. 2023. Application of Synthetic DINCAE–BME Spatiotemporal Interpolation Framework to Reconstruct Chlorophyll–a from Satellite Observations in the Arabian Sea. *Journal of Marine Science and Engineering* 11(4). doi: 10.3390/jmse11040743.

Yang, B., Wells, M.G., Li, J. and Young, J. 2020. Mixing, stratification, and plankton under lake-ice during winter in a large lake: Implications for spring dissolved oxygen levels. *Limnology and Oceanography* 65(11), pp. 2713–2729. doi: 10.1002/lno.11543.

Yang, S., Li, Z., Yu, J.Y., Hu, X., Dong, W. and He, S. 2018. El Niño-Southern Oscillation and its impact in the changing climate. *National Science Review* 5(6), pp. 840–857. doi: 10.1093/nsr/nwy046.

Yang, Y.C., Lu, C.Y., Huang, S.J., Yang, T.Z., Chang, Y.C. and Ho, C.R. 2022. On the Reconstruction of Missing Sea Surface Temperature Data from Himawari-8 in Adjacent Waters of Taiwan Using DINEOF Conducted with 25-h Data. *Remote Sensing* 14(12). doi: 10.3390/rs14122818.

Yao, F., Livneh, B., Rajagopalan, B., Wang, J., Crétaux, J.F., Wada, Y. and Berge-Nguyen, M. 2023. Satellites reveal widespread decline in global lake water storage. *Science* 380(6646), pp. 743–749. doi: 10.1126/SCIENCE.ABO2812.

Zhang, G. and Duan, S. 2021. Lakes as sentinels of climate change on the Tibetan Plateau. *All Earth* 33(1), pp. 161–165. doi: 10.1080/27669645.2021.2015870.

Zhang, K. and Yao, Y. 2023. Lake Heatwaves and Cold-Spells Across Qinghai-Tibet Plateau Under Climate Change. *Journal of Geophysical Research: Atmospheres* 128(16). doi: 10.1029/2023JD039243.

Zhang, R., Chan, S., Bindlish, R. and Lakshmi, V. 2021. Evaluation of global surface water temperature data sets for use in passive remote sensing of soil moisture. *Remote Sensing* 13(10). doi: 10.3390/rs13101872.

Zhao, S., Sun, H., Cheng, J. and Zhang, G. 2025. Water Surface Temperature Dynamics of the Three Largest Ice-Contact Lakes in the Patagonia Icefield over the Last 20 Years. *Water* 17(3). doi: 10.3390/w17030385.

Zhou, W., Melack, J.M., MacIntyre, S., Barbosa, P.M., Amaral, J.H.F. and Cortés, A. 2024. Hydrodynamic Modeling of Stratification and Mixing in a Shallow, Tropical Floodplain Lake. *Water Resources Research* 60(2), pp. 1–21. doi: 10.1029/2022WR034057.

Zhou, W., Wang, L., Li, D. and Leung, L.R. 2021. Spatial pattern of lake evaporation increases under global warming linked to regional hydroclimate change. *Communications Earth and Environment* 2(1), pp. 1–10. doi: 10.1038/s43247-021-00327-z.

Zolá, R.P. and Bengtsson, L. 2006. Long-term and extreme water level variations of the shallow Lake Poopó, Bolivia. *Hydrological Sciences Journal* 51(1), pp. 98–114. doi: 10.1623/hysj.51.1.98.

Zubieta, R., Molina-Carpio, J., Laqui, W., Sulca, J. and Ilbay, M. 2021. Comparative Analysis of Climate Change Impacts on Meteorological, Hydrological, and Agricultural Droughts in the Lake Titicaca Basin. *Water* 13(2), p. 175. doi: 10.3390/w13020175.

Appendices

Appendix A

Evaluating gap-filling techniques for satellite-derived surface water temperature: A case study of Lake Titicaca

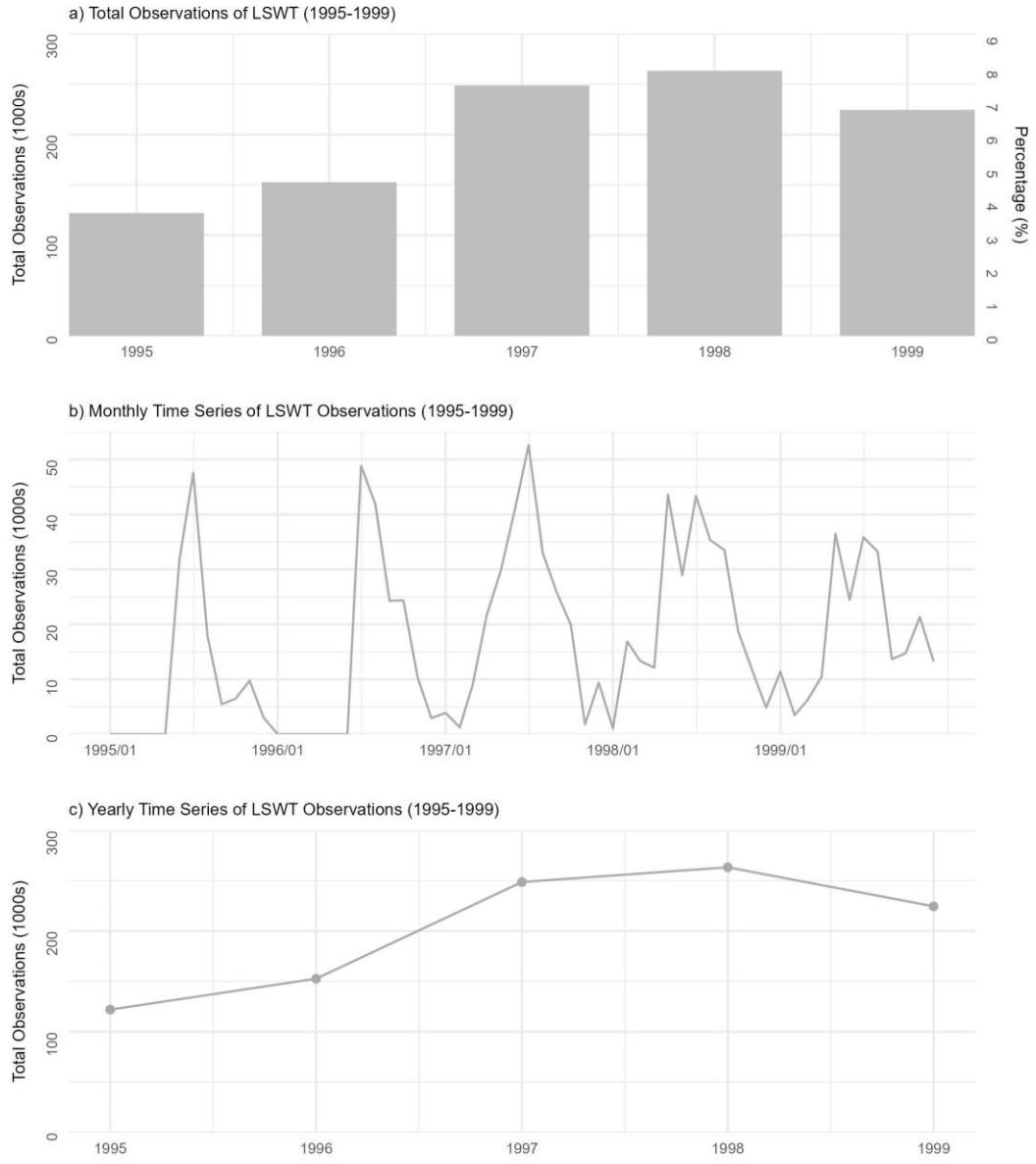


Figure A.1. Total observations of LSWT data (a), monthly (b) and yearly (c) time series of LSWT observations from 1995-1999

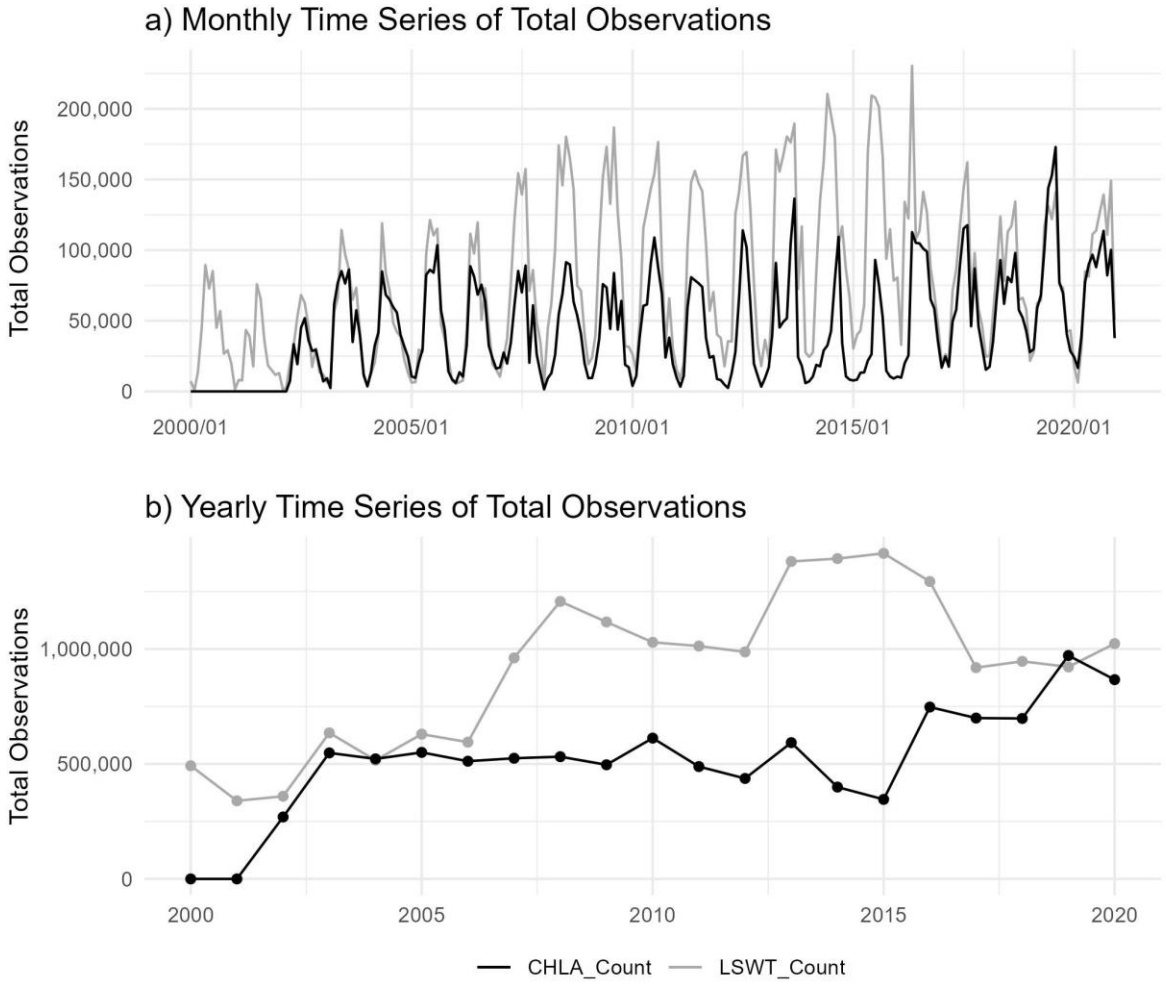


Figure A.2. Monthly/Annual Total Observations of LSWT and Chl-*a* from 2000 to 2020.

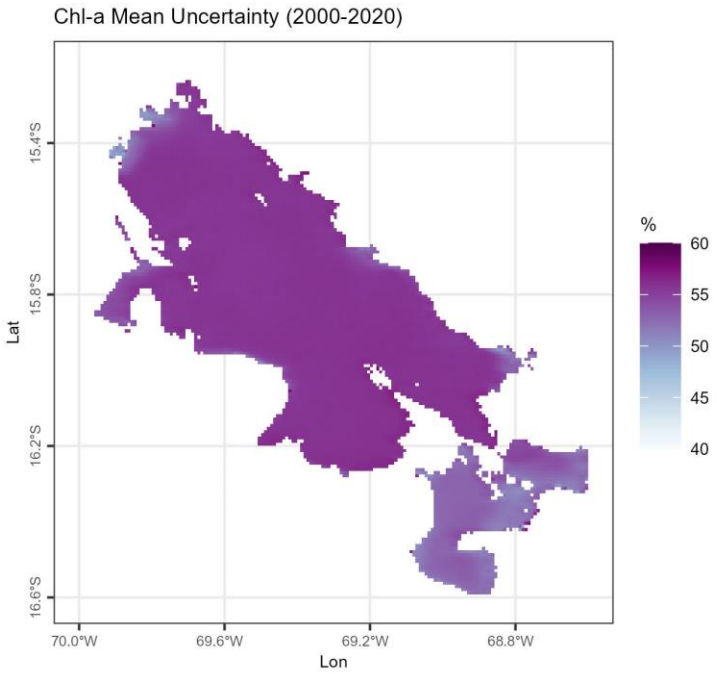


Figure A.3. Mean Chl-*a* Uncertainty (%) from 2002-2020 after removing outliers and uncertainty > 60%

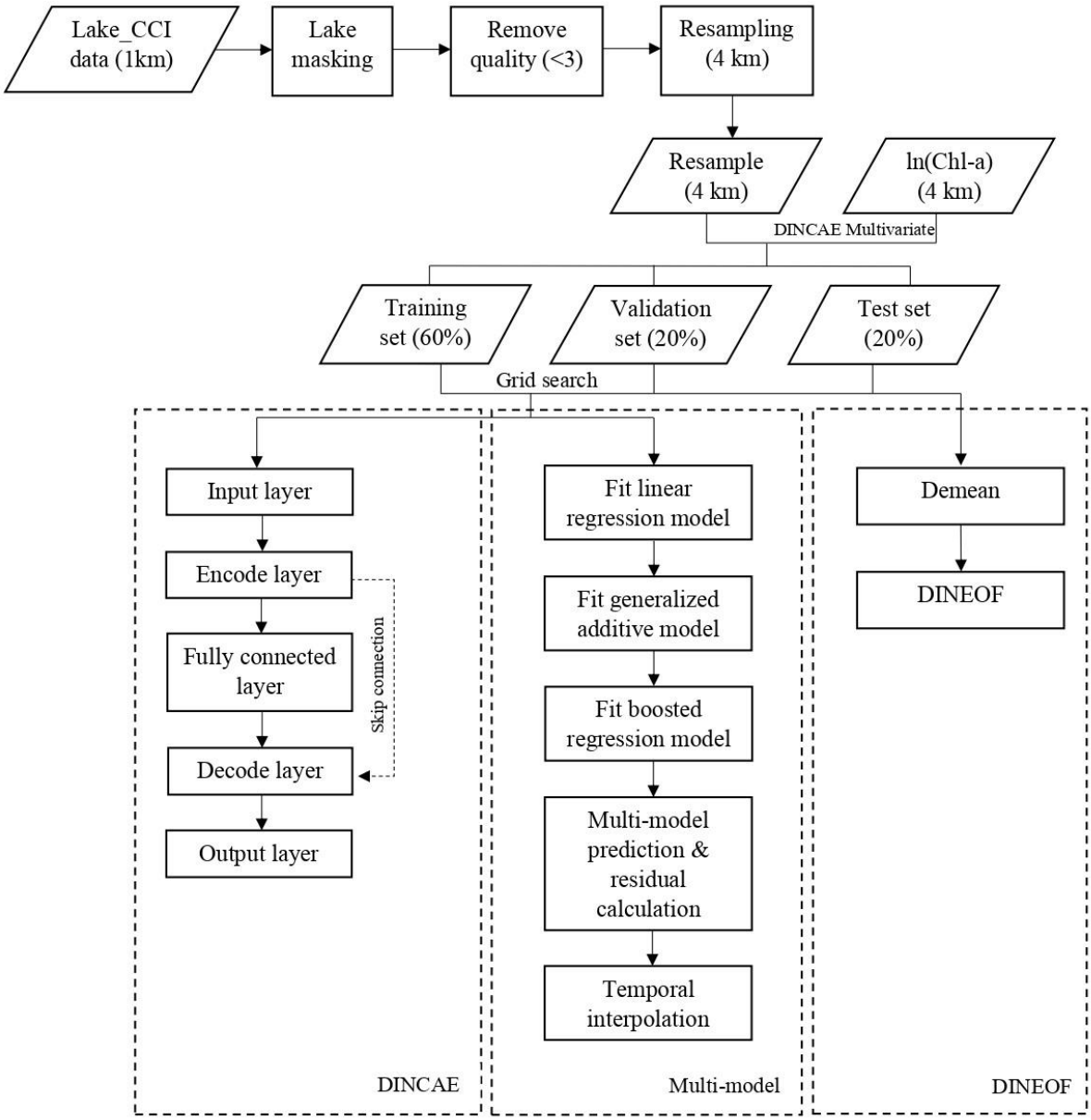


Figure A.4. Workflow

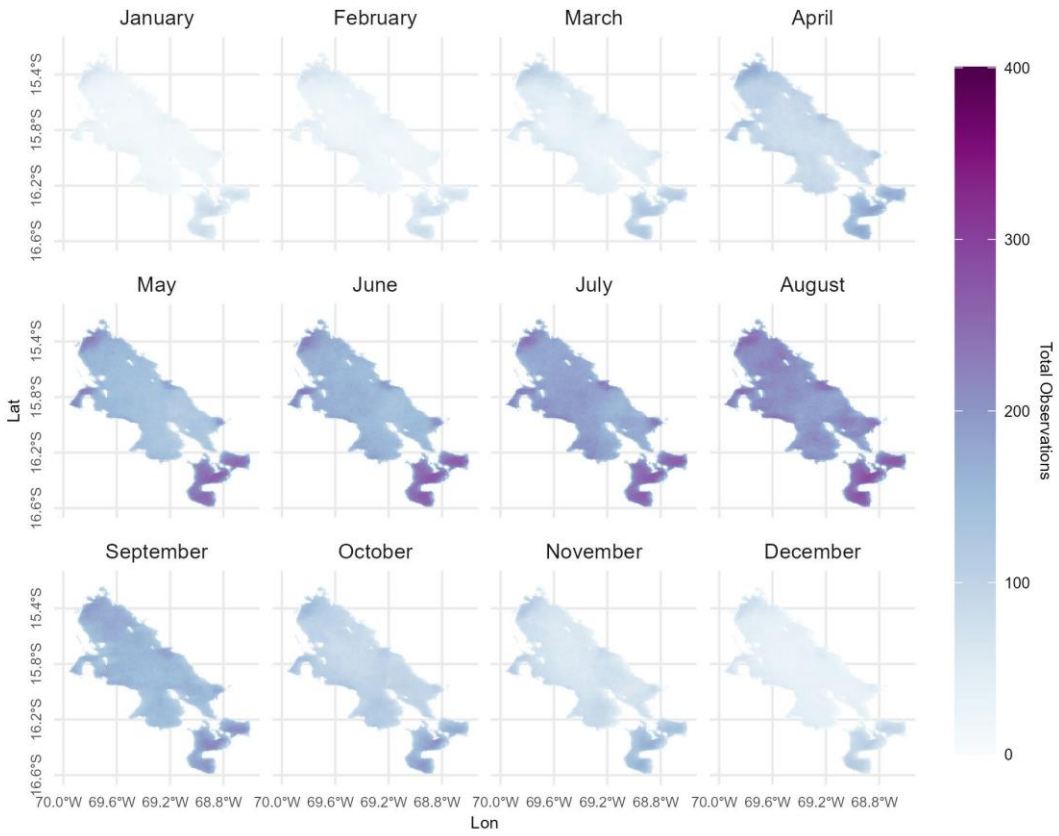


Figure A.5. Monthly observations per cell of Chl-*a* from 2000 to 2020. Observation count ranged between 0 and 400 per cell monthly.

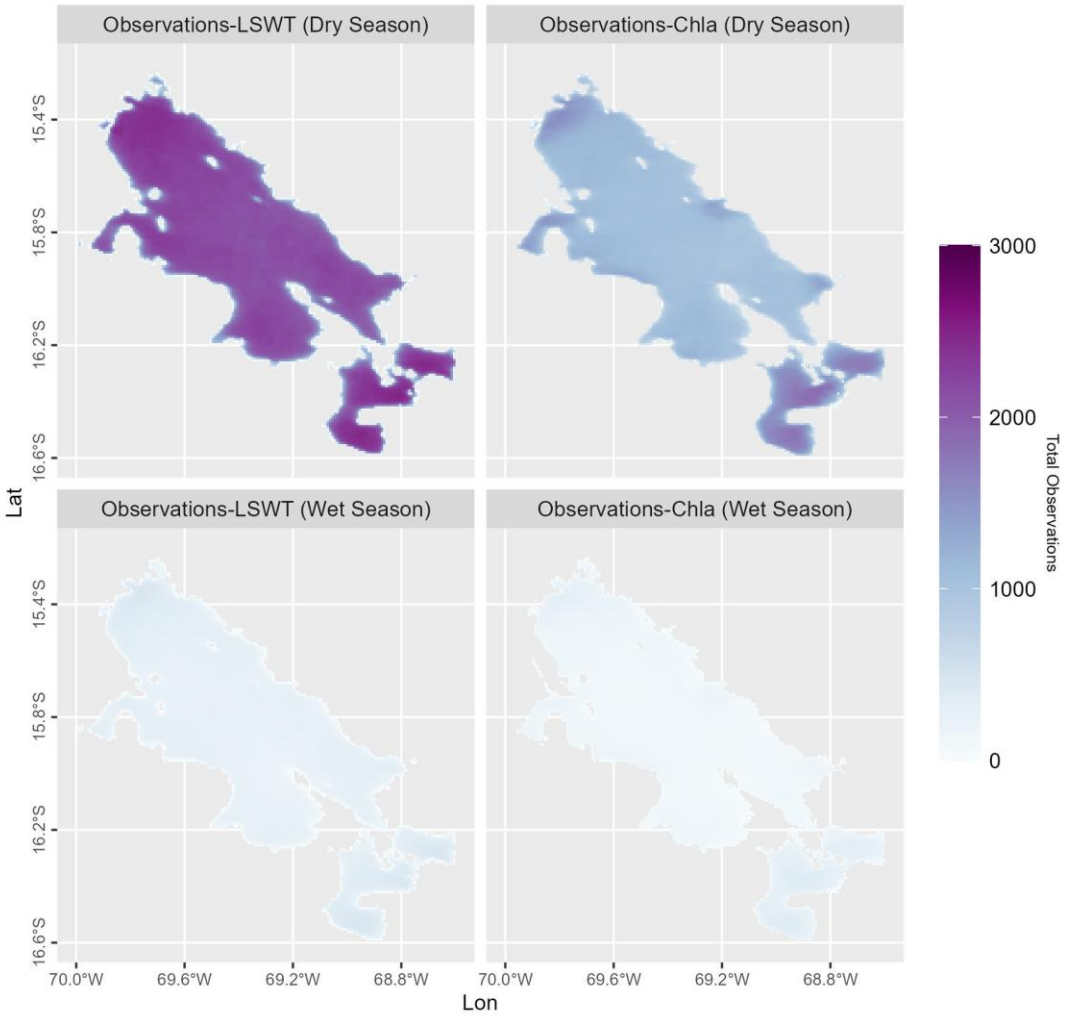


Figure A.6. Seasonal observations per cell of LSWT and Chl-*a* from 2000 to 2020. Seasonal observation count ranged between 0 and 3000 per cell seasonally.

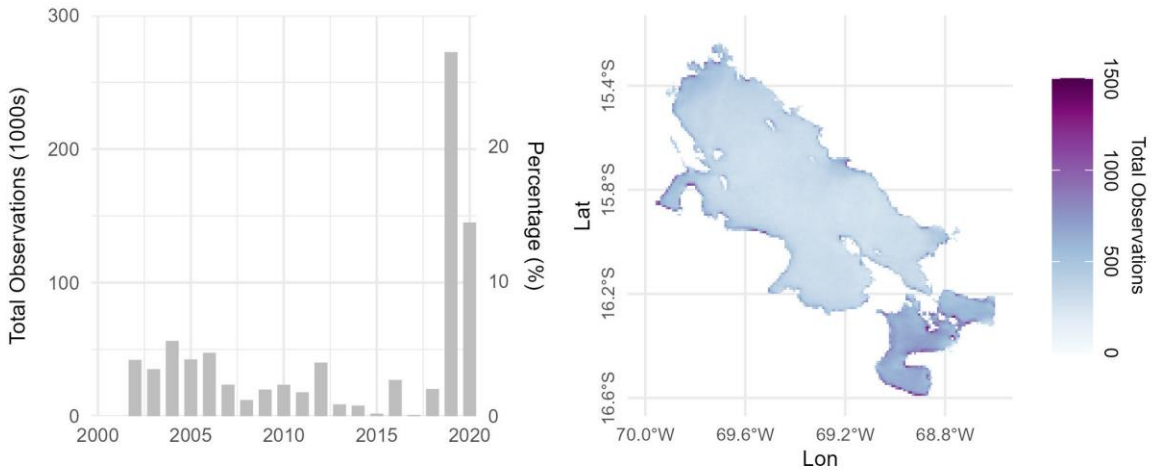


Figure A.7. Total observations of only Chl-*a* from 2000 to 2020.

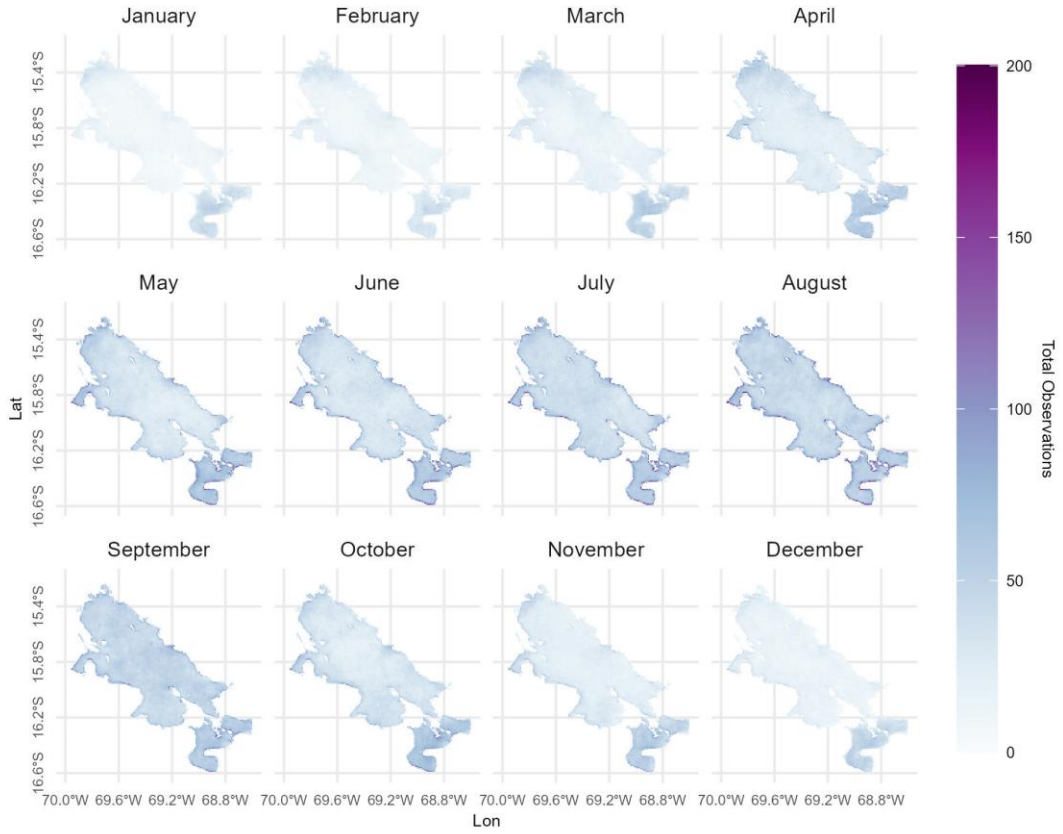


Figure A.8. Monthly observations per cell of only Chl-*a* from 2000 to 2020. Observation count ranged between 0 and 200 per cell monthly.

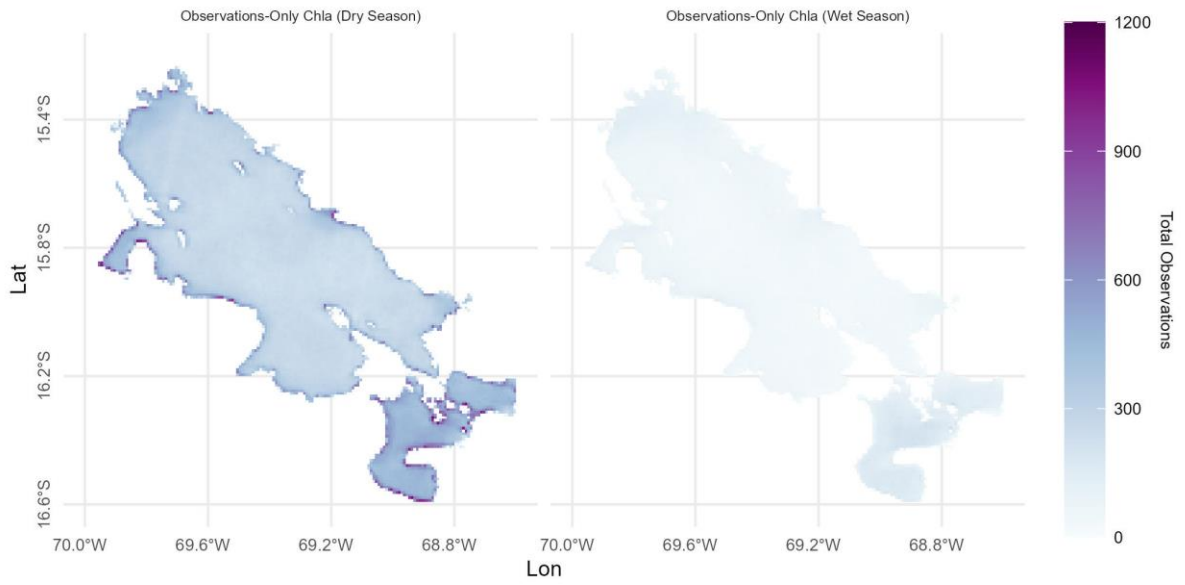


Figure A.9. Seasonal observations per cell of only Chl-*a* from 2000 to 2020. Seasonal observation count ranged between 0 and 1200 per cell seasonally.

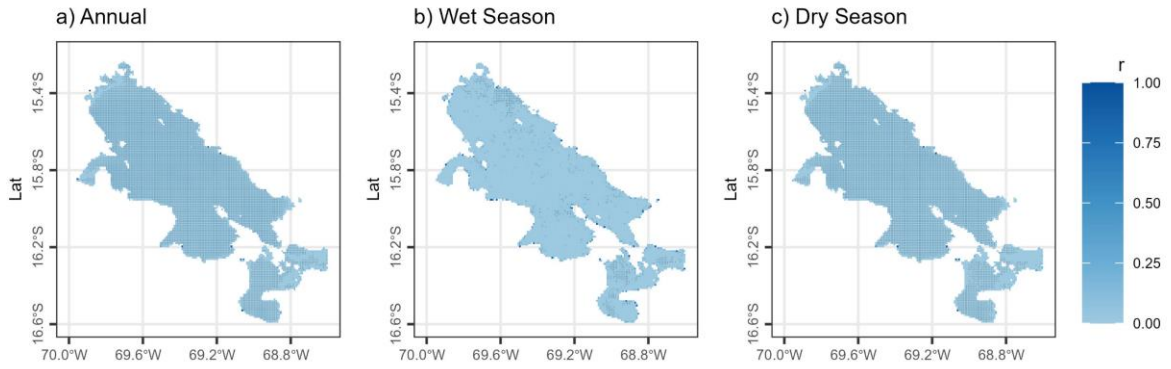


Figure A.10. Annual coefficient of determination between LSWT and Chl-*a*, the asterisk (*) shows statistically significant with $p < 0.05$.

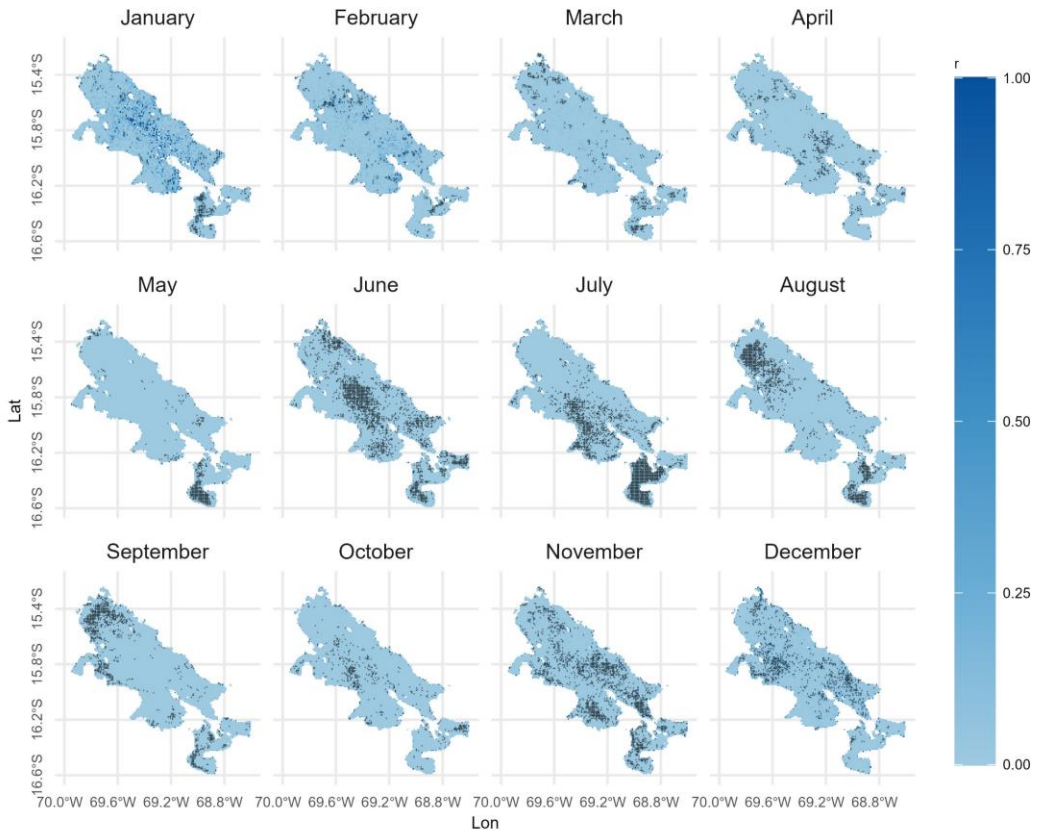


Figure A.11. Monthly coefficient of determination between LSWT and Chl-*a*, the asterisk (*) shows statistically significant with $p < 0.05$.

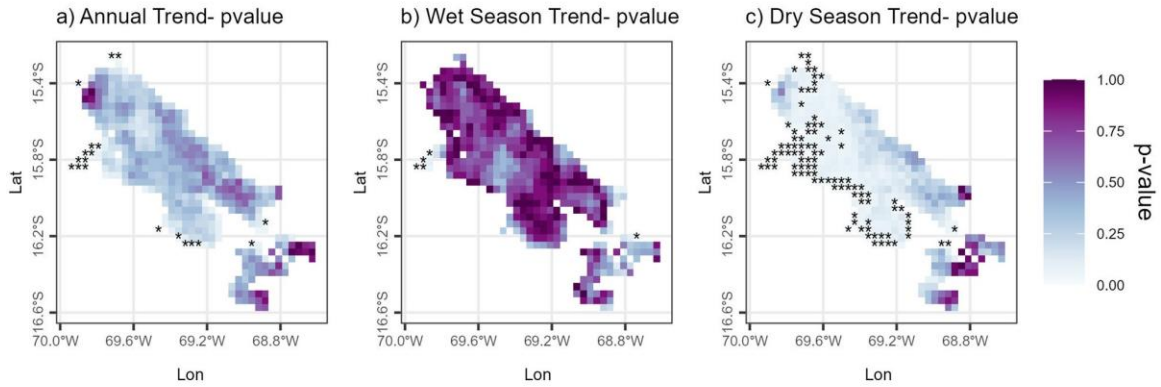


Figure A.12. Trend *p*-values of annual and seasonal LSWT, the asterisk (*) shows statistically significant with $p < 0.05$.

Appendix B

The current and future warming of Lake Titicaca

Text B1. Bias correction methods

B1.1. Linear Scaling (LS)

LS is a simple bias correction technique that uses mean values to adjust the models (Maraun 2016). LS is calculated based on the difference between the monthly mean of observed and historical climate model data in the same baseline period, then the future climate model values are subtracted by the difference (Maraun 2016). LS is calculated as follows:

$$X_{fut_corr} = X_{fut} - (\overline{X}_{cm_hist} - \overline{X}_{obs})$$

where: X_{fut_corr} is bias-corrected values, X_{fut} is future climate-modelled values, $\overline{X}_{cm_hist}$ is the mean of historical climate-modelled values, $\overline{X}_{obs}$ is observed values.

B1.2. Quantile Mapping (QM)

QM used a quantile-based modification of distributions of observed and climate-modelled data (Cannon et al. 2015). It can correct bias in mean, standard deviation and quantiles. QM is applied as follows:

$$X_{fut_corr} = F_{obs}^{-1}\left(F_{cm_hist}\left(X_{fut} + \overline{X}_{cm_hist} - \overline{X}_{fut}\right)\right) + \overline{X}_{fut} - \overline{X}_{cm_hist}$$

where: $\overline{X}_{fut}$ is the mean of future climate-modelled values, and F represents the Cumulative Distribution Function (CDF). CDF is a function that calculates the probability distribution of random values which is equal to or less than the specific values. F_{obs}^{-1} is the inverse CDF calculated by distribution fitting to observed data, and F_{cm_hist} is the CDF calculated by distribution fitting to historical climate-modelled data. F values range from 0 to 1 (Spuler et al. 2023).

QM used the output of Q-Q Mapping between the CDF of observed and historical climate-modelled values to adjust future projections (Spuler et al. 2023).

B1.3. Quantile Delta Mapping (QDM)

QDM is based on QM, however, the advantage of QDM is that it considers the variation between the historical and future simulations (Cannon et al. 2015). In QDM, CDF estimated for future climate-modelled data is fitting in a running window in order to obtain long-term variability in the future trend as well as the seasonality. QDM equation for temperature is:

$$X_{fut_corr} = X_{fut} + F^{-1}_{obs}\left(\hat{F}^{(t)}_{fut}\left(X_{fut}(t)\right)\right) - F^{-1}_{cm_hist}\left(\hat{F}^{(t)}_{fut}\left(X_{fut}\right)\right)$$

where: $\hat{F}^{(t)}_{fut}$ is future climate-modelled empirical CDF runs in a window around t. $F^{-1}_{cm_hist}$ is the inverse CDF calculated by distribution fitting to historical climate-modelled data (Spuler et al. 2023).

B1.4. Scaled Distribution Mapping (SDM)

The concept of SDM is similar to QM, which uses a quantile mapping approach to preserve trends (Switanek et al. 2017). SDM modifies the observed distribution by taking into account both magnitude changes and event likelihood, using additive scaling for temperature (Switanek et al. 2017). The scaling is calculated as follows:

$$scaling = \left[F^{-1}_{fut}(F_{fut}(X_{fut})) - F^{-1}_{cm_hist}(F_{fut}(X_{fut})\right) * \frac{\sigma_{obs}}{\sigma_{cm_hist}}$$

where: σ_{obs} and σ_{cm_hist} are the standard deviation of a normal distribution fitted to observed and historical climate-modelled data. Then recurrence intervals for observed, historical and future values are calculated:

$$RI = \frac{1}{0.5 - ||CDF - 0.5||}$$

Then RI and CDF are scaled:

$$RI_{scaled} = \max\left(1, \frac{RI_{obs} \,.\, RI_{fut}}{RI_{cm_hist}}\right)$$

$$CDF_{scaled} = 0.5 + sgn(CDF_{obs} - 0.5) \,.\, \left|0.5 - \frac{1}{RIscaled}\right|$$

Finally, bias-corrected values are calculated as follows:

$$F^{-1}_{obs}(CDF_{scaled}) + scaling$$

B1.5. ISIMIP3BASD (ISIMIP)

ISIMIP3BASD/ ISIMIP bias correction contains five steps. Firstly, time series of observed, historical and future data are detrended. A significant test is used to determine if the trend is to be removed, the linear regression is used to calculate the annual trend and the trend is removed from the daily values. Secondly, values over the threshold are randomized within the bound and threshold, and the ranks are maintained. Thirdly, by introducing a climate change signal into observed data using an additive method, pseudo-future observations are derived. Fourthly,

quantile mapping is used to map the future values to pseudo future observations to derive bias-corrected values. Finally, the trend is added back onto the debiased future values (Lange 2019; Lange 2021). This method is used in a running window in order to include seasonality (Spuler et al. 2023).

Table B.1. Bias correction results for 4 GCMs and 3 RCPs using 5 bias corrected methods (Linear Scaling- LS, Quantile Mapping- QM, Quantile Delta Mapping- QDM, Inter-Sectoral Impact Model Intercomparison Project- ISIMIP and Scale Distribution Mapping- SDM)

RCPs / GCMs	RCP2.6					RCP6.0					RCP8.5				
HadGEM2-ES	**LS**	**ISIMIP**	**QM**	**QDM**	**SDM**	**LS**	**ISIMIP**	**QM**	**QDM**	**SDM**	**LS**	**ISIMIP**	**QM**	**QDM**	**SDM**
RMSE	1.04	0.89	0.85	0.84	1.2	0.79	0.54	0.48	0.47	0.78	0.81	0.57	0.54	0.53	1.03
MAE	0.88	0.74	0.72	0.73	1.1	0.64	0.42	0.39	0.38	0.63	0.65	0.44	0.42	0.41	0.91
PBIAS	-0.25	-0.25	-0.25	-0.25	-0.38	0.02	0.02	0.02	0.01	-0.2	-0.08	-0.08	-0.08	-0.08	-0.31
r	0.93	0.91	0.93	0.94	0.93	0.93	0.92	0.93	0.93	0.92	0.92	0.92	0.92	0.93	0.92
GFDL ESM2M	**LS**	**ISIMIP**	**QM**	**QDM**	**SDM**	**LS**	**ISIMIP**	**QM**	**QDM**	**SDM**	**LS**	**ISIMIP**	**QM**	**QDM**	**SDM**
RMSE	0.98	0.64	0.52	0.58	0.88	1.01	0.72	0.64	0.66	0.96	1.1	0.7	0.65	0.66	0.96
MAE	0.81	0.51	0.42	0.48	0.73	0.85	0.57	0.51	0.53	0.83	0.9	0.55	0.51	0.53	0.82
PBIAS	0.01	0.01	0.01	0.01	-0.25	-0.14	-0.14	-0.14	-0.14	-0.29	-0.14	-0.14	-0.14	-0.14	-0.28
r	0.93	0.93	0.93	0.94	0.94	0.93	0.92	0.93	0.93	0.93	0.93	0.92	0.93	0.93	0.93
MIROC5	**LS**	**ISIMIP**	**QM**	**QDM**	**SDM**	**LS**	**ISIMIP**	**QM**	**QDM**	**SDM**	**LS**	**ISIMIP**	**QM**	**QDM**	**SDM**
RMSE	0.98	0.75	0.64	0.67	0.94	0.92	0.65	0.59	0.58	0.81	1.1	0.87	0.74	0.81	1.05

MAE	0.81	0.58	0.51	0.53	0.78	0.76	0.49	0.45	0.45	0.67	0.93	0.67	0.58	0.63	0.86
PBIAS	-0.13	-0.13	-0.13	-0.13	-0.27	-0.07	-0.07	-0.07	-0.07	-0.21	-0.09	-0.09	-0.09	-0.09	-0.27
r	0.93	0.91	0.93	0.93	0.93	0.91	0.89	0.91	0.91	0.91	0.87	0.84	0.87	0.86	0.86
IPSL-CM5A-LR	**LS**	**ISIMIP**	**QM**	**QDM**	**SDM**	**LS**	**ISIMIP**	**QM**	**QDM**	**SDM**	**LS**	**ISIMIP**	**QM**	**QDM**	**SDM**
RMSE	0.89	0.61	0.57	0.58	1.14	0.88	0.53	0.53	0.53	1.01	0.87	0.54	0.5	0.51	1.1
MAE	0.77	0.48	0.45	0.46	1.05	0.76	0.41	0.4	0.41	0.9	0.73	0.43	0.39	0.41	1
PBIAS	-0.13	-0.13	-0.13	-0.13	-0.36	-0.09	-0.09	-0.09	-0.09	-0.31	-0.08	-0.8	-0.08	0.09	-0.35
r	0.94	0.93	0.94	0.94	0.94	0.94	0.94	0.94	0.94	0.94	0.94	0.93	0.94	0.94	0.94

Table B.2. Simulations for relative contribution of meteorological variables using FLake model

Simulation	Air temperature	Longwave downward radiation	Specific Humidity	Shortwave downward radiation	Wind Speed
S1 (Reference)	1981-2020	1981-2020	1981-2020	1981-2020	1981-2020
S2	1981-2020	1981	1981	1981	1981
S3	1981	1981-2020	1981	1981	1981
S4	1981	1981	1981-2020	1981	1981
S5	1981	1981	1981	1981-2020	1981
S6	1981	1981	1981	1981	1981-2020

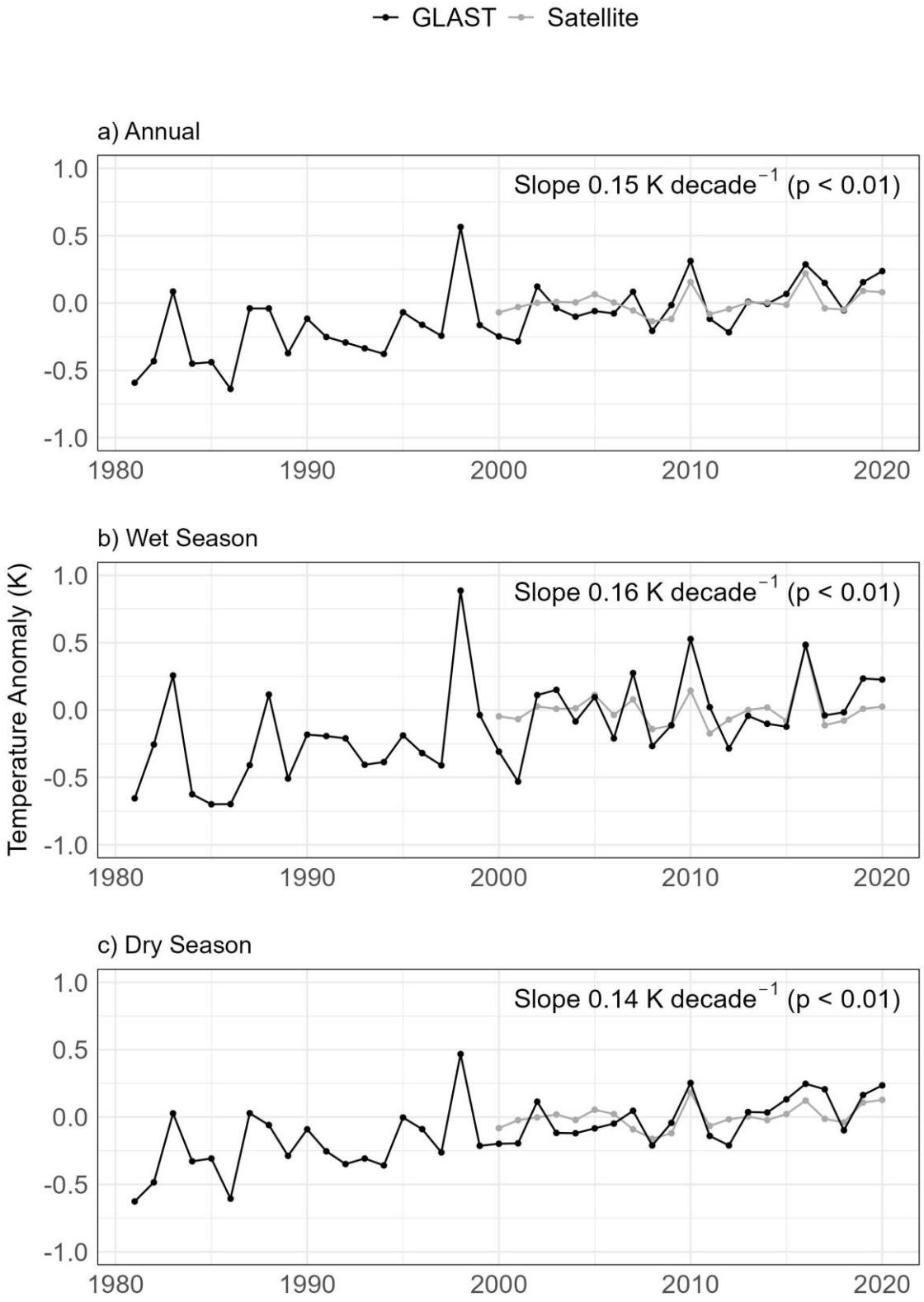


Figure B.1. Temperature anomalies derived from GLAST data (1981-2020) in black and satellite data (2000-2020) in grey; shown in a) Annual, b) Wet season, c) Dry season.

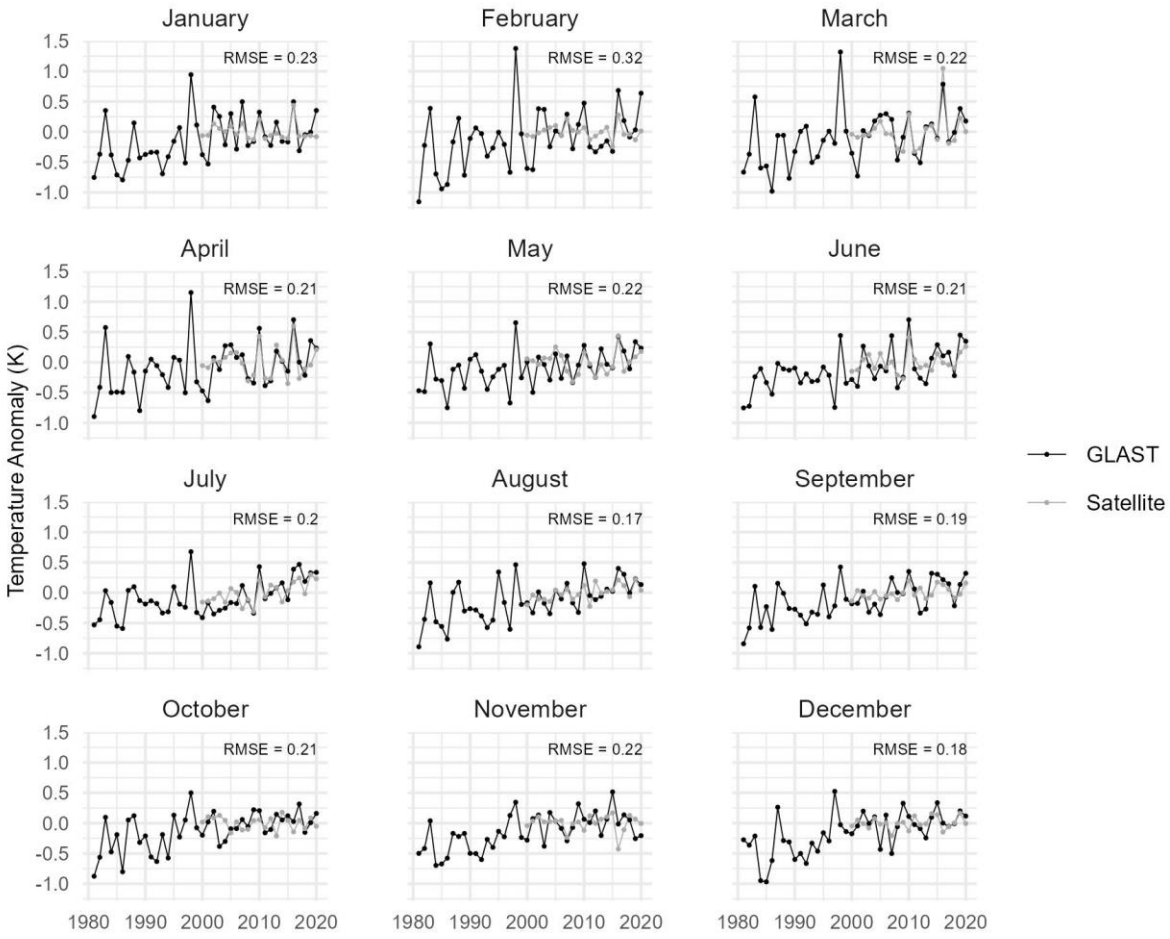


Figure B.2. Monthly temperature anomalies derived from GLAST data (1981-2020) in black and satellite data (2000-2020) in grey.

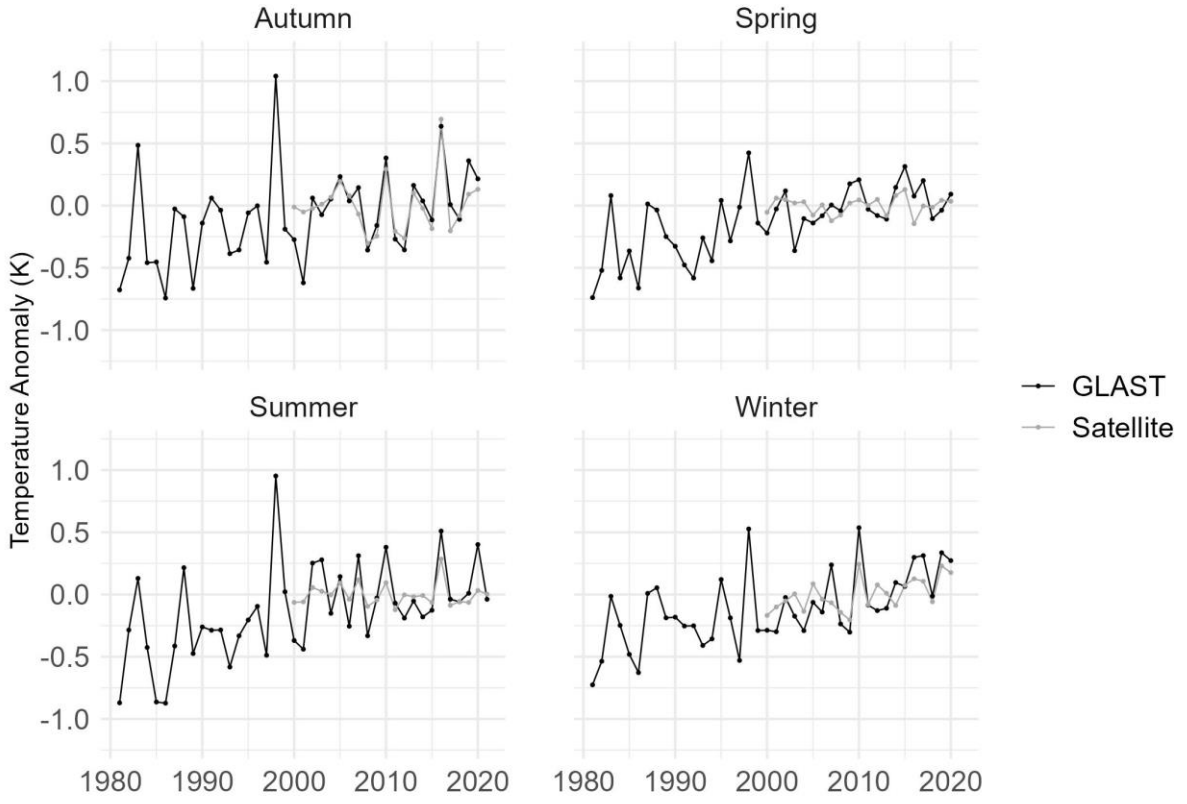


Figure B.3. Seasonal temperature anomalies derived from GLAST data (1981-2020) in black and satellite data (2000-2020) in grey.

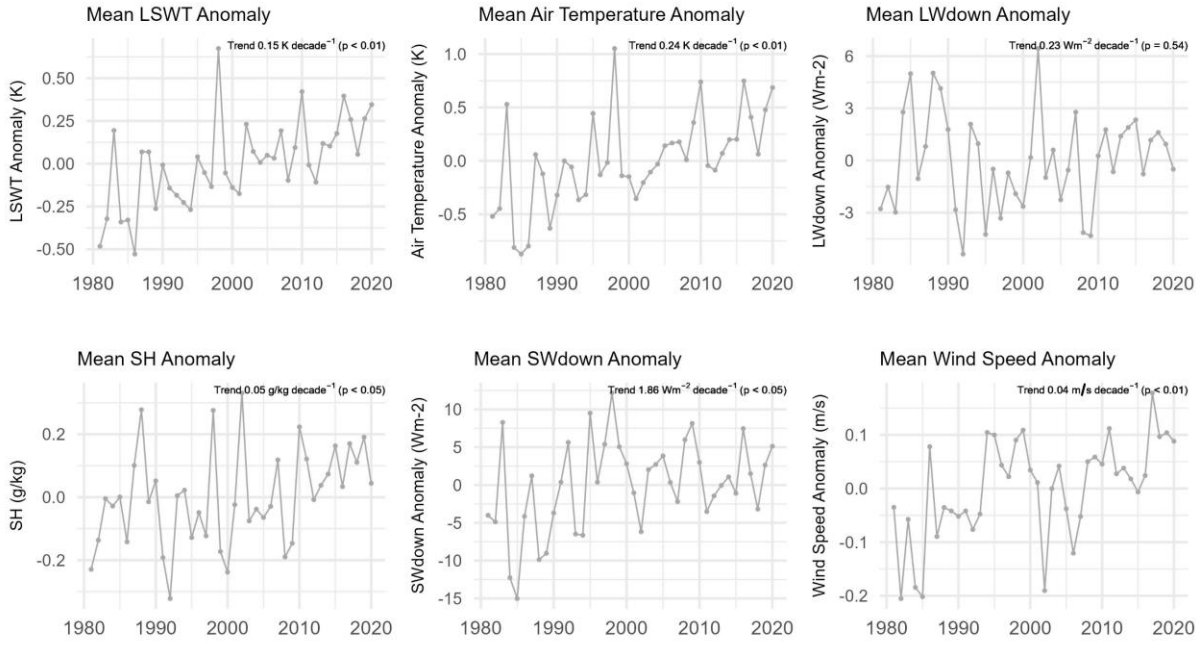


Figure B.4. Annual anomaly of LSWT and meteorological variables (1981-2020)

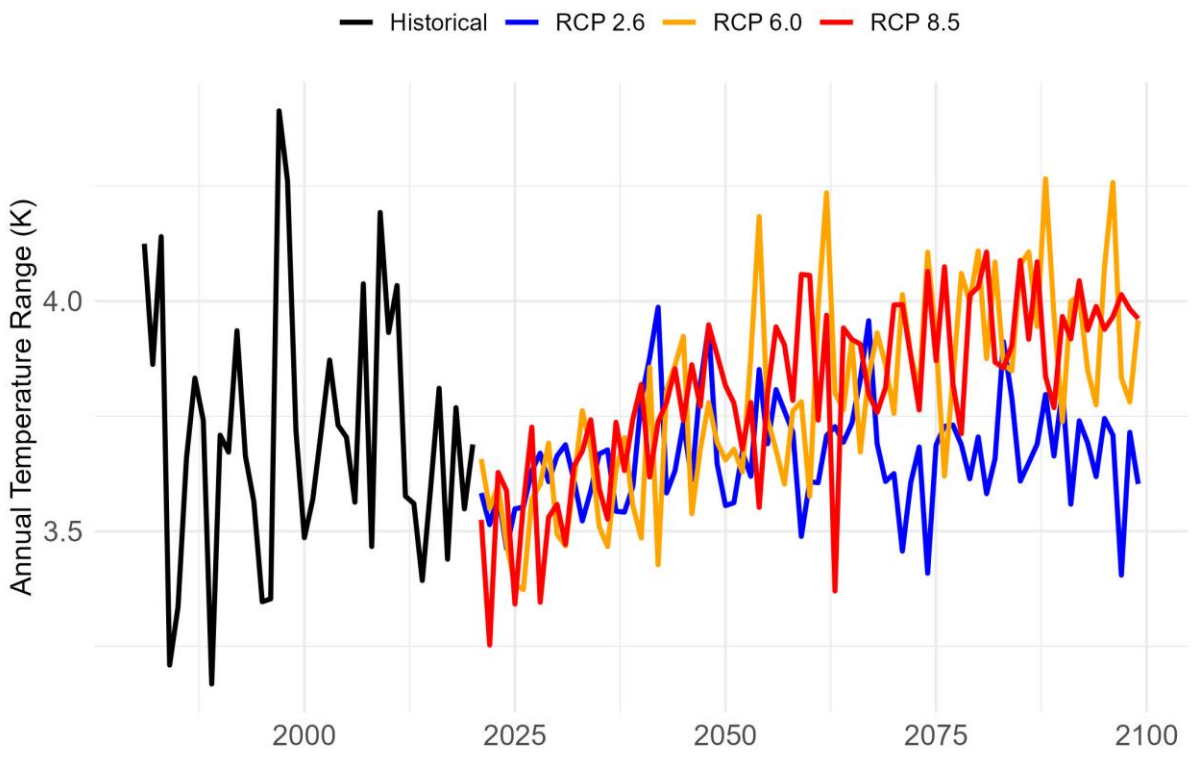


Figure B.5. Annual range during the historical and future periods driven under different RCPs.

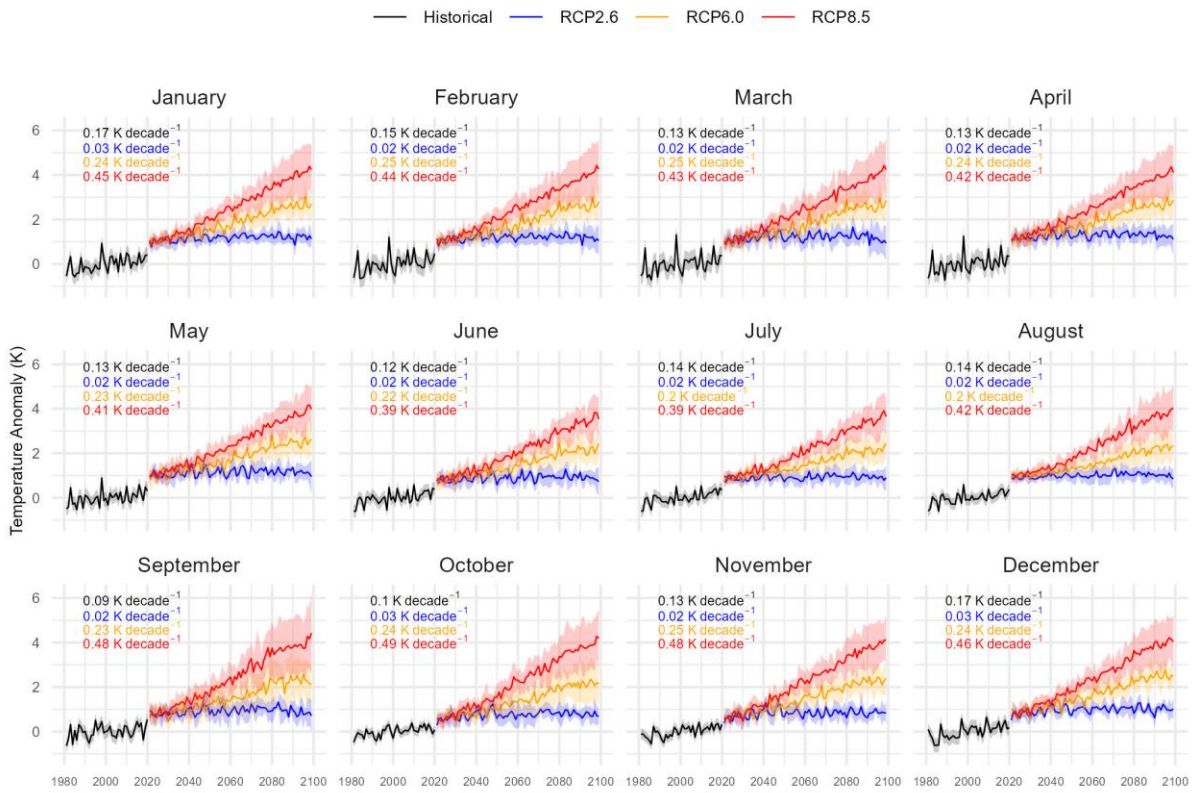


Figure B.6. Monthly historical and future projections of temperature anomalies driven under different RCPs. The thick lines represent mean temperature anomalies and the shaded areas show the standard deviation. The historical temperature anomalies (black) from 1981 to 2020, the projections under RCP 2.6 (blue), RCP 6.0 (orange), RCP 8.5 (red) scenarios from 2021 to 2099.

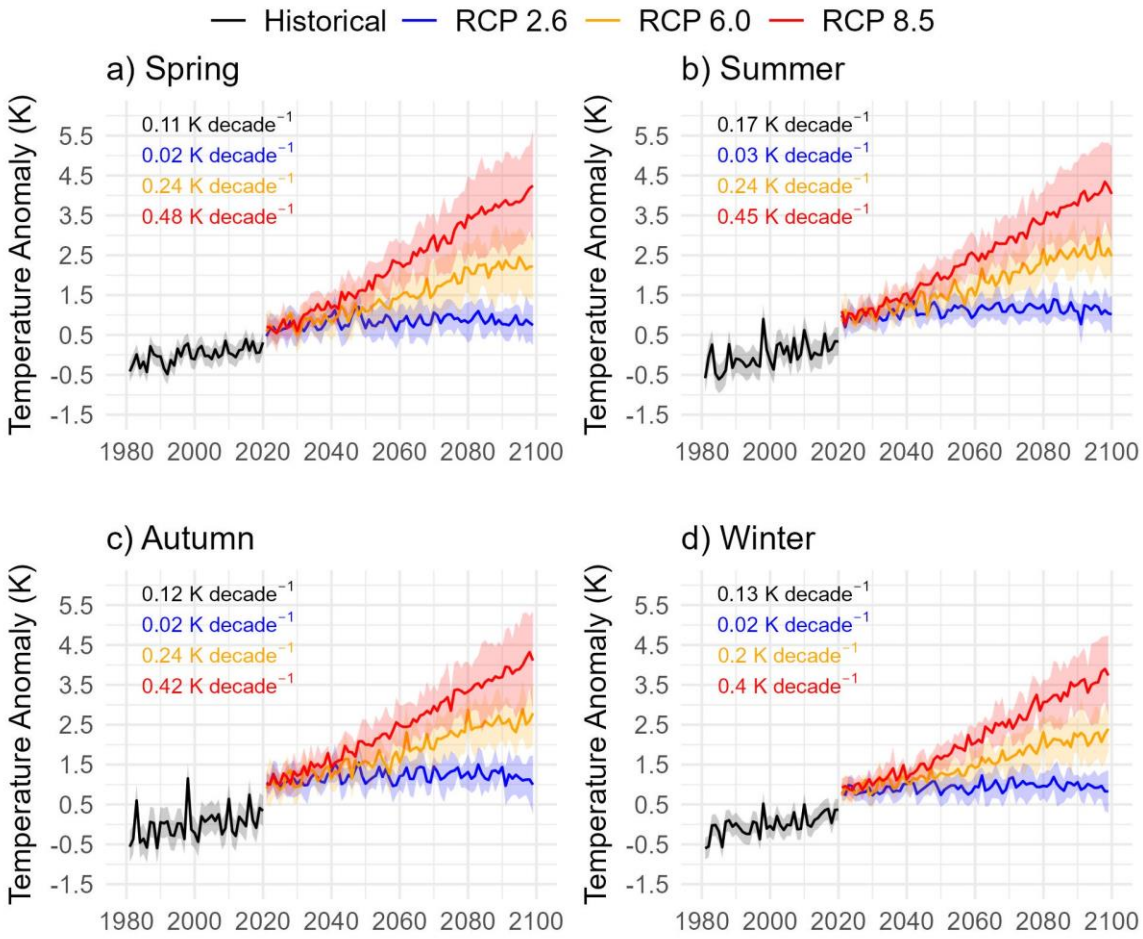


Figure B.7. Seasonal historical and future projections of temperature anomalies driven under different RCPs.

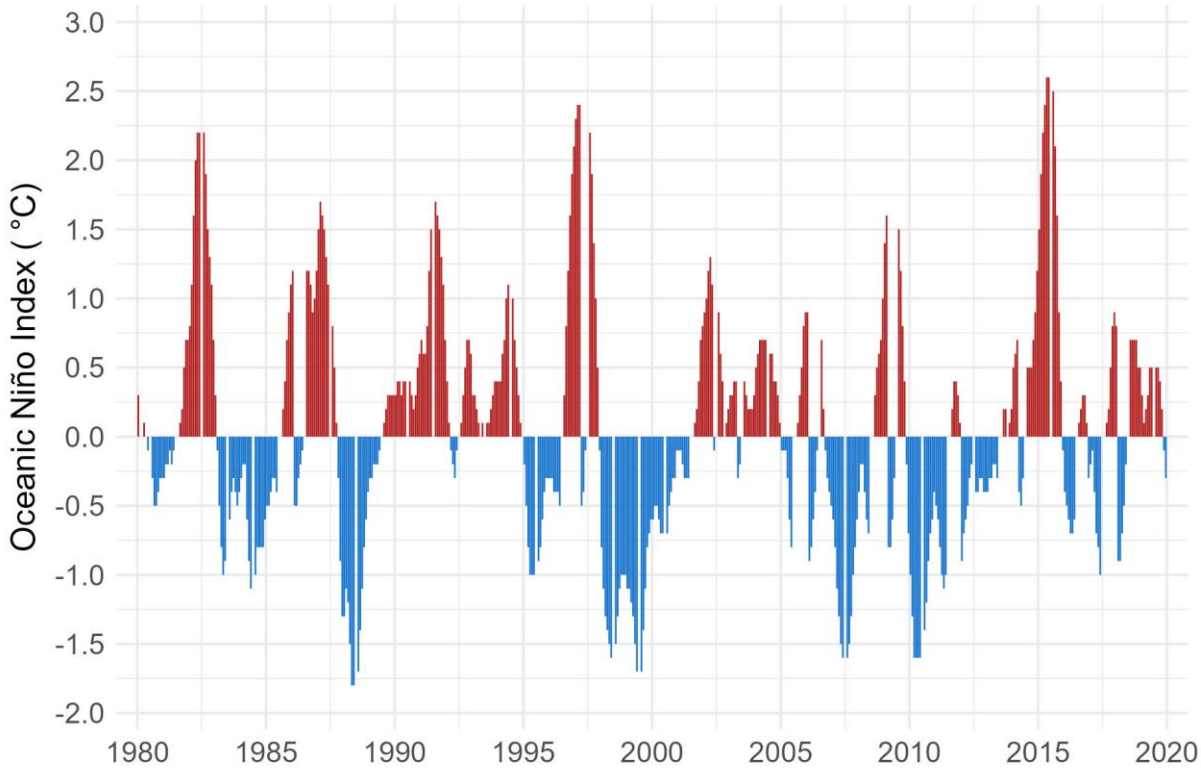


Figure B.8. Seasonal (3-month) sea surface temperature anomalies from 1980 to 2020. Warming phases show in red color while cooling phases show in blue color (Source: NOAA; https://www.cpc.ncep.noaa.gov/data/indices/oni.ascii.txt)

Appendix C

Emerging changes in lake temperature extremes and variability in South America

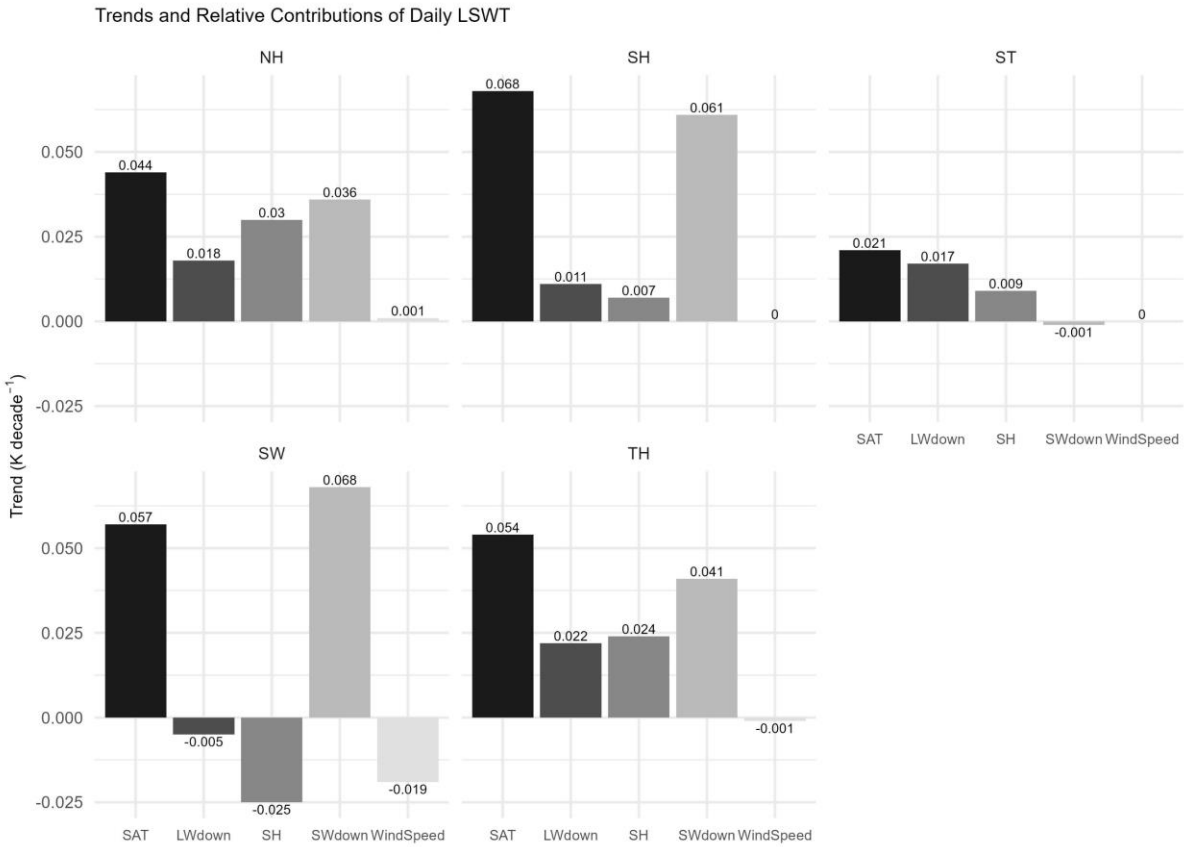


Figure C.1. Trend and relative contribution of daily LSWT (SAT- Surface Air Temperature, LWdown- Longwave Downward Radiation, SH- Specific Humidity, SWdown- Shortwave Downward Radiation, WindSpeed- Wind Speed) per thermal regions (NH- Northern Hot, SH- Southern Hot, ST- Southern Temperate, SW- Southern Warm, TH- Tropical Hot).

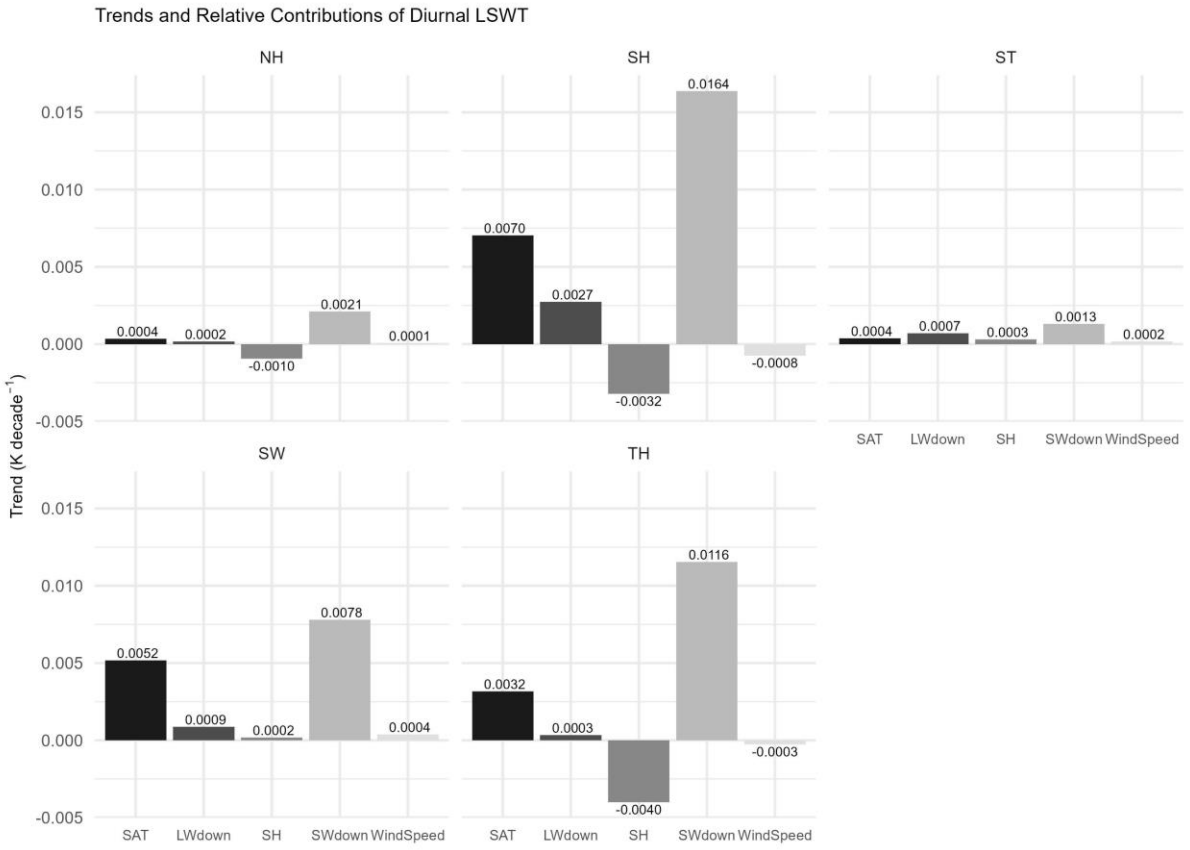


Figure C.2. Trend and relative contribution of diurnal LSWT per thermal regions (SAT- Surface Air Temperature, LWdown- Longwave Downward Radiation, SH- Specific Humidity, SWdown- Shortwave Downward Radiation, WindSpeed- Wind Speed).

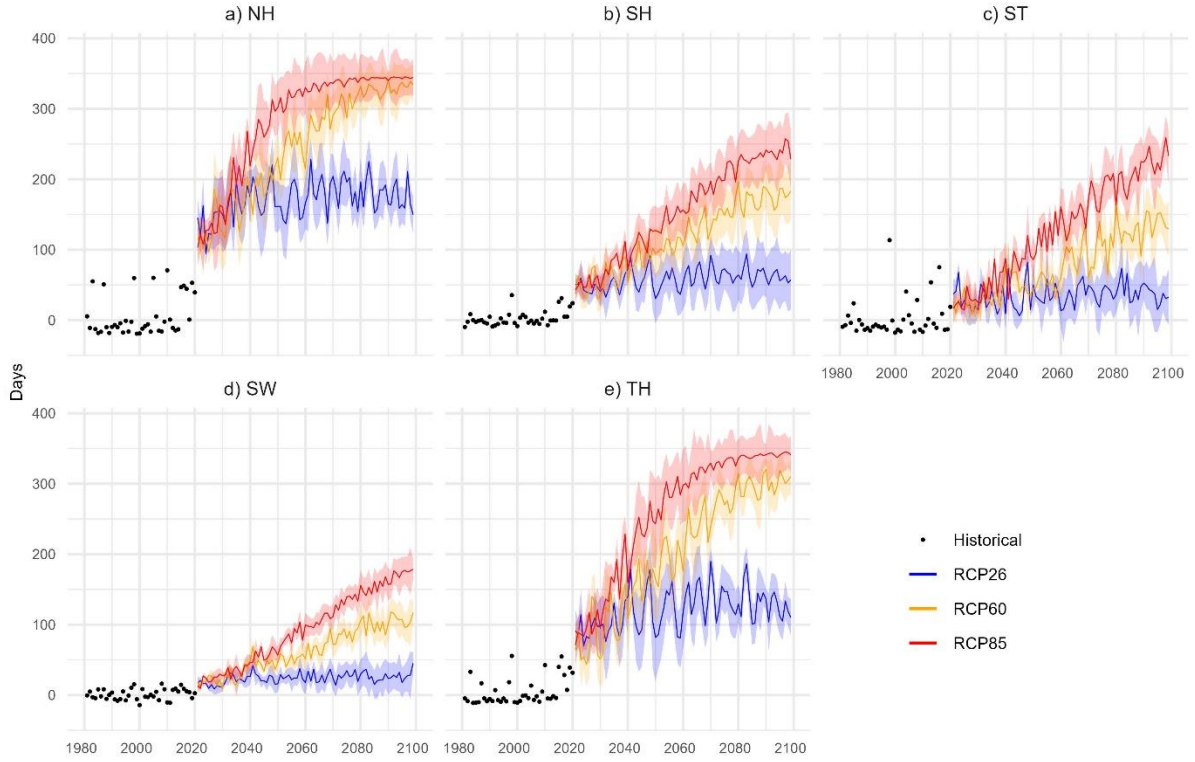


Figure C.3. Total heatwave day anomalies per thermal regions (a) Northern Hot, (b) Southern Hot, (c) Southern Temperate, (d) Southern Warm, and (e) Tropical Hot. The thick lines represent total heatwave day anomalies and the shaded areas show the standard deviation across the multi-model ensemble. The historical temperature anomalies (black) from 1981 to 2020, the projections under RCP 2.6 (blue), RCP 6.0 (orange), RCP 8.5 (red) scenarios from 2021 to 2099

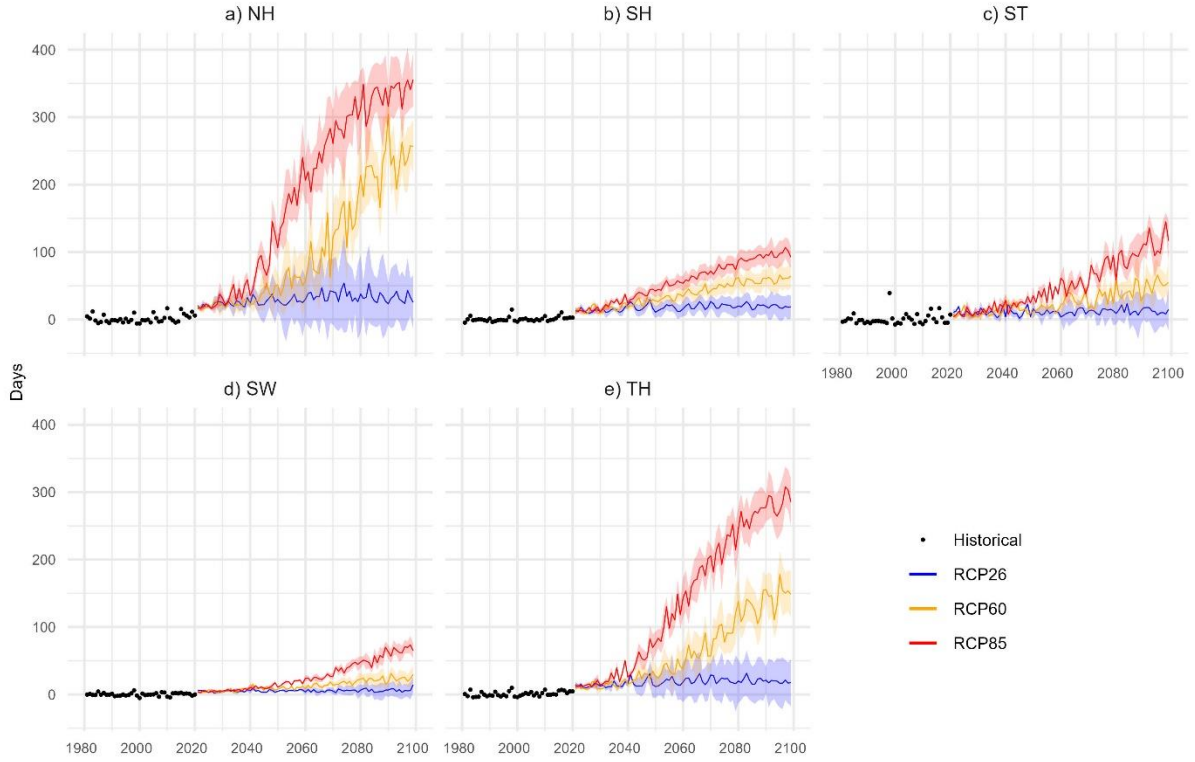


Figure C.4. Heatwave duration anomalies per thermal regions (a) Northern Hot, (b) Southern Hot, (c) Southern Temperate, (d) Southern Warm, and (e) Tropical Hot. The thick lines represent average anomalies and the shaded areas show the standard deviation across the multi-model ensemble. The historical temperature anomalies (black) from 1981 to 2020, the projections under RCP 2.6 (blue), RCP 6.0 (orange), RCP 8.5 (red) scenarios from 2021 to 2099.

.

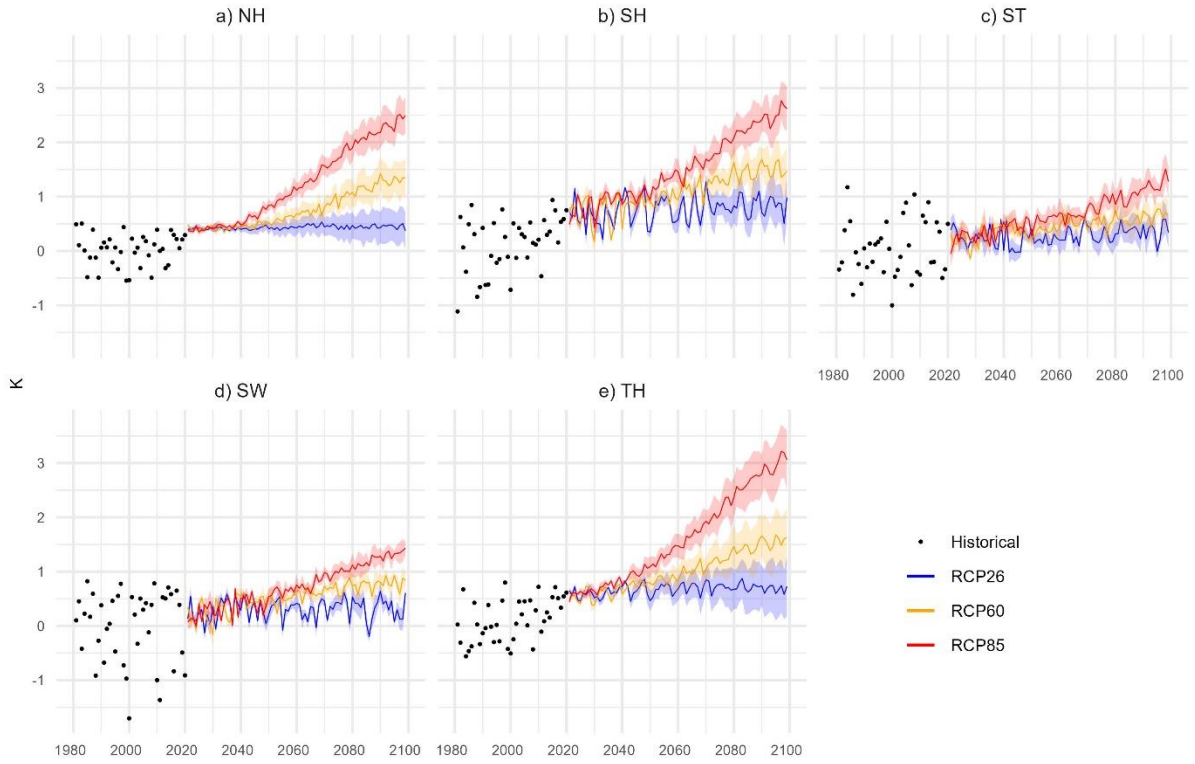


Figure C.5. Heatwave intensity anomalies per thermal regions (a) Northern Hot, (b) Southern Hot, (c) Southern Temperate, (d) Southern Warm, and (e) Tropical Hot. The thick lines represent average anomalies and the shaded areas show the standard deviation across the multi-model ensemble. The historical temperature anomalies (black) from 1981 to 2020, the projections under RCP 2.6 (blue), RCP 6.0 (orange), RCP 8.5 (red) scenarios from 2021 to 2099.

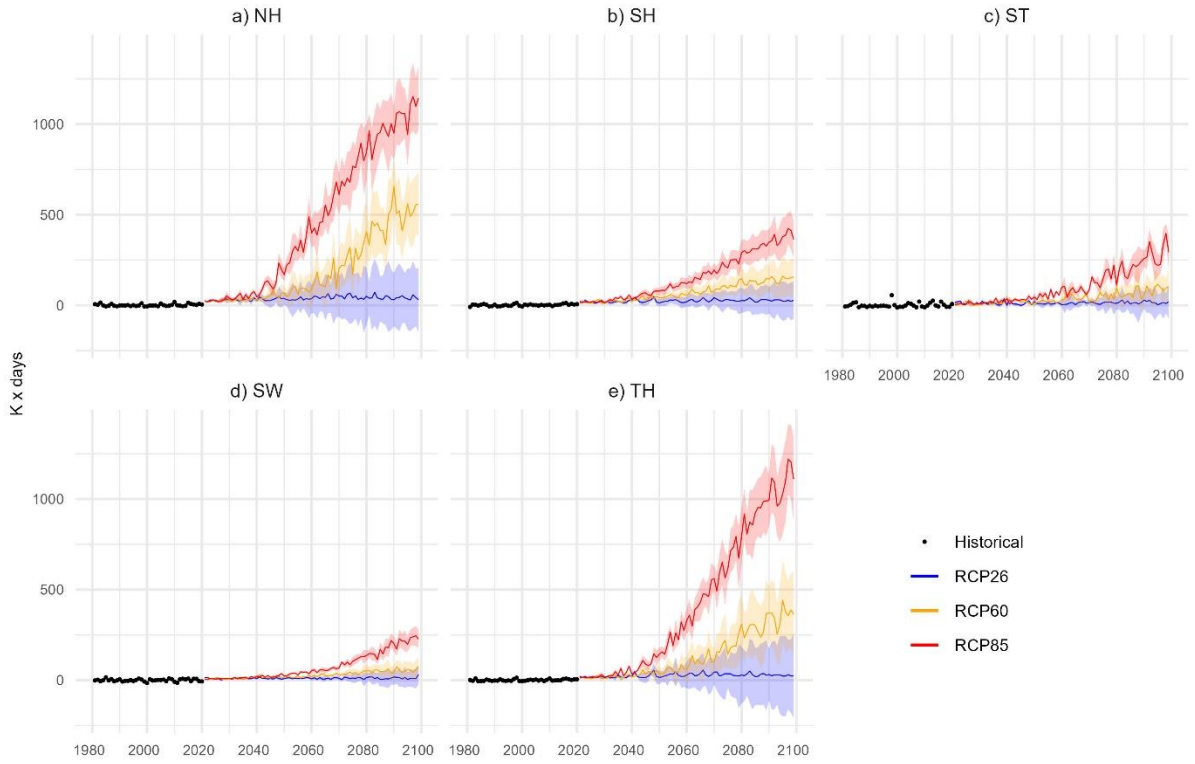


Figure C.6. Heatwave cumulative intensity anomalies per thermal regions (a) Northern Hot, (b) Southern Hot, (c) Southern Temperate, (d) Southern Warm, and (e) Tropical Hot. The thick lines represent average anomalies and the shaded areas show the standard deviation across the multi-model ensemble. The historical temperature anomalies (black) from 1981 to 2020, the projections under RCP 2.6 (blue), RCP 6.0 (orange), RCP 8.5 (red) scenarios from 2021 to 2099.

Appendix D. List of Publications, Conference Oral/Poster presentations and Trainings

D.1. List of Conference Oral/Poster presentations and Trainings

- **Participant**, Inventwater Workshop, at DKIT, Dundalk, Ireland on June 2022.

- **Participant**, Global Lake Ecological Observation Network GLEON 2023 Virtual All Hands' Meeting (virtual) on February 2023.

- Best **elevation pitch** on the project entitled "Remote Sensing of Global Surface Waters-RETINA" at the Irish Freshwater Science Association Meeting at the Atlantic Technological University, Galway on March 10, 2023.

- **Poster presentation** titled "Comparison of gap-filling methods for freshwater satellite data: a case study on spatial-temporal surface water temperature of Lake Titicaca" at the 13th Symposium for European Freshwater Sciences, Newcastle University, UK, on 18-23 June 2023.

- **Oral presentation** titled "Observed changes and future projections of surface water temperature in Lake Titicaca under a changing climate" at the European Geosciences Union General Assembly 2024, Vienna, Austria on 14-19 April 2024.

- **Oral presentation** titled "A Comparative Study of Gap-Filling Approaches for Surface Water Temperature Changes in Lake Titicaca Using Earth Observation Data" at the 35th International Geographical Congress, Dublin, Ireland on 24-30 August 2024.

- **Participant**, HydRoData (Hydrology and Data) Summer School, Unesco Chair on Water-related Disaster Risk Reduction & University of Ljubljana, Slovenia, 2-6 September 2024.

- **Participant**, the 14th CCI Colocation & CMUG Integration meetings, ESA's European Centre for Space Applications and Telecommunications, Harwell, UK, 16-18 October 2024.

- **Oral presentation** titled "Observed Changes and Future Projections of Daily and Diurnal Lake Surface Water Temperature in South America under a Changing Climate" at the American Geophysical Union (AGU) Annual Meeting, Washington DC, USA, 9-13 December 2024.

- **Oral presentation** titled “Exploring Historical and Future Changes of Lake Surface Water Temperature in South America” at the 35th Irish Environmental Researchers’ Colloquium (Environ 2025), Dublin, Ireland, 10-12 March, 2025.

D.2. List of Publications

This research is based on the publications below:

1. Dinh, D.A., McCarthy, V., Jennings, E., Jordan, S., Kraemer, B.M., Barth, A., Carrea, L., Simis, S., Liu, M. and Woolway, R.I. (2026). Evaluating gap-filling techniques for satellite-derived surface water temperature: A case study of Lake Titicaca. (Submitted)

2. Dinh, D.A., Tong, Y., Feng, L., McCarthy, V., Jennings, E., Jordan, S., Shi, K. and Woolway, R.I. (2026). The current and future warming of Lake Titicaca. *Journal of Great Lakes Research*, 102752. https://doi.org/10.1016/j.jglr.2026.102752

3. Dinh, D.A., Tong, Y., Feng, L., Fleischmann, A., Jennings, E., McCarthy, V., Jordan, S. and Woolway, R.I. (2026). Emerging changes in lake temperature extremes and variability in South America. *Climatic Change* 179, 41. https://doi.org/10.1007/s10584-026-04137-0

Additionally, I have contributed as a co-author to the publication listed below:

Woolway, R.I., Tong, Y., Feng, L., Zhao, G., Dinh, D.A., Shi, H., Zhang, Y. and Shi, K. (2024). Multivariate extremes in lakes. *Nature Communications* 15: 4559. https://doi.org/10.1038/s41467-024-49012-7